VALUE ENGINEERING AND COST EFFECTIVENESS OF VARIOUS FIBER REINFORCED POLYMER (FRP) REPAIR SYSTEMS

By

Sami Rizkalla
Principal Investigator

Owen Rosenboom
PhD Candidate

Anthony Miller
Graduate Research Assistant

Catrina Walter
Graduate Research Assistant

Research Project 2006-10

Final Report

In cooperation with the

North Carolina Department of Transportation

And

Federal Highway Administration
United States Department of Transportation

Department of Civil Engineering
North Carolina State University
Raleigh, NC 27695-7908

June 2007

Technical Report Documentation Page

1. Report No. FHWA/NC/2006-39	2. Government Accession No.	3. Recipient's Catalog No.
4. Title and Subtitle Value Engineering and Cost Effectiveness of Various Fiber Reinforced Polymer (FRP) Repair Systems, Phase II		5. Report Date June 2007 6. Performing Organization Code
7. Author(s) Sami Rizkalla, Owen Rosenboom, Anthony Miller and Catrina Walter		8. Performing Organization Report No.
9. Performing Organization Name and Address Department of Civil Engineering North Carolina State University Raleigh, NC 27695-7908		10. Work Unit No. (TRAIS) 11. Contract or Grant No.
12. Sponsoring Agency Name and Address North Carolina Department of Transportation Research and Analysis Group 1 South Wilmington Street Raleigh, North Carolina 27601		13. Type of Report and Period Covered Final Report July 2005 – December 2006 14. Sponsoring Agency Code 2006-10
Supplementary Notes:		

16. Abstract

This report is an extension to the final report for NCDOT project 2004-15 "Value Engineering and Cost-Effectiveness of Various Fiber Reinforced Polymers (FRP) Repair Systems", submitted in June 2005. In that report, seventeen 30-ft long prestressed concrete c-channels were tested under static and fatigue loading conditions using various carbon fiber reinforced polymer (CFRP) strengthening systems to determine their structural behavior, cost effectiveness and constructability. The 2004-15 final report also included the behavior of impact damaged AASHTO girders repaired by CFRP systems and tested under fatigue loading conditions.

This final report for NCDOT project 2006-10, summarizing the results of Phase II of the NCDOT project 2004-15, includes the behavior of four additional c-channel prestressed concrete girders strengthened with externally bonded high modulus CFRP sheets and high strength steel reinforced polymer (SRP) wire mesh. The report includes also the behavior of four additional AASHTO type II girders. Two long-span AASHTO girders were tested static loading conditions to assess the performances of FRP systems designed to repair impact damage. Two AASHTO girders were tested using short spans to determine the effectiveness of using FRP to restore the shear capacity of impact damaged girders with one girder tested as control specimen and one damaged then repaired with FRP. The repaired girder was stronger than the damaged girder, indicating that the FRP repair is effective in restoring the girder shear capacity.

Based on the above, the entire experimental program consisted of twenty-one girders strengthened with various FRP and SRP materials and five AASHTO girders repaired with FRP to restore their flexural and shear capacities. The research indicates that FRP systems are effective for the strengthening/repair of concrete highway bridges. The report provides detailed procedures for installation as well as efficient inspection procedures to ensure effectiveness of the strengthening/repair systems.

17. Key Words Fiber Reinforced Polymers, Prestressed Concrete, Flexural Behavior, Shear Behavior, Repair, Strengthening, Impact Damage, Fatigue	18. Distribution Statement

19. Security Classif. (of this report) Unclassified	20. Security Classif. (of this page) Unclassified	21. No. of Pages 248	22. Price

Form DOT F 1700.7 (8-72) **Reproduction of completed page authorized**

DISCLAIMER

ACKNOWLEDGEMENTS

The authors would like to acknowledge the support of the North Carolina Department of Transportation through Project 2004-15, the National Science and Engineering Research Council of Canada and the National Council of Scientific and Technological Development (CNPq), Brazil. Several industry members made much appreciated donations: David White of the Sika Corporation, Doug Gremel of Hughes Brothers, Akira Nakagoshi of Mitsubishi Chemical America, Peter Emmons of Structural Preservation Systems and Ed Fyfe of Fyfe Corporation. Special thanks to Structural Preservation Systems and Fyfe Corporation for carrying out the strengthening and repair work. Thanks are also extended to the personnel at the NCDOT Bridge Maintenance Department, especially Dallie Bagwell and Tracy Stephenson for providing Bridge Maintenance facilities and constructing steel substructures for the repair and strengthening work. The authors would like to thank Jerry Atkinson and Bill Dunleavy, technicians at the Constructed Facilities Laboratory at North Carolina State University, for their invaluable help.

SUMMARY

This report is an extension to the final report for NCDOT project 2004-15 "Value Engineering and Cost-Effectiveness of Various Fiber Reinforced Polymers (FRP) Repair Systems", submitted in June 2005. In that report, seventeen 30-ft long prestressed concrete c-channels were tested under static and fatigue loading conditions using various carbon fiber reinforced polymer (CFRP) strengthening systems to determine their structural behavior, cost effectiveness and constructability. The 2004-15 final report also included the behavior of impact damaged AASHTO girders repaired by CFRP systems and tested under fatigue loading conditions.

This final report for NCDOT project 2006-10, summarizing the results of Phase II of the NCDOT project 2004-15, includes the behavior of four additional c-channel prestressed concrete girders strengthened with externally bonded high modulus CFRP sheets and high strength steel reinforced polymer (SRP) wire mesh. The report includes also the behavior of four additional AASHTO type II girders. Two long-span AASHTO girders were tested static loading conditions to assess the performances of FRP systems designed to repair impact damage. Two AASHTO girders were tested using short spans to determine the effectiveness of using FRP to restore the shear capacity of impact damaged girders with one girder tested as control specimen and one damaged then repaired with FRP. The repaired girder was stronger than the damaged girder, indicating that the FRP repair is effective in restoring the girder shear capacity.

Based on the above, the entire experimental program consisted of twenty-one girders strengthened with various FRP and SRP materials and five AASHTO girders repaired with FRP to restore their flexural and shear capacities. The research indicates that FRP systems are effective for the strengthening/repair of concrete highway bridges. The report provides detailed procedures for installation as well as efficient inspection procedures to ensure effectiveness of the strengthening/repair systems.

TABLE OF CONTENTS

LIST OF TABLES

LIST OF FIGURES

1 INTRODUCTION

1.1 Background

The original agreement for the extension required repair of three impact damaged AASHTO Girders with fiber reinforced polymer (FRP) systems and then testing under static and fatigue conditions. The extension required also testing of two C-Channel girders strengthened with steel reinforced polymer (SRP) material under static and fatigue loading. The actual experimental program consisted of four AASHTO Girders, two tested in flexure and two tested in shear, under static conditions. Four C-Channels, two strengthened with SRP and two strengthened with carbon fiber reinforced polymer (CFRP) produced by Hexcel, were also tested. A summary of the total experimental program for strengthening, including those discussed in the previous report (Rizkalla et al. (2005)), can be found in Table 1.1. Summary of the experiment proposal for repair of AASHTO girders are given in Table 1.2.

1.2 Research Objectives and Scope

The primary objective of the research project is to evaluate the feasibility of using CFRP sheets as a repair system for severely laterally impact-damaged girders. The secondary objective of the research is to evaluate the application of typical design methods for the design of FRP repair systems for impact-damaged prestressed bridge girders. The scope also includes evaluation of the effectiveness of the new steel reinforced polymers (SRP) method for strengthening prestressed concrete bridge girders. The final objective of the research includes review of the current inspection methods and recommends the most practical inspection methods to ensure proper installation of the FRP system under field conditions.

Table 1.1 Summary of the entire experimental program for strengthening of c-channel girders

Static Tests - 11 Total		
	Beam #	Strengthening Technique
Type I	CS	Control Unstrengthened
	NSM1S	NSM CFRP Bars (20%)*
	NSM2S	NSM CFRP Strips (20%)*
	EB1S	Externally Bonded CFRP Strips (20%)*
	EB2S	Externally Bonded CFRP Sheets (20%)*
	EB3S	Externally Bonded HM CFRP Strips (20%)*
	EB4S	Externally Bonded CFRP Sheets (60%)*
	EB7S	Externally Bonded CFRP Sheets (30%)*
	SRPS	Externally Bonded Steel-Reinforced Poylmer (SRP)Sheets (30%)*
Type II	EB5S	Externally Bonded CFRP Sheets (40%)*
	EB6S	Externally Bonded HM CFRP Sheets (20%)*
Fatigue Tests - 10 Total		
	Beam #	Strengthening Technique
Type I	CF1	Control Unstrengthened
	EB1F	Externally Bonded CFRP Strips (20%)*
	EB4F	Externally Bonded CFRP Sheets (60%)*
	NSM1F	NSM CFRP Bars (20%)*
	NSM2F	NSM CFRP Strips (20%)*
	EB7F	Externally Bonded CFRP Sheets (30%)*
	SRPF	Externally Bonded Steel Reinforced Polymer (SRP) Sheets (30%)*
Type II	CF2	Control Unstrengthened
	EB5F	Externally Bonded CFRP Sheets (40%)*
	EB6F	Externally Bonded HM CFRP Sheets (20%)*

*Note: Desired Level of Strengthening is shown in parentheses

Table 1.2 Summary of the entire experimental program for repair of AASHTO girders

Specimen Designation	Loading Configuration	Loading Condition	Total number of PS strands	Number of strands ruptured	Main CFRP system
AASHTO1	Flexural	Fatigue	16	1	3 longitudinal layers 16 in
AASHTO2	Flexural	Static	28	4	3 longitudinal layers 16 in
AASHTO3	Flexural	Static	16	3	3 longitudinal layers 16 in
AASHTO2C	Shear	Static	28	--	--
AASHTO2R	Shear	Static	28	4	2 layers oriented at 45 degrees

2 LITERATURE REVIEW

2.1 Overview

Due to deficiencies in the built environment, many universities and research organizations have pursued the challenge to repair or strengthen existing structures with fiber reinforced polymer (FRP) materials in flexure. This section provides a summary of the literature in the field of flexural FRP repair or strengthening of concrete structures. Topics in this section include: 1) FRP systems and failure mechanisms, 2) History of FRP strengthening, 3) FRP strengthening of reinforced and prestressed concrete structures, 4) FRP repair of prestressed concrete, 5) Fatigue behavior of reinforced / prestressed concrete, 6) Fatigue behavior of reinforced / prestressed concrete strengthened with FRP materials, and 7) An overview of existing design guidelines for FRP repair / strengthening.

2.2 FRP Repair / Strengthening Systems

Fiber Reinforced Polymer (FRP) Materials

Fiber Reinforced Polymer (CFRP) materials consist of fiber filaments embedded in an adhesive matrix. There are various types of FRPs that are commonly used for structural strengthening of concrete members including pre-cured laminates and wet lay-up systems.

Pre-cured laminate FRPs are normally available commercially in the form of a bar or strip. The pre-cured laminate is manufactured by impregnation of fibers with adhesive, which is then pultruded and cured by the manufacturer. The controlled environment used in manufacturing of the pre-cured laminate can create laminates which are stronger and stiffer per unit volume than equivalent wet lay-up laminates. The laminates typically used for concrete strengthening are unidirectional and have all of the fibers oriented in the longitudinal direction. A laminate can come in various shapes and sizes. An externally bonded wet lay-up system consists of a fiber sheet which is typically field impregnated with a structural adhesive. A unidirectional fiber sheet consists of bundles of fibers held together by thin pieces of plastic material. Fiber sheets typically come in rolls 24 ft by 300 ft. The fibers in precured strips or wet lay-up systems are available in a variety of different materials including aramid (Kevlar®), carbon, or glass.

A steel reinforced polymer (SRP) system was also tested as part of this research, which is a wet lay-up system with embedded high-strength twisted steel wires embedded in an epoxy matrix. SRP have several benefits over traditional CFRP materials including lower cost, better fire resistance, and compatibility with anchorage systems, but may be more difficult to install and have untested corrosion resistance. The stress versus strain behavior of some typical CFRP and SRP materials are presented in Figure 2.1. Also shown in the figure are the traditional building materials used in tension: mild steel reinforcing and high strength steel used in prestressing strands.

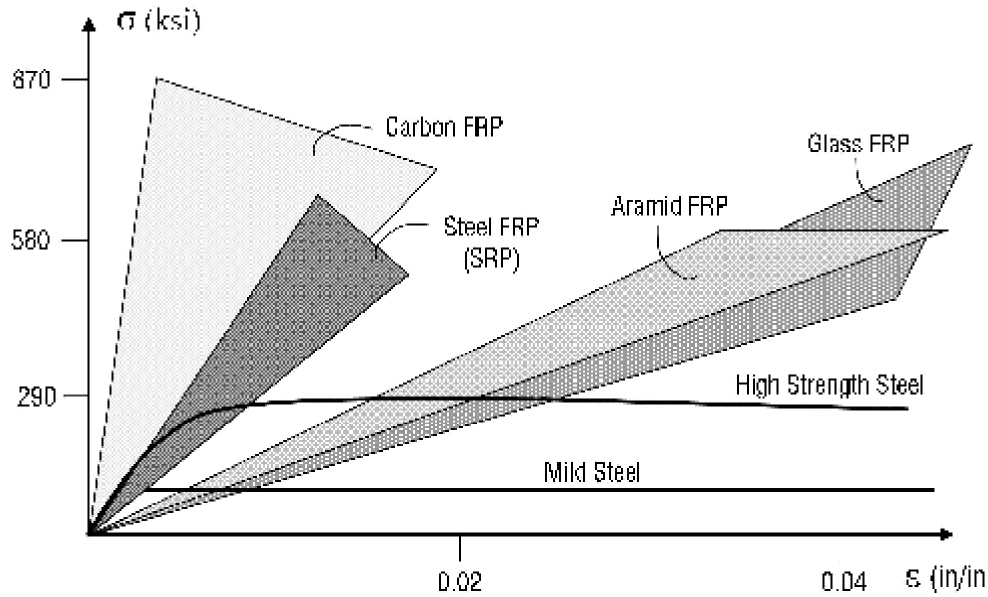

Figure 2.1 Stress-strain characteristics of steel, FRP, SRP materials

Adhesives

Structural adhesives are used to bond the CFRP material to the concrete surface. The most common form of adhesive used in structural strengthening is an epoxide adhesive which hardens by chemical reaction. The adhesive consists of two parts, a resin and a hardener, which when combined will harden and allow for the surface bonding of two dissimilar materials. The rate of hardening is highly dependent on the ambient temperature and the temperature of the two adherents. Typical cure times are 14 hours at room temperature, or 3 hours at 176° F (Adams 2004).

Since the tensile strength and flexural strength of the adhesive are typically much higher than the shear strength of the concrete, most of the failures occur within the concrete substrate during a debonding type failure. There is a large difference between the adhesives used during a wet lay-up type application, where the dry fiber FRP or steel filaments are field impregnated with the adhesive, and an installation of near surface mounted (NSM) FRP or externally bonded laminates, where the adhesive is bonding a pre-made FRP to the concrete. Due to sensitivity of adhesive properties to application temperatures, curing temperatures, surface preparation, thermal expansion, creep, abrasion and chemical resistance, the adhesives should be carefully selected to match the type of FRP system used (Täljsten 2002). As a result, critical adhesive selection was not done in the course of this research, and the adhesives used were recommended by the manufacturer for compatibility with the fiber sheet, pre-cured FRP, or steel fiber material being used.

2.3 Failure Mechanisms

Five different failure mechanisms have been identified for reinforced or prestressed concrete strengthened with FRP: 1) crushing of concrete, 2) FRP rupture, 3) shear failure, 4) plate-end (PE) debonding, and 5) intermediate crack (IC) debonding. Flexural failure is defined as either concrete crushing, or FRP rupture. Bond failure occurs either due to PE debonding or IC debonding. A figure illustrating the location of the five types of failure is given in Figure 2.2 for the loading configuration shown.

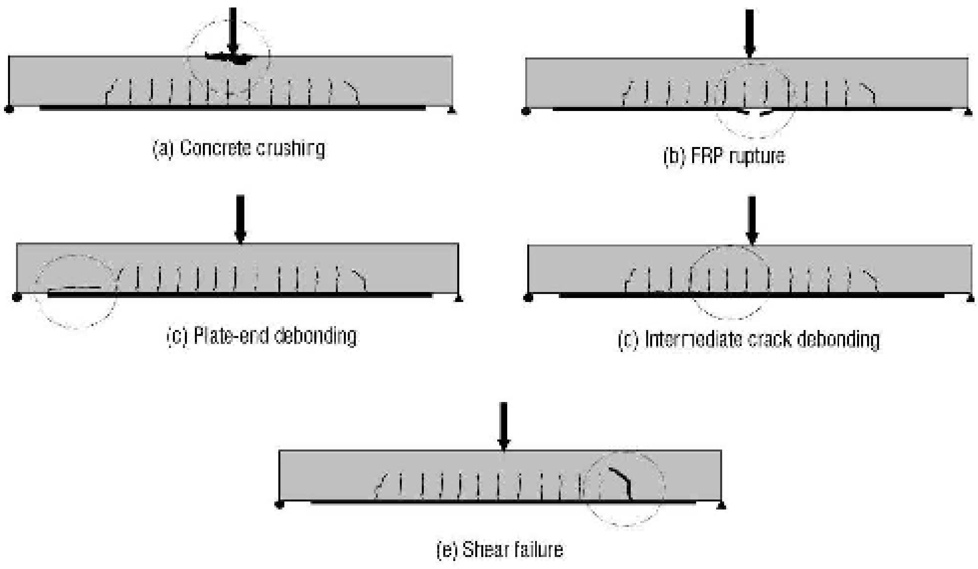

Figure 2.2 Failure modes of FRP strengthened RC structures

Bond failure in FRP strengthened reinforced or prestressed concrete girders propagates in one of two directions: from the FRP termination point (PE debonding), or from the intermediate flexural cracks (IC debonding).

Shear failure occurs when the shear resistance of the beam from the concrete, steel and/or FRP materials is lower than that of the applied shear force, and is not discussed in this dissertation.

Flexural failure, defined as crushing of concrete or rupture of FRP, can often occur in FRP strengthened reinforced or prestressed concrete members. Numerous situations may arise where designing a CFRP strengthened reinforced or prestressed concrete member results in crushing of concrete. FRP rupture is commonly encountered in beams which are strengthened with FRP having a low axial stiffness, or having a large amount of transverse anchorage provided for debonding mitigation. The background provided in this chapter is regarding CFRP repair or strengthening systems which are designed for flexural failure.

2.4 Historical Perspective

The use of fibers to increase the strength of various buildings and structures is an ancient technology – utilized when people first started using straw in clay bricks for residential walls and roofs (Nanni 1999). These early uses saw the advantage of using two materials with different material properties. After World War II, the use of fiber reinforced polymers was mainly confined to the military for boat hulls, submarine parts and aircraft components. Once it became economically feasible, industry took advantage of the excellent properties of FRP materials, manufacturing everything from fishing poles and bicycle frames to architectural components and bath tubs.

In the 1960's, FRP began to be used in structural applications mainly as a result of its non-corrosive properties. Bridge deck slabs, sea walls, and floor slabs in aggressive chemical environments were reinforced with Glass Fiber Reinforced Polymers (GFRPs) as an alternative to epoxy coated reinforcing (ACI 440 1996). Strengthening buildings and bridges using FRP was first used as an alternative to the bonding of steel plates to the soffits of reinforced concrete beams (Oehlers 1990). FRP strengthening gained popularity in Europe and Japan in the 1980's as a result of the high strength to weight ratio and easy installation of FRP materials. Throughout the 1990s, the use of FRP in North America, Europe and Asia has continued to become more prevalent with many repair and strengthening projects completed. The number of companies manufacturing FRP products has also increased, with numerous companies producing FRP sheets, reinforcing bars and pultruded laminates.

The primary reason that reinforced concrete beams are no longer commonly strengthened in flexure with externally bonded steel plates is simply because of the difficulty in installation. It is still widely believed that corrosion is a serious problem, but a study of RC beams strengthened with externally bonded steel plates by Swamy et al. (1995) proved otherwise through the experimental testing of the beams after 12 years of environmental exposure. The authors observed increases in the flexural strength of the beams over time in every case.

2.5 Reinforced Concrete Strengthened with CFRP

The flexural behavior of reinforced concrete strengthened with FRP has been extensively studied. Several studies which focus primarily on flexural failures (concrete crushing, FRP rupture) or field applications will be covered in this section. Predictions based on strain compatibility and equilibrium of internal forces provide accurate predictions of failure loads and ultimate displacements. With appropriate reduction factors applied to the material properties of the FRP to account for environmental degradation, manufacturing flaws, misalignment of the fibers, the desired modes of failure of concrete crushing or rupture of FRP can be achieved in many cases. The debonding failure mechanism is failure mechanism which must be carefully designed for.

Hag-Elsafi et al. (2001) installed FRP laminates to the tension side of reinforced concrete T-beams in a bridge in New York. After installation, load tests were performed on the bridge and the FRP strengthening system was shown to decrease tensile stresses in the steel reinforcing and increased concrete stresses. Although the load testing was halted before non-linear behavior was observed, the FRP strengthening was shown to be effective within the live load ranges examined.

Arduini et al. (2002) tested several decommissioned reinforced concrete bridge girders which had been heavily degraded over their service life. Four girders were strengthened longitudinally with several layers of FRP sheets, on top of which transverse U-wraps were placed. High interfacial shear stress was found in several of the girders due to local singularities such as a change in cross-sectional geometry, intersection with transverse members, and application of an applied load. Failure in one of the girders was due to debonding of longitudinal CFRP laminate between U-wraps, two of the girder failed due to FRP rupture and one failed due to concrete crushing. It was found that design guidelines based on ACI Committee 440 (2002) could adequately assess the flexural behavior.

El-Hacha and Rizkalla (2004) provided a comparison between externally bonded and near surface mounted FRP strengthening systems tested under static loading conditions. Besides several specimens which failed due to debonding, two of the T-beam specimens strengthened with NSM strips failed due to FRP rupture, at loads between 80 and 100 percent higher than the control specimen. The authors observed that the ultimate strength of the specimens was governed by the tensile strength of the NSM FRP material.

2.6 Prestressed Concrete Strengthened with CFRP

There has been little research on the strengthening of prestressed concrete with CFRP materials. There have been some field applications using CFRP on prestressed concrete yet few full scale specimens have been tested in the laboratory.

Takacs and Kanstad (2002) showed that prestressed concrete girders could be strengthened with externally bonded CFRP to increase their ultimate flexural capacity. CFRP pre-cured laminates were applied to the bottom and side surfaces of a T-beam soffit; no transverse U-wraps were provided. Of the strengthened beams, one failed due to debonding and the other experienced a shear failure. The beams achieved an increase in flexural moment capacity of 28 and 37 percent respectively. A finite element model based on the smeared crack methodology was used for predictions of the failure loads.

Hassan and Rizkalla (2002) and Hassan (2002) examined the flexural behavior of prestressed concrete bridge slabs strengthened with various CFRP systems. The half scale specimens were strengthened with near surface mounted (NSM) CFRP bars and strips as well as externally bonded CFRP strips and sheets. The flexural capacity of the slabs could be increased by as much as 50 percent using the CFRP strengthening, with the most cost effective solution being the CFRP sheets. A specimen strengthened with CFRP strips experienced debonding at 41 percent of the rupture strain of the material.

Reed and Peterman (2004) showed that both flexural and shear capacities of 30 year-old damaged prestressed concrete girders could be substantially increased with externally bonded CFRP sheets. Two single-tee girders were taken from an overloaded bridge, epoxy injected, strengthened with CFRP sheets and tested to determine their shear and flexural strength. A control specimen was also tested which was not epoxy injected. Both of the girders were strengthened using the same longitudinal CFRP configuration, but one girder had provided CFRP transverse U-Wraps throughout the length of the girder whereas the other had U-wraps provided only at the supports where the longitudinal CFRP was terminated. Both strengthened girders achieved approximately a 20 percent increase in strength over the control specimen. The failure modes were different however, as one failed due to CFRP rupture and the other due to debonding of the cover concrete between the CFRP strengthening and the prestressing. Reed and Peterman encouraged the use of CFRP transverse U-wraps along the length of the girder in externally bonded systems to delay debonding failure.

2.7 Steel Reinforced Polymer Strengthening

An innovative new material utilizing high strength twisted steel wires as fiber reinforcement is commonly known as steel reinforced polymer (SRP) when the steel fibers are impregnated in an epoxy matrix, and steel reinforced cementitious system (SRCS) when the fibers are embedded in a cementitious matrix. There are several variables that can be specified to achieve the desired properties: the amount of twist in the fibers affects the ductility of the wires and the resin penetration with lightly twisted wires can provide good mechanical interlock in the matrix (Prota et al. 2006). The density of the wires per millimeter can also be varied, to achieve the proper strengthening level. To date there has been only limited research in the area of SRP flexural strengthening of concrete structures.

Prota et al. (2006) tested eleven 12 ft long shallow reinforced concrete sections under static loading, seven strengthened with steel fibers (four SRP and three SRCS), and two strengthened with CFRP. The authors found that the steel fiber strengthening systems using epoxy resin outperformed the systems using a polymer-modified cementitious mortar as a result of the epoxy better engaging the concrete substrate prior to debonding failure. The specimens strengthened with CFRP outperformed the SRP specimens in terms of ultimate strength gains for similar (predicted) axial stiffnesses, but the SRP material had more ductility at failure. The authors pointed out that corrosion resistance of both the SRP and SRCS systems is a major concern and needs more research.

2.8 Repair of Reinforced and Prestressed Concrete with CFRP

The repair of damaged reinforced and prestressed concrete girders is an ever-growing practice in the US and around the world. Early methods such as external post-tensioning, strand splicing, and steel plates were used prior to the advent of FRP materials. This section will discuss a wide array of research performed during laboratory tests as well as field applications of both traditionally repaired and FRP repaired RC and PS concrete members. Lastly, existing FRP design guidelines will be presented.

Traditional Repair Methods

Extensive research literature is available for traditional repair methods of reinforced and prestressed concrete members. Several articles for various repair methods will be described; first for RC structures then for PS structures.

The use of bonding steel plates to RC members was reported by Aboutaha (1998). The advantages of using steel plates were: 1) improved serviceability and increased ultimate strength, 2) causes minimum changes to member dimensions and weight, and 3) they are cost effective and easy to maintain. Steel plates were also able to increase the flexural stiffness and reduce cracking of the test specimens. However, the largest drawback for the use of steel plates in strengthening concrete members is their poor resistance to corrosion.

Another traditional method of repairing shear-deficient RC members was examined by Khaloo (2000) using external post-tensioning. Twenty four members were tested to failure under shear-critical loading. Steel plates, bolts, and angles were used to achieve vertical post-tensioning of the members near the supports. The research was able to increase the shear capacity enough to change the mode of failure from shear failure to flexural failure, as well as increase the ductility of the post-tensioned member versus the control specimen.

The most common traditional repair method for damaged prestressed concrete bridge members is strand splicing. Two research studies by Olsen et al. 1992 and Zobel et al. 1998 found that severed prestressing strands could be effectively repaired using strand splicing. They both concluded that in many cases the strand splices were unable to restore the ultimate strength of the girder but were found to perform poorly during fatigue loading of the specimens. A more innovative technique was needed that could not only restore the ultimate strength capacity of the damaged girder, but withstand the repetitive service loadings that all bridge girders undergo.

CFRP Repair Methods and Field Applications

The advantage of using CFRP materials is not only can they restore the ultimate flexural or shear capacity of damaged sections, but they perform extremely well under repetitive service loading and in corrosive environments. Examples of reinforced and prestressed concrete members repaired using CFRP materials are presented below.

In Alabama, one span of a reinforced concrete bridge was chosen to repair damage due to aging (Stallings et al. 2000). CFRP precured laminates along with Glass FRP sheets were used to restore the repaired sections beyond their original capacities to increase posted load restrictions. Before installation of the repair systems designed by the researchers, load tests were performed to measure the behavior of the bridge superstructure under various static and dynamic loads. The same static and dynamic tests were performed after the completion of the FRP repair systems to compare with the prior results. The results of these load tests demonstrated that the FRP repair system reduced girder deflections ranging between 2 to 12 percent, as well as reducing rebar stresses by an average of 8 percent. The usage of CFRP plates to repair and strengthen reinforced concrete bridge girders was successfully installed and verified by field loading tests.

Three separate prestressed concrete bridges were repaired with CFRP systems in repair projects sponsored by the Missouri Department of Transportation. In the first project, eleven prestressed concrete bridge girders located on a bridge in Independence, MO were impact damaged due to an overheight vehicle and repaired with CFRP wet lay-up sheets (Schiebel et al. 2001). Although no prestressing strands were ruptured, all eleven girders had large cracks and spalling of concrete exposing prestressing strands. The CFRP repair system was designed using a simple section analysis procedure to ensure that the new flexural strength was equal to or greater than that of the original girder. Detailing of the CFRP repair system followed industry standards and provided transverse U-wraps at 15.75 in spacing and extension of the CFRP well away from the damaged concrete area. Experimental testing was limited to bond and adhesion tests to ensure proper bond of the CFRP to the concrete substrate. In the second project, a prestressed concrete bridge girder was repaired in-situ with CFRP wet lay-up sheets after impact damage ruptured two prestressing strands (Tumialan et al. 2001). The design of the repair system was determined by the rectangular stress block approach. Two layers of CFRP sheets were applied to the tension face, extending past the damaged location. CFRP U-wraps were also applied to prevent debonding failure. Following current industry standards, the CFRP repair system was successfully installed by a contractor. Field testing was not performed, however the repaired girder is performing well in service.

A third project sponsored by the Missouri DOT, repaired impact damage caused by a contractor who struck a girder during construction of a new bridge (Ludovico 2003). Two prestressing strands were ruptured and a significant loss of concrete occurred. The concrete section was restored and the girder repaired using CFRP sheets in both the longitudinal and transverse directions. Load testing was not performed on the repaired section, but the girder is currently performing well under traffic loading.

The Iowa Department of Transportation has sponsored several research projects that involved the use of CFRP to repair impact damaged prestressed concrete bridge girders. In the first project, several overheight impacts damaged all the girders on a bridge (Klaiber et al. 1999). Although no prestressing strands were ruptured, one girder had two prestressing strands which were visibly relaxed. The girders were load tested in-situ to examine their respective load-deflection behaviors. Two damaged girders were then cut out of the deck, replaced with new ones, and transported to a testing facility. The more severely damaged girder with two relaxed prestressing strands was tested to failure to observe the behavior of a beam with significant concrete loss and relaxed strands. The second girder, with only moderate damage, was then loaded to simulate service load conditions. The girder was then damaged to simulate a larger loss of concrete and rupturing of two prestressing strands. Following the simulated damage, the girder was then repaired by first restoring the concrete section using a cementitious mortar. CFRP plates were then bonded to the bottom flange of the beam to restore the flexural capacity of the member. CFRP sheets were added in the transverse direction to prevent debonding. Load tests after the CFRP installation indicated that the repaired girder exhibited 27 percent less deflection than the damaged girder. The repaired girder also exhibited a higher ultimate load capacity over the control specimen previously mentioned.

A second project, sponsored by the Iowa DOT, included the testing of a bridge before and after the installation of a CFRP repair system. All six prestressed concrete girders on one span of a bridge were damaged as a result of an overheight impact; however most damage only occurred to the first two girders. The first girder sustained spalled concrete as well as one ruptured prestressing strand. The second girder was damaged more significantly with a much larger loss of concrete, five prestressing strands visible and two of those ruptured. After restoration of the section was completed with patching material, CFRP plates were attached to the bottom flange of the beams. The researchers demonstrated through the before and after load tests that the midspan bridge deflections decreased following the installation of the CFRP plates. The researchers concluded that flexural strengthening of impact damaged PC girders is possible when up to 15 percent of the strands are severed. Higher ratios may be possible, but tests have not been performed to validate this assumption.

An experimental project was sponsored by the Florida Department of Transportation to create guidelines, standard practices, and experimental data for the repair of impact-damaged bridge girders using CFRP systems. The FDOT had previously repaired a damaged prestressed bridge girder on an acitive bridge, but did not have any design guidelines at the time to follow. All they had were the manufacturers engineeers to assist in the repair. In Green et al. (2004), six 44 ft long AASHTO Type II girders were tested in four point bending to examine effectiveness of various CFRP systems to restore the capacity of damaged girders back to their original strengths. The experiment was comprised of one control specimen, a second control specimen with simulated damage, and four specimens with simulated damage all repaired with different CFRP systems. All test results compared well with analytical predictions. The results show that one of the four repaired girders was able to achieve its orignial capacity. Wet lay-up CFRP sheets were used in the first repaired specimen. The girder failed prematurely, at 91 percent of the control specimen’s ultimate strength, due to plate-end debonding. The researchers did not provide any U-wraps along the length of the longitudinal CFRP. It is believed that the presence of U-wraps would have prevented the plate-end debonding. The second repaired specimen was repaired using pre-impregnated CFRP fabric sheets. Four layers of pre-preg sheets were installed in the longitudinal direction, along with bi-directional CFRP sheet U-wraps which were bolted into the web. The girder achieved 92 percent of the experimental capacity of the control girder, with failure due to adhesive failure immediately followed by rupture of the longtitudinal CFRP. The third girder incorporated a spray-on FRP repair system. This system achieved 95 percent of the original capacity, with failure caused by FRP rupture. The researchers found after the failure that the desired thickness of the spray was 0.50 in but the actual thickness as 0.27 in. The final repaired girder emplyoyed the usage of wet lay-up CFRP sheets. One transverse U-wrap was provided at the end of the longitudinal sheets to provide achorage. The girder failed after the longitudinal FRP pulled away from the U-wraps, leading to an achorage failure, but not until after the girder had achieved a 7 percent increase in strength over the control specimen. The researchers concluded that FRP can be used to restore a significant portion of the strength capacity of an impact damaged girder, however they observed that proper detailing at termination points is critical to any FRP system.

In Di Ludovico et al. (2005), three 36 ft prestressed concrete Missouri Type II bridge girders, with a 32 in composite cast-in-place slab, were tested monotonically to failure to assess the flexural behavior of repaired damaged sections with CFRP wet lay-up laminates. After the first girder was tested as a control specimen, the other two were damaged at midspan by removing the concrete cover and rupturing two and four prestressing strands, respectively. They were then repaired with cementitious mortar and repaired with two or three layers of longitudinal CFRP sheets below numerous transverse CFRP U-wraps. The results show that the CFRP system can restore the ultimate capacity and stiffness of the original girder, but the two repaired girders could not match the original serviceability. The failure mode observed for both of the repaired girders was rupture of a U-wrap on the undamaged side followed by intermediate crack debonding of the longitudinal CFRP system. The researchers provided numerous CFRP U-wraps throughout the repaired area, but they only extended around the bottom flange of the girder to the bottom of the web. It is possible that this detailing led to the premature debonding failures at 56 and 46 percent of the ultimate nominal FRP strain. The authors also provide an analysis procedure to calculate the prestress force, the cracking moment and the ultimate moment based on strain compatibility and equilibrium. For the design of the CFRP system, they applied the bond reduction factor (κ_m) from ACI Committee 440 (2002), but not the environmental reduction factor (C_E).

2.9 Fatigue Behavior

The behavior of a reinforced or prestressed concrete beam strengthened with CFRP under fatigue loading may be the critical point of design of the member. For proper serviceability, the effect of repeated live load should be properly designed for, especially for members with a large amount of cyclic loading such as bridges. In this section the fatigue behavior of the constituent materials (FRP, concrete, steel) are reviewed, along with studies examining the fatigue behavior of reinforced and prestressed concrete strengthened with CFRP.

Fatigue of Constitutive Materials

To properly assess the resistance of a structure or bridge against cyclic loading, the fatigue characteristics of the constituent materials should be assessed. For most materials there exists an endurance limit, an alternating maximum stress which a material can withstand for an infinite number of cycles. Cumulative damage models are the most effective way to assess fatigue degradation of materials within a structure, but these models are beyond the scope of this report. Through experimental testing, the fatigue resistance of materials has been defined using stress ratio versus number of cycle curves, or S-N curves, which offer fatigue life predictions when the stress ratio and other parameters are known.

The fatigue resistance of concrete was first studied extensively when reinforced concrete began being used to construct railroad bridges. Defining $S=f_{max}/f'_c$ and $R=f_{min}/f_{max}$, Aas-Jacobsen (1970) defined an equation for fatigue of concrete under compression-compression cyclic loading:

$$S = 1 - b\,(1-R)\log_{10} N \tag{2-1}$$

where β=0.064 and N is the number of cycles to failure.

The performance of concrete under tension-tension cyclic loading is less known (Ahmad 2004). Saito and Imai (1983) found that there is no endurance limit for concrete in tension under fatigue loading and that after 2 million cycles the residual strength was 73% of its original tensile strength.

The most extensive report on fatigue on reinforced and prestressed concrete constituent materials in the United States is published by ACI Committee 215 (1997). From extensive experimental studies, S-N curves are presented in graphical format for concrete under compression-compression loading, in addition to the tension-tension loading of regular reinforcing bars and prestressing strands. The effects of different variables such as bar geometry, load history and rate of loading are examined.

The fatigue resistance of prestressed concrete members is often dependent on the stress ratio applied to the prestressing strands. Various equations have been proposed to estimate the fatigue life of a prestressing strand in air, two of which are:

$$\log_{10}(N) = 10 - 3.6 \cdot \log_{10}(100 \cdot SR) \tag{2-2}$$

$$\log_{10}(N) = 7.07 - 8.13 \cdot (SR) \qquad (2\text{-}3)$$

from Collins and Mitchell (1997) and Naaman (1991) respectively. Both of these equations are plotted in Figure 2.3.

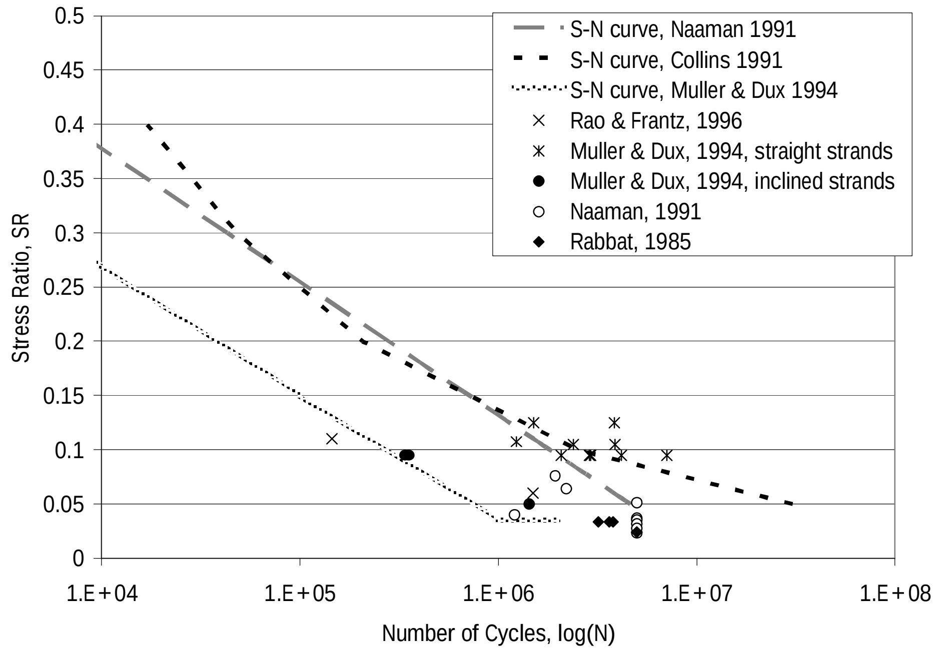

Figure 2.3 S-N Behavior of prestressing strands

Unidirectional Fiber Reinforced Polymer (FRP) materials have good fatigue resistance and very little stiffness degradation under cyclic load (Barnes and Mays 1999). Walton and Yeung (1986) found that the fatigue performance of composite materials was superior to that of other engineering materials, including steel. Adimi *et al*. (2000) observed that for carbon fiber bars embedded in concrete cycled at a frequency of 4 Hz, the maximum stress should not exceed 35 percent of its ultimate tensile strength in order to achieve 4 million cycles of loading.

Fatigue of Prestressed Concrete

From 1950 to 1990, the fatigue of prestressed concrete bridge girders was extensively investigated. Many studies concluded that the fatigue critical component of a prestressed concrete bridge girder is the prestressing strands. One exhaustive study by Overman (1984) tested full scale precast prestressed concrete bridge girders with cast-in-place composite decks under fatigue loading. This study and others (Rao and Franz, 1996, Rabbat et al., 1985) have found that if a prestressed concrete girder remains in an uncracked condition the fatigue life of the prestressing strands are infinite. The AASHTO (2004) code specifies a maximum nominal tensile stress in concrete at service load of $6.0*(f'_c)^{0.5}$ (ksi) in corrosive environments and

$3.0*(f'_c)^{0.5}$ (ksi) in non-corrosive environments. This value is meant to maintain the service load of the girder under the cracking load so that the strands can withstand load indefinitely.

The use of inclined strands normally reduces the fatigue resistance of prestressed concrete bridge girders as a result of the fretting fatigue which occurs at the hold down points. Muller and Dux (1994) proposed an S-N curve for prestressed concrete girders with inclined strands, which is valid from 300,000 to 2 million cycles:

$$SR = -0.12\log_{10} N + 0.75 \geq 0.035 \qquad (2\text{-}4)$$

This equation is shown in Figure 2.3.

Rabbat et al. (1985) first examined the effect of draped strands in prestressed concrete girders with full size testing. Through the testing of six full-size AASHTO Type II girders under fatigue loading corresponding to a nominal bottom tensile stress in the concrete of

$6.0*(f'_c)^{0.5}$ (ksi), they recommended that straight strands with blanketing at the ends be employed in new constructions as their fatigue life is equivalent to that of draped strands.

A recent investigation examining the fatigue resistance of prestressed concrete was performed by Rao and Franz (1996). They conducted fatigue tests on two 56 ft, 27 year old prestressed concrete box beams. One of the beams was tested under loading designed to simulate a nominal bottom tensile stress in the concrete of $6.0*(f'_c)^{0.5}$ (ksi) corresponding to a stress ratio in the prestressing strands of . An additional test was performed on a girder to simulate a tensile stress in the concrete of $9.0*(f'_c)^{0.5}$ (ksi) corresponding to a stress ratio in the prestressing strands of $0.11*f_{pu}$. The girder with the lower level of loading survived over 1.5 million cycles retaining excellent performance whereas the girder with the higher loading experienced a ruptured prestressing strand at 145,000 cycles. They recommended that all calculations to find stresses in concrete and prestressing strands be based on a cracked section analyses because of the possibility of unintentional overloads.

2.10 Fatigue of Reinforced Concrete Strengthened with FRP

Barnes and Mays (1999) tested five reinforced concrete beams under fatigue loading, three strengthened with externally bonded CFRP plates. The 3.5 in x 0.05 in plates were bonded to the tension surface of a 5 in x 9 in x 90.5 in beam. The plate was terminated near the beam supports and mechanically anchored to the concrete by way of a steel plate bonded to the plate surface and bolted to the concrete. The results show that the fatigue performance of CFRP strengthened beams is superior to unstrengthened beams at the same level of loading due to reduced crack widths and shorter spacing of cracks. Using a criteria based on the stress ratio in the regular steel reinforcing was also deemed to give a more accurate representation of the fatigue behavior rather than applying the percent increase in ultimate capacity to the fatigue loading range.

Shahawy and Beitelman (1999) examined the performance of CFRP strengthened reinforced concrete beams through the testing of ten beams under static loading conditions, and seven beams under fatigue loading conditions. The main variables in the experimental program were the amount and configuration of FRP strengthening, the concrete strength, and amount of damage prior to strengthening. The load range used was 25 percent of the ultimate strength of the control specimen, which corresponds to a stress range in the steel of $0.25f_y$. The strengthened beams subjected to fatigue loading were strengthened along the entire stem of the reinforced concrete T-beam, and had superior performance to the control girder tested under the same loading conditions.

In an analytical study, El-Tawil et al. (2001) estimated the fatigue response of several specimens from Barnes and Mays (2000) and Shahawy and Beitelman (2001). The beams were discretized into several layers, and a fiber section approach was used with several models estimating the fatigue characteristics of the constituent materials. The compressive fatigue behavior of concrete was estimated using the model of Holmen, which gives an effective modulus of elasticity after a certain number of fatigue cycles. Concrete tensile fatigue was deemed not to be significant, as was CFRP and epoxy fatigue relaxation. Steel fatigue was not deemed to be significant while the steel is still in the elastic range. The analytical model shows that the beams experience redistribution of internal stresses similarly to what would be obtained in a creep analysis.

Carolin (2003) examined the effect of repeated live load during strengthening of reinforced concrete with CFRP through the testing of 12 beams strengthened with externally bonded FRP plates and near surface mounted systems. They found that the effect of fatigue loading during strengthening was small for FRP strengthening using normal two-part structural epoxies, but that there was a significant effect for FRP strengthening using cementitious adhesives.

A very similar conclusion was reached in a study by Heffernan and Erki (2004) in which 9.8 ft and 16.4 ft reinforced concrete beams were tested under static and fatigue loading conditions. The authors found that the stress ratio in the steel reinforcement controlled the fatigue failures and that increasing stress ratios were observed due to concrete softening during the repeated loading.

Breña et al. (2005) examined the flexural fatigue behavior of ten reinforced concrete beams, eight of which were strengthened with two types of CFRP: wet lay-up sheets and pultruded laminates. The CFRP sheet strengthened specimens were 9.5 inches in length and the CFRP plate specimens 10.5 inches in length with cross sectional dimensions configured to give a span to depth ratio of 8.15 for both series of tests. Out of the eight strengthened beams, three failed due to the fatigue loading – one of the CFRP sheet strengthened beams due to rupture of reinforcing steel and two of the CFRP plate strengthened beams due to debonding of CFRP. Although the stress ratio in the reinforcement was identified to be an important factor in the fatigue life of the strengthened system because some of the beams failed due to debonding, the authors concluded that the stress ratio in the composite system was critical in this case. It is possible that the detailing of the CFRP system could have prevented the premature debonding failures observed in the research.

Budelman and Husemann (2005) tested 13 reinforced concrete slabs strengthened with CFRP laminates to assess the effect of fatigue load on the CFRP systems. They found that the embedded reinforcement would fail prior to the CFRP material and that very little bond degradation occurred at service load. The strains found during an analytical and parametric investigation of reinforced concrete strengthened with CFRP show that service loads determined from the fatigue resistance of the internal material will not cause degradation of the bond between CFRP laminate and concrete.

Aidoo et al. (2006) examined the fatigue behavior of eight reinforced concrete beams, four strengthened with CFRP strips and sheets. The authors observed that the fatigue life of the strengthened members was controlled by the stress ratio in the regular reinforcing steel, but stressed that the increase in fatigue life behavior is limited by the quality of bond between the CFRP and the concrete substrate.

2.11 Fatigue of Prestressed Concrete Strengthened with FRP

Larson, et al. (2005) examined the fatigue behavior of prestressed concrete T-beams strengthened with CFRP wet lay-up sheets. Of the five beams tested, one was tested statically to failure as a control girder (Beam 1), two were strengthened with CFRP to resist an AASHTO (1998) determined stress range of 18 ksi (Beams 2 and 3), and two were strengthened with CFRP to resist double the AASHTO stress range 36 ksi (Beams 4 and 5). Of the four strengthened girders, two were tested statically to failure and two were tested under fatigue loading conditions. The control girder failed due to rupture of prestressing, which shows that the sections were under-reinforced since this is an uncommon failure mode in prestressed concrete. All of the strengthened girders failed due to rupture of flexural CFRP near midspan. The T-beam specimens were 16 in wide, and 14 in deep, with a 4 in soffit. The girders were 198 inches in length and were prestressed with two-0.37 in 270 ksi straight prestressing strands located 2 in and 4 in from the bottom of the web.

Beams 2 and 3 were strengthened with one layer of CFRP sheets wrapped 2.24 in up the bottom of the web sides, and transverse CFRP sheets 5.51 in wide spaced at 12 in throughout the length of the girder. Beam 2 failed due to rupture of CFRP at an applied load 70 percent higher than the control beam. Beam 3 survived 1,065,000 cycles of fatigue loading and failed due to rupture of CFRP at a load 68 percent higher than the control beam. The fatigue loading was designed such that the stress range in the prestressing strands was equivalent to 18 ksi, the AASHTO specified limit for straight prestressing strands. Significant degradation in the beam behavior could be noted after 1 million cycles as shown in Figure 2.4perhaps indicating that one or more of the prestressing wires had ruptured. Further fatigue loading of this beam most likely would have lead to rupture of prestressing strands.

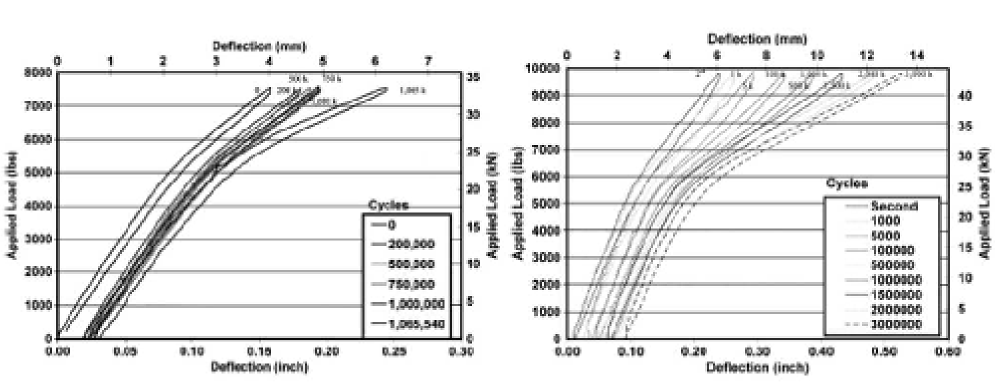

Figure 2.4 Load versus displacement hysteresis (from Larson, et al.2005)

Beams 4 and 5 were flexurally strengthened with two layers of CFRP sheets: one layer wrapped 0.5 in, and another layer wrapped 3 in up the sides of the beam soffit. Beam 4 failed due to rupture of CFRP at a load 113 percent higher than the control beam. Beam 5 failed due to rupture of CFRP after 3 million cycles of fatigue loading, which was designed to simulate double the AASHTO specified allowable stress range in straight prestressing strands. The ultimate load of Beam 5 was 74 percent higher than the control beam, but significantly less than its twin girder tested monotonically to failure. The authors admit that this girder might not have lasted much longer after 3 million cycles, as large amounts of residual deformation can be seen in the load versus displacement hysteretic response shown in Figure 2.4. Some conclusions that Larson, et al. (2005) determined from their study are the following:

1. CFRP strengthening of prestressed concrete T-beams can increase the ultimate capacity by up to 113 percent.
2. Member ductility was enhanced by the addition of the CFRP strengthening system.
3. The member stiffness from the cracking load up to yielding of the prestressing strands was much reduced due to fatigue loading.
4. The magnitude of strain in the CFRP increased after flexural cracking due to their superior bond performance across cracks, relieving the stress range in the prestressing.

Larson et al. (2004) presented a procedure for designing CFRP strengthening systems for prestressed concrete by limiting the stress range in the prestressing strands under levels prescribed in the AASHTO specification. Their non-linear section analysis used a layer by layer approach to determine the cracked section moment-curvature response, and designing the amount of CFRP to limit the stress range over a certain increase in service load value. They also presented a procedure to determine the width and spacing of their CFRP U-wraps based on a shear friction model in ACI 318 (1999). The load deflection behavior determined from their analysis and from experimental results correlate well.

2.12 Durability of FRP Systems

FRP systems externally bonded or near surface mounted to concrete as a retrofit material may see significant effects due to environmental exposure. As the FRP material is bonded to the concrete, the durability of the concrete at the bond line is important in determining the long-term effectiveness of the strengthening or repair system. Items that could affect the performance include moisture and humidity, high alkaline environments, elevated temperature, freeze-thaw cycles, creep and fatigue, UV exposure, and corrosion of internal reinforcement (ACI Committee 440, 2002).

Grace and Singh (2004) showed in a comprehensive study of many parameters such as alkaline exposure, freeze-thaw cycling and fatigue cycling, that the most detrimental effect was from humidity exposure. They observed a 33% reduction in strength of CFRP plates after 10,000 hours of exposure to 100% humidity. Very little effect was found due to repeated cycling, but they found that CFRP precured plates to be more susceptible to aggressive environmental conditions than CFRP wet lay-up sheets.

2.13 Design Guidelines for Concrete Retrofitted with FRP

Various code writing organizations around the world have proposed design guidelines for the repair or strengthening of concrete structures with FRP. An overall review of the guidelines is presented here.

The American Concrete Institute released a document in 2002 concerning design and construction of externally bonded FRP systems for strengthening concrete structures (ACI Committee 440, 2002). Many different aspects of using FRP are included, such as system installation guidelines, including various types of surface preparation techniques, inspection and field evaluation procedures, as well as guidelines for the repair of minor damage observed after CFRP installation. The document discussed fire endurance ratings, and strengthening limits to be used in design in the event of fire or vandalism. They recommend that an environmental reduction factor (C_E) be applied to the modulus of elasticity and the rupture strain of the FRP to account for environmental degradation over time. Under sustained and cyclic load, the document recommends that CFRP materials be kept below a stress range of 55 percent. CFRP detailing concerns are also addressed in conjunction with FRP anchorage and lap splice recommendations. Design examples are also given with procedures shown for calculating reduced FRP material properties and a complete FRP flexural and shear strengthening problem. A revised version with a possible publication date in 2006 plans to include the strengthening of prestressed concrete with bonded or unbonded tendons.

The Concrete Society (2004) of the United Kingdom has proposed design guidance for the strengthening of concrete structures with fiber composites. A state of the art application review of various FRP installations throughout Europe and North America is first presented. Using numerous experimental studies, they propose safety factors to be applied to the FRP material properties to account for environmental degradation and misalignment of fibers. The safety factors are applied to the rupture strain, elastic modulus, and tensile strength and have values which depend on the type of material used and the method of installation. Flexural design follows from strain equilibrium and compatibility of the section. The flexural design procedures for near surface mounted FRP reinforcement are similar for externally bonded FRP, with recommendations on anchorage design taken from Hassan and Rizkalla (2004). Under fatigue loading, a stress ratio of 80 percent is recommended as an upper limit for CFRP materials. Installation procedures, quality control and guidelines on destructive and non-destructive testing are presented.

The Fédération Internationale du Béton (fib) (2001) has published guidelines on externally bonding FRP to reinforced concrete structures. For FRP material properties, the guidelines provided safety factors to be employed for different types of material and applications to account for long term behavior. The failure modes of flexurally strengthened members are described and guidance is given to prevent various debonding failures. An entire chapter of the document is devoted to detailing rules. For flexural strengthening, the anchorage of externally bonded CFRP is their primary concern, with U-wrap transverse reinforcements or other mechanical anchorages recommended at the CFRP termination points.

The Japan Society of Civil Engineers (2001) has proposed recommendations for the upgrade of concrete structures with continuous fiber sheets. They propose material safety factors to be used for safety, reliability, and serviceability. To prevent peeling of FRP sheets, the recommendation provided an equation to determine the maximum permissible stress in the sheets based on the interfacial fracture energy between the concrete and FRP as well as other material properties. Guidance is also given regarding anchorage and splice design. Detailed specifications are presented in order to experimentally determine various FRP material properties and degradation due to environmental effects.

The Canadian Standards Association (2000) published a document for the design and construction of building components with FRP. Although mainly concerned with the use of FRP materials in new constructions, the standard specifies basic design guidelines and requirements for the use of surface bonded FRP for concrete or masonry structures.

Following closely from an earlier text (Oehlers et al., 2004), Australian researchers have submitted a document for publication as the code standard for the retrofitting of reinforced concrete with FRP (Oehlers et al., 2006). Specialized solely for the upgrading of beams and slabs, the document provides detailed guidance on various debonding mechanisms for adhesively bonded and mechanically anchored FRP and metal plates. Following the US code (ACI Committee 440, 2002) the Australian standard specifies environmental reduction factors to be applied to the properties of the FRP material. A flexural design approach that assumes full interaction between the FRP material and the concrete is a starting point for design.

Ye et al. (2005) outline several provisions that are present in the Chinese design code for strengthening reinforced concrete structures with FRP. Provisions for plate-end and intermediate crack debonding are presented in the following section.

The National Research Council of Italy (2004) has published a document on guidelines for FRP strengthening of reinforced concrete, prestressed concrete, and masonry structures. The guideline specifies the various strengthening systems and provides acceptance criteria along with providing complete design guidelines for strengthening in flexure, shear and torsion. Provisions for plate-end debonding and IC debonding are summarized in the following section.

The document AC125 from ICC Evaluation Service (2003) provides interim criteria for FRP systems to be used for reinforced concrete repair and strengthening, mainly as a provisional document to be used for acceptance by building code officials. It provides design equations for the enhancement of axial force provided by FRP materials, as well as a value for maximum bond stress.

2.14 Conclusions

This section has provided a summary of the literature in the field of flexural FRP repair or strengthening of reinforced and prestressed concrete structures. Various different topics were examined including background on the FRP system types, failure mechanisms, and history of FRP strengthening along with a critical review of FRP strengthening and repair of reinforced and prestressed concrete. The fatigue behavior of such systems was also examined and overviews of the existing design guidelines for FRP repair/strengthening. There are very few studies which have examined FRP strengthening for prestressed concrete structures, but the importance of several factors should be highlighted: 1) the fatigue stress range is an important consideration in the design of any FRP strengthening system, and 2) the existing state of strain on the beam soffit, as a result of the current load posting, is important and should be considered in any design.

3 EXPERIMENTAL PROGRAM – C-CHANNEL GIRDERS

3.1 Introduction

This chapter will provide specifics related to the tested girders, design of the various strengthening systems, test setup, loading scheme, instrumentation, and detailed descriptions of the individual tests. Constitutive material testing was performed on all the materials encountered, including material properties for the various CFRP systems, and these results are also included. Test results are presented in Chapter 5.

3.2 Test Girders

The C-Channel Bridge

The C-Channel prestressed concrete girder is a superstructure member commonly used for short two-span bridges ranging in length from 40 to 60.4 ft in rural areas of North Carolina, typically used to span small streams or estuaries. Bridges using this type of girder were built between the late 1950's to the mid 1970's. During erection, each precast C-Channel was delivered to the bridge site, along with the bridge cap beams (which were also precast). The bridge was typically supported by a timber substructure. Once the girders were in place side by side, they were post-tensioned transversely as shown in Figure 3.1. All of the girders tested in this research project were interior girders, with no integral parapet walls connected to the deck.

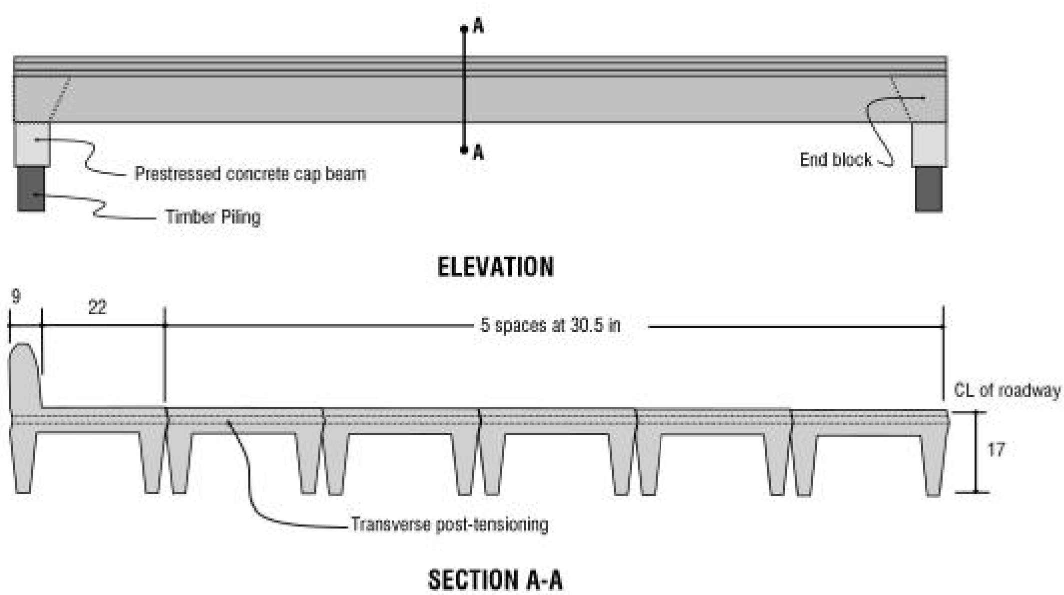

Figure 3.1 C-Channel Bridge Layout

Prestressing Strands

According to the North Carolina State Highway Commission Design Standards, the C-Channel type prestressed concrete bridge girder was prestressed by various prestressing strand configurations. The configurations were used to accommodate the loads for either exterior or interior girders corresponding to spans of 20 ft, 25 ft, or 30 ft. All of the girders tested had a length of 30 ft, of which there were only two different prestressing configurations. The four girders tested had a Type I prestressing strand configuration using ten 250 ksi stress-relieved 7- wire prestressing strands. The Type I configuration consisted of five strands in each web, three of which were inclined with a hold down point located at midspan. The bottom two strands were straight. The prestressing strand configuration is shown in Figure 3.2.

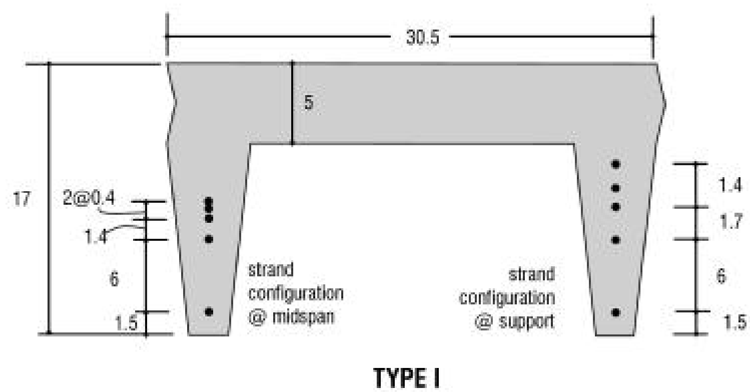

Figure 3.2 Cross section showing prestressing strand configurations

Material testing was carried out on the prestressing steel strands encountered in the tested Type I girders. Once testing of the girder was complete, two of the bottom prestressing strands were extracted near the supports. Care was taken in removal of the strands to prevent any unraveling of the strands while cutting.

The prestressing strands were tested in tension according to ASTM A416 specification using a 220 k MTS closed-loop universal testing machine used to apply a constant rate of displacement. The prestressing strands were clamped into the MTS grips using two 0.43 in multiple-use super chucks provided by Prestress Supply, Inc, Lakeland, Florida. Displacement during the test was measured by a 2.0 in extensometer placed at the middle of the gauge length. The extensometer was removed prior to rupture of the strands, and the rupture strain was determined from the stroke of the MTS machine for four of the specimens. Table 3.1shows the yield strength, ultimate strength, modulus of elasticity and rupture strain for the tested prestressing strands.

Table 3.1 Prestressing steel properties

System Designation	Yield Strength (ksi)	Ultimate Strength (ksi)	Rupture strain (%)	Modulus of Elasticity (ksi)
EB7F	205	265.8	9.50	2.9e4

The Ramberg-Osgood function (Collins and Mitchell 1991) was used to match the stress versus strain behavior of the prestressing strands.

$$f_p = E_p e_{ps} \left[A + \frac{1-A}{\left[1+\left(Be_{ps}\right)^C\right]^{1/C}} \right] \tag{3-1}$$

where f_p is the prestressing strand stress, E_p is the modulus of elasticity of the prestressing strand, ε_{ps} is the strain in the prestressing strand, and A,B and C are material constants. A, B and C can be determined from the stress-strain relationships generated from the tension tests. For the Type I girders with 250 ksi strands, the average values for A, B and C were 0.025, 138.7 and 6 respectively.

Regular Reinforcing

The thickness of the deck (or flange) of the C-Channel girders was 5.0 in. Shear keys were provided on both ends of the deck to achieve continuity between the girders after transverse post-tensioning. The deck was reinforced with regular reinforcing: D10 bars at 7.08 inches in the longitudinal direction and D12 bars at 13 inches in the transverse direction. Two D12 bars at 13 in were used as stirrups.

Concrete

The nominal concrete strength specified for the C-Channel prestressed concrete girders was 5 ksi at 28 days, and the specified concrete strength at transfer of prestressing force was 4 ksi. During the design stage for strengthening of these girders, as described in Section 3.2, the concrete compressive strength was estimated using the following equation which accounts for the strength increases due to aging. (MacGregor 1997).

$$f'_c(t) = f'_c(28)\left[\frac{t}{4+0.85(t)}\right] \tag{3-2}$$

where f'_c is the concrete compressive strength as a function of time and t is time in days. Three concrete core samples were obtained from most of the tested girders with the exception of one girder (CF2). These cores were taken by qualified NCDOT personnel, and tested in compliance with ASTM C42 specification in a Forney type compression testing machine. By inspection, it was observed that the concrete had river rock type aggregate varying in diameter from approximately 0.5 in to 1.0 in. Due to the difficulty in obtaining a typical sized sample of 8 in long, the cores were drilled in the deck where a core of 5 inches in length was obtained, as shown in Figure 3.3. The appropriate correction factor from ASTM C42 was then applied to obtain the compressive strength of each core sample. Results of the compression tests are given in

Table 3.2. Based on these results, the average concrete strength was 9.3 ksi for the Type I girders.

Figure 3.3 Concrete core drilling operation for C-Channel girders

Table 3.2 Results from concrete compression tests

Girder Type	Girder Designation	Compressive Strength (ksi)			
		Core 1	Core 2	Core 3	Mean
Type I	EB7S	6.135	6.628	6.323	6.367
	EB7F	7.396	7.179	7.454	7.338
	SRP1S	6.628	7.396	6.381	6.802
	SRP1F	7.614	8.122	8.861	8.209

Carbon Fiber Reinforced Polymers (CFRP)

One of the materials used for flexural strengthening of the C-Channel girders, the main point of interest in this report, was Carbon Fiber Reinforced Polymer (CFRP) materials. As mentioned earlier, the use of CFRPs in the built environment is gaining popularity in the United States, mainly because of its high strength to weight ratio, non-corrosive properties, and ease of installation. Two types of CFRP systems were used in this research: externally bonded wet lay-up type systems and externally bonded pre-cured laminates systems. The shape, type and amount of CFRP applied to the soffits of the C-Channel girder are shown in Figure 3.4. The strengthening system EB7 consisted of various configurations of either normal or high modulus CFRP wet lay-up sheets. System SRP consisted of two layers of steel reinforced polymer material. Design of the CFRP systems is discussed in the next section.

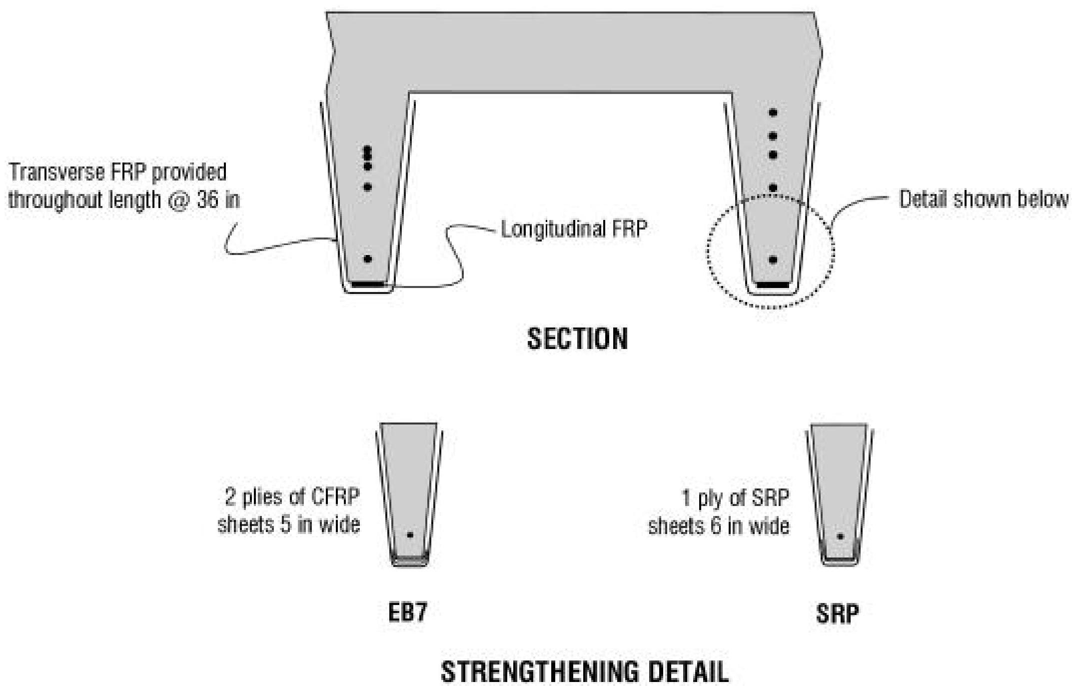

Figure 3.4 C-Channel strengthening configurations

Each type of CFRP material used in this research was tested to determine their characteristics including their tensile strength, elastic modulus, and rupture strain according to ASTM D3039 specification with the exception of CFRP bars manufactured by Hughes Brothers, where data was provided by the manufacturer. Descriptions of the various CFRP systems, along with their manufacturers, are shown in
Table 3.3. The material samples for the wet lay-up CFRP sheets were taken from witness panels created at the time of strengthening and kept at the same location as the girders during the curing process. All samples were bonded to aluminum tabs using Wabo MBrace© Saturant. The width of the CFRP samples varied from 1.0 in to 2.0 in and the gauge length was kept constant at 6.0 in.

The prepared specimens were tested using a MTS machine. The strain of the CFRP was measured using a 0.24 in TML FLA-6-11 120 Ω electric resistance strain gauge placed at the center of the width and gauge length of the specimen. Two distinct modes of failure were observed during the tension testing. The first behavior was characterized by sudden and brittle rupture of the fibers through the CFRP matrix as shown in Figure 3.4. The second possible mode of failure was less violent and rupture occurred through the cross section as shown in Figure 3.5. In general, failure of the pre-cured laminate strips was according to the first mode, while the wet lay-up laminates failed according to the second mode. This behavior is due to the fiber volume fraction in the pre-cured laminates which is significantly greater than the wet lay-up sheets. The only exception was the high modulus pre-cured laminates, which failed due to a smooth rupture through the cross section. If the rupture of the CFRP occurred in the vicinity of the aluminum grips the test was not included. Test results for all the CFRP tension tests are given in Table 3.3.

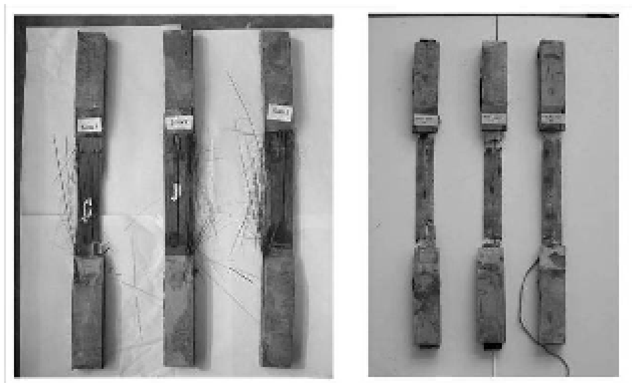

Figure 3.5 Typical pre-cured (left) and wet lay-up (right) specimens after tension testing

Table 3.3 Tension test results – C-Channels

System Designation	Epoxy	Girders Strengthened	Thickness (in)	Tensile Strength (ksi)	Modulus of Elasticity (ksi)	Ult Strain (%)
Hexcel	Sika Hex 306	EB7S, EB7F	0.046	88.62	9412.9	1.02
		Manufacturer	0.039	101.5	10152.6	1.00
Hardwire	Fox Ind.	SRPS, SRPF	0.076	60.77	6787.8	1.55
		Manufacturer	0.047	155	10384.7	1.50

Steel Reinforced Polymers (SRP)

In addition to the CFRP materials tested as part of this research, an additional type of strengthening system was examined consisting of high strength steel fibers embedded in an epoxy matrix, commonly called steel reinforced polymer (SRP) material. The SRP material was tension tested in the same manner as the CFRP strengthening systems and the results are provided in

Table 3.3.

3.3 Design of Strengthened Girders

The design of the strengthened girders proceeded after testing the control girder. Results of the static test on the Type I girder were assumed as the base for the design of the strengthened girders. A 30 percent increase in the ultimate load carrying capacity with respect to the control girder was examined. The design of each strengthened girder was expedited through the use of a cracked section analysis program, Response 2000© (Bentz 2000) discussed in Chapter 6. The base curve of the concrete compression model used in the cracked section analysis program was the Popovics curve, compression softening was determined using the Vecchio-Collins model and the tension stiffening was determined from the Bentz model (Bentz 2000). In the preliminary design, the compression strength of the concrete used was 6 ksi and was based on the compression strength specified in the original NCDOT drawings modified according to Equation (3-2) to account for the age of concrete at the time of testing. The prestressing strands were all assumed to be 250 ksi for Type I prestressing configuration modeled using the Ramberg-Osgood equation with 0.030, 121 and 6 for the coefficients A, B, and C respectively. The CFRP systems used in the design were modeled as linear elastic up to failure using material properties provided by the manufacturer. The material properties used in the design of the high modulus CFRP sheets were based on extensive prior material testing conducted by another graduate student (Schnerch 2005).

Flexural failure, defined as rupture of the FRP or crushing of the concrete in compression, was the desired mode of failure. It was recognized that externally bonded systems are more prone to debonding failures than near surface mounted systems. According to Malek et al., 1998, shear stresses developed at the FRP cut-off point for the externally bonded systems were significantly lower than the shear strength of the concrete. Therefore, plate-end debonding is not expected to occur and is not of great concern. To delay FRP delamination-type failures along the length of the girder, 6.0 in wide U-wraps were installed at 36 in spacing for all externally bonded strengthened girders. This arrangement was selected to simulate typical anchorage details commonly used by the construction industry for reinforced concrete members strengthened with FRP. Girders strengthened with system EB7 and SRP were strengthened to achieve a 30 percent increase in capacity.

3.4 Static Tests

Test Setup, Procedure and Instrumentation

All girders were tested using a 110 k MTS hydraulic actuator, with the exception of girder CS which was tested using a 450 k MTS hydraulic actuator. The actuator was mounted to a steel frame placed at the midspan of the girder. To simulate field loading conditions, a set of truck tires filled with silicon rubber were used as a contact surface while applying the load for the Type I girders. The footprint of the two tires was approximately 6 in by 9.8 in, the same area as the design loading area specified by AASHTO (AASHTO 2004). Typical C-Channel prestressed concrete bridges constructed in the early 1960s usually have a substructure of wooden piles that is difficult to mimic in the laboratory. However, in order to simulate small displacements at the supports, the girder was supported at both ends on a 2.5 in thick neoprene pad which in turn rested on a 1.0 in steel plate. Hydrostone was used at the supports for leveling purposes. The width of the neoprene pad was 8.5 in which provided a clear span of 342 in for each tested girder.

The displacement behavior of the girders during testing was monitored using three sets of string potentiometers, placed at quarter spans, and two linear potentiometers to measure vertical displacement over the supports. The compressive strain in the concrete was measured using a combination of PI gauges (a strain gauge mounted to a spring plate) and two 2.4 in TML FLA-60-11 120 Ω electric resistance strain gauges located at midspan. PI gauges were also placed at various locations at the level of the lowest prestressing strand to measure the crack width and to determine the strain profile along the depth of the girder. The tensile strain in the CFRP reinforcement was measured using six 0.24 in TML FLA-6-11 120 Ω electric resistance strain gauges: two at midspan, two at 6 in from midspan and two at 12 in from midspan. Additional tensile strain gauges were provided for the girders tested as part of the bond study, and these are discussed in the next part of this dissertation. Figure 3.6 shows a typical test setup for the C-Channel girders under static loading conditions.

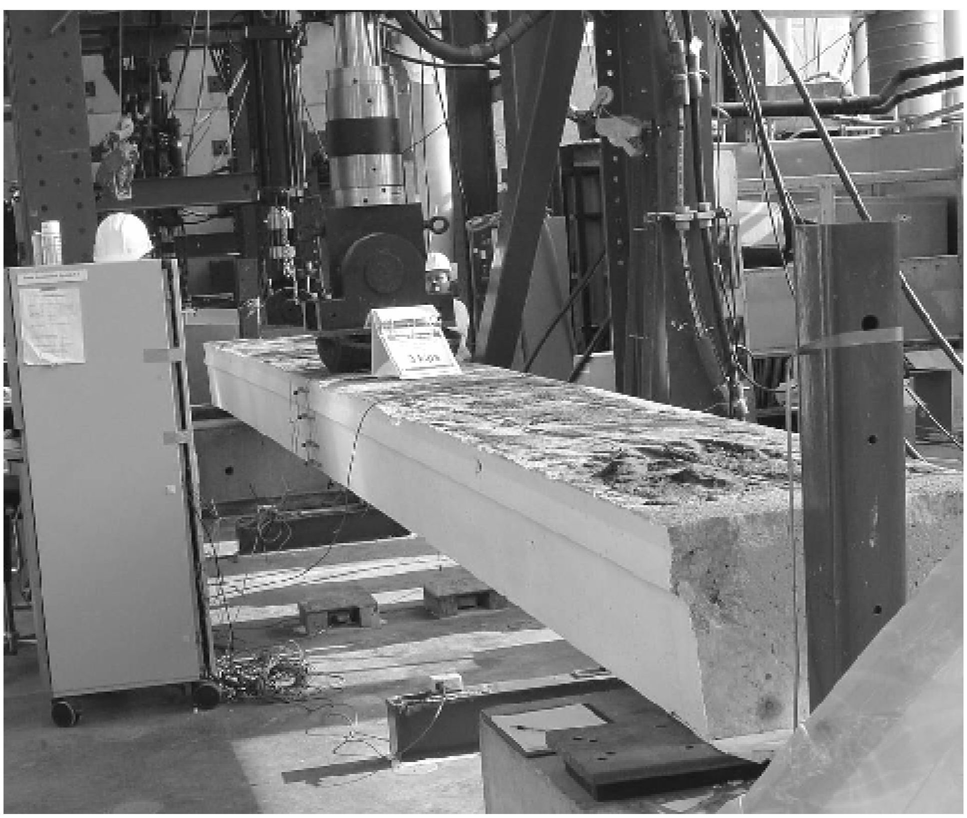

Figure 3.6 Typical test setup for C-Channel girders tested under static loading conditions

The loading sequence of the girders began by increasing the applied load up to a load level slightly higher than the cracking load. The girder was then unloaded, and reloaded again at a rate of 0.1 in/min up to the load level equivalent to yielding of the prestressing strands. This loading sequence was selected to determine the effective prestressing force in the girders by observing the re-opening of the flexural cracks. For the given measured load at reopening of the flexural crack at midspan, P_{ro}, the average effective prestressing force, P_{eff}, can be determined according to the following equation:

$$0 = \frac{M_D}{S_b} + \frac{L \cdot P_{ro}}{4 \cdot S_b} - \frac{10 \cdot P_{eff}}{A_c} - \sum \frac{d_i \cdot P_{eff}}{S_b} \tag{3-3}$$

where M_D is the moment due to the dead load, S_b is the bottom section modulus, L is the span, A_c is the area of the concrete section, n is the number of prestressing strands, and d_i are the locations of the different layers, i, of prestressing strand measured from the neutral axis of the section.

When the girders were loaded beyond yielding of the prestressing strands, the rate of the applied load was increased to 0.2/min up to failure. The average prestress force for Type I girders was 15.5 k. Details of the various strengthening systems and material properties are summarized in Table 3.4.

Table 3.4 Details of the strengthened girders

Specimen Designation	EB7	SRP
Date of testing	1/06S 3/06F	4/06S 5/06F
Date of strengthening	12/05	2/06
Prestressing Configuration	Type I	Type I
Strengthening technique	EB Sheets	EB SRP
FRP details	2 plies per web	1 ply per web
FRP shape	sheets are 0..39 x 5 in	SRP is 0.049 x 5.98 in
Groove size	-	-
A_{FRP}, in^2	0.787	0.561
E_{FRP} ksi (material testing)	X	X
f_{uFRP}, ksi (material testing)	X	X
f'_c, ksi*	X	X

* this is the average of the girder tests performed for the specified type of strengthening

Control Girder

The physical description as well as the experimental set up and results for the control girder (CS) can be found in the Final Report 2005.

Figure 3.7 Failure due to concrete crushing of girder CS

Externally Bonded CFRP Strengthened Type I Girders

A Type I C-Channel girder (EB7S) was strengthened to achieve a 30 percent increase in ultimate load carrying capacity using two 5.0 in CFRP wet lay-up sheets per web. This girder was tested under static loading conditions in January 2006. There were several purposes of testing this girder (and an identical girder under fatigue loading conditions): 1) to verify design procedures which have been developed as part of this research, 2) to test an additional CFRP strengthening system, and 3) to perform a cost-effectiveness analysis with one more contractor. The observed cracking load of the girder was 13.3 k. Due to the unloading sequence, the effective prestress force was determined to be 16.5 k . There was a greater distribution of cracks at failure, and smaller crack widths than was present in the static test of the control girder (CS). The failure was due to concrete crushing at a load of 43.2 k, which represents a 30.2 percent increase in ultimate capacity over the control girder

Externally Bonded SRP Strengthened Type I Girder

A type I prestressed concrete girder strengthened with steel reinforced polymer (SRP) material was tested under static loading conditions (SRPS). The girder was strengthened to achieve a 30 percent increase in ultimate capacity. The girder was delivered to the laboratory in good condition with no visible flexural cracking. In the deck at midspan, there was a 7.0 in diameter hole cut in the concrete. Using techniques described in the AASHTO repair experimental program, the hole was filled in with high strength polymer-modified repair mortar with 0.5 in round aggregates.

During the initial loading cycle, the observed cracking load was 13.2 k and the observed crack re-opening load was 8.5 k, which corresponds to an effective prestress force of 15.6 k per strand. Failure was due to crushing of the concrete followed by debonding of SRP material at midspan at a load of 48.8 k as shown in Figure 3.8, an increase of 46.5 percent compared to girder CS. Immediately after concrete crushing, a large shear crack propagated at a 45 degree angle from a flexural crack near midspan to the compression zone causing catastrophic failure.

Figure 3.8 Concrete crushing failure of girder SRPS

3.5 Fatigue Tests

Test Setup, Procedure and Instrumentation

The test setup and instrumentation for the girders tested under fatigue loading conditions was similar to that of the girders tested under static loading conditions with the following exceptions: 1) a 10 in by 20 in by 1 in loading plate was used in lieu of the loading tires to ensure adequate stability during the cyclic loading, and 2) two 6 in linear potentiometers were placed at midspan to measure displacement instead of string potentiometers due to their superior performance in fatigue. After completion of the fatigue loading, string potentiometers were used for the final static test. The initial applied loading for the girders tested in fatigue was also identical to that of the girders tested statically to failure: the girder was loaded up a load equal to the cracking load, unloaded and reloaded in order to determine the effective prestressing force in the girder. Due to the large scale of the C-Channel girders, they were loaded at a frequency of 2 Hz.

Fatigue Load Determination

The fatigue load range used for testing the C-Channel girders was designed to simulate typical loading of an actual bridge under service loading conditions. The range varies from a minimum load equivalent to the dead load and a maximum equivalent to the dead load plus the live load. For the tested C-Channel girders, the minimum load, in addition to the girder's own weight, included a load producing a moment equivalent to the moment due to an asphalt wearing surface typically used for these types of bridges. Assuming a wearing surface thickness of 4 in and density of 0.15 k/ft^3, the dead load was calculated as 0.127 k/ft, which corresponds to a midspan moment of 14.35 k-ft. Thus, the minimum concentrated load at midspan was calculated to be 1.9 k. A value of 2.0 k was used.

The maximum load was determined based on a truck configuration specified by AASHTO HS-15 type loading depicted in Figure 3.9. The axle load of 24 k was multiplied by the impact factor and the distribution factor according to AASHTO specifications (2004). The impact factor used was 1.33 as specified by AASHTO Article 3.6.2.1. The load distribution factor was determined from Table 4.6.2.2.2b-1 of the AASHTO specifications. Based on a two lane bridge 30 ft wide supported by twelve C-Channel girders, the distribution factor used was 0.24.

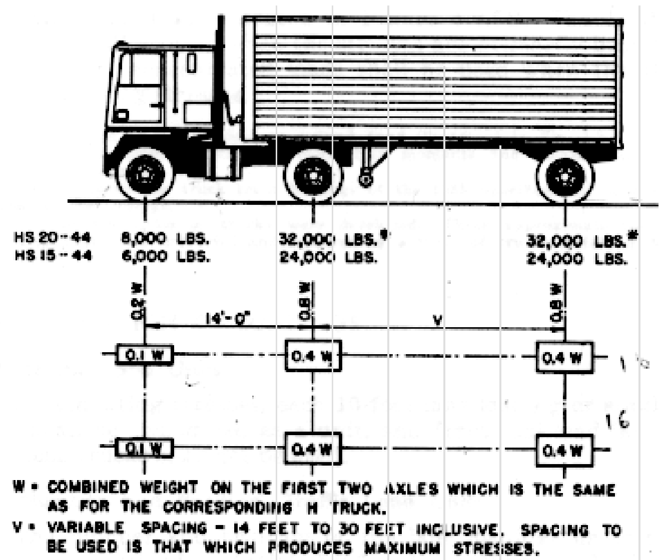

Figure 3.9 AASHTO Design Truck

Applying the appropriate factors to the middle and rear axle loads can be determined as: (Axle Load)(Impact Factor)(Distribution Factor)=(24)(1.33)(0.24)=7.7 k. When the design axle loads were applied as moving truck loads along the girder span of 30 ft, the maximum moment occurred when the middle axle was at a distance of 11.5 ft from the right support and the rear axle was at a distance of 25.5 ft from the right support. The analysis indicates that the front axle of the truck would be acting on an adjacent span. Based on the maximum moment induced by the truck loading, the equivalent concentrated load at midspan was determined to be 9 k as shown in Figure 3.10.

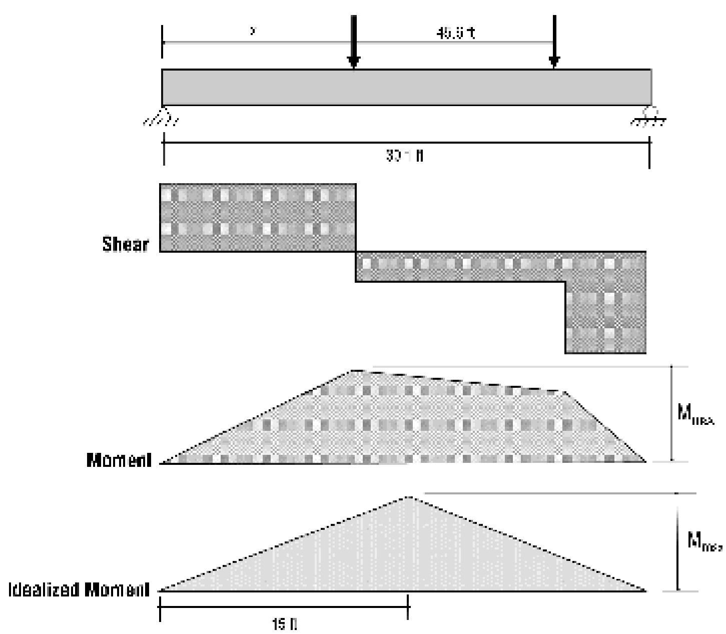

Figure 3.10 Shear and moment diagram for moving AASHTO axle loads

In June 2005 a more clear copy of the 40 year old Standard Specification for C-Channel Girders (the original design document) was obtained. It was noticed that the HS-15 type loading was specified only for girder spans of 19.7 ft or 25 ft. For girders with a 19.7 ft span, HS-13 type loading was the specified design loading. Applying the impact, distribution, and moment correction factors discussed above to the HS-13 loading, the equivalent concentrated load simulating the live load is 7.8 k which is 13.3 percent less than the HS-15 type loading originally used.

Control Girders

The control girder was prestressed with a Type I prestressing configuration (CF1). At the initial stage of loading of C-Channel girder CF1, a sudden load of approximately 22.5 k was applied to the girder due to problems related to the load control system of the actuator. The load was large enough to cause flexural cracking. Following the unfortunate incident, the girder was loaded statically to determine the load causing reopening of the crack to determine the effective prestress forces as described earlier, the measured value of which was 9 k, which corresponds to a loss of prestress of 14.3 percent, comparable to the level measured for the other girders. The fatigue cycles varied between an upper and lower load levels of 2 k and 11 k respectively which corresponds to HS-15 type loading, or 15.4 percent higher than HS-13 loading. The girder failed due to a ruptured lower prestressing strand after completion of 1,076,000 cycles; therefore the girder was not tested by the typical final static loading test.

Externally Bonded CFRP Strengthened Type I Girders

A C-Channel girder designed to achieve a 30 percent increase in capacity using CFRP wet lay-up sheets (EB7F) was tested under fatigue loading conditions. From the initial loading sequence, the cracking load was measured at 12.9 k, and the effective prestress force calculated as 15.7 k. The fatigue load applied varied from 2 k to 12.1 k, which represents a 30 percent increase in live load based on HS-13 type loading. After 1.25 million cycles an accidental overload condition of 30 k was applied to the girder, which caused a residual displacement of 1.77 in. The fatigue test was then resumed and the girder completed 2 million cycles of fatigue loading with little additional degradation. A final static test was performed on the girder to assess the damage due to fatigue loading. The ultimate load achieved during the final static test was 44.2 k, which is a 2.2 percent increase in ultimate load compared to girder EB7S. Failure was due to rupture of the externally bonded CFRP sheets as shown in Figure 3.11. After the ultimate load was achieved, the girder continued to resist load, behaving similarly to the control specimen. Catastrophic failure occurred due to concrete crushing at a load of 37.6 k.

Figure 3.11 Concrete crushing after FRP rupture of girder EB7F

Externally Bonded SRP Strengthened Type I Girders

A type I prestressed concrete girder strengthened with steel reinforced polymer (SRP) material was tested under fatigue loading conditions (SRPF). This girder was similar to a girder strengthened with SRP and tested under static loading conditions (SRPS). The girder was delivered to the laboratory in good condition with no visible flexural cracking. During the strengthening operation difficulty was encountered in wrapping the SRP with 0.03937 wires per in. around the beam soffit. It was envisioned that the material would conform to the rounded soffit edge and bond to the concrete without leaving voids. For one of the soffits in this girder the SRP material was cut in the longitudinal direction in two places to relieve pressure that was present due to the wrapping. On the other soffit the SRP was left in one piece per layer, a configuration which resulting in sagging that was observed post-strengthening. The strengthening on this soffit was repaired according to procedures described in Mirmiran et al. (2004).

Girder SRPF was strengthened to achieve a 30 percent increase in ultimate capacity, and was tested under cyclic loading between the load levels of 2 k and 12 k, which corresponds to a 30 percent increase in HS12 live load. During the initial loading cycle, the observed cracking load was 14 k and the observed crack re-opening load was 9.4 k, which corresponds to an effective prestress force of 16.7 k per strand. The girder achieved over 2 million cycles of loading with very little degradation. During the final static test, failure was due to crushing of the concrete at midspan at a load of 50.9 k, an increase of 52.8 percent compared to girder CS. Underneath the loading area at midspan the SRP material was partially debonded between the flexural cracks, but this did not lead to failure due to the wrapping and the U-wrap debonding mitigation. Immediately after concrete crushing, a large shear crack propagated at a 45 degree angle from a flexural crack near midspan to the compression zone causing catastrophic failure. Compared to a similar girder tested under static loading conditions (SRPS), SRPF failed at a load 4.28 percent higher, mainly due to a higher effective prestress force. The failure of girder SRPS is shown in Figure 3.12.

Figure 3.12 Concrete crushing failure of girder SRPF

4 EXPERIMENTAL PROGRAM – AASHTO GIRDER

4.1 Introduction

In October 2003, a tractor trailer carrying improperly secured excavating equipment impacted the prestressed concrete superstructure of NC Bridge 169 shown in Figure 4.1, in Robeson County, North Carolina. The impacted bridge was located on Green Springs Road (SR 1718) over Interstate 95. Originally built in 1959, the bridge consisted of four 55 ft long spans. Each span was made up of four AASHTO Type II prestressed concrete girders spaced at 7 ft intervals. The impact of the excavating equipment heavily damaged the first exterior girder by nearly severing it in half. The second and third girders were missed, and the last girder was then struck, causing a large loss of the concrete section and rupturing one prestressing strand.

This was not the first time that the bridge had been hit; therefore the bridge maintenance engineers with the North Carolina Department of Transportation decided to replace all four girders in the eastern span with cored slab units. The cored slab units would provide more ground clearance and therefore reduced the probability of future impacts. The bridge girders were identified by members of the North Carolina State University Civil Engineering Department as a potential research source. These girders were then transported to the NCDOT Bridge Maintenance Facility in Raleigh, NC for future repair work. Figure 4.2 shows the three girders at the DOT maintenance facility. The first phase of the project focused on repairing the severely damaged girder with rupture of one prestressing strand. The results of the first phase can be found in Rizkalla *et al* (2005). The other two structurally sound interior girders were set aside for phase two of the project, which involved simulating varying degrees of impact damage and then repairing them.

Figure 4.1 Undamaged eastern span of NC Bridge 169

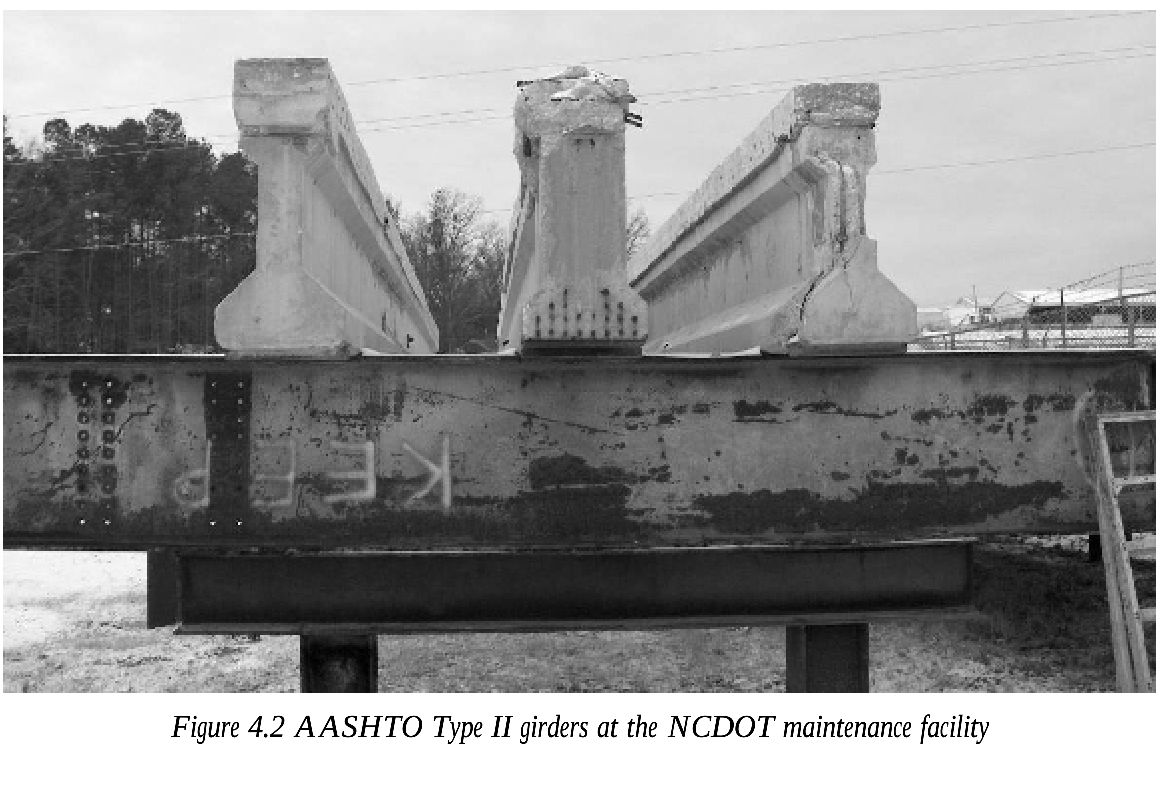

Figure 4.2 AASHTO Type II girders at the NCDOT maintenance facility

During the first phase, the impact damaged AASHTO Type II girder previously reported was repaired using a polymer modified cementitious material to rebuild the concrete section and CFRP wet lay-up sheets to restore the nominal section capacity. The second phase included simulating damage to the two 55 ft long specimens by removing part of the concrete section and rupturing three or four prestressing strands, respectively. The girders were damaged at midspan to simulate a flexurally critical situation. The girders were then repaired in the same manner as the first AASHTO girder. Following the completion of testing these two girders, one girder was then cut into thirds in order to create short spans, which is typically critical for shear resistance. One of these short spans was tested as a control specimen and the second was damaged to simulate an impact near the girder's support. This girder was then repaired, using PCI and ACI Committee 440 design guidelines, and tested statically to failure. This chapter presents the experimental program for the five test specimens. Complete test results and discussion are given in Chapter 5.

4.2 Test Girder

Two Type II AASHTO girders (AASHTO2 and AASHTO3) were tested to examine the flexural behavior of CFRP repaired girders damaged by vehicular impact. The girders were artificially damaged near midspan location to examine different damage scenarios, including varying the amount of prestressing strands ruptured. This chapter will provide details and descriptions of the various tests conducted in this study.

Two short span girders were tested under shear-critical loading conditions. Following the flexural testing of AASHTO2, the girder was saw-cut into thirds, with the two identical end pieces used for the shear study. One section of the girder was used as a control specimen (AASHTO2C), while the other specimen was damaged near the support and repaired with CFRP sheets (AASHTO2R). AASHTO3 was saw-cut in a similar manner and saved for future research. This chapter will provide details and descriptions of the individual tests. Complete test results are discussed in Chapter 5.

AASHTO2

Test girder AASHTO2 was an interior girder of the bridge and therefore was not damaged by direct impact like AASHTO1 (Rizkalla et al. 2005). This AASHTO Type II girder was older than the others; based on the presence of a large endblock and 28-7/16 in diameter 250 ksi prestressing strands it was determined the girder was cast in the 1960's. The girder was prestressed with twenty four straight and four harped prestressing strands using a hold down system at midspan. The total length of the girder was 54.5 ft, with a span length of 53.06 ft from center-to-center of the supports. Based on measurements taken at two foot intervals, the average width of the composite deck was determined to be 16.5 in. Cross section and elevation drawings of AASHTO2 are shown in Figure 4.3.

As previously mentioned in Section 4.1, AASHTO2 was received by the researchers undamaged, except for several transverse cuts approximately 0.4 in wide in the composite deck after the removal of the diaphragms. In order to simulate impact damage, a large portion of the tension flange of the girder was removed (Figure 4.4), and four prestressing strands were ruptured (Figure 4.5), corresponding to a reduction in prestressing force of 14.3 percent. The length of the damage was extended to a total of 2.0 ft on either side of midspan on the front side of the girder only. Approximately 2.2 ft^3 of concrete was removed, as shown in Figure 4.5.

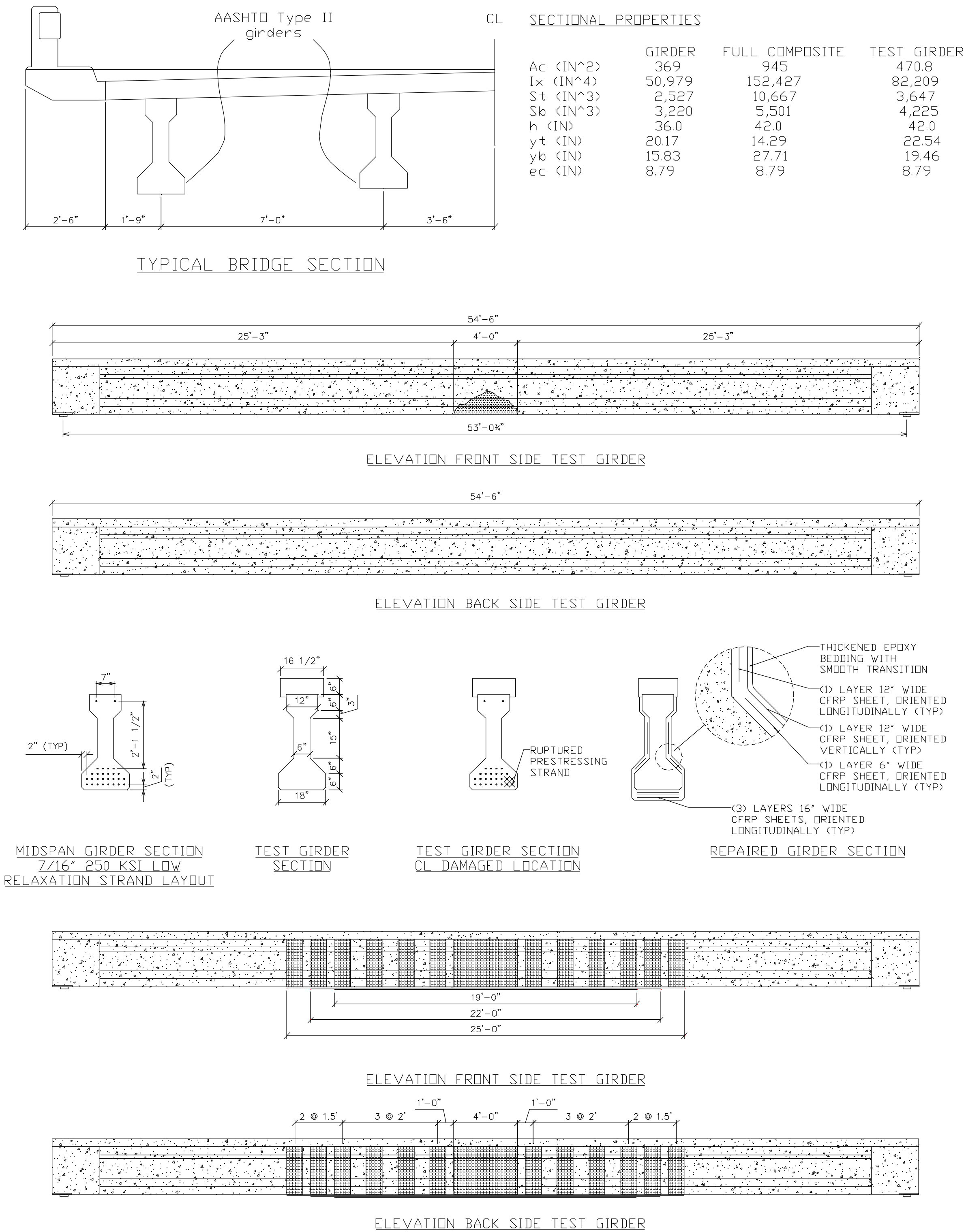

SECTIONAL PROPERTIES

	GIRDER	FULL COMPOSITE	TEST GIRDER
Ac (IN^2)	369	945	470.8
Ix (IN^4)	50,979	152,427	82,209
St (IN^3)	2,527	10,667	3,647
Sb (IN^3)	3,220	5,501	4,225
h (IN)	36.0	42.0	42.0
yt (IN)	20.17	14.29	22.54
yb (IN)	15.83	27.71	19.46
ec (IN)	8.79	8.79	8.79

Figure 4.3 AASHTO2 girder cross section, elevation, and CFRP design details

Figure 4.4 AASHTO2 during removal of concrete

Figure 4.5 Simulated damage of AASHTO2 girder

Design drawings were provided by the NCDOT; however they were illegible and it was difficult to discern most information. Initially it was assumed that the concrete strength for the girder was 5000 psi when it was first erected 40 some years ago. For preliminary calculations, a girder concrete strength of 6000 psi was used to reflect the age of 40 years plus. The composite deck slab was estimated at 3000 psi. Material test results of the prestressing strands and concrete core samples taken after testing girder AASHTO2 are presented in Section 4.3.

AASHTO3

The second girder tested in flexurally critical conditions was AASHTO3. This exterior girder was an AASHTO Type II girder, but was only 10 years old because a previous girder in the same location had been struck by an overheight vehicle and required replacement. AASHTO3 was comprised of 16-0.5 in diameter 270 ksi straight prestressing strands. The total length of the girder was 54.5 ft. The testing span length of this girder had to be shortened to avoid the damage at one end of the girder, caused during transportation, as shown in Figure 4.6. The center-to-center length between the testing supports was 49.0 ft. Based on measurements taken at two foot intervals, the average width of the composite deck was determined to be 13.5 in. Cross section and elevation drawings of AASHTO3 are shown in Figure 4.7.

Figure 4.6 Damage to right support of AASHTO3 caused during transportation of girder

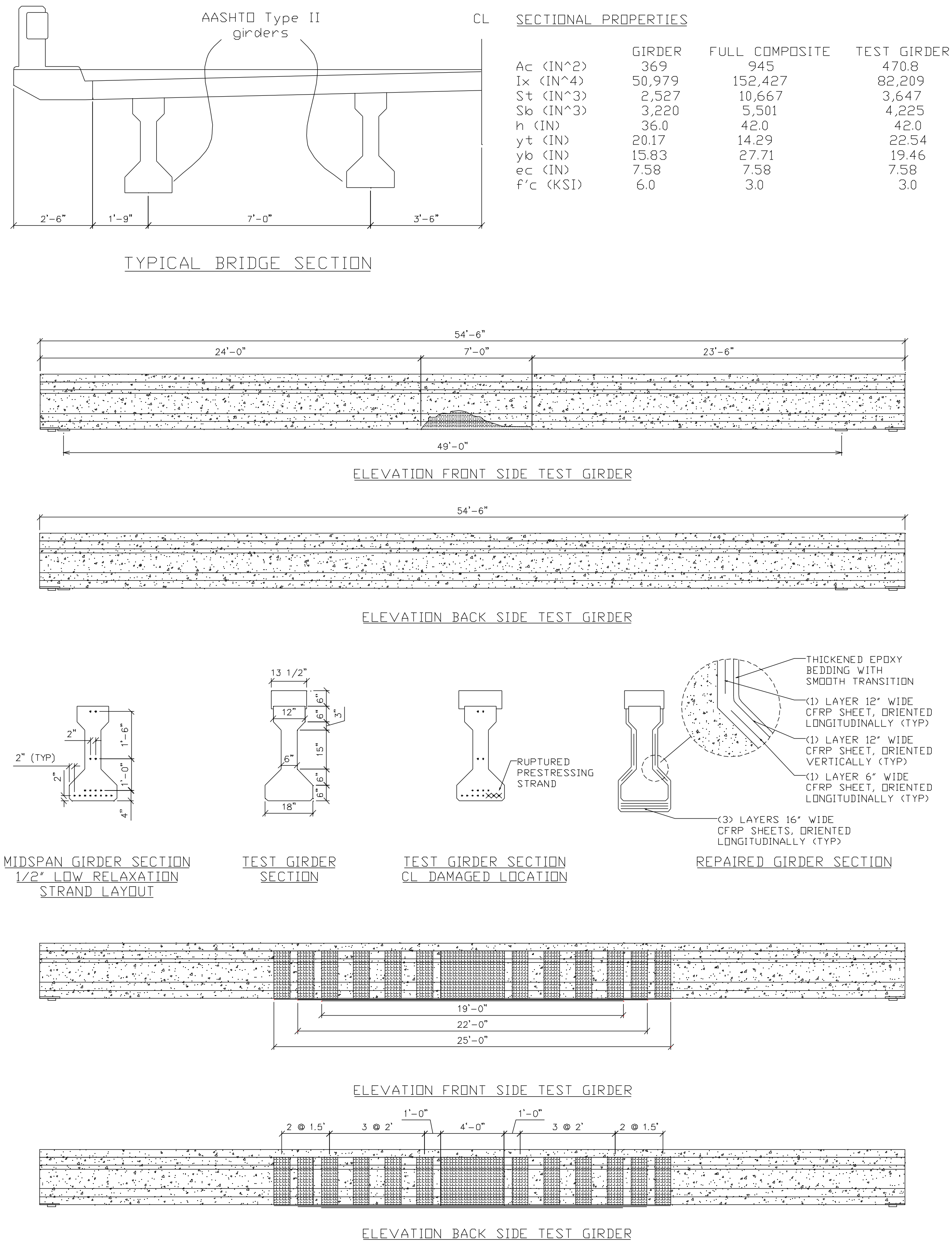

Figure 4.7 AASHTO3 girder cross section, elevation, and CFRP design detail

AASHTO3 had been impacted several times prior to being removed from the bridge. Figure 4.8 shows one section where an earlier concrete repair had been performed along with epoxy injection of the cracks caused by vehicular impacts. In order to simulate impact damage to this girder, a large portion of the tension flange was removed, similar to girder AASHTO2, and three prestressing strands were ruptured (Figure 4.9), corresponding to a reduction in prestressing force of 18.8 percent. The length of the damage was 2.0 ft to the left of midspan and approximately 5.0 ft to the right on the front side only. It was intended for the damage to be symmetrical about midspan, but the presence of earlier repairs made it difficult to cut as planned. A total of approximately 2.4 ft^3 of concrete was removed, as shown in Figure 4.9.

Figure 4.8 AASHTO3 defects after arriving at the testing facility

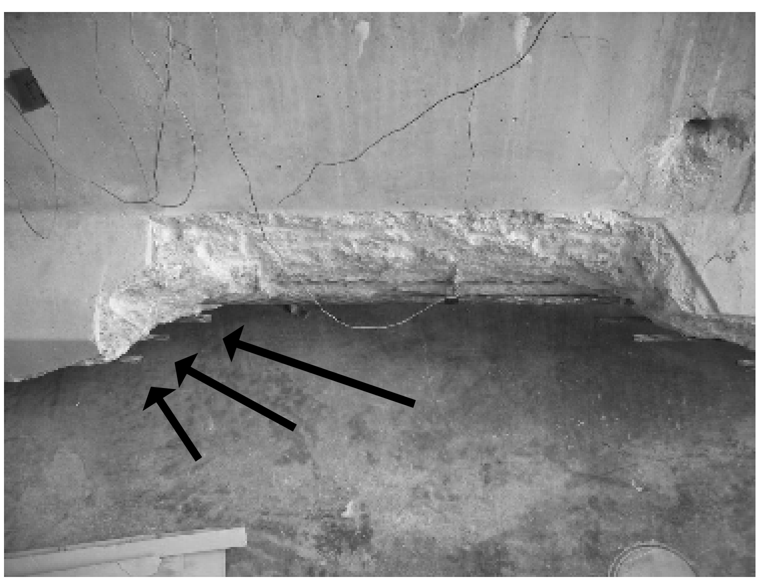

Figure 4.9 Simulated damage of AASHTO3 girder

Design drawings provided by the NCDOT indicated that the concrete strength for the girder was 5000 psi and 3000 psi for the bridge deck. Material test results of the prestressing strands and concrete core samples taken after testing girder AASHTO3 are presented in Section 4.3.

AASHTO2C

The first girder tested during the shear study, AASHTO2C, was tested monotonically to failure as a control specimen. The girder, shown in Figure 4.10 was prestressed with 28-7/16 in diameter 250 ksi strands. The total length of the girder was 20.67 ft, with a span of 17.83 ft from center-to-center of the supports. Based on measurements taken at two foot intervals, the average width of the composite deck was determined to be 16.5 in. Cross section and elevation drawings of AASHTO2C are shown in Figure 4.11.

Figure 4.10 AASHTO2C test specimen

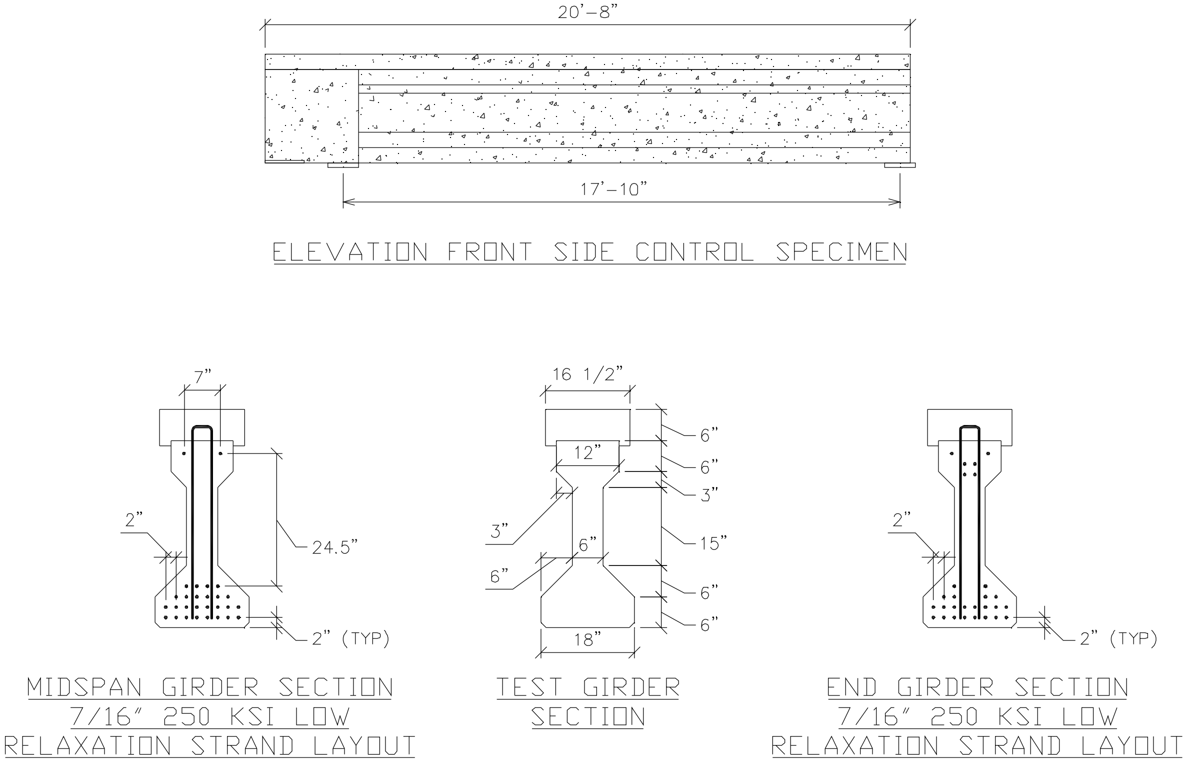

SECTIONAL PROPERTIES

	GIRDER	TEST GIRDER
Ac (IN^2)	369	470.8
Ix (IN^4)	50,979	82,209
St (IN^3)	2,527	3,647
Sb (IN^3)	3,220	4,225
h (IN)	36.0	42.0
yt (IN)	20.17	22.54
yb (IN)	15.83	19.46
ec (IN)	8.79	8.79

Figure 4.11 AASHTO2C girder cross section and elevation

AASHTO2 was received by the researchers undamaged, except for several transverse cuts which were repaired as mentioned previously in Section 4.2. Concrete strengths were the same as those specified for girder AASHTO2. Material test results of the prestressing strands and concrete core samples are presented in Section 4.3.

AASHTO2R

AASHTO2R was tested monotonically to failure as a shear critical member with simulated damage repaired with CFRP sheets as shown in Figure 4.12. The girder was prestressed with 28-7/16 in diameter 250 ksi strands. The total length of the girder was 20.67 ft, with a span of 17.83 ft from center-to-center of the supports. Based on measurements taken at two foot intervals, the average width of the composite deck was determined to be 16.5 in. Cross section and elevation drawings of AASHTO2R, including CFRP repair details, are shown in Figure 4.13. It should be noted that the section properties for AASHTO2R are the same as AASHTO2C but were not included for clarity.

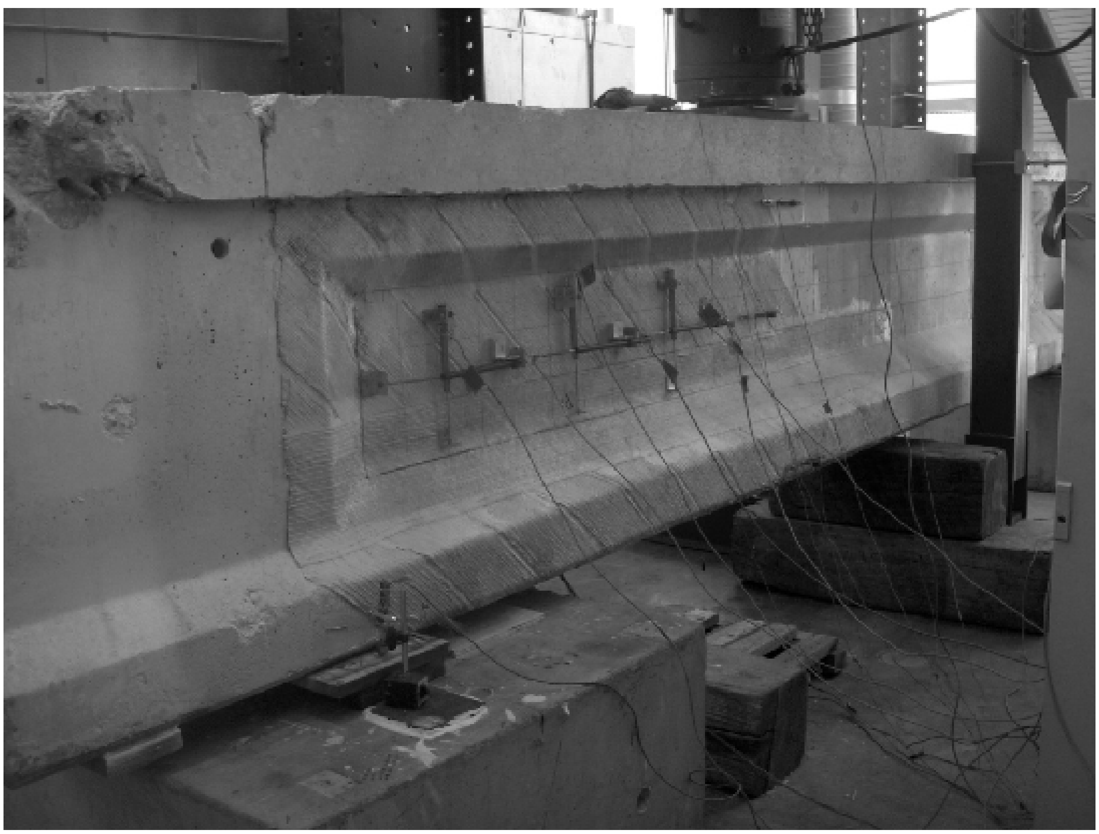

Figure 4.12 AASHTO2R test specimen

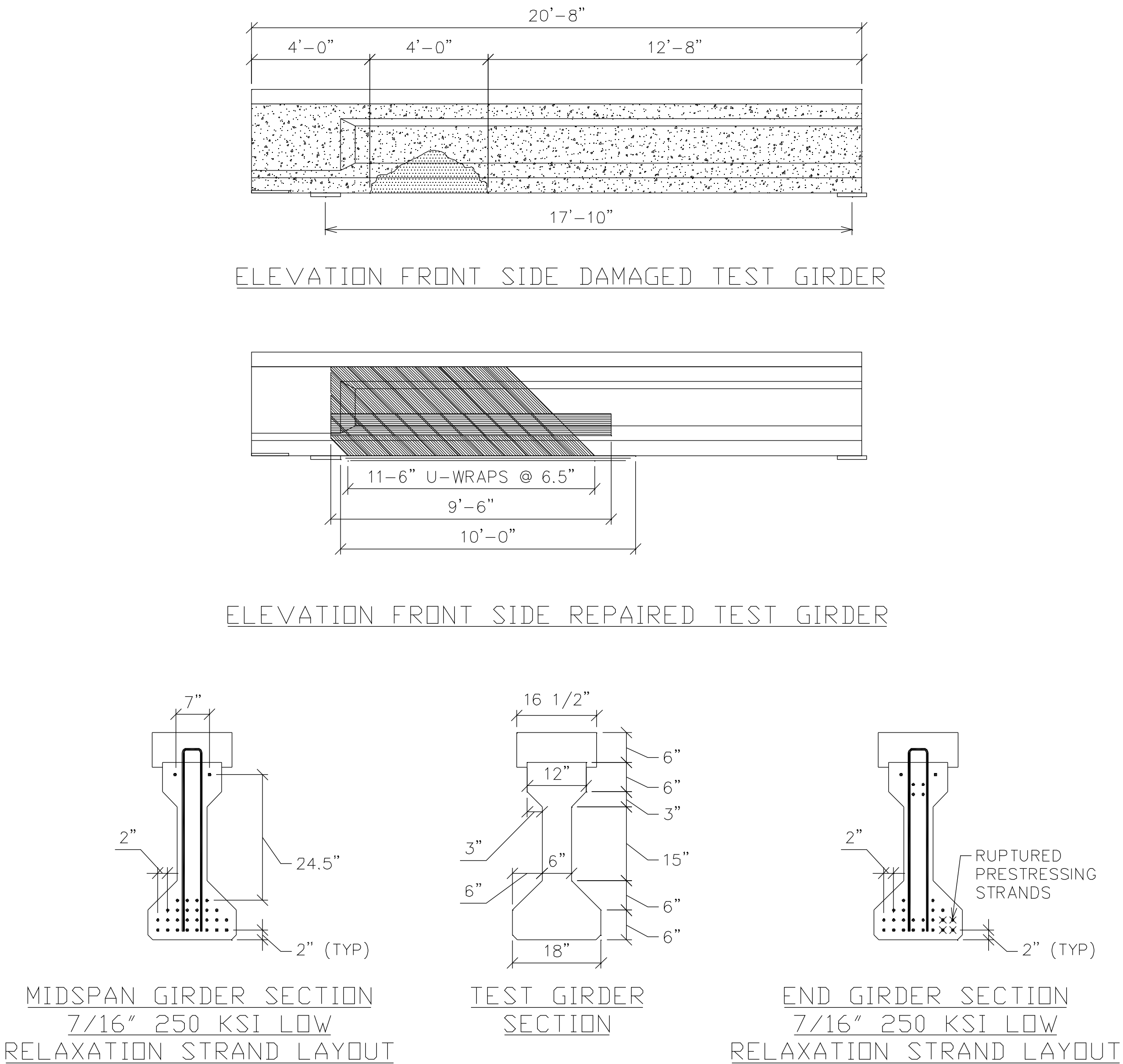

Figure 4.13 AASHTO2R girder cross section, elevation, and CFRP design details

In order to simulate impact damage, a large portion of the tension flange of the girder was removed, and four prestressing strands were ruptured (Figure 4.14), corresponding to a reduction in prestressing force of 14.3 percent. The length of the damaged began 1 ft past the face of the left support and extended 4 ft to the right. A total of approximately 1.5 ft^3 of concrete was removed, as shown in Figure 4.14.

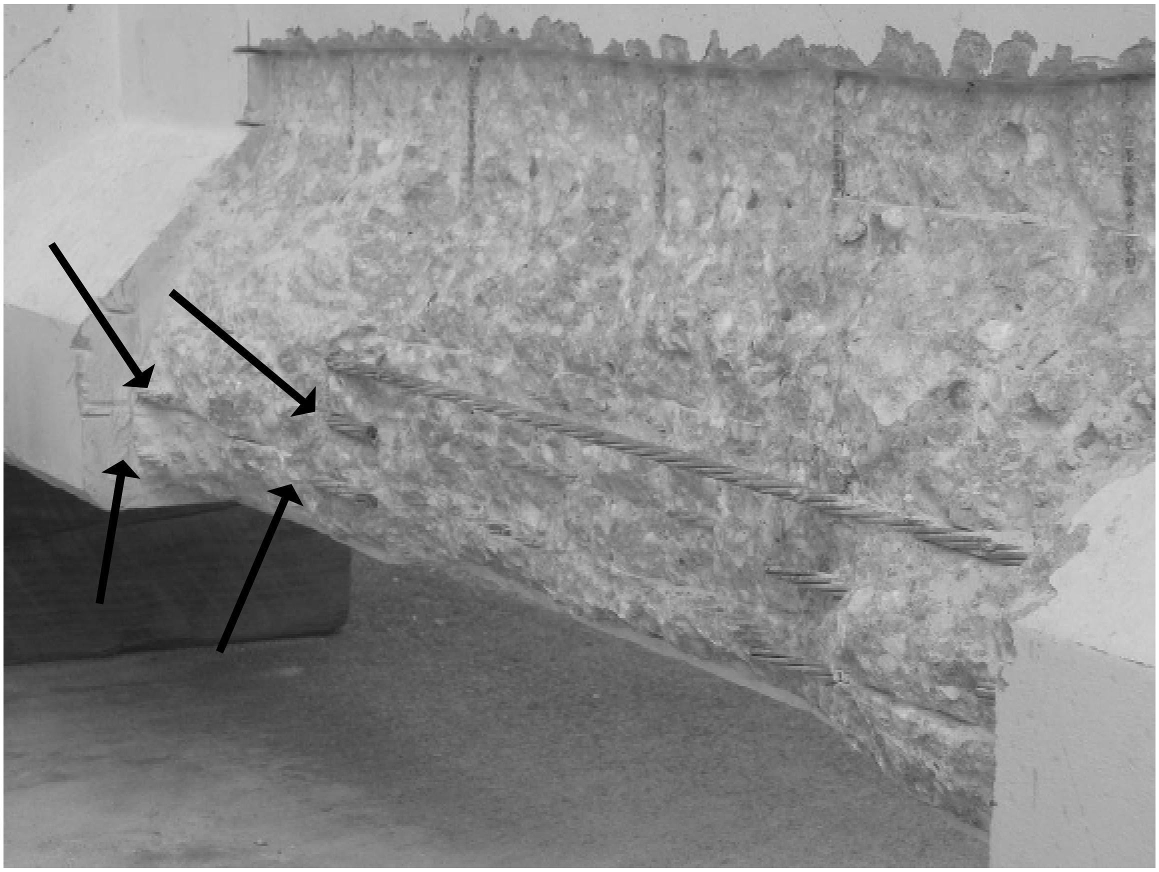

Figure 4.14 AASHTO2R after completion of simulated damage

4.3 Material Properties

This section will present testing methods and results of material tests performed on prestressing strands, concrete core samples, and CFRP sheets. The material properties for AASHTO1 are included in the section as a result of the tests not being performed prior to the publication of the previous report.

Prestressing Strands

Two different types of prestressing strands were encountered during the experimental program of this research project. Specimens AASHTO1 and AASHTO3 utilized the same prestressing strand pattern with 270 ksi strands, while specimens AASHTO2, AASHTO2C, and AASHTO2R utilized the same prestressing strand pattern with 250 ksi strands. The 270 ksi strand pattern (Figure 4.15 left) consisted of 16-0.5 in straight prestressing strands. The 250 ksi strand pattern (Figure 4.15 right) consisted of 28-7/16 in prestressing strands, 24 of which were straight and four of which were harped with a hold-down system located at midspan.

Material testing was carried out on prestressing strands encountered in each of the three main girders, after testing of each girder was complete. In order to test the strands, several were extracted from the bottom layer as close to the supports as possible. The strands were removed from the supports to ensure the strands had not yielded under the effect of loading. Special care was taken during removal of the strands to prevent unraveling.

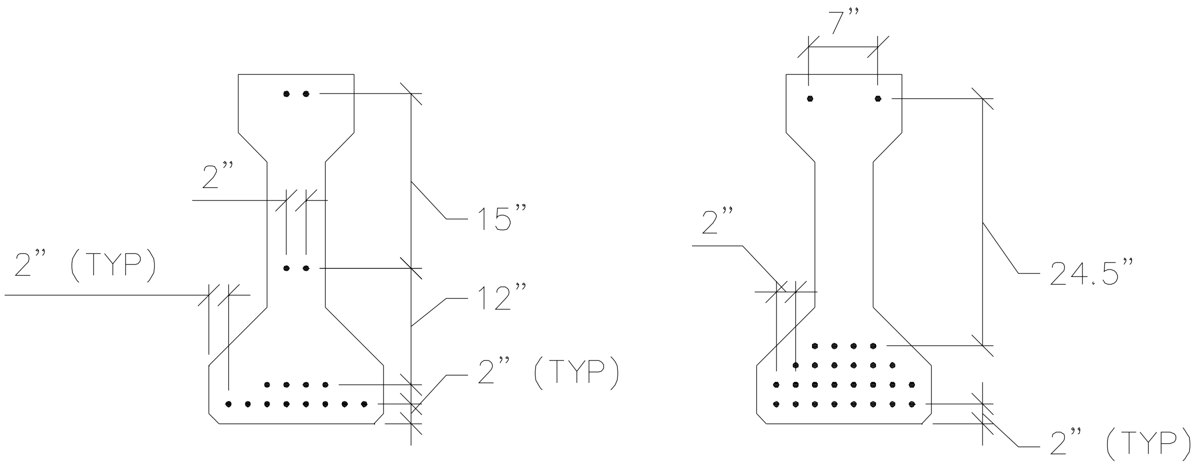

Figure 4.15 270 ksi (left) and 250 ksi (right) midspan strand patterns

The prestressing strands were tested in tension according to ASTM A416 specifications using a 220 k MTS closed-loop universal testing machine used to apply a constant rate of displacement. The prestressing strands were clamped into the MTS grips using multiple-use super chucks. A 1 in extensometer was placed at the middle of the specimen during the test to measure displacement and to obtain modulus of elasticity measurements. Figure 4.16 shows a typical prestressing strand specimen. Prior to rupture of the strand, the extensometer was removed to prevent any damage caused by the violent nature of the failure. The stroke of the MTS machine was then used to determine the rupture strain of the specimens. Table 4.1 shows the average yield strength, ultimate strength, modulus of elasticity, and rupture strain for each set of tested prestressing strands.

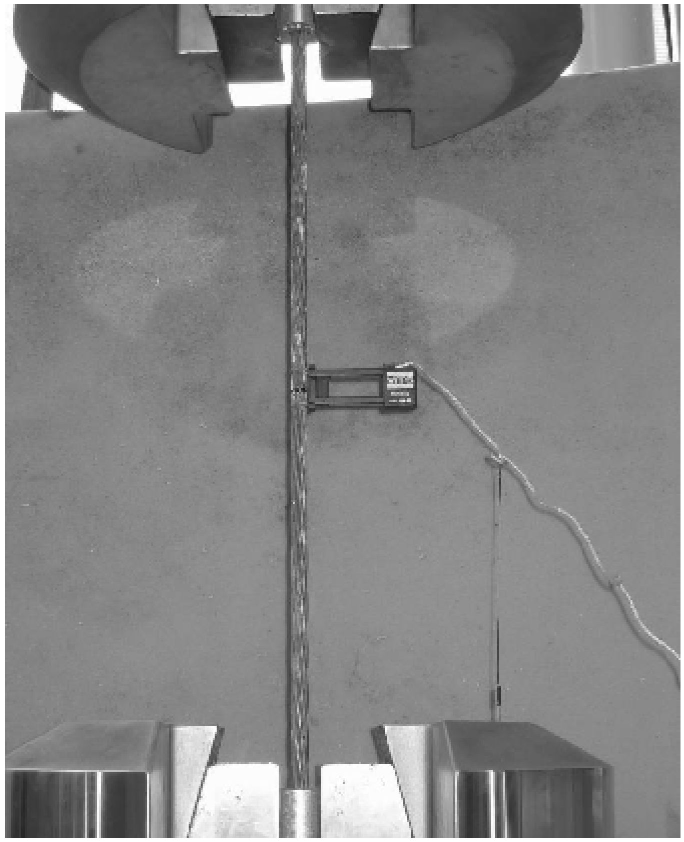

Figure 4.16 Typical prestressing strand test setup

Table 4.1 Prestressing steel properties

Specimen Designation	Strand Type, ksi	σ_y, ksi	σ_u, ksi	ε_u, %	E, ksi
AASHTO1 and AASHTO3	270	262	279	5.10	28,500
AASHTO2	250	210	255	5.62	28,900

The Ramberg-Osgood function (Collins and Mitchell 1991) was used to match the stress-strain behavior of the prestressing strands with material constants.

$$f_p = E_p e_{ps}\left[A + \frac{1-A}{\left[1+\left(Be_{ps}\right)^C\right]^{1/C}}\right] \tag{4-1}$$

where f_p is the prestressing strand stress, E_p is the modulus of elasticity of the prestressing strand, e_{ps} is the strain in the prestressing strand, and A, B, C are material constants.

Constants A, B, and C were determined by fitting the stress-strain curve generated by the Ramberg-Osgood equation with the stress-strain curve generated from the tension tests. For the 270 ksi strands, the average values for A, B, and

C were 0.015, 108, and 10 respectively. These values compared well with similar test values obtained from previous research by Rizkalla (2005). For the 250 ksi strands, the average values for A, B, and C were 0.025, 139, and 6 respectively, which also compared well with the values from earlier research by Rizkalla (2005). Figure 4.17 shows the measured stress-strain behavior compared to the Ramberg-Osgood function for both types of prestressing strands encountered.

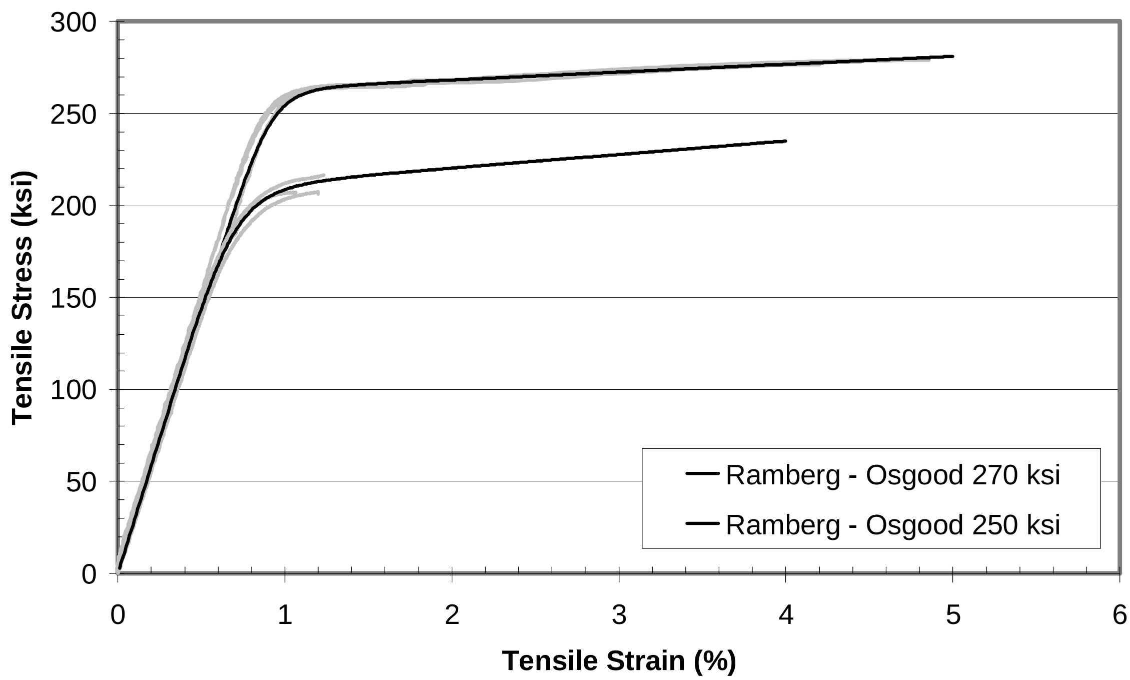

Figure 4.17 Stress-strain behavior of 270 ksi and 250 ksi prestressing strands

Reinforcing Bars

Due to the difficulty to extract any straight reinforcing bars, no tests were conducted to examine the characteristics of the reinforcing bars in the deck or the stirrups of each girder. The material properties used in the analysis were based on the specifications provided on the design drawings provided by NCDOT.

Concrete

The specified nominal concrete strength for all of the AASHTO girders was 5000 psi at time of erection. The design strength of these girders, as described in Section 4.2, was estimated to increase by at least 1000 psi as a result of the significant aging of the concrete. The following equation proposed by MacGregor (2005) accounts for the strength increases due to aging:

$$f'_{c(t)} = f'_{c(28)}\left[\frac{t}{4+0.85(t)}\right] \tag{4-2}$$

where $f'_{c(t)}$ is the concrete compressive strength as a function of time and t is time in days.

Several core samples were taken from both the girders and deck slab by qualified NCDOT personnel (Figure 4.18). The cores were then tested in accordance with ASTM C42 in an MTS closed-loop universal testing machine used to apply a constant rate of displacement. Concrete strains were measure using the stroke of the MTS machine. Eight inch long core samples were not able to be obtained due to the configuration of the AASHTO girders. The cores taken from the deck slab were approximately 5 inches in length. Likewise, the only feasible place to take cores from the girder itself was from the web, which was 6 inches in width. 4 in by 8 in cylinders were also cast of the various concrete repair materials used during the research. Table 4.2 lists the average results of all concrete testing for each AASHTO girder.

Figure 4.18 NCDOT personnel removing core samples

Table 4.2 AASHTO core sample test results

Specimen Designation		Compressive strength of concrete, f'c (ksi)	Aggregate description
AASHTO1	girder	7.1	Crushed and round ¼" – 1"
	deck	6.7	Gritty ¼" – ½"
	repair mortar	6.3	N/A
AASHTO2	girder	6.8	1" rounded quartz and river rock
	deck	5.1	½" – ¾" crushed sandstone
	repair mortar	6.3	3/8" crushed
AASHTO3	girder	6.6	Crushed and round ¼" – 1"
	deck	7.1	¾" crushed
	repair mortar	6.3	3/8" crushed

Carbon Fiber Reinforced Polymers (CFRP)

Carbon Fiber Reinforced Polymer (CFRP) wet lay-up sheets were used in the repair of every specimen, as mentioned in Section 4.1. The design of the repair systems are presented in Section 4.4. Although several girders were repaired using the same CFRP system, samples were made during installation and kept at the same location as the girder to determine their tensile strength, modulus of elasticity, and rupture strain. All tests were performed in accordance with ASTM D3039 specifications and tested using the MTS equipment described previously in Section 4.3. Test results for each girder, along with the manufacturer's specifications, are shown in Table 4.3.

Table 4.3 CFRP tension test results

CFRP system	Specimen Designation		Tensile strength, (ksi)	E (ksi)	ε_u (%)	Average thickness (in)
Tyfo SCH-41 Composite	AASHTO1	Test	76	6,350	1.2	.08
		Manufacturer	143	13,890	1.0	.04
	AASHTO2	Test	109	9,730	1.08	.096
		Manufacturer	143	13,890	1.0	.04
	AASHTO3	Test	109	9,730	1.08	.096
		Manufacturer	143	13,890	1.0	.04
	AASHTO2R	Test	98	8,480	1.12	.099
		Manufacturer	143	13,890	1.0	.04

All CFRP samples were cut out of witness panels to a width of 1 in and a length of 17.5 in. The samples were then bonded to aluminum tabs using Wabo MBrace© Saturant (Wabo 2002) to produce a gauge length of 6 in. Figure 4.19 shows a typical CFRP tension test setup. The strain of the CFRP was measured using a 0.236 in TML FLA-6-11 120 Ω electric resistance strain gauge placed at the center of the width and gauge length of the specimen. The primary mode of failure was the sudden and brittle rupture of the fibers in the CFRP, as shown in Figure 4.20 (left). The second, and less frequent mode of failure, was rupturing of the CFRP matrix through the cross section, as shown in Figure 4.20 (right).

Figure 4.19 Typical CFRP tension test setup

Figure 4.20 Failure through the fibers (left) and failure through cross section (right)

4.4 Design of CFRP Repair Systems

The purpose of applying CFRP to the various damaged AASHTO girders was to restore their original ultimate flexural and shear strengths. Based on previous research by Rizkalla *et al*. (2005), it was decided to use externally bonded CFRP wet lay-up sheets to restore the original flexural and shear capacity of all the girders. The wet lay-up sheets were chosen for two reasons: 1) transverse U-wraps would be needed to encapsulate the restored concrete section to stabilize crack growth, thus meaning that two CFRP systems would be needed if wet lay-up sheets were not chosen as the main longitudinal reinforcement and 2) based on previous research by Rizkalla *et al*. (2005), and in consultation with NCDOT officials, CFRP wet lay-up sheets were found to be the most cost-effective repair system, and thus most likely to be used by the NCDOT in future field applications.

AASHTO2

The first task in the design of the CFRP repair system for AASHTO2 was to determine the ultimate flexural strength and load vs. deflection behavior of the undamaged specimen. The ultimate capacity of the section was predicted using RESPONSE 2000©, a cracked section analysis program (Bentz 2000), and was verified by loading the girder as described in Section 4.6. The base curve of the concrete model used in the cracked section analysis program was the Popovics curve, which included compression softening based on the Vecchio-Collins model, as well as tension stiffening based on the Bentz model (Bentz 2000).

Following the simulated impact damage described earlier, the concrete section was restored using Emaco® T430 rapid-strength repair mortar with extended working time (ChemRex 2002). Due to the vast size of the damaged region, 3/8 in rounded aggregate was added to increase the strength of the mortar, minimize shrinkage, and maintain an equivalent modulus of elasticity value. The compressive strength of the repair mortar was 6300 psi, as shown in Section 4.3.

To restore the loss of four prestressing strands, or 14.3 percent of prestressing, in AASHTO2, the Fyfe© CH-41 composite and Tyfo© S two part epoxy (Fyfe 2006) system was chosen. The amount of CFRP repair material required to restore the original capacity of AASHTO2 was determined using RESPONSE 2000©. Several of the input parameters follow: 1) the compressive strength of the girder was estimated to be 6000 psi, and 3000 psi for the deck, and 2) the 250 ksi prestressing strands were modeled using the Ramberg-Osgood function (Equation 4.1) for low relaxation strands. The design material properties for the CFRP system were provided by the manufacturer’s data sheet:

Ultimate tensile strength for design laminate:	143,000 psi
Laminate thickness:	0.04 in
Tensile Modulus:	13.9×10^6 psi

Ultimate elongation: 1.0%

Following a procedure similar to that described in Appendix A, it was concluded that three layer of 16 in wide longitudinal CFRP sheets were needed to restore the original ultimate flexural capacity of the girder. In order to minimize the initiation of new cracks in the repaired concrete, addition longitudinal sheets were provided; a 6 in wide sheet was placed on the top of the bottom flange and a 12 in sheet was placed in the middle of the web. These sheets were provided on both sides of the girder to ensure symmetry of the section. In order to ensure proper utilization of the CFRP's strength and strain capacity, adequate development length of the sheets was provided. Twelve 12 in wide transverse CFRP U-wraps were provided along the repaired section to prevent interfacial debonding of the longitudinal sheets. Full details of the CFRP reinforcement are described below, as well as a full schematic shown in Figure 4.3:

1. The three bottom layers of longitudinal CFRP reinforcement were extended 7.5 ft past the location of the ruptured prestressing strand. This length was chosen to ensure full development of a 0.5 in diameter prestressing strand, as well as full development of the CFRP sheet.
2. The termination points of the longitudinal CFRP were staggered at a distance of 1.5 ft to prevent plate-end debonding.
3. Two 6 in sheets and two 12 in sheets were installed on the top face of the bottom flange and middle of web, respectively. These four sheets were to control cracking in the non-prestressed, damaged location. These sheets extended the same length as the longest longitudinal CFRP sheet. Twelve inch wide transverse CFRP U-wraps were spaced along the entire length of the longitudinal CFRP reinforcing sheets. The U-wraps were placed at the termination point of each longitudinal CFRP sheet, as well as at three other locations beyond the damaged region. The U-wraps extended from the top flange of the girder on one side, down to the bottom of the girder and back up to the top flange of the other side.
4. An additional two U-wraps, 2 ft in width, were provided to completely encapsulate the area of repaired concrete. The sheets were overlapped by 1 in to prevent the formation of cracks between the sheets. These two sheets were provided to control crack growth within the non-prestressed repair mortar. It should be noted that completely encapsulating the entire length of the girder should be avoided because of the concern of moisture build-up between the CFRP and concrete.

The completed installation of the CFRP system for AASHTO2 is shown in Figure 4.21

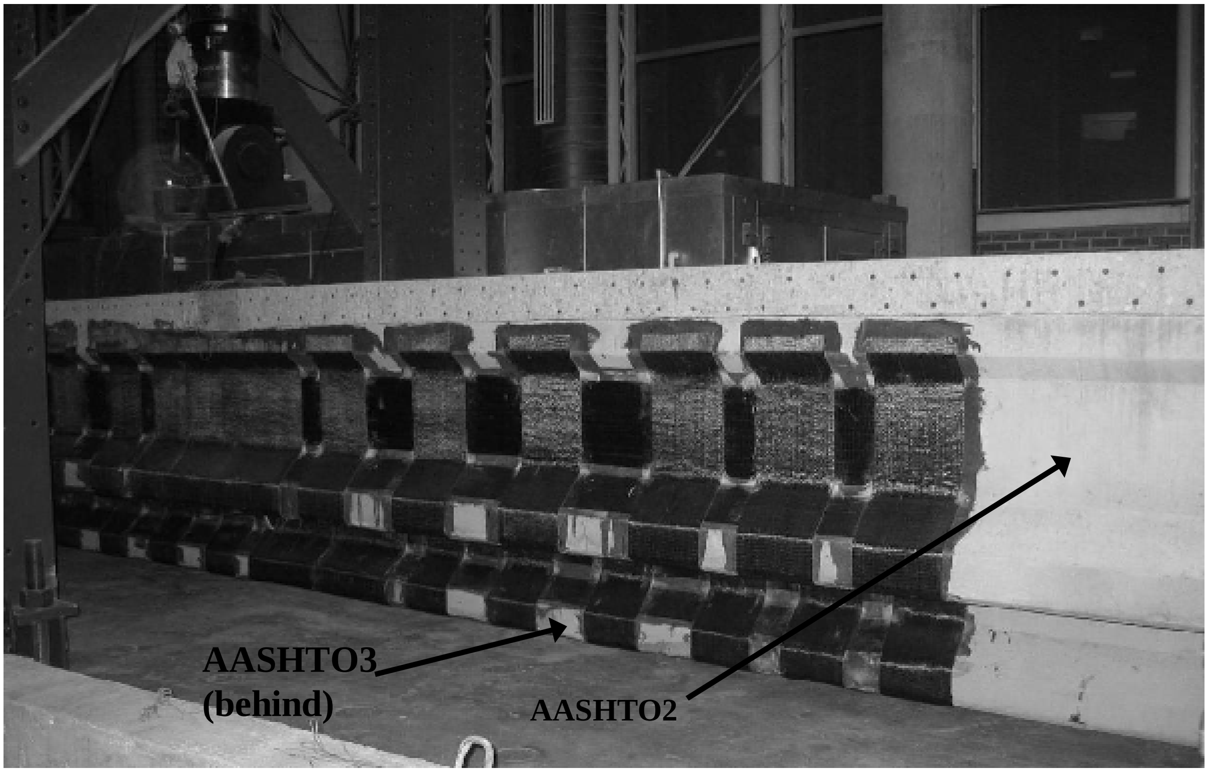

Figure 4.21 CFRP repaired AASHTO2 girder

AASHTO3

As with AASHTO2, the first task in the design of the CFRP repair system for AASHTO3 was to determine the ultimate flexural strength and load vs. deflection behavior of the undamaged specimen. The ultimate capacity of the section was predicted using the previously described cracked section analysis program RESPONSE 2000© and was verified by loading the girder as described in Section 4.6.

The restoration of the concrete section was performed in the same manner previously described for AASHTO2. Likewise, the same design procedure and same CFRP materials were used in AASHTO3. However, unlike AASHTO2, AASHTO3 was comprised of 270 ksi prestressing strands.

Following a procedure similar to that described in Appendix A, it was concluded that three layers of 16 in wide longitudinal CFRP sheets were needed to restore the original ultimate flexural capacity of the girder. The full details of the CFRP reinforcement are the same as those previously described for AASHTO2. The CFRP repair details are shown in Figure 4.7.

AASHTO2R

The purpose of applying CFRP to the damaged AASHTO2R girder was to restore the original ultimate shear strength, as well as the flexural capacity of the section. Wet lay-up sheets were chosen as the CFRP repair system for the reasons previously described in Section 4.4. The shear and longitudinal CFRP sheets were designed according to the analysis procedures outlined in Chapter 5. The full CFRP repair system is outlined below:

1. Three 16 in longitudinal sheets were installed on the bottom flange of the girder to restore the moment capacity of the damaged section. The amount of CFRP was the same required for the AASHTO2 flexural test specimen.
2. The termination points of the longitudinal CFRP were staggered at a distance of 2 in to minimized plate-end debonding effects.
3. Two layers of 6 in wide transverse CFRP sheets were oriented perpendicular to the anticipated shear cracks to fully utilize their unidirectional strength. A 0.5 in space was left between each sheet to allow for moisture evaporation and allow for possible inspection. The transverse sheets started at the top flange of the girder, and made a 45 degree angle to the bottom of the girder. Once it reached the bottom, the sheet was smoothly transitioned and extended to the opposite side of the bottom flange before being terminated. This configuration created a crossing pattern on the bottom of the girder, as shown in Figure 4.22. This pattern of diagonal sheets began at the left support and ended below the loading point.
4. Two 10 in sheets were installed on the intersection of the top face of the bottom flange and bottom of web. These two sheets were placed over the diagonal struts to control cracking in the non-prestressed, damaged location, smear the distribution of stresses and prevent straightening of the sheets caused by tension in the struts at the location of the chamfer between the web and bottom flange. These sheets extended the same length as the longest longitudinal CFRP sheet.

The completed installation of the CFRP repair system for AASHTO2R is shown in Figure 4.23.

Figure 4.22 CFRP crossing pattern on bottom of AASHTO2R girder

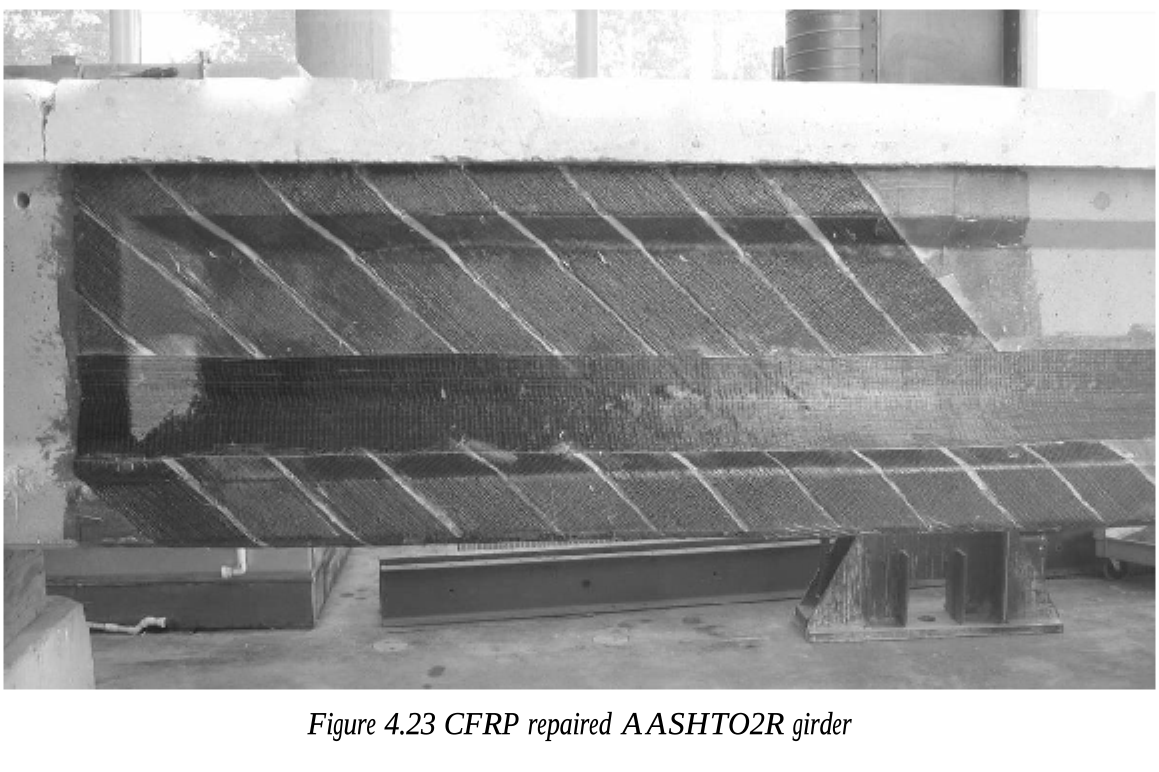

Figure 4.23 CFRP repaired AASHTO2R girder

4.5 Test Setup

This section discusses test setup for all five AASHTO Type II test specimens. AASHTO1 was first tested under fatigue loading conditions, which will be described later, before being tested to failure monotonically. AASHTO2 and AASHTO3 were tested in several cycles to failure. AASHTO2C and AASHTO2R were tested to failure under one loading cycle.

AASHTO1

The repaired AASHTO1 specimen was tested under fatigue loading conditions using a 110 k MTS hydraulic actuator. The 110 k actuator was chosen based on its high capacity servo-valve. This servo-valve allowed the girder to be tested at a higher frequency of cycles. The actuator was mounted to a steel frame which was located at midspan of the girder. As specified in AASHTO (2004), a 10 in by 20 in steel loading plate was placed in contact between the actuator and girder. A neoprene pad 11 x 21 x 0.5 in was placed below the load plate to evenly distribute the forces over any uneven surfaces on the girder. Figure 4.24 shows a drawing of the test setup for AASHTO1.

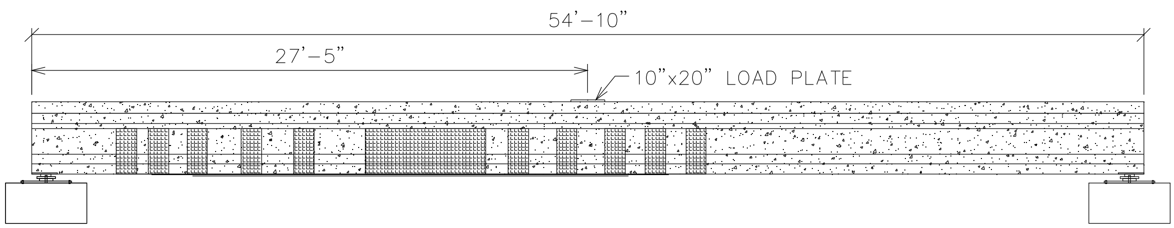

Figure 4.24 AASHTO1 test setup

For the end supports, 22 x 9 x 2.5 in neoprene pads were placed between two 1 in steel plates. The bottom plate measured 22 in by 30 in and the top plate measured 11 in by 30 in. The entire assembly was supported by a concrete block measuring 4 x 4 x 2 ft, as shown in Figure 4.25. The girder arrived at the testing facility with an 18 by 15 in flat steel plate built into each end, and an 18 in by 6 in curved steel plate then welded onto it. This latter plate was centered over the top of the support system.

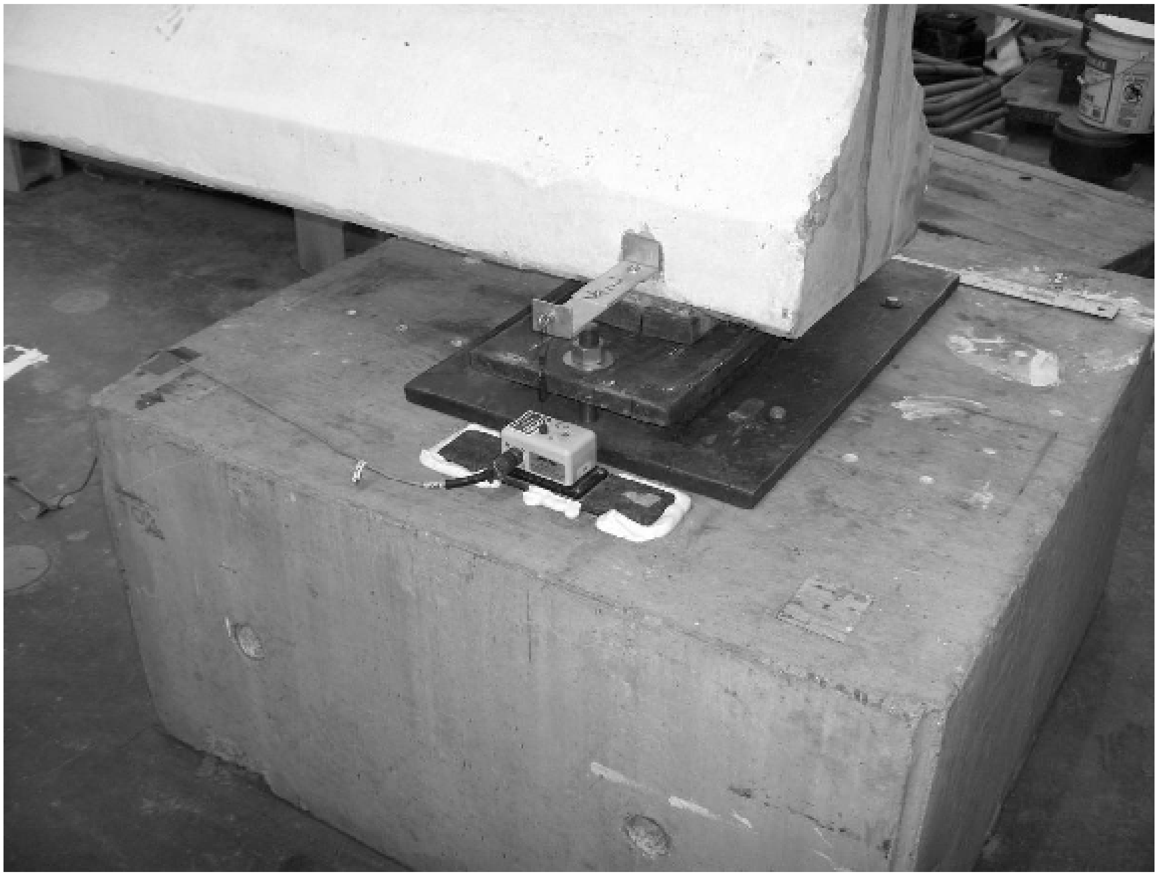

Figure 4.25 AASHTO1 girder support assembly

Fatigue Loading Range for AASHTO1

The fatigue loading range for AASHTO1 was described in detail in the previous report, Rizkalla *et al*. 2005.

AASHTO2 and AASHTO3

The repaired AASHTO2 and AASHTO3 specimens were cycled monotonically to failure using a 440 k MTS hydraulic actuator mounted to a steel frame located directly at midspan of the girder. The same load plate and neoprene pad described previously for AASHTO1 were placed between the actuator and girder. Figure 4.26 and Figure 4.27 show a drawing of the test setup for AASHTO2 and AASHTO3.

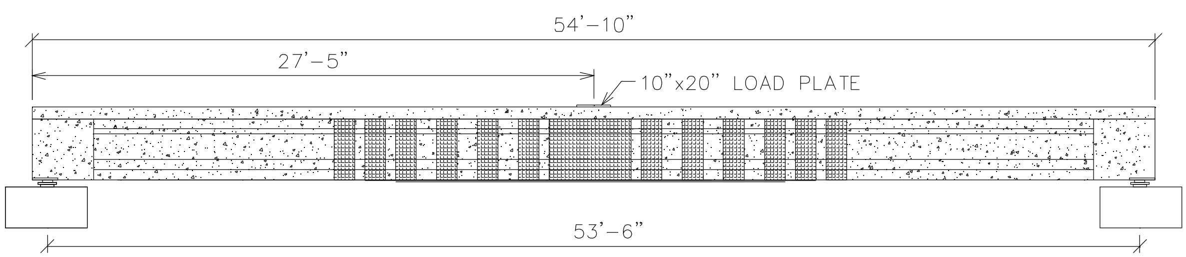

Figure 4.26 AASHTO2 test setup

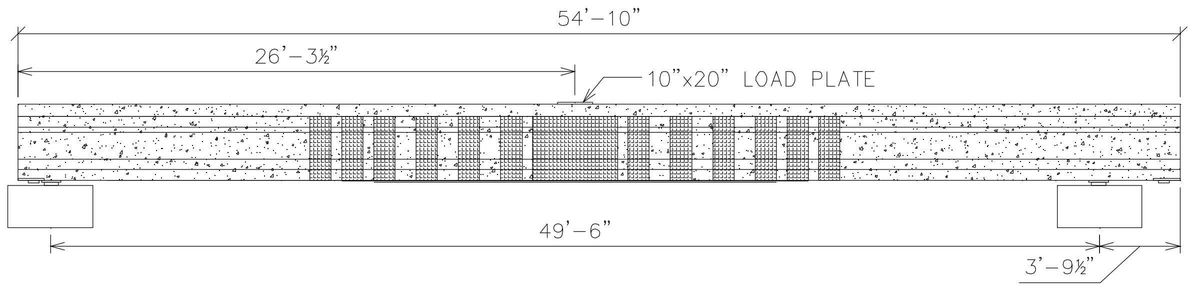

Figure 4.27 AASHTO3 test setup

The end supports for AASHTO2 and AASHTO3 were slightly different than the setup used for girder AASHTO1 Rizkalla et al. (2005). The supports were comprised of the 4 x 4 x 2 ft concrete support block, on which directly rested a 22 x 9 x 2.5 in neoprene bearing pad, and on which sat an 11 x 30 x 1 in steel plate. These were all placed beneath the 18 by 6 in curved steel plate already welded to the girder (Figure 4.28). The test setup for AASHTO3 was similar in that it used the previously mentioned concrete support block, neoprene bearing pad, and steel plate, however the difference is that since the supports were moved in to avoid the damaged end region, the 1 in steel plate was placed directly in contact with the concrete surface of the girder, as shown in Figure 4.29.

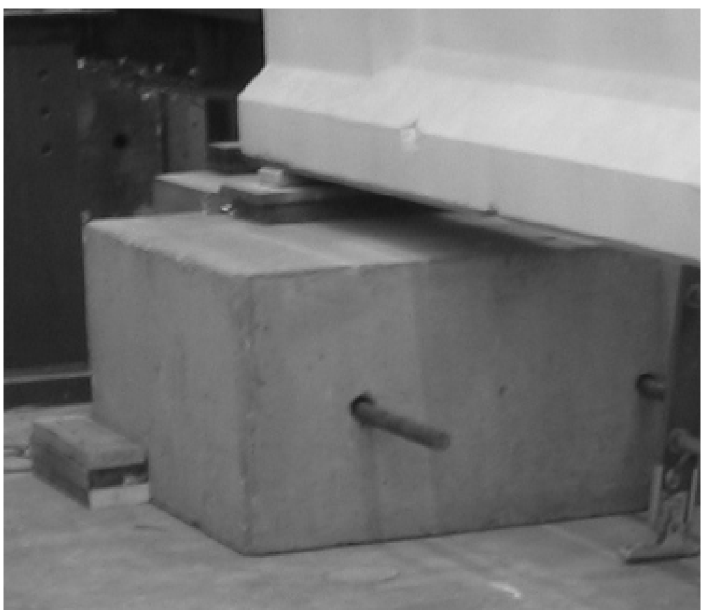

Figure 4.28 AASHTO2 girder support assembly

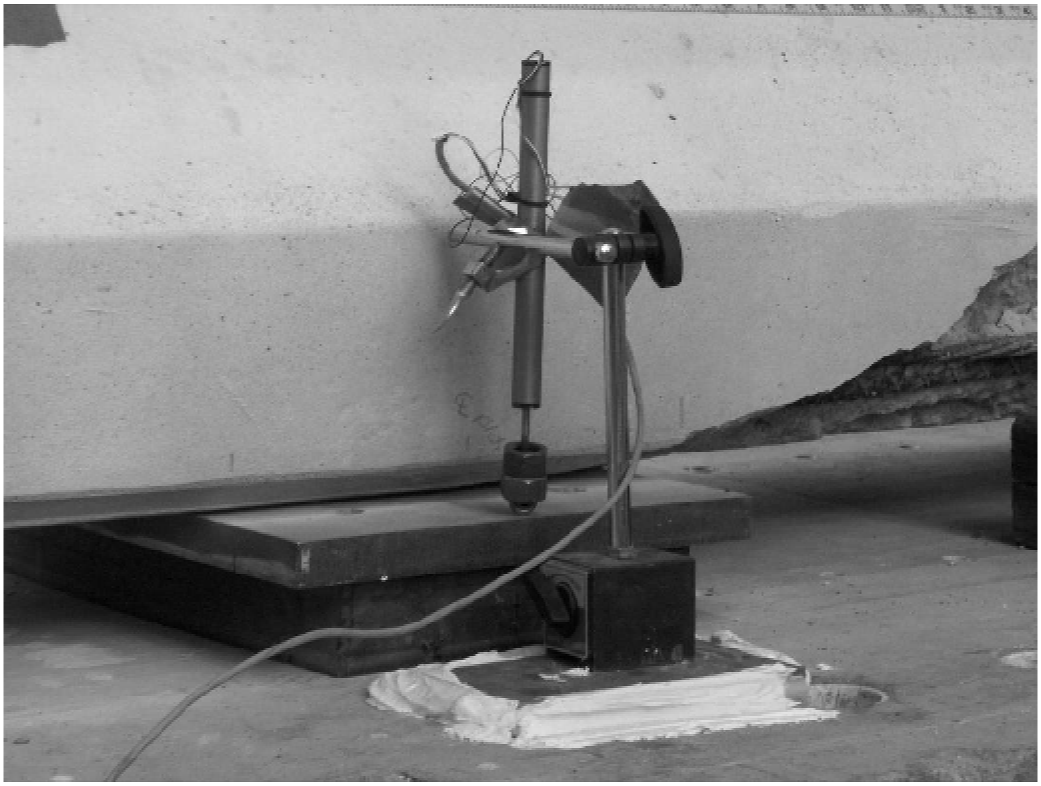

Figure 4.29 AASHTO3 girder support assembly

AASHTO2C and AASHTO2R

The test setup for both of the shear tests, AASHTO2C and AASHTO2R, were identical except for the loading mechanisms. AASHTO2C was tested to failure in one load cycle using a 440 k MTS hydraulic actuator mounted to a steel frame, while AASHTO2R was tested to failure using a 600 k hydraulic jack mounted to the same steel frame. A drawing of the test setup is shown in Figure 4.30. The loading mechanism was placed at 5.5 ft from the face of the left support of each girder, resulting in a shear span to depth ratio, a/d, of 1.57. The load was transferred to the girder through a 10 by 20 in and 11 x 21 x 0.5 in neoprene pad.

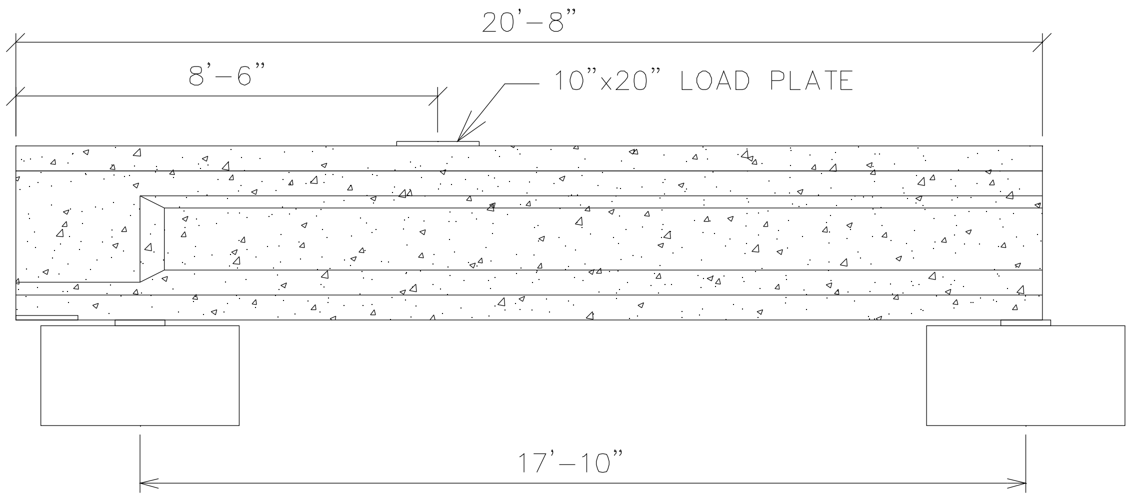

Figure 4.30 Test setup for shear study

The end supports for both AASHTO2C and AASHTO2R were the same as those previously described for AASHTO3 in Section 4.5. The right support was placed below the extreme right end of the girder, while the left support was placed beneath end block transition region in order to avoid any affects on the shear capacity that the end block would create.

4.6 Loading Scheme

AASHTO1

The loading of AASHTO1 consisted of three stages that all occurred after the installation of the CFRP repair system: 1) initial loading, 2) fatigue loading, and 3) final static loading to failure.

During the initial loading phase, the girder was loaded up to a level of 51 k, applied using displacement control loading. This load was selected to simulate a bottom tensile stress in the girder of $3\sqrt{f'_c}$ ksi, in order to evaluate the observed stress ratio in the lower prestressing strands and load-deflection behavior of the girder at this load level. The fatigue loading regime was performed by oscillating between 18.7 k and 45.2 k to simulate the dead load to the dead load plus live load, as determined in Section 4.5. The load was applied using a 110 k actuator, at a frequency of 2 Hz, for two million cycles. At regular intervals, the fatigue test was stopped to record data during intermediate static tests. The final static test of the girder consisted of several intermediate cycles of progressively increasing load up to a failure load of 136.1 k.

AASHTO2 and AASHTO3

The loading of AASHTO2 and AASHTO3 consisted of four stages: 1) initial loading of undamaged specimen, 2) loading after removal of concrete section, 3) loading after cutting of prestressing strands, 4) final static loading to failure after CFRP repair.

During the initial loading of AASHTO2, the girder was first loaded to 75.6 k then unloaded to 5.0 k. Immediately following the previous cycle, the girder was loaded to 105.9 k. Similarly, AASHTO3 was first loaded to 62.6 k, unloaded to 2.0 k, then reloaded to 89.0 k. These loads were selected to evaluate the cracking and crack reopening loads of the girder, as well as the load-deflection behavior of undamaged specimen. Initially loading of both girders was also intended to ease the removal of the desired concrete section. After the desired amount of concrete was removed from each girder, AASHTO2 and AASHTO3 were loaded to examine any changes in the load-deflection behavior; 60.3 k and 50.3 k, respectively. Following the cutting of prestressing strands, AASHTO2 and AASHTO3 were again loaded 50.3 k and 50.2 k, respectively. The final static test of each girder consisted of two cycles up to a failure load of 135.1 k for AASHTO2 and 145.4 k for AASHTO3.

AASHTO2C and AASHTO2R

The loading of AASHTO2C and AASHTO2R was performed in one cycle up to failure. No initial tests were performed after the removal of the concrete or cutting of prestressing strands for fear that an unexpected brittle failure could ruin the test specimens. The ultimate failure load of AASHTO2C was 413.7 k. The ultimate failure load of AASHTO2R was 446.3 k.

4.7 Instrumentation

AASHTO1, AASHTO2, and AASHTO3

The displacement profile along the length of each girder was measured using string potentiometers. The tensile strain in the longitudinal CFRP was measured using 0.236 in TML FLA-6-11 120 Ω electrical resistance strain gauges. The compressive strain in the deck and girder were measured using both PI gauges (a strain gauge mounted to a spring plate) and 2.36 in TML FLA-60-11 120 Ω electrical resistance strain gauges. The location of the instrumentation was selected to determine: 1) the strain profile at the damaged region, 2) the behavioral differences between the damaged and undamaged section, if applicable, and 3) the tensile strain in the CFRP to determine the bond characteristics between the CFRP and concrete. Figure 4.31 shows a drawing of the instrumentation used during the testing of AASHTO1. Figure 4.32 shows a drawing of the instrumentation used during the final testing of AASHTO2 and AASHTO3.

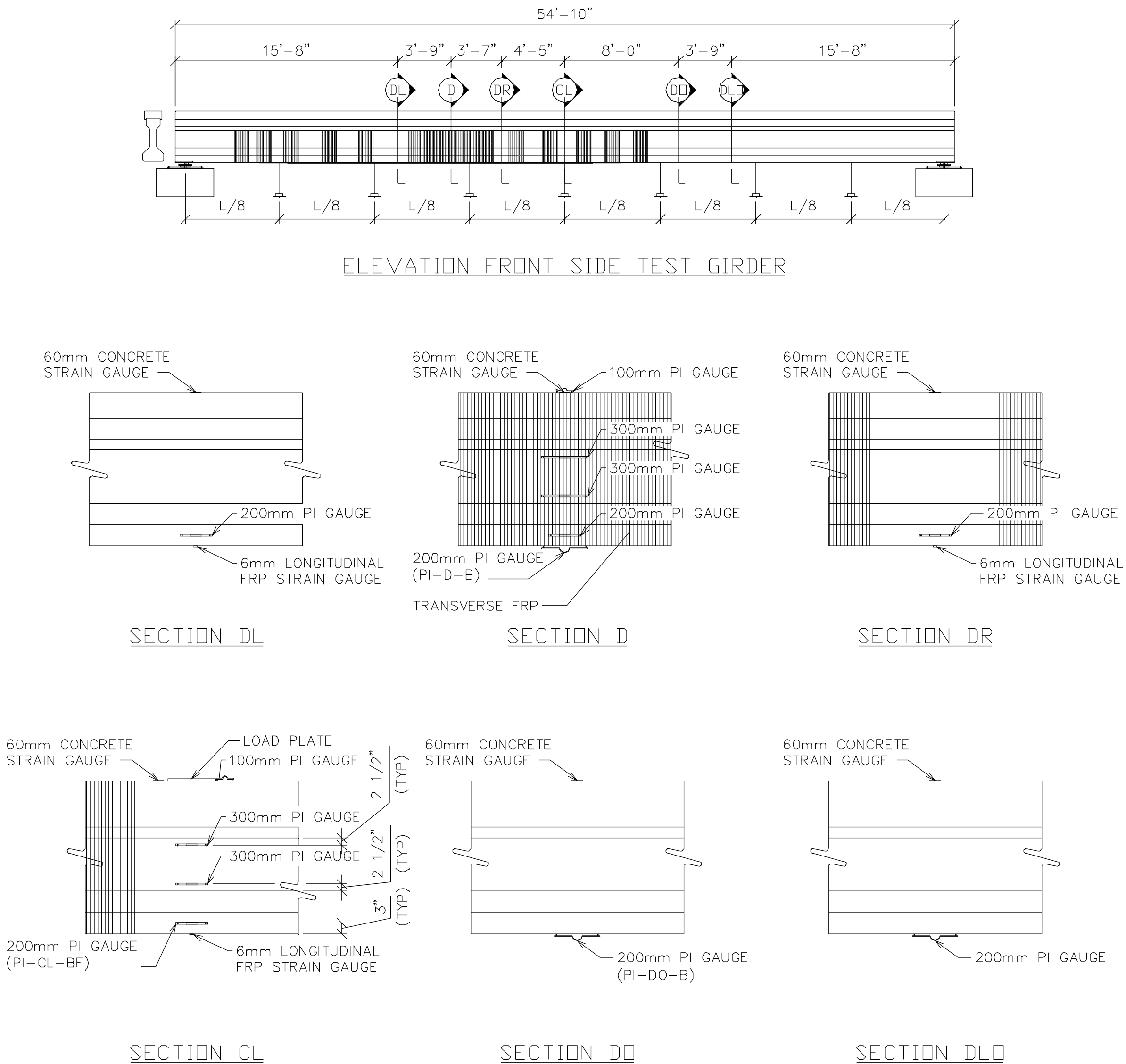

Figure 4.31 Repaired AASHTO1 instrumentation plan

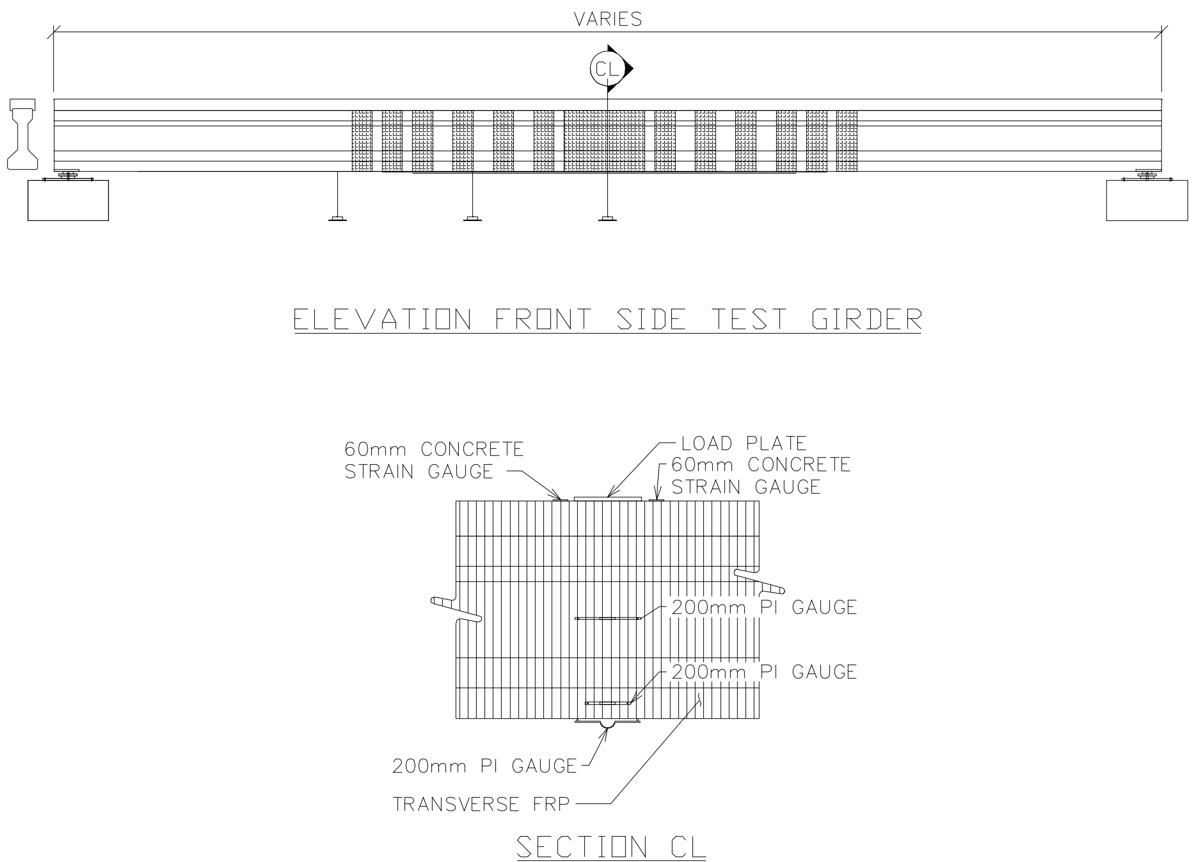

Figure 4.32 Instrumentation plan for AASHTO2 & AASHTO3 final static test

AASHTO2C and AASHTO2R

The displacement beneath the load point of each girder was measured using two string potentiometers. The compressive strain in the deck and girder were measured at midspan using both PI gauges (a strain gauge mounted to a spring plate) and 2.36 in TML FLA-60-11 120 Ω electrical resistance strain gauges. The shear crack widths were measured using three sets of two linear potentiometers oriented perpendicular to each other as shown in Figure 4.33. The location of the instrumentation for both girders was selected to determine: 1) the strain profile below the load point, and 2) to compare the crack widths of the control specimen with those of the repaired specimen. AAHTO2R was instrumented with 0.236 in TML FLA-6-11 120 Ω electrical resistance strain gauges along the CFRP diagonal struts to determine the strain distribution along the length of the girder.

Figure 4.33 Typical layout of linear potentiometers for AASHTO2C and AASHTO2R

4.8 Test Descriptions

AASHTO1

Visual cracking was first observed just outside the transverse U-wraps enclosing the damaged region at 42.0 k. The crack formed on the side of the girder with the ruptured prestressing strand. After the first three initial loading cycles, three additional visible cracks formed at the edge of the CFRP U-wraps in the damaged region. These cracks formed on the same side as the previous crack and extended from the edge of the CFRP U-wrap to the top of the bottom flange. It should be noted that the three cracks that formed during the initial static test did not significantly propagate during the fatigue loading phase. After the completion of 2 million cycles of fatigue loading, the midspan deflection of the girder, at 45.2 k, degraded from an initial value of 0.771 in to 0.922 in. This resulted in a total midspan residual deflection of 0.12 in due to fatigue-creep of the concrete (ACI 215 1997). As well, very little degradation in stiffness was observed in the girder.

The final static test of AASHTO1 was performed in various deflection increments. The girder was first loaded up to a level of 76.2 k at a rate of 0.1 in/min, resulting in a total deflection of 1.5 in. Both the midspan and damaged region flexural cracks extended through the bottom flange of the section as a result of this loading. The girder was then unloaded and reloaded up to a level of 90.0 k, resulting in a total deflection of 2.0 in. Cracking within the area of the longitudinal CFRP did not extend during this cycle, but new flexural cracks formed just beyond the right termination point of the longitudinal CFRP. The test was stopped because the capacity of the girder unexpectedly exceeded the capacity of the actuator.

The final test to failure began after installation of a 220 k actuator was completed. At a load of 101 k, the flexural cracks outside the longitudinal CFRP extended into the web. The presence of the longitudinal tension strut in the web prevented cracks in the damaged region from extending beyond the top of the bottom flange. Concrete crushing was observed in two locations at a load of 131.0 k: 1) on both sides of the loading plate at midspan and, 2) above the damaged region at the location of a saw cut in the deck. The maximum measured load was 136.0 k at a midspan deflection of 5.78 in. After the maximum load was achieved, a sudden drop of 2.0 k occurred. The load rate was then increased to 0.2 in/min until at a displacement of 6.17 in a large flexural-shear crack suddenly extended from the right termination point of the longitudinal CFRP to the concrete crushing zone near the loading plate. This flexural-shear crack caused catastrophic failure, as shown in Figure 4.34. Complete test results are presented in Chapter 6.

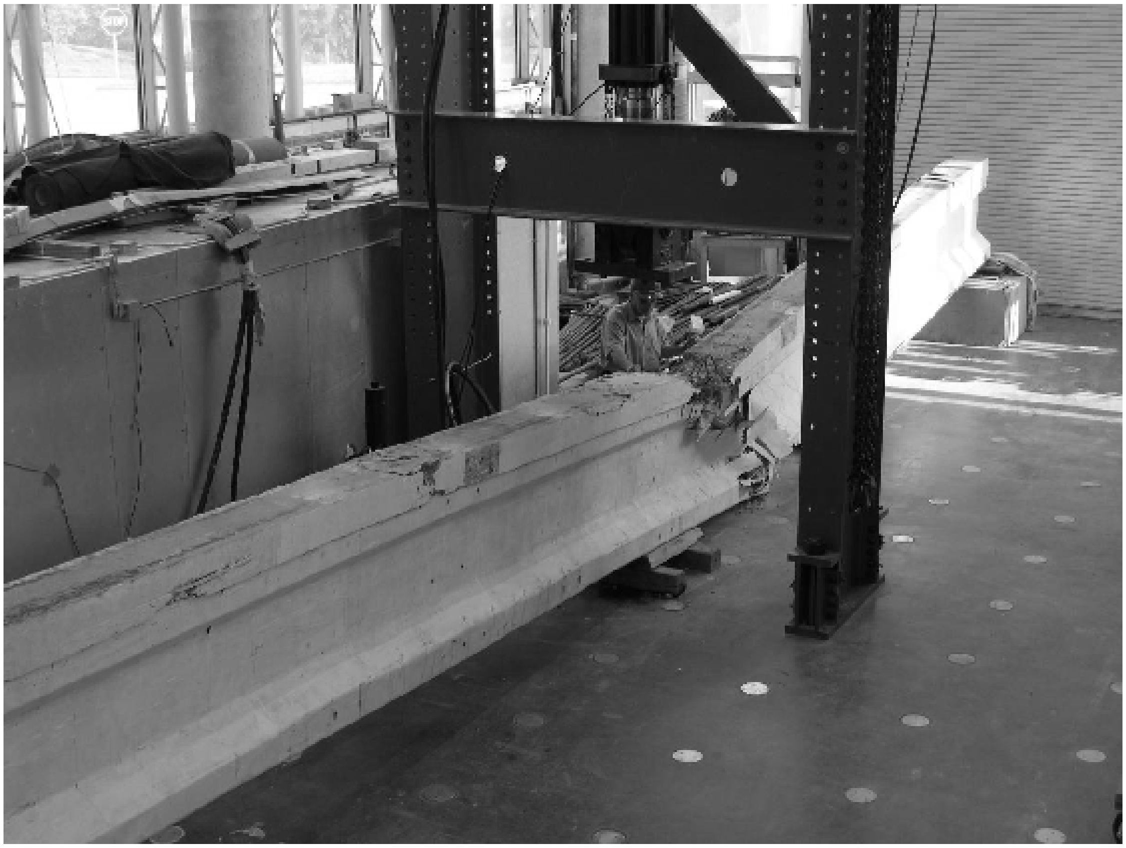

Figure 4.34 AASHTO1 girder after failure

AASHTO2

During the initial loading phase described in Section 3.6, visual flexural cracking of the undamaged specimen was first observed at 75.0 k, occurring directly below the loading plate at midspan. All loading in the initial phase was performed at 0.1 in/min and was unloaded at a rate of 0.25 in/min. The specimen was then reloaded again to 93.4 k to observe the crack reopening load, which was approximately 50.5 k. The girder was then unloaded and reloaded one final time to 104.7 k at a displacement of 3.09 in, which was estimated to be 90 percent of the girder's ultimate load capacity. The final initial load level caused a residual midspan deflection of 0.257 in.

Following the removal of the concrete section previously described in Section 4.2, the girder was loaded up to 60.0 k at a rate of 0.15 in/min then unloaded at a rate of 0.25 in/min after the behavior of the girder became nonlinear. A residual deflection of 0.415 in formed between the first initial loading up to 60.0 k and the loading after the removal of the concrete section. After the cutting of prestressing strands, the girder was again loaded up to 49.3 k to examine the fully damaged behavior of the member, only resulting in an increase in girder deflection of 0.018 in. However, a loss of stiffness occurred due to the cutting of the prestressing strands. The test was terminated because of the sudden non-linear behavior of the girder.

After repaired using CFRP sheets, the final static test of AASHTO2 was performed in one cycle, monotonically to failure, at a load rate of 0.1 in/min. Cracking first occurred at midspan in the non-prestressed repair mortar at a load of 10.6 k and occurred at the undamaged side at 51.4 k. These cracks were not visible but were detected by instrumentation. The loading was continued up to 90.0 k then held to look for cracks, but none were visible. The girder continued to be loaded up to 112.9 k, but still no cracks were visible outside of the CFRP repaired region despite the load being significantly higher than the cracking load determined during the initial test. Localized concrete crushing occurred at the left edge of the loading plate on the side with the simulated damaged at a load of 125 k. Loading continued until the girder noticeably shifted approximately 1.0 in out-of-plane towards the damaged side. The maximum load achieved was 135 k with a midspan deflection of 4.77 in. The concrete crushing failure is shown in Figure 4.35. Complete test results are presented in Chapter 5.

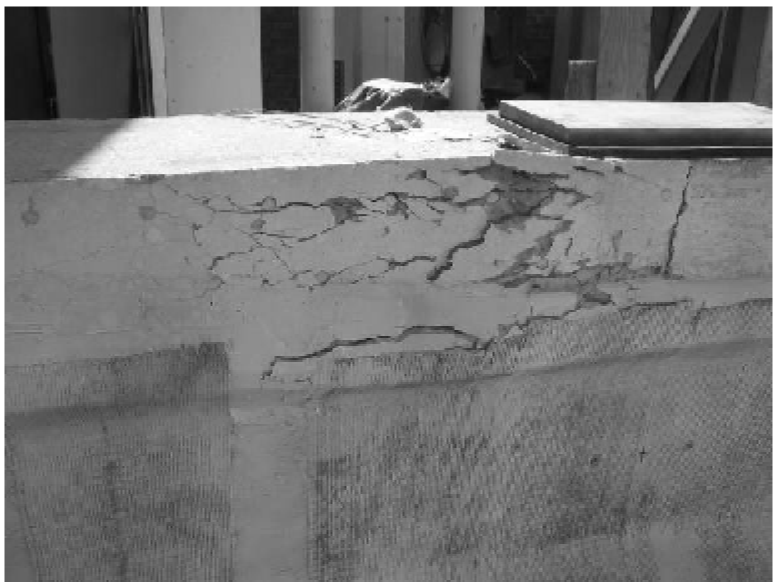

Figure 4.35 AASHTO2 girder localized concrete crushing

AASHTO3

During the initial loading phase described in Section 4.6, visual cracking of the undamaged specimen was first observed at a load of 59.0 k, occurring directly below the loading plate at midspan. All loading in the initial and post damaging phases was performed at 0.1 in/min while unloading occurred at 0.25 in/min. Additional flexural cracks formed as an additional three cycles were performed up to a load of 89.0 k. It should be noted that several small cracks did not form during the loading regime, but one large crack and several medium width cracks formed instead. The large crack extended all the way up through to the interface between the girder and deck. The final initial load was approximately 80 percent of the estimated ultimate capacity of the undamaged section. This load caused a residual midspan deflection of 0.240 in.

Following the removal of the concrete section described in Section 4.2, the girder was loaded up to 50.3 k at the same rate as the initial tests. A residual deflection of 0.024 in resulted after this test. After cutting the three prestressing strands, the girder was again loaded up to 50.2 k to examine the fully damaged behavior of the member, resulting in a residual deflection of 0.021 in. A loss of stiffness occurred in the girder after cutting of the prestressing strands.

The final static test of AASHTO3 was performed monotonically to failure in two cycles at a load rate of 0.1 in/min. The first visible crack appeared between two CFRP U-wraps just to the right of the fully encapsulated area; at a load of 65.0 k. The first cycle continued to load the specimen to 84.3 k where cracking was heard beneath the CFRP but was not visible. The girder was unloaded and reloaded to a maximum load of 145.5 k and a midspan deflection of 5.41 in. Failure of the girder was caused by crushing of the concrete beneath the left side of the load plate at 144.7 k, followed later by catastrophic failure as a flexural crack extended into the deck, splitting the member in two. Figure 4.36 shows the progressive failure of the AASHTO3 girder, and Figure 4.37 shows catastrophic failure of AASHTO3.

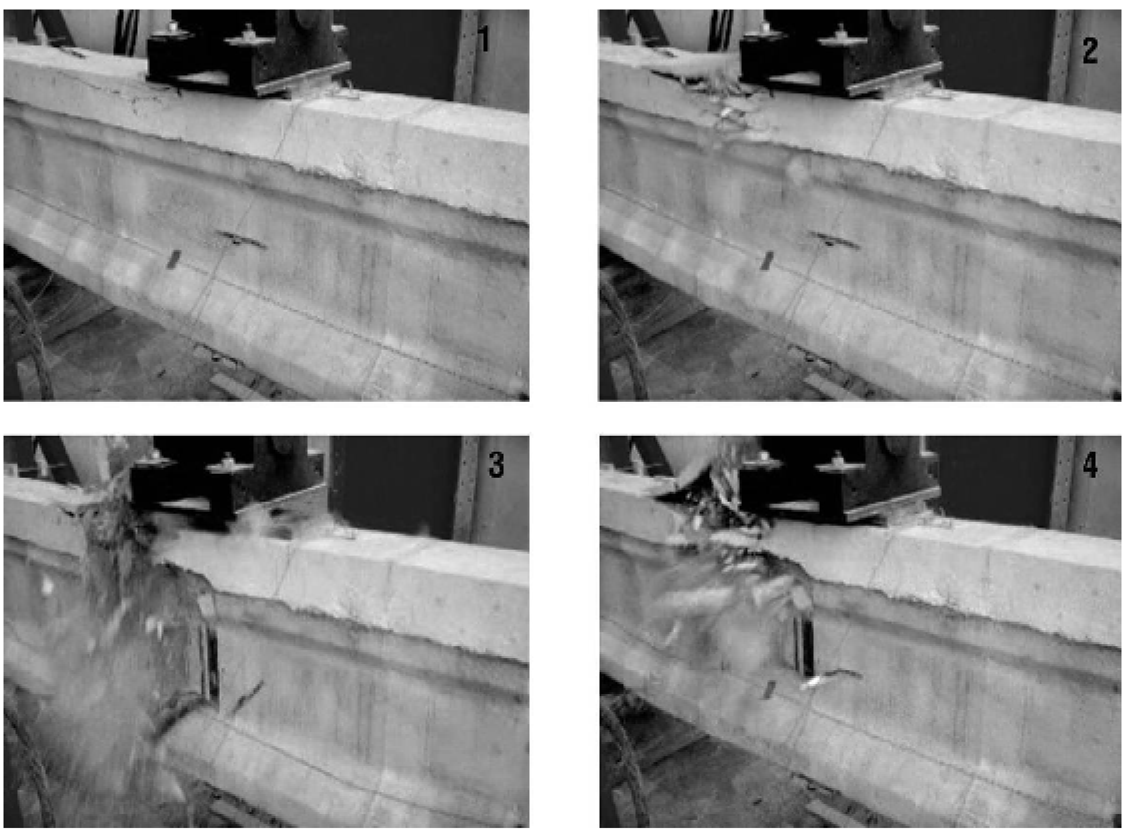

Figure 4.36 Progressive failure of AASHTO3 girder

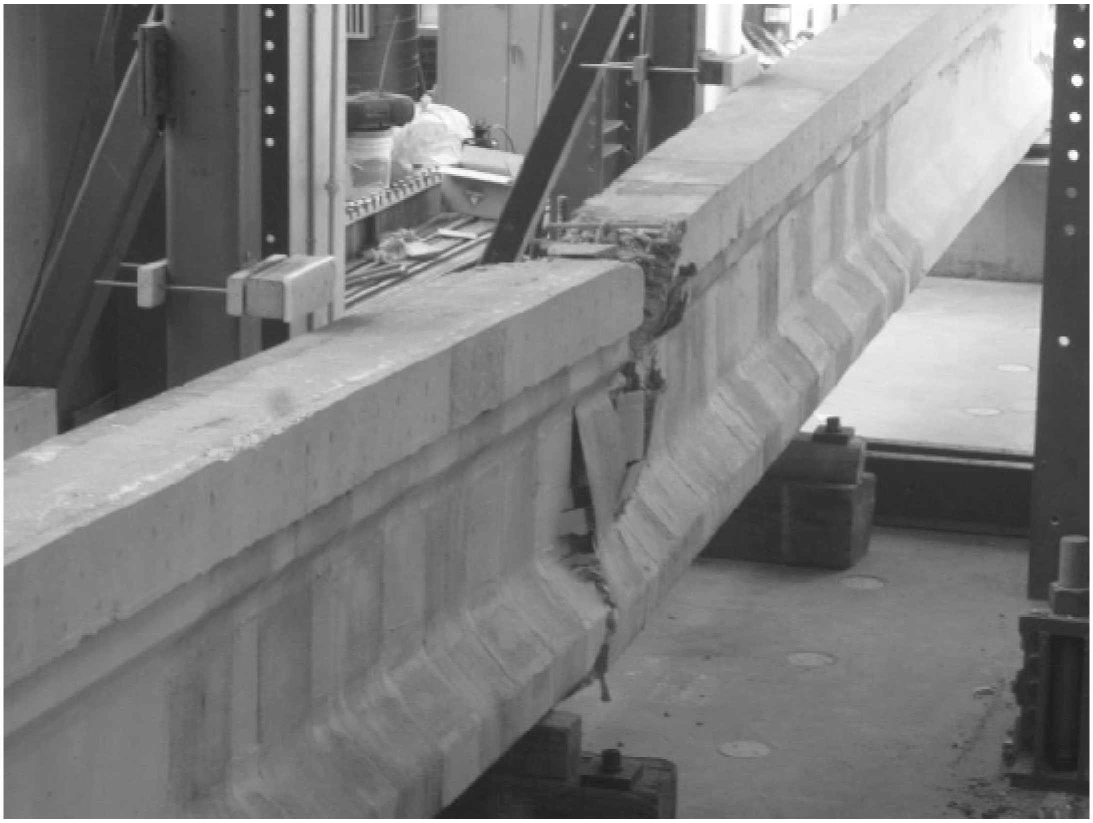

Figure 4.37 AASHTO3girder after failure

AASHTO2C

AASHTO2C was loaded at a constant rate of 0.05 in/min up to a load of 275 k, then loaded at a rate of 0.02 in/min up to failure. The first visual crack formed in the web at 45 degrees from the left support on the back side of the girder at a load of 225 k. Additional shear cracks formed in the web as the girder continued to be loaded up to its ultimate capacity of 413.7 k before failing in web shear. At ultimate, a shear crack on the shear critical span, left side, of the girder in the web propagated toward both the left support and left edge of the loading plate, causing the section to split along this line. The initial web shear cracks on the back side of the girder are shown in Figure 4.38, while the catastrophic web shear failure is shown in Figure 4.39. Complete test results are presented in Chapter 5.

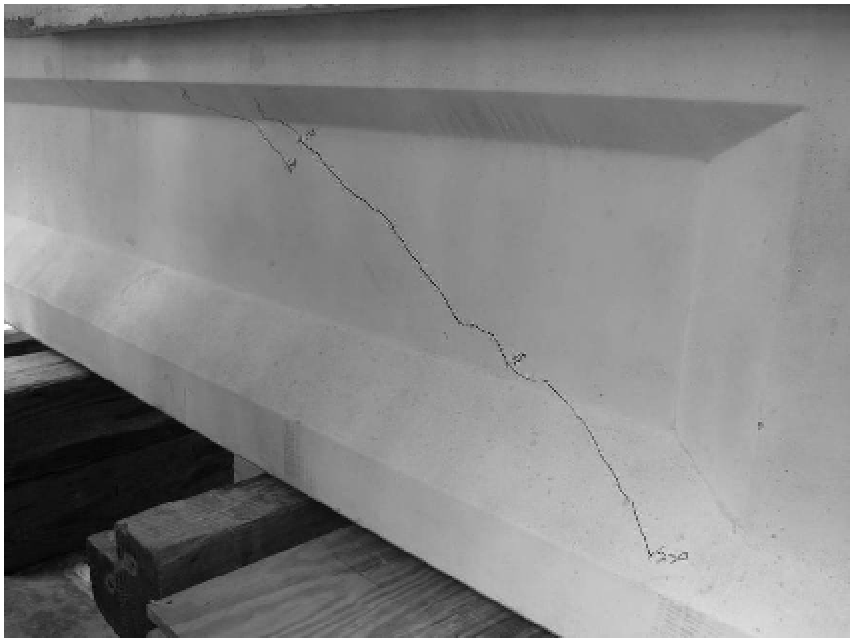

Figure 4.38 Initial shear cracks in AASHTO2C girder (back side)

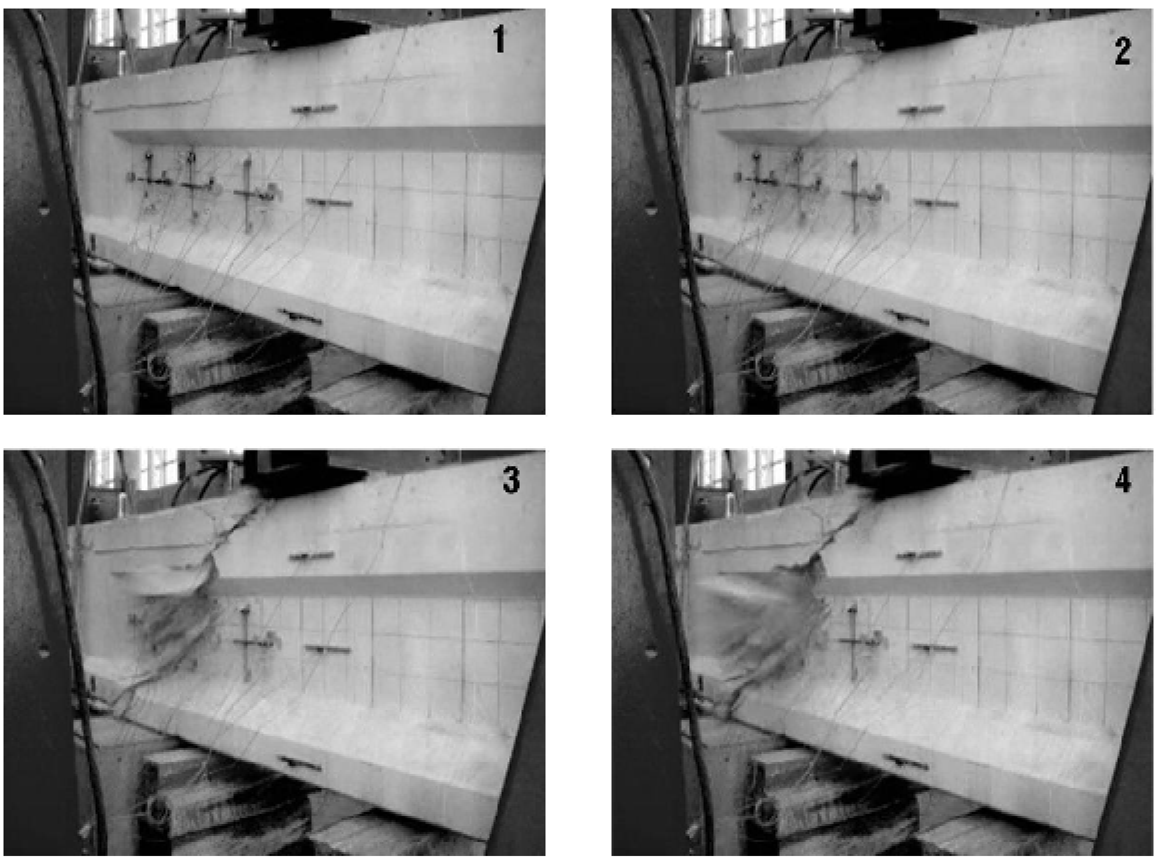

Figure 4.39 Progressive failure of AASHTO2C girder (front side)

AASHTO2R

AASHTO2R was loaded using a 600 k hand-controlled jack. The girder was loaded as evenly as was possible with the hand-controlled hydraulic unit. The first visible crack formed on the test specimen at a load of 344 k just beyond the right termination point of the CFRP on the front side of the girder. The crack that formed was a flexural crack, however other cracks were heard prior to this, but they were located beneath the diagonal CFRP struts and thus not visible. The girder was then loaded to an ultimate load of 446.3 k before shear forces in the right transfer region began debonding the prestressing strands, as shown in Figure 4.40. This debonding led to decreased flexural capacity on the right side of the girder, which ultimately resulted in a flexural-shear crack propagating through the right, undamaged, side of the specimen from the load point to the support. Plate end debonding at the right termination point of the bottom longitudinal CFRP also occurred in this same region. The flexural-shear failure is shown in Figure 4.41. It should be noted that the transverse CFRP sheets that are visibly debonded were not part of the shear study, but were left over from the flexural repair of the specimen. Complete test results are presented in Chapter 5.

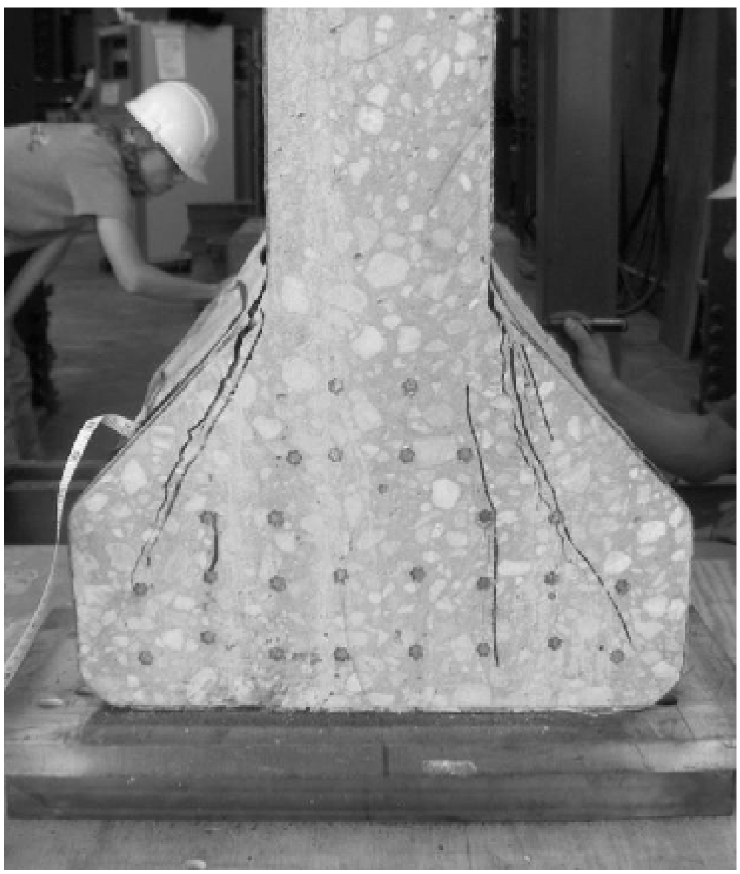

Figure 4.40 Failure in transfer zone of girder AASHTO2R

Figure 4.41 Failure of AASHTO2R girder (front side)

5 C-CHANNEL TEST RESULTS AND DISCUSSION

In order to present the test results along with their analytical predictions, the results of the tested girders as well as descriptions of several analytical procedures are presented in this section. Test results are presented to compare the behavior of the various strengthening systems used in this research and the capability of the analytical modeling to predict the behavior. Three types of analytical modeling are described in this section: a flexural model developed to predict the short term response of the strengthened girders, a finite element simulation, and a cracked section analysis computer program. Test results for the strengthened C-Channel girders tested under static and fatigue loading are presented as well as the test results of the repaired AASHTO girders tested under static and fatigue loading conditions.

5.1 Modeling

Flexural Model

The short-term response of the FRP strengthened prestressed concrete members tested experimentally in this research was determined using a layer-by-layer moment-curvature analysis. Using the plane sections remain plane assumption, the strain profile at any depth through the section can be determined from two variables: the strain in the extreme compression fibers (ε_t) and the depth to the neutral axis (c), as shown in Figure 5.1. The procedure begins by fixing ε_c and assuming a value for c. The integration of the internal stresses over any section must be equal to the sectional force or, in the case of no externally applied axial load, equal to zero. It is an iterative process: if equilibrium condition is not satisfied, the value of c must be changed and the process begun anew. Once equilibrium is satisfied, the external bending moment applied to the section is found through integrating the moment resultant of the internal stresses. For a strengthened section,

$$\int_{A_c} f_c dA_c + \int_{A_s} f_s dA_s + \int_{A_{ps}} f_{ps} dA_{ps} + \int_{A_f} f_f dA_f = 0 \qquad (5\text{-}1)$$

$$\int_{A_c} f_c \, y \, dA_c + \int_{A_s} f_s \, y \, dA_s + \int_{A_{ps}} f_{ps} \, y \, dA_{ps} + \int_{A_f} f_f \, y \, dA_f = -M \qquad (5\text{-}2)$$

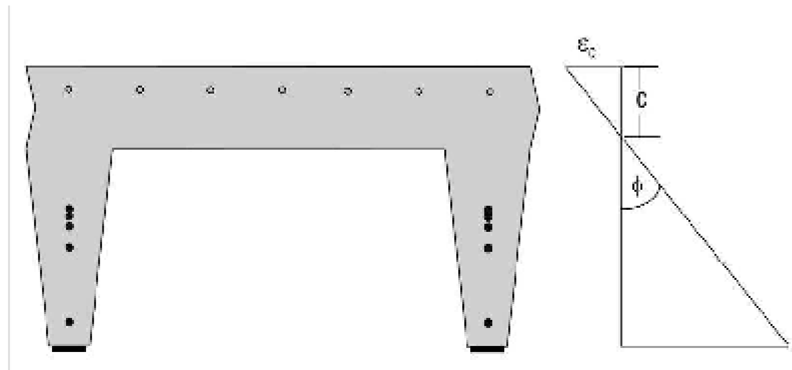

Figure 5.1 Cross-section and strain profile of strengthened girder

The full stress-strain relationship for concrete used is shown in Figure 5.2. Three separate behaviors are present which will be discussed individually: compressive (f_{c1}), uncracked tensile (f_{c2}), and cracked tensile (f_{c3}).

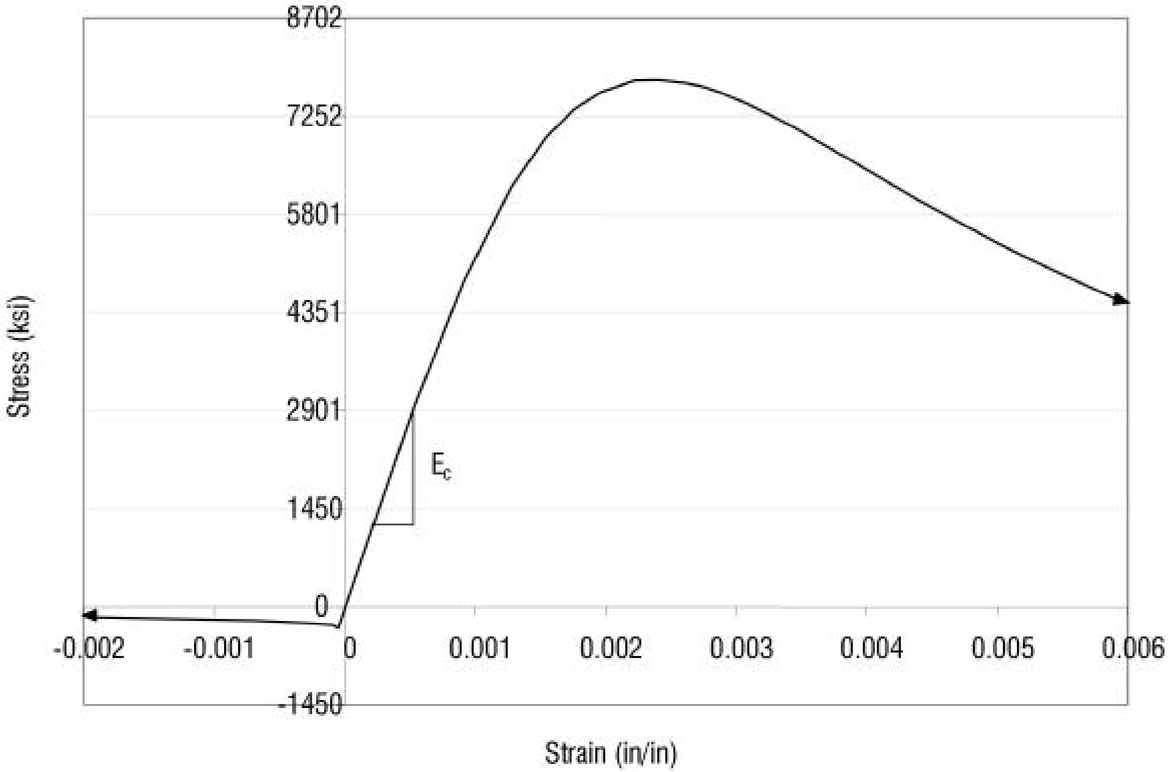

Figure 5.2 Stress-strain relationship of concrete

The compressive stress-strain relationship of concrete in flexural members will differ in shape and magnitude from that obtained through representative cylinder tests and can be attributed to the effects of casting the cylinders in forms having different compaction, curing and drying conditions than that of larger structural elements (Hognestad, 1951). Since the majority of the concrete cylinders tested under uniaxial compression in this study were taken from core samples taken from the tested structural elements, no calibration factor is warranted to account for this difference. The compressive model used (Collins and Mitchell, 1997) is based on an earlier model predicting the response of normal weight concrete cylinders to uniaxial compression (Popovics, 1973).

$$f_c = f'_c \frac{n(e_c/e'_c)}{n-1+(e_c/e'_c)^{nk}} \quad (5\text{- }3)$$

where ε'_c is the maximum value of the concrete compressive strain (ε_c). The factor n depends on the ratio E_c/E'_c, and the factor k describes the descending branch of the relationship and can be determined from cylinder tests. If only the maximum concrete strength (f'_c) is known, these factors can be determined for normal weight concrete from the following equations.

$$n = 0.8 + \frac{f_c^{'}}{17} \quad (5\text{- }4)$$

$$k = 0.67 + \frac{f_c^{'}}{62} \;\geq\; 1 \quad (5\text{- }5)$$

$$e'_c = \frac{f_c^{'}}{E_c}\frac{n}{n-1} \quad (5\text{- }6)$$

The initial tangent stiffness of the concrete, or modulus of elasticity of the concrete (E_c), was calculated by using the ACI Code (ACI 318, 2005) equation for normal strength concretes. For high strength concrete this equation has shown to overestimate E_c so the following equation was used if f'_c was greater than 6 ksi (Bentz, 2000):

$$E_c = 40{,}000\sqrt{f_c^{'}} + 1{,}000{,}000 \quad (5\text{- }7)$$

The uncracked tensile behavior of concrete was modeled as linear-elastic up to failure with the cracking strength (f_t) taken as (Bentz, 2000):

$$f_t = 5.4\left(f_c^{'}\right)^{0.4} \quad (5\text{- }8)$$

which corresponds to a cracking strength at any value of concrete tensile strain (ε_{ct}) as:

$$f_{c2} = E_c e_{ct} \leq f_t \quad (5\text{- }9)$$

The initial tangent tensile stiffness of concrete was assumed to have the same value as the compression stiffness.

Well reinforced cracked concrete still exhibits strength in tension, primarily in the effective embedment zone surrounding the longitudinal reinforcement. The tension stiffening effect is a result of bond stresses present below the neutral axis and between the flexural cracks. Tension stiffening can also be found away from the effective embedment zone, and the following model was used to estimate the effect (Bentz, 2000):

$$f_{c3} = \frac{f_t}{1+\sqrt{500(e_2)}} \tag{5- 10}$$

where ε_2 is the concrete tensile strain beyond cracking and can be expressed as $\varepsilon_2=\varepsilon_{ct}- f_t/E_c$.

From earlier compatibility assumptions and using the coordinate system shown in Figure 5.3, the compressive and tensile strains in the concrete can be shown to be:

$$e_c = f\,y_1 \tag{5- 11}$$

$$e_{ct} = f\,y_2 \tag{5- 12}$$

where f is the curvature of the section. The total resultant of the internal stresses in the concrete can be expressed as:

$$\int_{A_c} f_c dA_c = C_c - T_{c1} - T_{c2} \tag{5- 13}$$

where C_c is the resultant of the concrete compressive stress, Tc_1 is the resultant of the uncracked concrete tensile stress, and Tc_2 is the resultant of the cracked concrete tensile stress. With strain relations shown above, these resultants can be expressed as:

$$C_c = \int_0^c f'_c \frac{n(f\,y_1/e'_c)}{n-1+(f\,y_1/e'_c)^{nk}} b(y_1)dy_1 \tag{5- 14}$$

$$T_{c1} = -\int_0^{f_t/E_c} E_c f\,y_2 b(y_2)dy_2 \tag{5- 15}$$

$$T_{c2} = -\int_{f_t/E_c}^{h-c} \frac{f_t}{1+\sqrt{500(f\,y_2 - f_t/E_c)}} b(y_2)dy_2 \tag{5- 16}$$

where h is the height of the section and $b(y_1)$ and $b(y_2)$ are the variable widths of the concrete section above and below the neutral axis depth respectively.

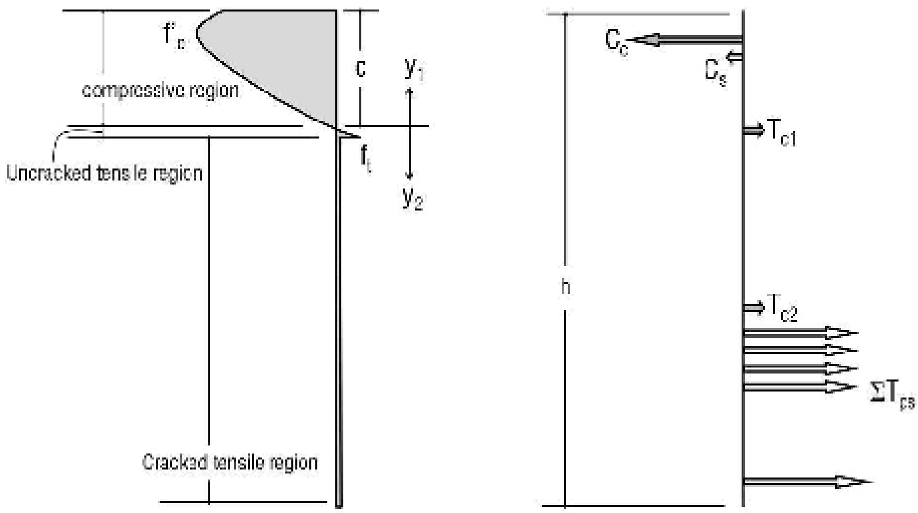

Figure 5.3 Internal stress resultants of FRP strengthened girder

The solutions to these integrals are best found using Simpson's rule:

$$\int_a^b f(x)dx \approx \frac{b-a}{3n}\left[f(x_0)+4f(x_1)+2f(x_2)+4f(x_3)+\cdots+4f(x_{n-1})+f(x_n)\right] \quad (5\text{- }17)$$

where n is the number of quadratic elements in the discretization.

The lever arms of the concrete resultants (d_{cc}, d_{ct1}, d_{ct2}) from the extreme compression fiber can be found by finding the centroid, or the first moments of the area divided by the area.

It is a more straightforward procedure to calculate the force resultants in a particular section curvature for the steel and FRP material. Since they can be broken down into discreet elements, no integration is necessary: just a solution of the closed-form stress-strain relationships. For the steel elements (both the regular reinforcing, and the prestressing strands) the Ramberg-Osgood equation was used to model the tensile behavior (Collins and Mitchell, 1997):

$$\left(f_s, f_{ps}\right) = E_s e_s \left\{ A + \frac{1-A}{\left[1+\left(Be_s\right)^C\right]^{1/C}} \right\} \leq f_u \quad (5\text{- }18)$$

where f_s is the steel tensile stress, f_{ps} is the prestressing steel tensile stress, E_s is the steel modulus of elasticity and ε_s is the steel tensile strain. The constants *A, B, C* can be calibrated with results from tension tests. Strain hardening effects in the regular reinforcing steel were not modeled.

The stress-strain relationship of FRP tensile coupons shows nearly linear-elastic behavior to failure. The behavior of FRP used as strengthening material on a reinforced or prestressed concrete member is quite different, and depends on many bond-related mechanisms. Assuming perfect bond, the material can be modeled as:

$$f_f = E_f e_f \leq f_{fu} \tag{5- 19}$$

where f_f and ε_f are the stress and strain in the FRP material, respectively, and E_f and f_{fu} are the elastic modulus and ultimate stress at rupture of the FRP material.

Through applying compatibility conditions, the strains in the steel and FRP material can be expressed as:

$$e_{si} = e_c \left(\frac{d_{si} - c}{c} \right) \tag{5- 20}$$

$$e_{psi} = e_c \left(\frac{d_{psi} - c}{c} \right) \tag{5- 21}$$

$$e_f = e_c \left(\frac{d_f - c}{c} \right) \tag{5- 22}$$

where ε_c is the strain in the extreme compression fiber of concrete, c is the neutral axis depth, and d_{si}, d_{pi} and d_f are the depth to the internal steel, prestressing strands and FRP materials respectively.

Next the force resultants in the steel (T_s), the individual prestressing strands i (T_{ps}), and the FRP material (T_f) can be found by multiplying the stresses with the corresponding areas:

$$T_{si} = \frac{E_{si} e_{si}}{A_{si}} \left\{ A + \frac{1 - A}{\left[1 + \left(B e_{si} \right)^C \right]^{1/C}} \right\} \leq f_y A_{si} \tag{5- 23}$$

$$T_{psi} = \frac{E_{psi} e_{psi}}{A_{psi}} \left\{ A + \frac{1 - A}{\left[1 + \left(B e_{psi} \right)^C \right]^{1/C}} \right\} \leq f_{pu} A_{psi} \tag{5- 24}$$

$$T_f = e_f n E_f t_f b_f \leq f_{fu} n t_f b_f \tag{5- 25}$$

where f_y and f_{pu} are the yield strength of the regular steel reinforcing and the ultimate strength of the prestressing strands. t_f and b_f are the thickness and width of the FRP material, and n represents the number of layers of FRP.

Using equilibrium conditions, the resulting force of the section can now be found by:

$$N = C_c + C_s - T_{c1} - T_{c2} - \sum T_{psi} - T_f \tag{5- 26}$$

If $N=0$, then the value for neutral axis depth (c) should be changed until equilibrium is obtained.

From the forces acting on the section as shown in Figure 5.3, the moment (M) acting on the section is:

$$M = T_{c1}d_{ct1} + T_{c2}d_{ct2} + \sum T_{psi}d_{psi} + T_f d_f - C_c d_{cc} - C_s d_s \tag{5- 27}$$

As different values of strain in the extreme compression fiber of concrete (ε_c) are assumed, a moment-curvature (M-f) relationship will be obtained. The load versus deformation response of the member can be calculated from the M-f relationship by numerically integrating the first moment of the curvatures over half the length of the beam:

$$\Delta = \int_0^{0.5l} f\, x dx \tag{5- 28}$$

The M-f behavior of the flexural model is shown in Figure 5.4. For the particular cross-section shown, which is modeled after girder EB1S, the model predicts a mode of failure of FRP rupture at a moment of 3208.4 k-ft. Soon after the rupture of the FRP, the lowest two prestressing strands rupture. After further curvature is applied to the section, the second layer of prestressing strands ruptures. Also shown in the figure is the M-f relationship determined from the computer program Response 2000, which is discussed later in this section.

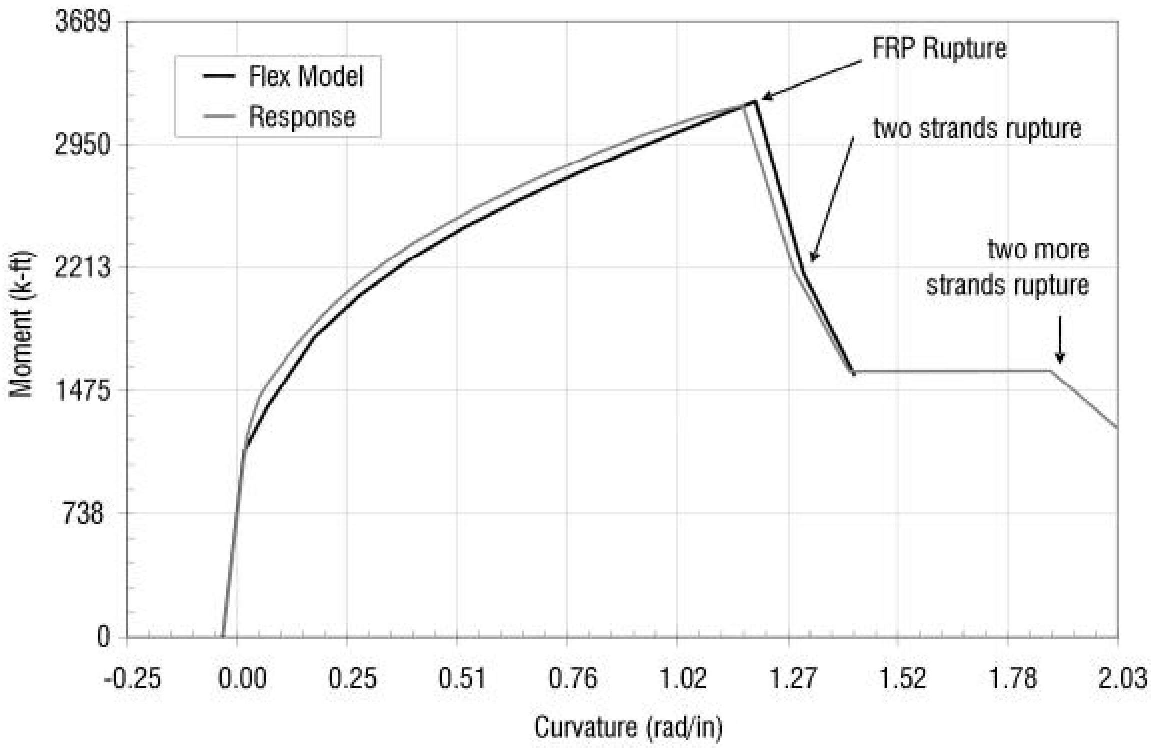

Figure 5.4 Comparison of flexural model with analysis program Response.

Finite Element Simulations

ANACAP is a non-linear finite element program for analysis of plain, reinforced and prestressed concrete members and structures and was developed by the ANATECH Corporation. The program was used to run finite element simulations on all the tested girders with the various repair and strengthening configurations. The 3-D modeling capabilities of ANACAP, along with advanced analytical models for the constituent materials, provide accurate predictions of the behavior of concrete structures (James 1997).

ANACAP uses the smeared cracking methodology for modeling of concrete where cracking is assumed to be distributed over an entire element. This mechanics-based philosophy uses plasticity theory that incorporates cracking and other concrete properties. Values for the elastic modulus and nominal compressive strength of concrete were obtained from testing of the concrete cores extracted from the tested girders. The effect of concrete confinement at different stress levels was incorporated into the analysis as well as an elastic modulus allowing for changes between the three distinct zones of the stress-strain curve of concrete – the initial linear region, strain hardening region and strain softening region. Opening and reopening of cracks can also be simulated for cyclic loading regimes and the program considers the effects of aggregate interlock and their effect in lowering shear capacity as crack widths increase at high load levels.

The stress-strain characteristics of the prestressing steel were based on material testing of prestressing strands. The ANACAP program considers other factors inherent in the behavior of reinforcing in concrete such as: 1) Bond slip, 2) Anchorage loss, 3) Discontinuities in strain at locations of cracks, and 4) Buckling of compression reinforcement after crushing of concrete. Characteristics of the CFRP material were also based on material testing and presented as perfectly linear elastic to failure. Since the original program was not designed for these types of materials, it was required to analyze the load-deflection response and terminate the behavior if the strain in the CFRP reached the desired rupture strain value.

The concrete cross section of the girder was modeled with 20 node elements using quadratic isoparametric displacement interpolation. The prestressing steel and the CFRP were modeled as sub-elements within the concrete section elements. Modeling the loading and supports reflected the conditions encountered during laboratory testing. The applied load was distributed at midspan over an area of 10 in x 20 in, and spring supports used to simulate the behavior of the neoprene pads. The load-deflection response of the modeled girders was obtained using ANACAP by the incremental application of the load up to failure. At each load interval, equilibrium is obtained and the stiffness of the member recalculated to adjust for nonlinearity. Experimental verification of the accuracy of the program can be found elsewhere (Hassan and Rizkalla 2003, 2004).

Cracked Section Analysis

In addition to the flexural model and the non-linear finite element simulations, a cracked section analysis was performed for the repaired and strengthened girders using Response 2000© software. Verification of this program can be found elsewhere (Bentz 2000). Due to limitations of the geometry input of the program, the concrete section of the C-Channel girders was modeled as a single-tee type section by combining the two webs of test girders. The cross section of the AASHTO girder was directly used without modification. Strength of the concrete for each girder was based on material testing of concrete core sample. The concrete behavior was modeled using the Popovics curve. Tension stiffening was included in the analysis. The prestressing steel was modeled using the Ramberg-Osgood function, using constants corresponding to the behavior observed in tension tests on samples taken from each girder. The CFRP was assumed to be linear-elastic up to failure with modulus of elasticity and rupture strain values determined from tension coupon tests.

Shear Model

An analysis technique utilizing two different design approaches was used to model the girder repaired with CFRP in shear. A method from the Precast/Prestressed Concrete Institute (PCI) (2006) design manual was combined with the shear analysis approach from ACI Committee 440 (2002). A brief summary and description of the model is provided here. A complete design example is provided in Miller (2006). There are several steps in the model for prediction of the shear capacity of an impact-damaged and CFRP repaired AASHTO girder:

1. The first step is to determine the shear capacity of the undamaged girder using the PCI (2006) guidelines.
2. The second step is to determine the flexural capacity of the undamaged girder.
3. The shear capacity of the damaged section is then evaluated using the PCI (2006) guidelines. The repaired section is modeled with the appropriate number of prestressing strands missing and concrete damaged. The difference in shear capacity between the damaged and undamaged is restored using CFRP sheets modeled using the recommendations of ACI Committee 440 (2002).
4. The last step is to restore the flexural capacity of the repaired section with CFRP sheets.

Step 1: Calculation of Shear Strength of Undamaged Section

The shear strength of the undamaged section was determined using the PCI Design Handbook (2006). The nominal shear strength along the length of the girder (V_n) was determined by finding the shear strength contribution from the concrete section (V_c) and the shear strength contribution from the steel stirrups. The detailed analysis included determining the web shear capacity (V_{cw}) and the flexure-shear capacity (V_{ci}) at each section:

$$V_{ci} = 0.6\sqrt{f_c^{'}}b_w d + V_d + \frac{V_i M_{cr}}{M_{\max}} \qquad (5\text{- }29)$$

$$V_{cw} = \left(03.5\sqrt{f_c^{'}} + 0.3 f_{pc}\right) b_w d + V_p \qquad (5\text{- }30)$$

where V_d is the shear force caused by the unfactored dead load, V_i is the factored shear force at a section due to externally applied loads, M_{cr} is the cracking moment of the section, M_{max} is the maximum factored moment at a section due to externally applied loads, f_{pc} is the compressive stress in concrete at the centroid due to effective prestressing forces, and V_p is vertical component of the effective prestress force at the section centroid. M_{cr} is the cracking moment and can be calculated as:

$$M_{cr} = \left(\frac{I}{y_t}\right)\left(6\sqrt{f_c^{'}} + f_{pe} - f_d\right) \qquad (5\text{- }31)$$

where I is the moment of inertia, y_t is the distance from the top of the girder to the center of gravity, f_{pe} is the compressive stress in concrete at extreme tension fiber due to effective prestressing forces, and f_d is the stress due to service dead load.

The shear strength contribution from the internal steel reinforcing (V_s) can be calculated as:

$$V_s = \frac{A_v f_y d}{s} \qquad (5\text{- }32)$$

where A_v is the area of the shear reinforcement, f_y is the yield stress of the shear reinforcement, and s is the spacing between stirrups. The nominal shear strength (V_n) is then determined by $V_n=V_c+V_s$ for several points along the length of the girder.

Step 2: Calculation of Flexural Strength of Undamaged Section

The moment capacity of the undamaged section can be calculated using a cracked section analysis approach similar to the one described in the previous section.

Step 3: Restore the Shear Capacity using CFRP

The third step in the shear model gives an analysis of the damaged prestressed concrete beam repaired with CFRP. This task was performed using the same procedure described in step one, with the application of an additional term to account for the presence of FRP materials (V_f) based on ACI Committee 440 (2002) guidelines. First the shear capacity of the damaged section should be calculated with an appropriate reduction in prestressing force contribution, and a reduced value for the concrete contribution (V_c) corresponding to the level of damage in the section. The nominal shear strength (V_n) can be calculated using:

$$V_n = \left(V_c + V_s + \psi_f V_f\right) \qquad (5\text{- }33)$$

where (ψ_f) is a reduction factor set equal to 0.95 for completely wrapped members and 0.85 for U-wraps. The shear contribution from the FRP material can be calculated using:

$$V_f = \frac{A_{fv} f_{fe} \left(\sin\alpha + \cos\alpha\right) d_{fv}}{s_f} \qquad (5\text{- }34)$$

where A_{fv} is the area of CFRP shear reinforcement, f_{fe} is the tensile stress in the CFRP shear reinforcement at ultimate, α is the angle of the CFRP, d_{fv} is the depth of CFRP shear reinforcement, and s_f is the spacing of the CFRP shear reinforcement. The tensile stress in the shear reinforcement can be calculated using $f_{fe}=\varepsilon_{fe}E_f$, where ε_{fe} is the effective strain in the CFRP system and E_f is the tensile modulus of elasticity of the CFRP.

The type of CFRP system used for shear strengthening determines the effective tensile strain permitted. The effective tensile strain for U-wrap systems was calculated using:

$$\varepsilon_{fe} = \kappa_v \varepsilon_{fu} \le 0.004 \qquad (5\text{- }35)$$

where κ_v is the bond-reduction coefficient, and ε_{fu} is the design rupture strain of the CFRP. The bond reduction coefficient is a function of the concrete strength, type of wrapping scheme, and laminate stiffness, and can be computed as follows:

$$\kappa_v = \frac{k_1 k_2 L_e}{11900\varepsilon_{fu}} \le 0.75 \qquad (5\text{- }36)$$

where k_1 and k_2 are modification factors that account for the concrete strength and type of wrapping system, and L_e is the active bond length over which the majority of the bond stress is maintained. The active bond length and modification factors are calculated as follows:

$$L_e = \frac{23300}{\left(nE_f t_f\right)^{0.58}} \tag{5- 37}$$

$$k_1 = \left(\frac{f_c^{'}}{27}\right)^{2/3} \tag{5- 38}$$

$$k_2 = \begin{cases} \dfrac{d_{fv} - L_e}{d_{fv}} & \text{for U-wraps} \\ \dfrac{d_{fv} - 2L_e}{d_{fv}} & \text{for two sides bonded} \end{cases} \tag{5- 39}$$

where n is the number of layers and t_f is the thickness of the FRP material.

Step 4: Restoration of the Flexural Strength of the Section

The damaged section may have lost significant flexural strength, and this should be restored using longitudinal FRP placed on the tension side of the beam. Using the cracked section analysis approach described earlier, a design for sufficient longitudinal FRP can be obtained.

5.2 Results and Discussion: Strengthening

A total of twenty-one prestressed concrete C-Channels were tested as part of the Strengthening Study: eleven girders under static loading conditions and ten girders tested under fatigue loading conditions. The experimental test results, discussion, and modeling predictions are provided in this section, divided into two sections representing the applied loading conditions. Part II of this study tested four concrete C-Channels: EB7F, EB7S, SRPS and SRPF.

C-Channel Static Tests

Eleven girders were tested monotonically to failure as part of the Strengthening Study: one was a control specimen, nine were strengthened with various carbon fiber reinforced polymer (CFRP) materials, and one was strengthened with steel reinforced polymer (SRP) material. The four girders for Part II of this study were prestressed with a Type C1 configuration (as designated in Chapter 3).

Type C1 Girders

Nine Type C1 girders were tested monotonically to failure, one control girder and eight strengthened girders. Summarized test results for Part II of this study are shown in Table 5.1.

Crack Development

Each of the girders was loaded up to the cracking load, unloaded, and reloading again to determine the cracking load and the effective prestress force which are shown in Table 5.1. Initiation of the flexural cracks was determined either by visual inspection or by analysis of the test data. Typically, cracking occurred between the loads 11.9 k and 14.1 k. Flexural cracks were located at the bottom of the C-Channel soffit near midspan, with a length near midspan equal to the depth of the girder from the edge of the loading area. Spacing of the cracks was approximately 13 in, which corresponds to the distance between the transverse stirrups used for the C-Channels. As the applied load increased, all the girders developed additional flexural cracks along the span at the same spacing.

Table 5.1 Summarized test results for Type C1 girders tested under static loading

Specimen Designation	CS	EB7S	SRPS
Strengthening	None	EB sheets	EB SRP
Cracking load, k	12.59	13.3	13.39
Ultimate load, k	33.2	43.23	48.58
Prestress losses, %	15.3	13.0	17.6
Effective prestress, k	16	16.46	15.58
% Increase in capacity	--	30.2	46.3
Ultimate concrete compressive strain, με	3000	3200	2800
Ultimate CFRP tensile strain, με	--	10500	10200
Exp/Manufacturer tensile strain in CFRP	--	103	65.8
Failure Mode*	C	C	C
Initial Stiffness**, k/in	28.4	27.9	27.3
Secondary Stiffness†, k/in	0.999	4.39	5.71
Structural Efficiency, %/k	--	4.07	12.14

* R = rupture of CFRP near midspan, C=Concrete Crushing
** defined from 2 k to 10.1 k
† defined from 28.1 k to 33 k

Beyond an applied load level corresponding to yielding of the prestressing strands (approximately 22.5 k), the cracking pattern of the control and strengthened girders diverged. Increasing load initiated more cracks between the existing cracks. At ultimate, the flexural cracking of the control specimen extended approximately 6.6 ft from each side of midspan. The flexural cracks of the strengthened girders extended farther at ultimate, up to 9.8 ft from each side of midspan. The CFRP strengthening reduced crack spacing, crack width and crack growth for all of the strengthened girders with respect to the control girder. For the girders whose failure was due to crushing of the concrete, it was observed that flexural cracks within the loading area changed their direction near ultimate and extended towards the loading area and formed a compression fan. The curvature of both the control and strengthened girders at failure was not sufficient to cause the flexural cracks to bifurcate, or fork, near the compression zone. The cracking pattern and crack widths generated from a Response 2000© analysis of the control girder, a girder strengthened 20 percent, and a girder strengthened 60 percent is shown in Figure 5.5 which is representative of the crack patterns and widths observed during the individual tests.

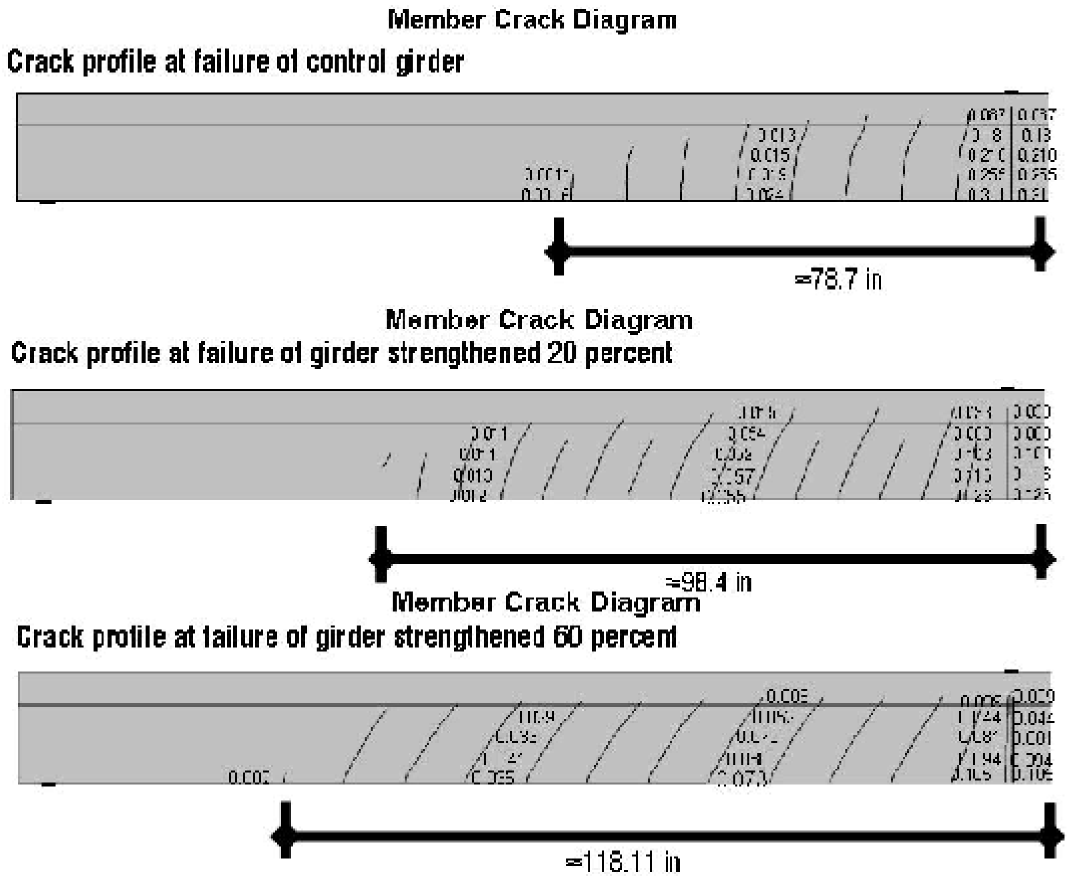

Figure 5.5 Response 2000© crack widths

PI gauges mounted near the bottom of the C-Channel soffit at midspan were used to measure the tensile strain in the concrete at various load levels. The average crack width at midspan can be calculated using the measured strains at any applied load level from the following equation:

$$CW_{ave} = \frac{(e_{ci} - e_{ccr}) \times l_{PI}}{n} \qquad (5\text{- }40)$$

Where ε_{ci} is the measured strain at a certain applied load level, ε_{ccr} is the measured strain in the concrete at the flexural cracking load, l_{PI} is the length of the PI gauge, and n are the number of cracks observed within the PI gauge length. The load versus the average crack width at midspan for the Type C1 girders is shown in Figure 5.6. The figure indicates that the presence of the strengthening system restrained crack opening and growth with respect to the control girder, CS. At ultimate, the crack widths of the strengthened girders were as much as 400 percent less than the control girder.

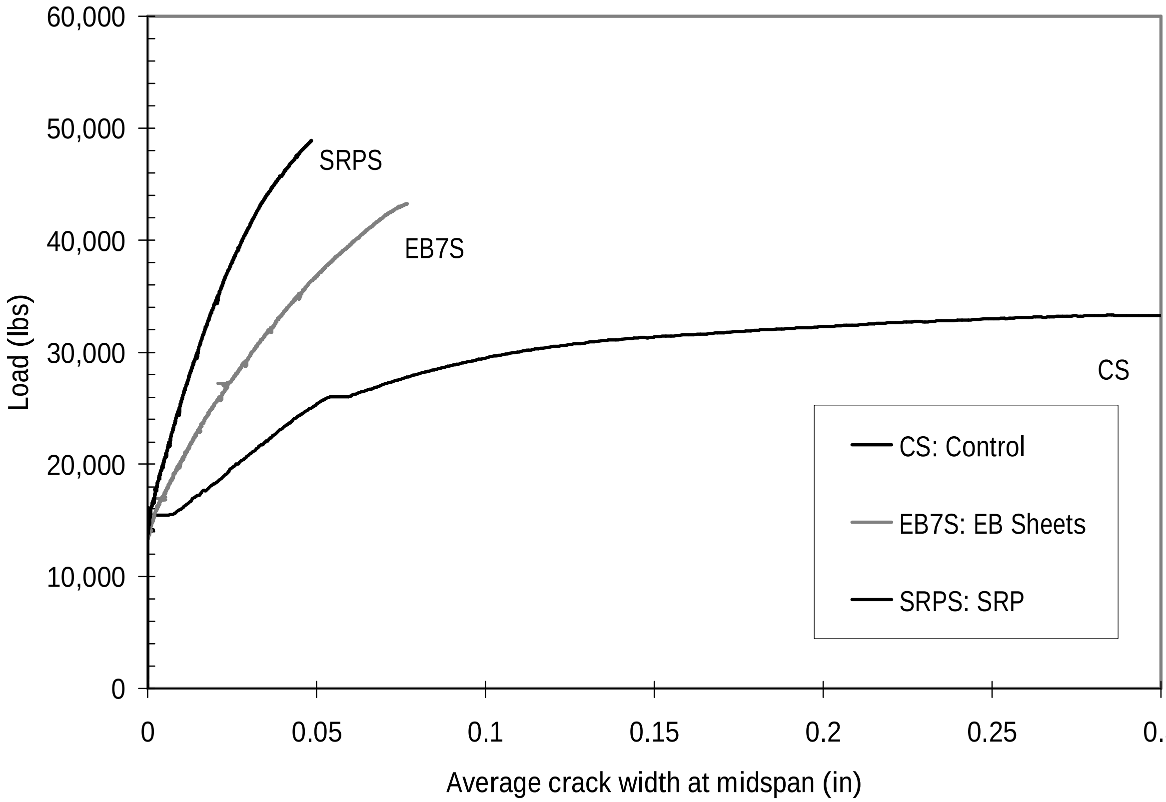

Figure 5.6 Load versus crack width for Type C1 girders tested under static loading

Stiffness

Prior to cracking, the strengthened girder and the control girder behaved elastically. Based on the load versus displacement relationships measured during the test, the initial flexural stiffness (k_i) of the C-Channels was determined for each tested girder and shown in Table 5.1.

Comparing the initial stiffness of the strengthened girders with the initial stiffness of the control girder, it was obvious that the strengthening system has very little effect on the initial stiffness. However, using a strengthening system to achieve a 60 percent increase in ultimate capacity, modest increases in initial stiffness can be obtained. The girder strengthened with high modulus strips increased the initial stiffness 14.7 percent above than the control specimen. The measured secondary stiffness, calculated within the load range 28.1 k to 33 k is shown in Table 5.1. This value represents the stiffness which is expected during an extreme overloading type event. Since girder EB3S did not reach loads corresponding to yielding of the prestressing strands before rupture of the CFRP, the stiffness was not calculated, although stiffness before rupture was high. As expected, the girder strengthened to achieve a 60 percent increase in ultimate capacity had the highest secondary stiffness for the Type C1 girders, six times the value determined for the control girder CS.

Effective Prestress

The effective prestress force in one strand (P_{eff}) of the Type C1 girders was determined from the loading and unloading scheme adopted at the beginning of each test. From the crack reopening load (P_{ro}) the effective prestress can be solved from:

$$\frac{10 \times P_f}{A_c} + \sum \frac{P_f e_i}{S_b} - \frac{w_D L}{8} \times \frac{1}{S_b} - \frac{P_{ro} L}{4} \times \frac{1}{S_b} = 0 \tag{5- 41}$$

where ω_D is the distributed self weight of the girder, e_i is the eccentricity of the prestressing strand with respect to the neutral axis of the section, L is the clear span length, A_c is the cross-sectional area of the girder, and S_b is the section modulus of the girder below the neutral axis. The measured values of effective prestress force per strand varied between 14.9 k and 16.2 k for girders with Type C1 prestressing configuration. From the C-Channel specifications, the initial jacking force was 18.9 k, equivalent to $0.7f_{pu}$ where f_{pu} was specified as 250 ksi. Long-term losses calculated using the initial jacking force varied between 13.0 percent to 21.2 percent for the girders with Type C1 prestressing configuration. Many of the experimentally determined values for losses are less than the value of 20.1 percent given in Collins and Mitchell (1991) for typical prestress losses in 250 ksi prestressing strands and the losses of 28.5 percent calculated using the AASHTO specification (2004) lump-sum method.

In some cases where the load corresponding to crack reopening was not determined, the cracking load itself was used to calculate the effective prestress in the strands by using the modulus of rupture for the concrete (AASHTO 2004) substituted for zero in Equation 5.30:

$$7.5\sqrt{f'c} \tag{5- 42}$$

Structural Efficiency

The structural efficiency (SE) of a CFRP strengthening system was evaluated using the following expression:

$$SE = \frac{S}{E_f A_f} \tag{5- 43}$$

where S is the percent increase in ultimate flexural capacity achieved using a CFRP system compared to the control girder and E_f and A_f are the elastic modulus and area of CFRP material respectively. Material properties of the CFRP, including thickness of the laminates, were measured for each case. The structural efficiency as defined represents how efficient the CFRP strengthening system is with respect to the amount of material and its stiffness. The CFRP systems failed due to the limited strain achieved at ultimate or debonding such was the case for the high modulus material and the CFRP strips respectively. The girders strengthened with externally bonded normal modulus sheets or steel reinforced polymer material achieved a high percentage of structural efficiency. In these cases, the amount of

CFRP material installed using the wet lay-up system, and as a result lower values of stiffness, gave lower values of structural efficiency.

Ultimate Load and Displacement

Test results indicate that the addition of a brittle material such as CFRP to a ductile structural member such as prestressed concrete does not reduce the overall ductility of the member. As shown in Figure 5.7, the ultimate loads of a prestressed concrete girder can be substantially increased using CFRP materials without sacrificing the ductility of the section.

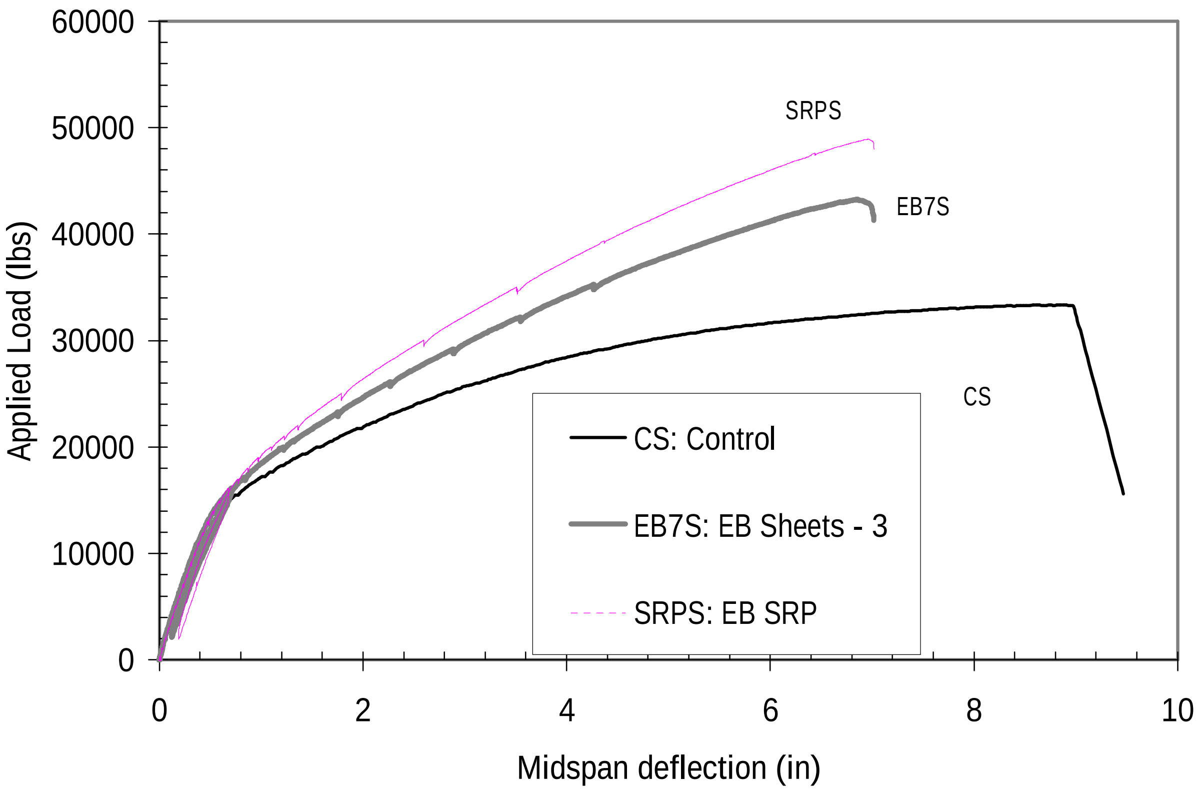

Figure 5.7 Load versus displacement response of Type C1 girders

The failure of girders EB7S and SRPS was due to concrete crushing, and the measured value of maximum concrete compressive strain was around 3000 $\mu\varepsilon$.

C-Channel Fatigue Tests

Total, ten girders were tested under cyclic loading conditions including two unstrengthened girders used as control specimens and eight CFRP strengthened girders. For Part II of the study one of the control girders had a Type C2 prestressing strand configuration while the other two were Type C1. The results of the control girder with a Type

C1 configuration are presented here, but due to a testing equipment error, the girder was accidentally subjected to a high load which could have altered the behavior from what is typically measured. Even though the load-deflection response and ultimate capacity of the control girders with Type C1 and Type C2 prestressing strand configuration are very similar, all the test results are separated according to each type. As discussed in Chapter 3, the fatigue loading applied to the girders was determined assuming that the design load was HS-15, but it was later discovered that the design load for the original girders was a HS-13 type loading. Therefore, when the specified live load for the fatigue testing was designed to represent a 20 percent increase over the assumed design load of HS15, it was actually representing a 41.0 percent increase over the original design load of HS-13. Similarly, the loading for the girders designed to represent a 60 percent increase over HS-15, was actually representing an 84.6 percent increase over the original design load of HS-13. This admittedly severe loading provides the research work with an upper limit value for the possibilities of strengthening prestressed concrete with CFRP.

Type C1 Girders

Total, seven girders with a Type C1 prestressing configuration were tested under fatigue loading conditions. For Part II of the study one control girder, one girder strengthened with CFR and one girder strengthened with SRP were tested. Summarized test results are presented in Table 5.2.

Table 5.2 Summarized test results for Type C1 girders tested under fatigue loading

Specimen Designation	CF1	EB7F	SRPF
Strengthening	-	EB sheets	EB SRP
Cracking load, k	--	12.9	14
Prestress losses, %	14.3	16.7	11.7
Effective prestress, k	16.2	15.74	16.7
Upper fatigue load, k	10.99	12.14	12.14
N, number of cycles achieved, thousands	1076	2000	2000
Failure Mode*	RPS	R	C
Ultimate load (residual), k	--	44.197	50.89
% change from virgin	--	2.24	4.28
Initial Stiffness**, k/in	20.24	35.46	35.17

* RPS = rupture of prestressing strand, IC = Intermediate crack debonding, C=concrete crushing
** defined from 2 k to 10.1 k

Load versus Displacement Hysteric Response

After the completion of each fatigue cycling regime, a static test was performed. Several static tests were performed at the beginning of the fatigue cycling since most of the degradation was expected to occur early in the fatigue regimen (Ahmad 2004). The load versus displacement characteristics of five strengthened Type C1 girders, as well as the control girder, are shown in Figure 5.8 to 5.9. The Type C1 control girder, CF1, failed due to a ruptured lower prestressing strand after 1.1 million cycles of fatigue loading equivalent to HS-15 type loading, which is equivalent to loading 15.3 percent higher than HS-13 type loading. As mentioned previously, this girder was subjected to a sudden unmeasured load due to an error in the loading system. The initial stiffness of this girder after the sudden loading was 39.6 percent less than the initial stiffness of an identical girder tested under static loading conditions, girder CS. It is believed that the sudden and unmeasured load was high enough to cause yielding of the prestressing strands resulting in residual displacement and reduced fatigue life of this control girder.

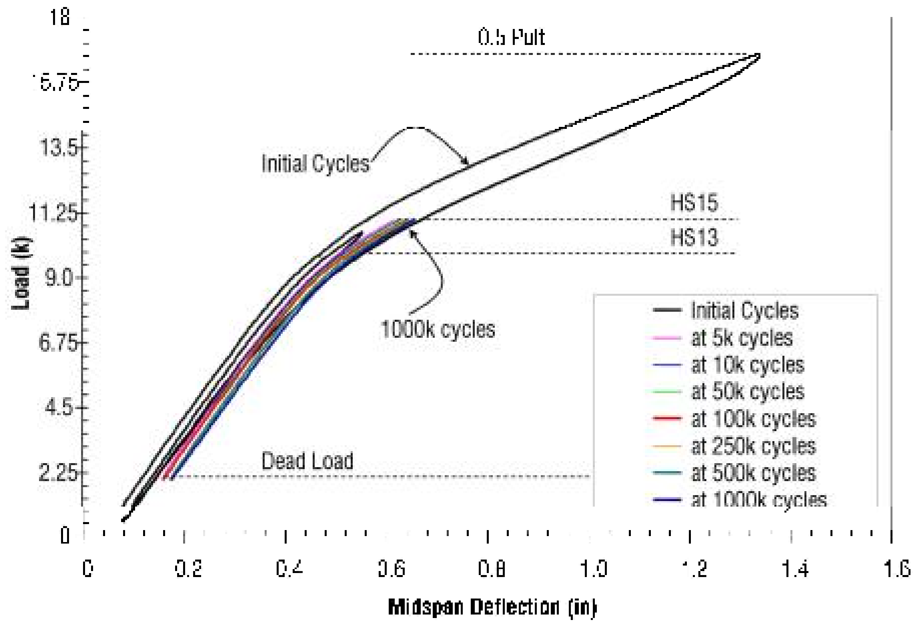

Figure 5.8 Load versus displacement for girder CF1

Girder EB7F, strengthened with two 5 in layers of CFRP sheets, survived 2 million loading cycles equal to a 30 percent increase over HS-13 loading. As explained earlier, an accidental malfunction of the load controller lead to application of an overload condition of 30 k. This overload caused significant residual displacement equal to approximately 0.40 in, and may have yielded the prestressing strands due to the slightly non-linear behavior observed in subsequent fatigue cycles. The load versus displacement response of the girder is shown in Figure 5.9.

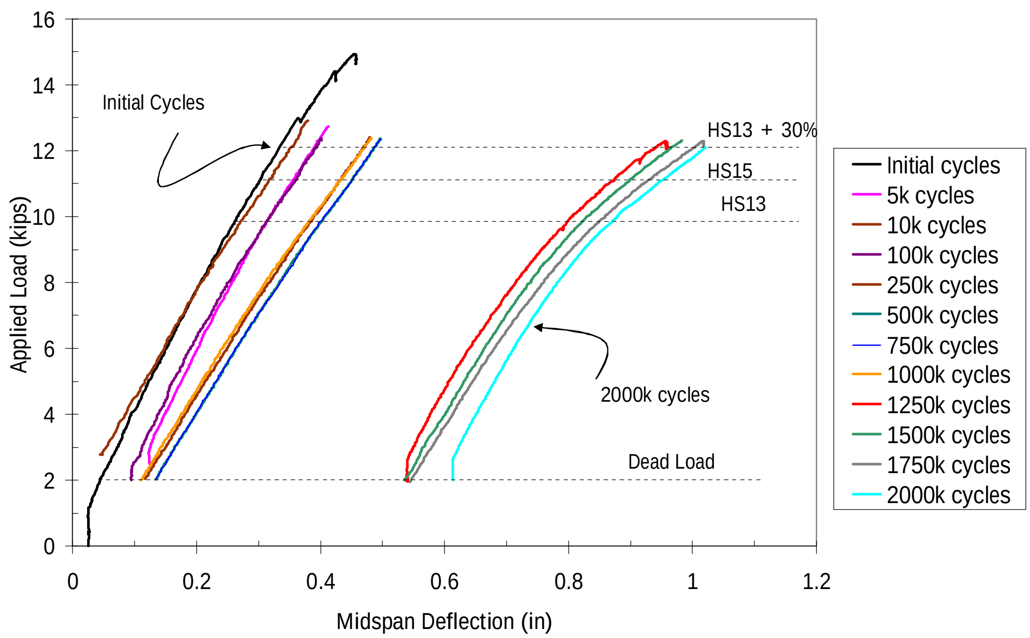

Figure 5.9 Load versus displacement for girder EB7F

Girder SRPF, strengthened with steel reinforced polymer material, was subjected to a fatigue load equivalent to a 30 percent increase over HS-13 loading. Very little fatigue degradation was observed during testing and the girder survived over 2 million cycles. The load versus displacement response of the girder is shown in Figure 5.10.

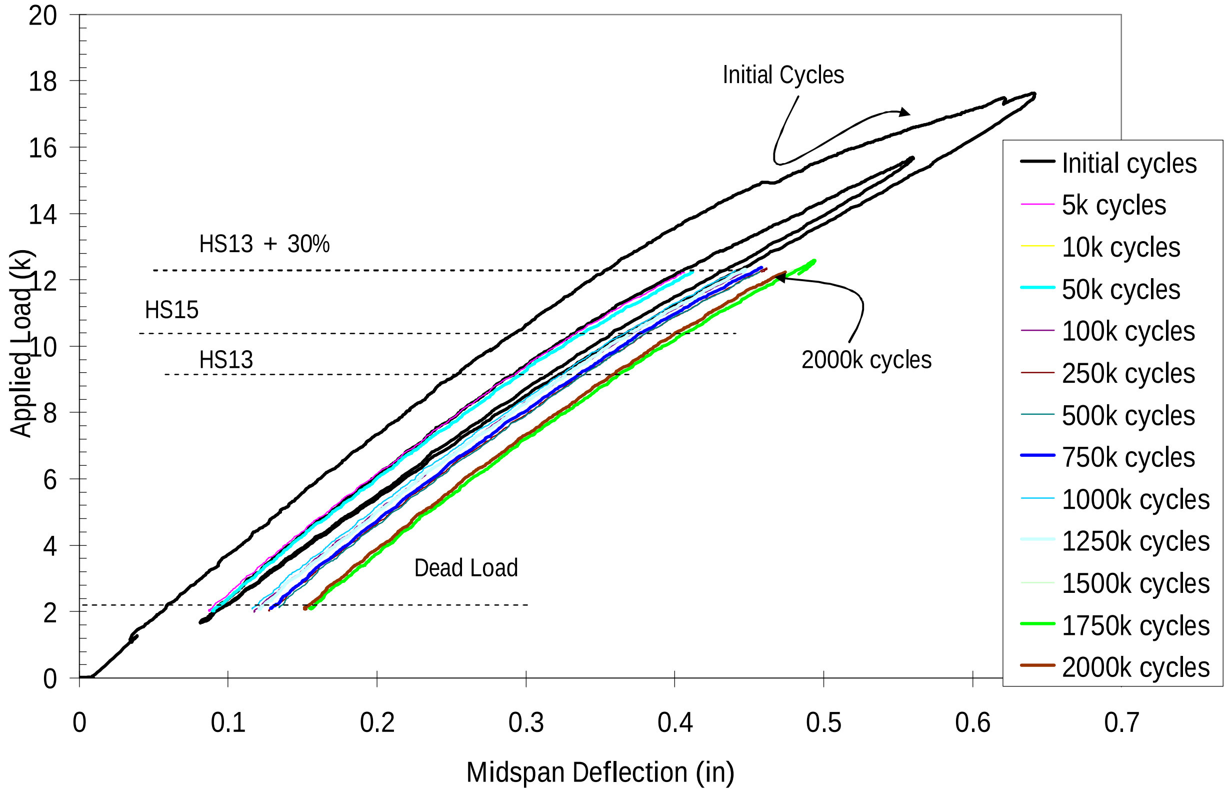

Figure 5.10 Load versus displacement for girder SRPF

Stress Ratio in Prestressing Strands

Based on the literature review of the behavior of prestressed concrete in fatigue (see Chapter 2), the prestressing strands have been identified as the most critical component affecting the fatigue life of a prestressed concrete member. The stress ratio in a prestressing strand during fatigue cycling can be defined as:

$$SR_{ps} = \frac{f_{ps2} - f_{ps1}}{f_{pu}} \times 100 \tag{5- 44}$$

where f_{ps1} and f_{ps2} are the upper and lower stress values in the prestressing strand as a result of the fatigue loading, and f_{pu} is the ultimate tensile strength of the strand. The stress ratio in the lower prestressing strand was determined from experimental data by first determining the strain present in the strand from measured values:

$$e_{ps} = e_i + e_{psPI} \qquad (5\text{- }45)$$

where ε_i is the initial strain in the prestressing strand after losses (determined from the effective prestress force) and ε_{psPI} is the strain in the strand determined from PI gauge readings at a specific load level. Once the strain in the strand was determined for the upper and lower fatigue loads for any given girder, the stress in the strands can be determined by applying the Ramberg-Osgood function (Equation 3.1) with the appropriate material constants A, B and C (see Chapter 3). The stress ratio in the lower prestressing strand versus the number of cycles is shown in Figure 5.11.

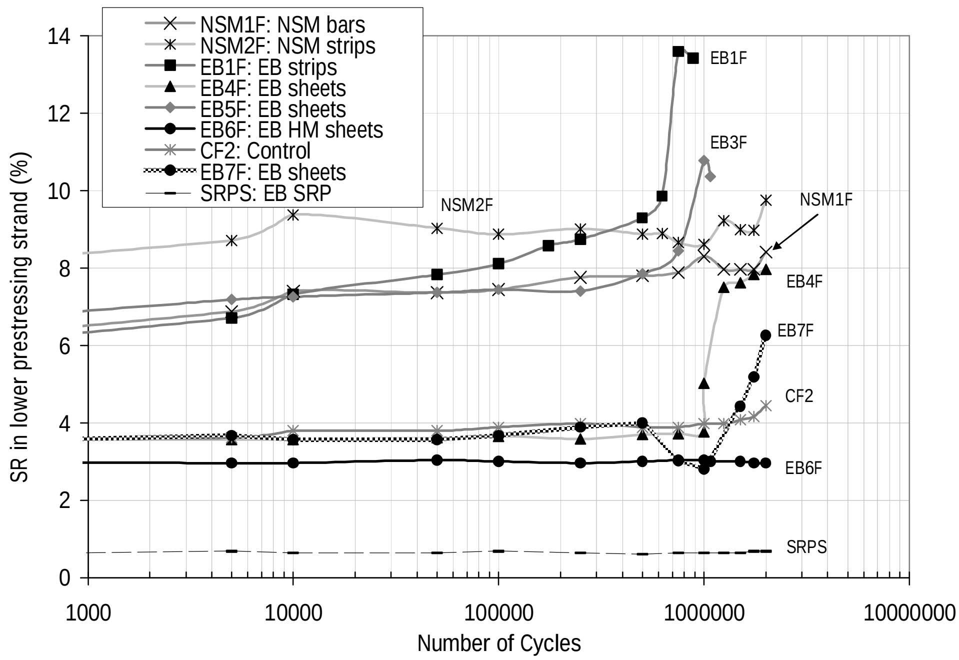

Figure 5.11 Stress ratios in prestressing strands versus number of cycles for Type C1 girders

At midspan, the stress ratio for the lower prestressing strand is typically higher because of the higher eccentricity with respect to the neutral axis. However, since the lower prestressing strands are straight in this prestressing configuration, they may not rupture first. At the hold down points at midspan, the inclined strands are subjected to high stress concentrations and therefore they may rupture first under the effect of the applied stress ratio. Since the stress ratio in the first inclined strand is typically the highest, this is the strand which was analyzed. The stress ratios for the lowest prestressing strand and for the first inclined prestressing strand can be determined using the cracked section analysis program Response 2000© and are given in

Table 5.3 for each of the Type C1 girders tested in fatigue. The stress ratios applied to many of the girders were accurately predicted using the Response 2000© analysis. The stress ratios given by the Response analysis for girder SRPF is conservative.

Table 5.3 Summarized test results for Type C2 girders tested under fatigue loading

Stress Ratio	In lower prestressing strand (%)	In first inclined prestressing strand
EB7F	4.0	1.9
SRPS	4.2	1.9

The stress ratios induced in lower prestressing strands for the Type C1 girders tested in fatigue versus the number of cycles achieved are shown in Figure 5.12 along with three S-N curves to predict fatigue life, as discussed in Chapter 2. The five girders which survived 2 million cycles are shown with arrows. The early rupture of girder EB5F discussed in Rizkalla et al. (2005) was due to rupture of an inclined prestressing strand. The early rupture of girders CF1 and EB1F was mainly due to corrosion of the straight prestressing strands. The behavior shows that both Naaman (1991) and Collins (1991) provide good estimation of the fatigue life behavior of a prestressed member with straight prestressing strands, while Muller and Dux (1994) gives a lower bound estimation of the life of a prestressed member with inclined prestressing strands.

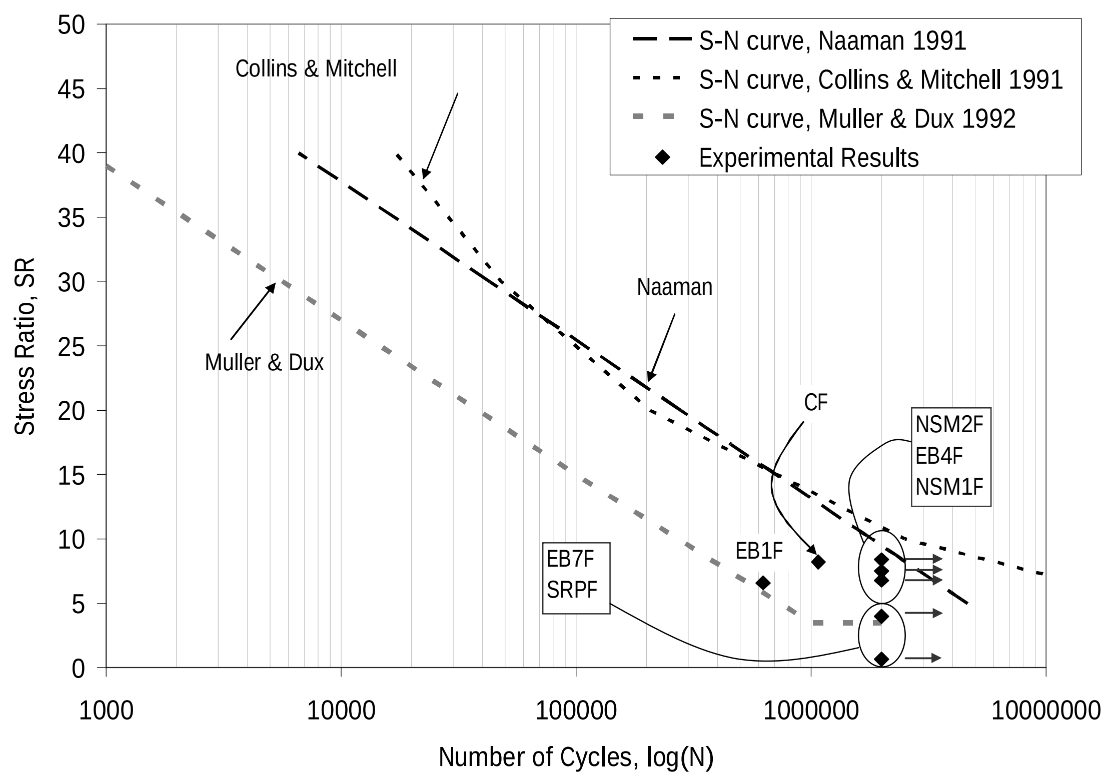

Figure 5.12 Stress ratios in lower prestressing strands versus number of cycles

Compressive Stress Ratio in Concrete

The compression stress ratio of concrete (SR_{conc}) can be calculated from the experimental results from:

$$SR_{conc} = \frac{f_{c\max} - f_{c\min}}{f'_c} \qquad (5\text{-}46)$$

where f_{cmax} and f_{cmin} are the experimental values for concrete stress in extreme compressive fiber corresponding to the upper and lower load levels. The compression stress ratio versus the number of cycles is shown in Figure 5.13. Due to the impact loading exerted on the girder CF1, the concrete stress ratio shown is artificially high. Similarly for girder EB7F, the unexpected loading after 1.25 million cycles caused the rise in stress ratio shown.

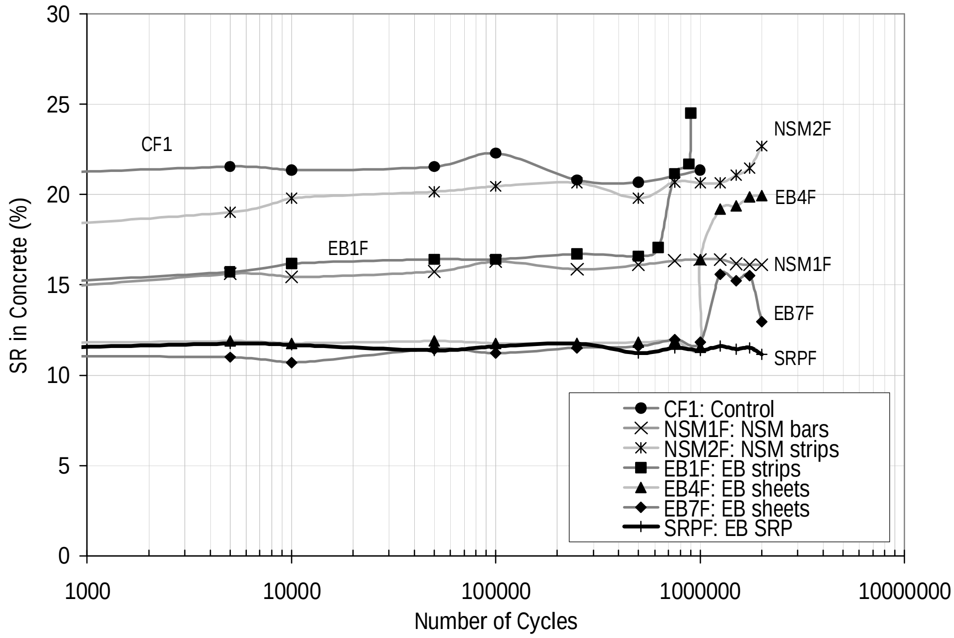

Figure 5.13 Compressive stress ratios in concrete for Type C1 girders

In order to determine the minimum and maximum range of the compressive stresses in the extreme compression zone of the concrete, the initial compressive stress in the concrete due to the dead load and the applied effective prestress force can be evaluated due to prestressed concrete theory. For Type C1 girders strengthened to 20 percent, using average values for the effective prestress force, the maximum and minimum concrete stresses are 2 ksi and 362 psi. For a value of concrete strength equal to the average for the Type C1 girders, the compressive stress ratio in the concrete is equal to 19.5 percent, which is similar to the measured values shown in Figure 5.13.

Using the predicted values for f_{cmax} and f_{cmin}, a prediction of the fatigue life of the concrete can be evaluated using Equation 2.1 (Aas-Jacobsen 1970). For the girders strengthened to achieve a 20 percent increase in ultimate capacity, the fatigue life is 7.75 x 10^{12} cycles, and for the girder strengthened to achieve a 60 percent increase in ultimate capacity the fatigue life is 7.62 x 10^{9} cycles. Based on the results, it was concluded that compression-compression concrete fatigue is not a concern, even at a loading 84.6 percent higher than HS-13 truck loading.

Tensile Stress Ratio in FRP

The stress ratio in the extreme tensile fiber of the CFRP material at midspan (SR_{FRP}) can be defined as:

$$SR_{FRP} = \frac{f_{FRP\max} - f_{FRP\min}}{f_{fu}} \qquad (5\text{- }47)$$

where f_{FRPmax} and f_{FRPmin} are the measured values for stress in the CFRP corresponding to the upper and lower fatigue loading values, and f_{fu} is the ultimate tensile strength of CFRP as determined from material testing. A recent study on the topic of fatigue of CFRP (Adimi et al 2000) has shown that CFRP pre-cured laminates can withstand over 4 million cycles subjected to a stress ratio of 35 percent of their ultimate tensile strength. From Figure 5.14, the stress ratio in the FRP for all strengthened girders is less than 35 percent and therefore the fatigue rupture of the FRP should not be a concern. The degradation in the stress ratio of FRP for girder EB1F shown in Figure 5.14 is a result of ruptured prestressing strands which induce a larger demand on the FRP during the remaining fatigue cycles. The degradation shown for girder EB7F is due to the unexpected load event which may have put a greater demand on the FRP system due to yielding of the prestressing strands.

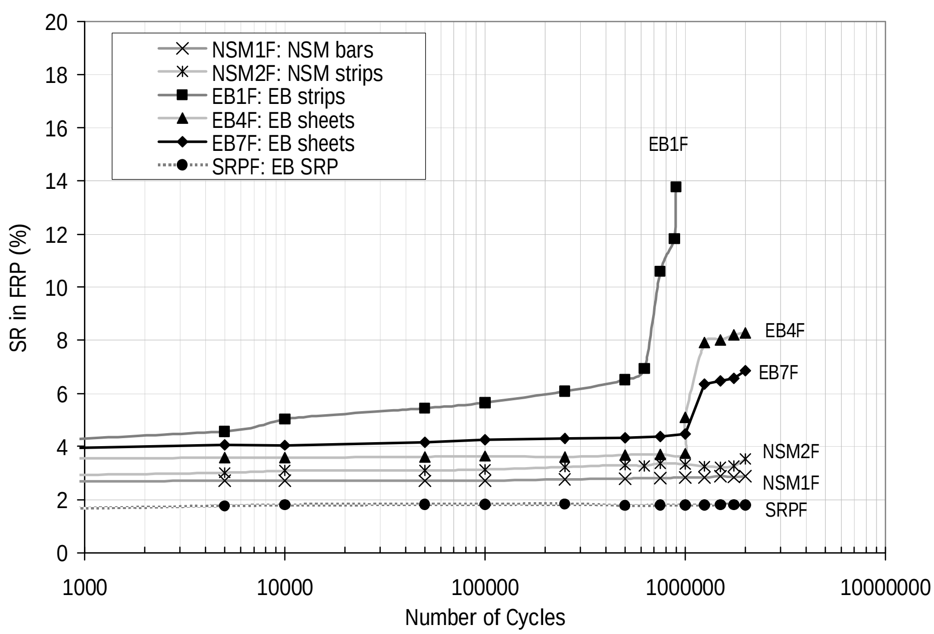

Figure 5.14 Tensile stress ratios in FRP (or SRP) material for Type C1 girders

Residual Strength

A final static test to failure was performed on the two strengthened Type C1 girders. Compared with their counterparts tested under static loading conditions, the behavior of the fatigue cycled girders was nearly identical. The girders varied with their counterpart tested under static loading conditions in ultimate load by up to 4 percent. The variation could be attributed to variations in the cross-sectional dimensions, effective prestress forces or slight misalignment of the CFRP (or SRP) material in the externally bonded girders.

6 AASHTO TEST RESULTS AND DISCUSSION

6.1 Introduction

Four AASHTO Type II girders were tested in this research project. Two were damaged (by simulated impact) at or near midspan, and repaired using CFRP sheets (AASHTO2, AASHTO3). Two additional AASHTO Type II short span girders were tested under induced shear critical loading, one as a control specimen (AASHTO2C), and one intentionally damaged near the support and repaired with CFRP sheets (AASHTO2R). Summarized test results for the AASHTO girders are provided Table 6.1for the flexural tests and Table 6.2for the shear tests

6.2 Modeling

The following modeling procedures were used in the design of the repair systems for each of the test specimens. It should be noted that the first step of any repair system is to determine if the shear capacity or the flexural capacity of the section will be the critical failure mode of the member. Once the critical failure mode is determined, the proper repair model, presented below, can be chosen

Introduction

A combination of various design and analysis procedures were used throughout the research project. A cracked section analysis was performed to predict the undamaged, damaged and repaired flexural capacity of girders AASHTO1 (Rizkalla *et al*. (2005)), AASHTO2, and AASHTO3. The analysis of the undamaged shear strength of AASHTO2C and AASHTO2R was determined using Prestressed/Precast Concrete Institute (PCI (2006)) guidelines. The same PCI guidelines were combined with ACI Committee 440 (2002) design guidelines to determine the repaired capacity of AASHTO2R. The cracked section analysis procedure, PCI guidelines, and ACI Committee 440 guidelines will be presented in this section. A complete design example using RESPONSE 2000© for repairing a flexurally critical specimen with CFRP, is presented in Appendix A. Likewise, a complete design example for shear repair of a member using CFRP is presented in Appendix B.

Flexural Modeling

RESPONSE 2000© Cracked Section Analysis

A cracked section analysis was performed on all five of the AASHTO Type II girder test specimens using RESPONSE 2000© software to analyze their flexural capacities. Verification of this program can be found in Bentz (2000). The default cross section of the AASHTO Type II girder was used without any modification. The width of the composite deck was modified using the modular ratio of concrete strengths. The strength of the concrete for the girder and the deck was based on material testing of concrete core samples previously described in Section 4.3. The behavior of the concrete was modeled using Popovics curve; tension stiffening was also included in the analysis. The prestressing steel for each girder was modeled using the Ramberg-Osgood function, using constants derived from the tension tests taken from each girder. The CFRP was modeled as a linear-elastic material up to failure with the modulus of elasticity, rupture strain, and ultimate tensile strength values determined from coupon tension tests.

The results of the cracked section analyses for both the undamaged and repaired specimens showed very good agreement with the experimental results presented in Section 6.3. Finite element simulation was not included in this research based on the good agreement of the predicted versus experimental results.

Shear Modeling

An analysis technique combining two different design approaches was used in the modeling of the girder repaired with CFRP in shear. The method combined guidelines from the Precast/Prestressed Concrete Institute (PCI) (2006) design manual with the CFRP shear analysis approach from ACI Committee 440 (2002). Below are the steps used in the model for the prediction of the shear capacity of an impact damaged and CFRP repaired AASHTO girder:

1. The first step is to determine the shear capacity along the undamaged girder using the PCI (2006) guidelines. The nominal shear capacity envelope was then plotted to determine the maximum applied load.
2. The second step is to determine the flexural capacity of the undamaged section using cracked section analysis to ensure that the expected ultimate load determined in step one will not produce flexural failure of the girder.
3. The third step is to restore the shear capacity along the member using PCI (2006) and ACI Committee 440 (2002) design guidelines. The difference in shear capacity between the damaged and undamaged girder is restored using CFRP sheets modeled using ACI Committee 440 (2002) recommendations.
4. The last step is to check the flexural capacity of the damaged section and restore with CFRP sheets if needed.

Step 1: Calculation of Shear Strength of Undamaged Section

Using the PCI Design Handbook (2006), the nominal shear strength along the length of the girder (V_n) was determined by finding the shear strength contribution from the concrete section (V_c) and steel stirrups (V_s). The detailed analysis method was used in the determination of V_c; the web shear capacity (V_{cw}) and the flexure-shear capacity (V_{ci}) were both examined at each section:

$$V_{ci} = 0.6\sqrt{f_c^{'}}b_w d + V_d + \frac{V_i M_{cr}}{M_{\max}} \tag{6-1}$$

$$V_{cw} = \left(3.5\sqrt{f_c^{'}} + 0.3 f_{pc}\right) b_w d + V_p \tag{6-2}$$

where V_d is the shear force caused by the unfactored dead load, V_i is the factored shear force at a section due to externally applied loads, M_{cr} is the cracking moment of the section, $M_{\max}$ is the maximum factored moment at a section due to externally applied loads, f_{pc} is the compressive stress in concrete at the centroid due to effective prestressing forces, and V_p is the vertical component of the effective prestress force at the section centroid. M_{cr} can be calculated as:

$$M_{cr} = \left(\frac{I}{y_t}\right)\left(6\sqrt{f_c^{'} + f_{pe} - f_d}\right) \tag{6-3}$$

where I is the moment of inertia, y_t is the distance from the top of the girder to the center of gravity, f_{pe} is the compressive stress in the concrete at the extreme tension fiber due to the effective prestressing force, and f_d is the stress due to service dead load. The shear strength contribution of the steel stirrups (V_s) can be calculated as:

$$V_s = \frac{A_v f_y d}{s} \tag{6-4}$$

where A_v is the area of the shear reinforcement, f_y is the yield stress of the shear reinforcement, and s is the spacing between stirrups. The total nominal shear strength (V_n) is then determined by $V_n = V_c + V_s$ for every section along the length of the girder.

Step 2: Calculation of Flexural Strength of Undamaged Section

The moment capacity of the undamaged section is determined using cracked section analysis approach similar to the one described in the previous section.

Step 3: Restore the Shear Capacity Using CFRP

Step three of the shear model is to restore the shear capacity of the damaged girder using CFRP sheets. This task was performed using the same procedure described in step one, with the application of ACI Committee 440 (2002) guidelines for the usage of CFRP materials. First the shear capacity of the damaged section should be calculated with an appropriate reduction in prestressing force, and a reduced value for the concrete contribution (V_c) corresponding to the level of damage in the section. The shear strength contribution of CFRP materials was included in the nominal shear strength equation (V_n) with an additional term (V_f) used to account for the presence of CFRP materials:

$$V_n = \left(V_c + V_s + \Psi_f V_f\right) \tag{6-5}$$

where (y_f) is a reduction factor of 0.85 for members using U-wraps. The shear contribution from the FRP material can be calculated using:

$$V_f = \frac{A_{fv} f_{fe} (\sin a + \cos a) d_{fv}}{s_f} \qquad (6\text{-}6)$$

where A_{fv} is the area of CFRP shear reinforcement, f_{fe} is the tensile stress in the CFRP shear reinforcement at ultimate, a is the angle of the CFRP, d_{fv} is the depth of CFRP shear reinforcement, and s_f is the spacing of the CFRP shear reinforcement. The area of CFRP shear reinforcement was calculated using the following:

$$A_{fv} = nt_f \mathrm{w}_f \qquad (6\text{-}7)$$

where n is the number of layers of transverse CFRP sheets, t_f is the thickness of each transverse CFRP sheet, and w_f is width of the transverse CFRP plies. The tensile stress in the CFRP shear reinforcement at ultimate was calculated as follows:

$$f_{fe} = e_{fe} E_f \qquad (6\text{-}8)$$

where e_{fe} is the effective strain, or maximum strain that can be achieved in the CFRP system, and E_f is the tensile modulus of elasticity of the CFRP. The type of CFRP system used for shear strengthening determines the effective tensile strain permitted. The effective tensile strain for U-wrap systems is calculated using:

$$e_{fe} = k_v e_{fu} \le 0.004 \qquad (6\text{-}9)$$

where k_v is the bond-reduction coefficient, and e_{fu} is the design rupture strain of the CFRP. The bond reduction coefficient is a function of the concrete strength, type of wrapping scheme, and laminate stiffness, computed as follows:

$$k_v = \frac{k_1 k_2 L_e}{468 e_{fu}} \le 0.75 \qquad (6\text{-}10)$$

where k_1 and k_2 are modification factors that account for the concrete strength and type of wrapping system, and L_e is the active bond length over which the majority of the bond stress is maintained. The active bond length is calculated as follows:

$$L_e = \frac{2500}{\left(nt_f E_f\right)^{0.58}} \qquad (6\text{-}11)$$

The modification factors are calculated as follows:

$$k_1 = \left(\frac{f_c^{'}}{4000} \right)^{2/3} \tag{6-12}$$

$$k_2 = \frac{d_{fv} - L_e}{d_{fv}} \tag{6-13}$$

Step 4: Restoration of the Flexural Strength of the Section

The last step in the modeling process of a shear-critical specimen is to check the flexural capacity of the damaged section. If it is found to be deficient, the flexural repair procedures described in Section 6.2 are to be used.

6.3 Flexural Study

Two AASHTO Type II girders were damaged (by simulated impact) at or near midspan, and repaired using CFRP sheets (AASHTO2, AASHTO3). The girders were damaged and repaired as previously described in Chapter 4. Summarized test results for the flexural tests are provided in Table 6.1.

Table 6.1 Summarized test results for AASHTO girders tested in flexure

Specimen Designation	AASHTO2	AASHTO3
Repair system	CFRP sheets	CFRP sheets
Initial cracking load*, k	59.5	63.2
Cracking load**, k	58.9	65.0
Prestress losses*, %	18.2	12.9
Effective prestress*, k	15.5	27.5
Predicted ultimate load of undamaged girder, k	119.1	126.5
Predicted ultimate load of repaired girder, k	140.5	143.0
Measured ultimate load, k	134.1	145.3
Maximum compressive strain in concrete, με	2630	3090
Maximum tensile strain in CFRP, με	4620	5760
Failure mode	Crushing of concrete	Crushing of concrete

* For the girders which were tested prior to simulated impact damage
** The cracking load of the repaired material

AASHTO2

Girder AASHTO2 was intentionally damaged at midspan with four out of twenty-eight prestressing strands ruptured, corresponding to a 14.3 percent loss of prestressing force. The girder was then repaired with CFRP sheets and tested in several stages to failure. A description of the test and other set-up details can be found in Chapter 4.

Behavior of Girder during Initial Loadings

Girder AASHTO2 was subjected to four cycles of initial loading. Two of those cycles were performed on the undamaged girder, with only minor repair of the composite deck performed prior to testing. One of these initial cycles loaded the girder up to 90 percent of the predicted ultimate load value. The resulting flexural cracks during this loading stage were well spaced, a result of the numerous and well distributed prestressing strands. The third and fourth cycles of loading that the girder was subjected to occurred after the simulated impact damage was applied to the girder, as described in detail in Chapter 4. The third loading cycle followed the concrete removal around midspan, and the fourth cycle was after four prestressing strands, representing a 14.3 loss of prestress force, were ruptured in the damaged zone. A comparison of the stiffness of girder AASHTO2 in each of these cycles is provided in Table 6.2. The largest drop in stiffness was a result of the severe initial loading combined with the concrete damage, for a reduction of approximately 17 percent. A further reduction was observed after the cutting of the prestressing strands. The load versus deflection curve for girder AASHTO2 due to the initial loading scheme is shown in Figure 6.1.

Table 6.2 Stiffness comparison of AASHTO girders tested in flexure (lb/in)

Specimen Designation		AASHTO2	AASHTO3
Prior to CFRP repair	Initial cycle 1*	78.8	77.7
	Initial cycle 2*	81.1	77.7
	Post concrete damage*	68.0	65.7
	Post cutting of prestressing strands*	62.8	60.5
After CFRP repair	Final cycle 1	69.1	68.0
	Final cycle 2	67.4	70.2

* For the girders which were tested prior to simulated impact damage

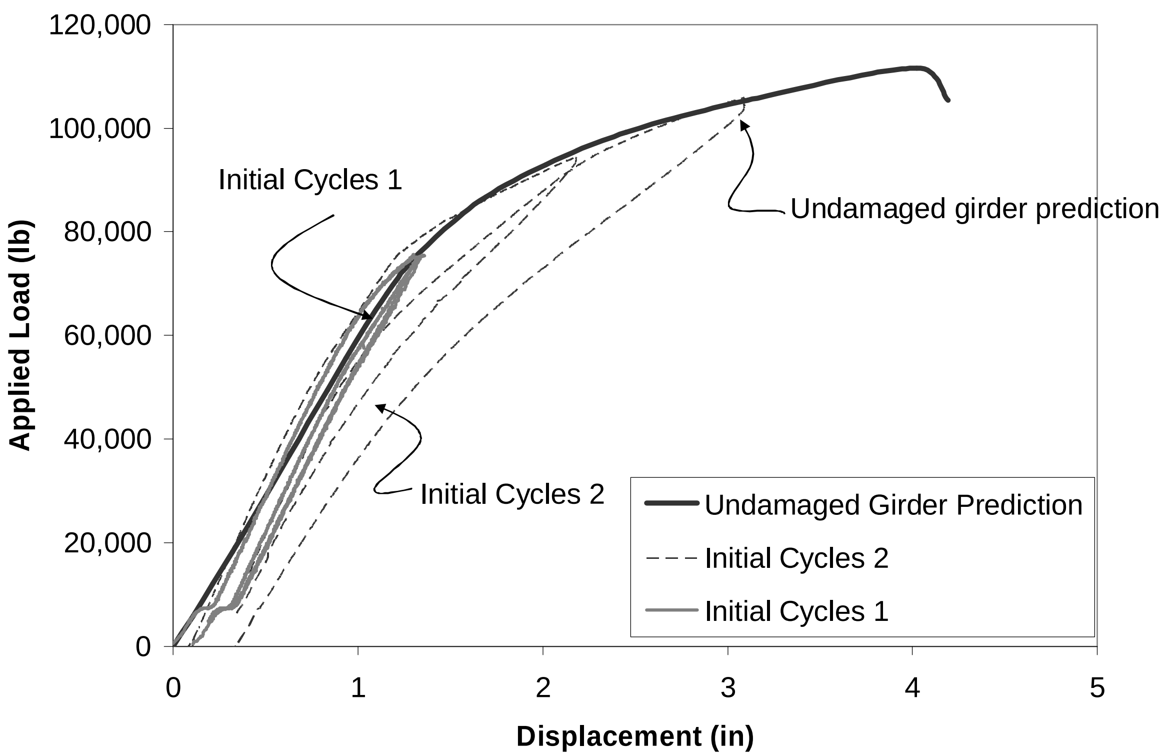

Figure 6.1 Initial load versus deflection of girder AASHTO2

In addition to stiffness loss, there was also increasing residual deflections following each of the loading cycles. The largest residual deflection came as a result of the initial cycles on the undamaged girder, where a residual deflection of 0.25 in was observed. The residual deflection after the concrete damage, prestressing strand cutting, and subsequent cycles was 0.36 in. The stiffness change and the residual deflections in the girder through the various cycles can be seen in Figure 6.2, which plots a detail of the load versus deflection behavior of all loading cycles.

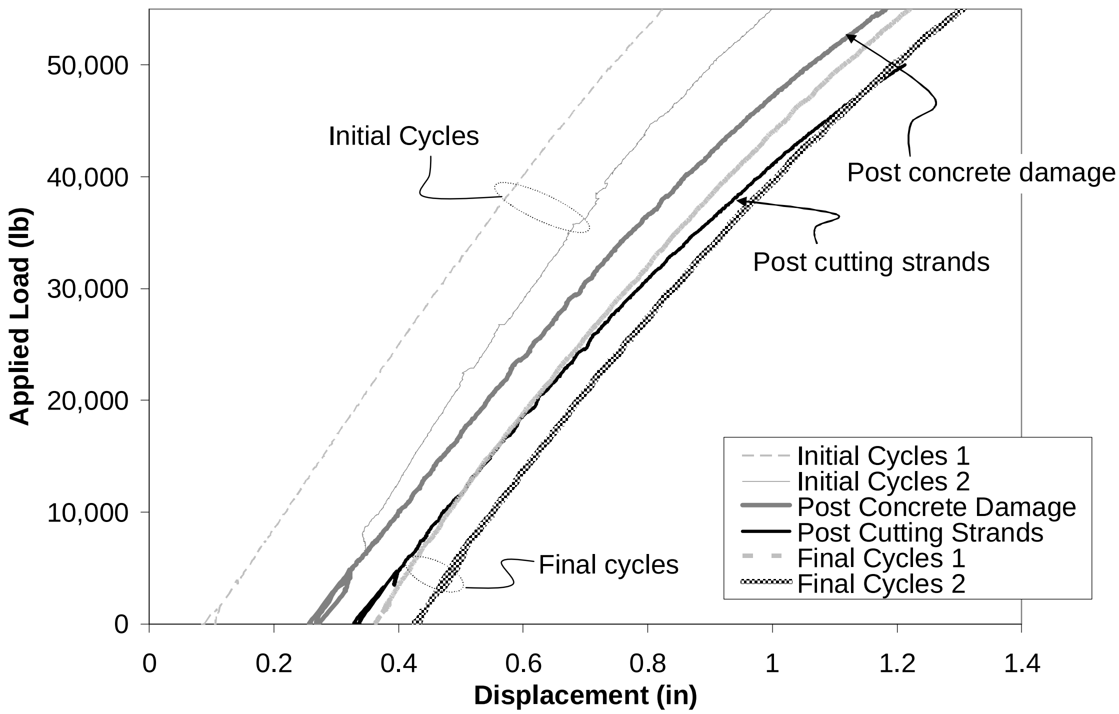

Figure 6.2 Close-up of load versus deflection of girder AASHTO2

Behavior at Ultimate

After the section was restored with repair mortar and CFRP sheets were installed, girder AASHTO2 was subjected to two loading cycles up to failure. A full description of the final static test is provided in Chapter 3. Failure initiated in the concrete material around the loading plate, where localized crushing led to out-of-plane behavior rapidly causing failure. The maximum measured value of concrete compressive strain was 2630 $\mu\varepsilon$. The relatively low value at crushing of concrete was likely a result of the poor condition of the concrete at midspan due to extant transverse cuts. The damaged and repaired girder far exceeded the strength and ductility of the original undamaged girder, as shown in Figure 6.3. The longitudinal CFRP system was able to adequately carry the tensile forces, and showed very little debonding or damage even after the failure event. The transverse CFRP sheets were also virtually unaffected during the loading, with only the U-wraps positioned directly below the loading area becoming damaged at failure.

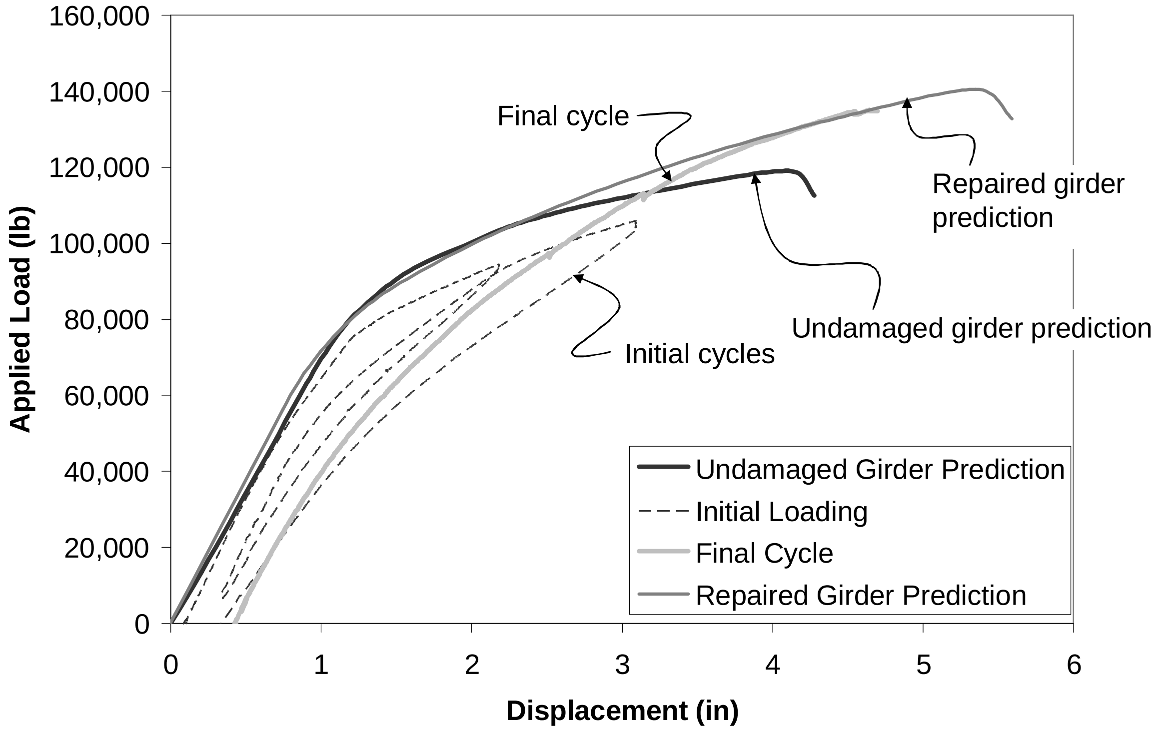

Figure 6.3 Load versus deflection of girder AASHTO2

The maximum tensile strain in the CFRP system at failure was 4620 $\mu\varepsilon$, very close to the maximum tensile strain observed during the test of girder AASHTO1(Rizkalla *et al*. (2005)). Due to the location of several wide transverse U-wraps used to encapsulate the damaged region, tensile strain gauges could only be located at a distance approximately 3.94 ft from midspan. Therefore, the maximum strain in the longitudinal CFRP was likely larger than the maximum measured value. Multiple strain gauges were affixed to the longitudinal CFRP throughout the repaired area, and the measured tensile strain profile is shown in Figure 6.4. Due to the thickness of the longitudinal CFRP, the presence of the transverse U-wraps, and the large distance between the gauges, the effect of stress concentrations at the toes of the flexural cracks is not manifested in the plot. At failure the large increase in tensile strain which can be seen around 78.7 in from the end of the CFRP repair is likely due to the yielding of the prestressing strands at that location along the length of the girder.

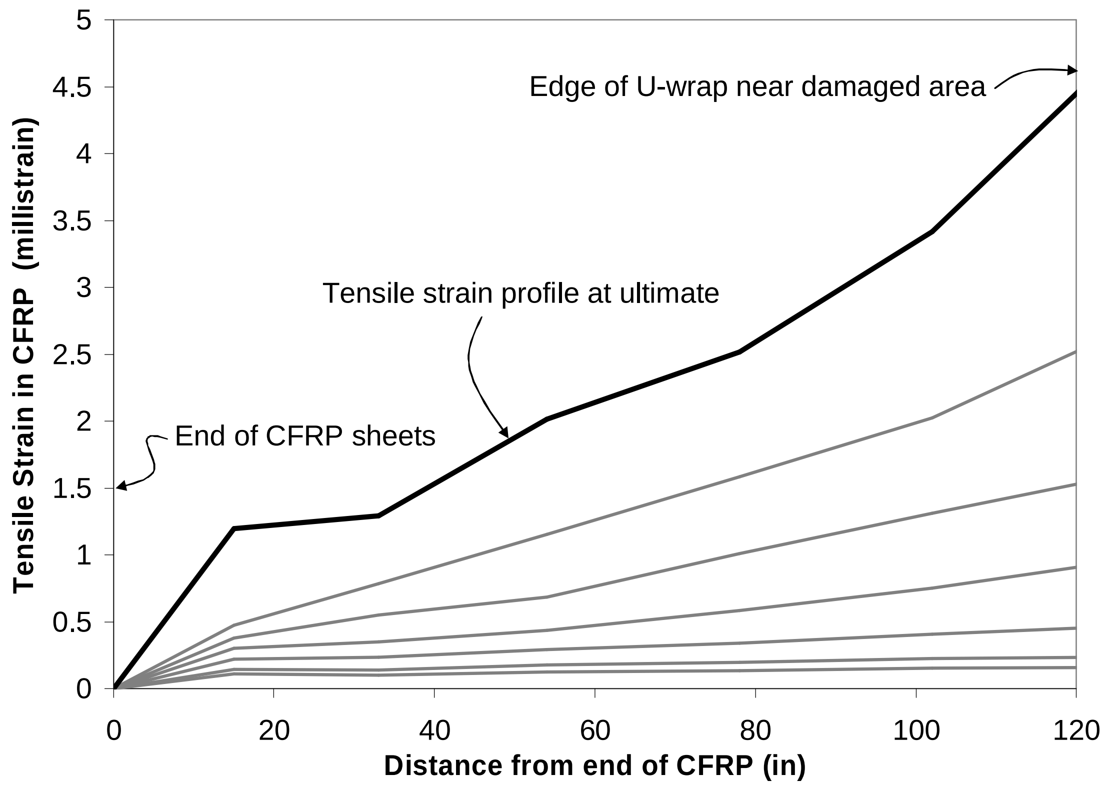

Figure 6.4 CFRP tensile strain profile during final static test of girder AASHTO2

Predicted versus Experimental

In Figure 6.3, the load versus deflection predictions are shown for two scenarios: 1) the undamaged girder, and 2) for a repaired girder modeled with a similar amount of CFRP as the actual repaired girder. Both of the predictions were made using cracked section analysis described earlier in this chapter and constituent properties taken from material testing. The prediction of the undamaged girder matches closely the measured values from the initial static test, in both load and deflection, until the static test was terminated at around 90 percent of ultimate. Based on experience gained from the testing of other girders and their predictions using cracked section analysis, it is possible that the ultimate deflection of the undamaged AASHTO2 girder could have been greater than that of the prediction (Rosenboom 2006). If four prestressing strands are taken out of the cracked section analysis and the total amount of CFRP used in the repair of girder AASHTO2 is included, counting all CFRP tension struts on the girder flange and web, a prediction can be made which closely matches the observed behavior. The ultimate load of the repaired girder is 13.4 percent greater than the undamaged girder prediction, and is similar to the repaired girder prediction.

AASHTO3

Girder AASHTO3 was intentionally damaged at midspan with three prestressing strands ruptured, corresponding to an 18.8 percent loss of prestressing force. The girder was repaired with CFRP sheets and tested in several stages to failure. A description of the test and other set-up details can be found in Chapter 4.

Behavior of Girder during Initial Loadings

Similar to girder AASHTO2, AASHTO3 was subject to four cycles of initial loading: two on the undamaged girder up to 80 percent of the predicted ultimate load value, one cycle after concrete damage, and one cycle after three prestressing strands were cut. As mentioned in Chapter 4, the original girder was delivered to the laboratory in poor condition, with numerous impact events and subsequent repairs evident on one side and significant permanent out of plane deflection. A comparison of the stiffness of girder AASHTO3 in each of these four cycles is provided in Table 6.2. Due to the simulated impact damage, the stiffness of the girder was reduced by 22.1 percent. The load versus deflection curve for girder AASHTO3 due to the initial loading scheme is shown in Figure 6.5.

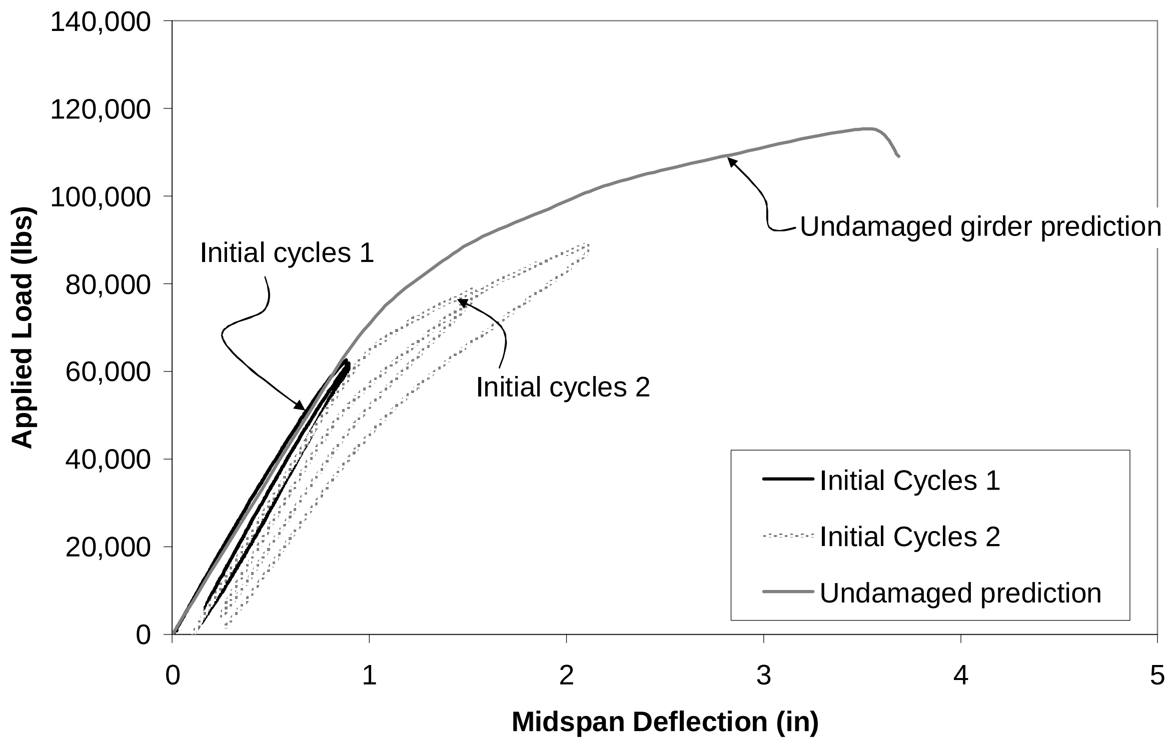

Figure 6.5 Initial load versus deflection of girder AASHTO3

Similar to girder AASHTO2, AASHTO3 also experienced residual deflections as a result of the simulated impact damage and initial cycling. The largest residual deflection came as a result of the initial cycles on the undamaged girder, where a residual deflection of 0.24 in was measured. The residual deflection after the concrete damage, prestressing strand cutting, and subsequent cycles was 0.36 in. The stiffness change and the residual deflections in the girder through the various cycles can be seen in Figure 6.6, which plots a detail of the load versus deflection behavior of all loading cycles.

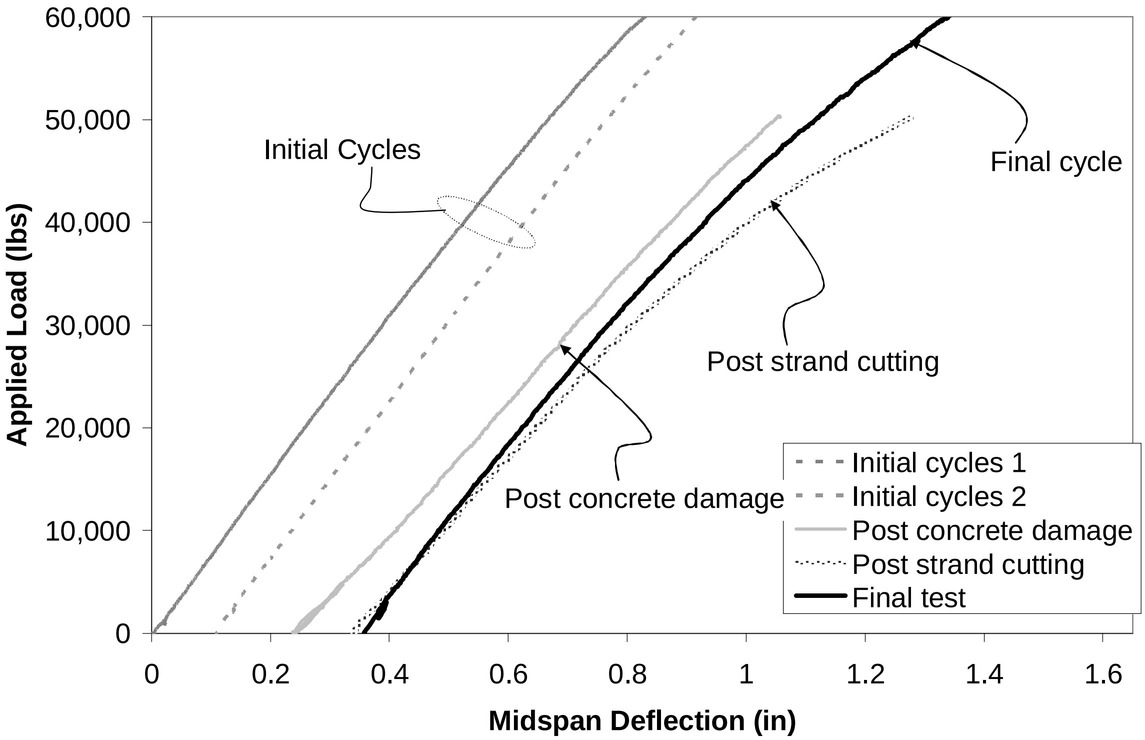

Figure 6.6 Close-up load versus deflection of girder AASHTO3

Behavior at Ultimate

After the section was restored with repair mortar and CFRP sheets were installed, girder AASHTO3 was subjected to two loading cycles up to failure. A full description of the final static test is provided in Chapter 4. Failure was due to concrete crushing in the compression region around the loading plate. The maximum measured value of concrete compressive strain at failure was 3090 $\mu\varepsilon$, significantly larger than the measured value for the previous AASHTO flexural tests. There was no evidence of debonding in the longitudinal CFRP at failure. The transverse U-wraps buckled at failure but contained most of the concrete damage. The load versus deflection behavior of girder AASHTO3 is shown in Figure 6.7.

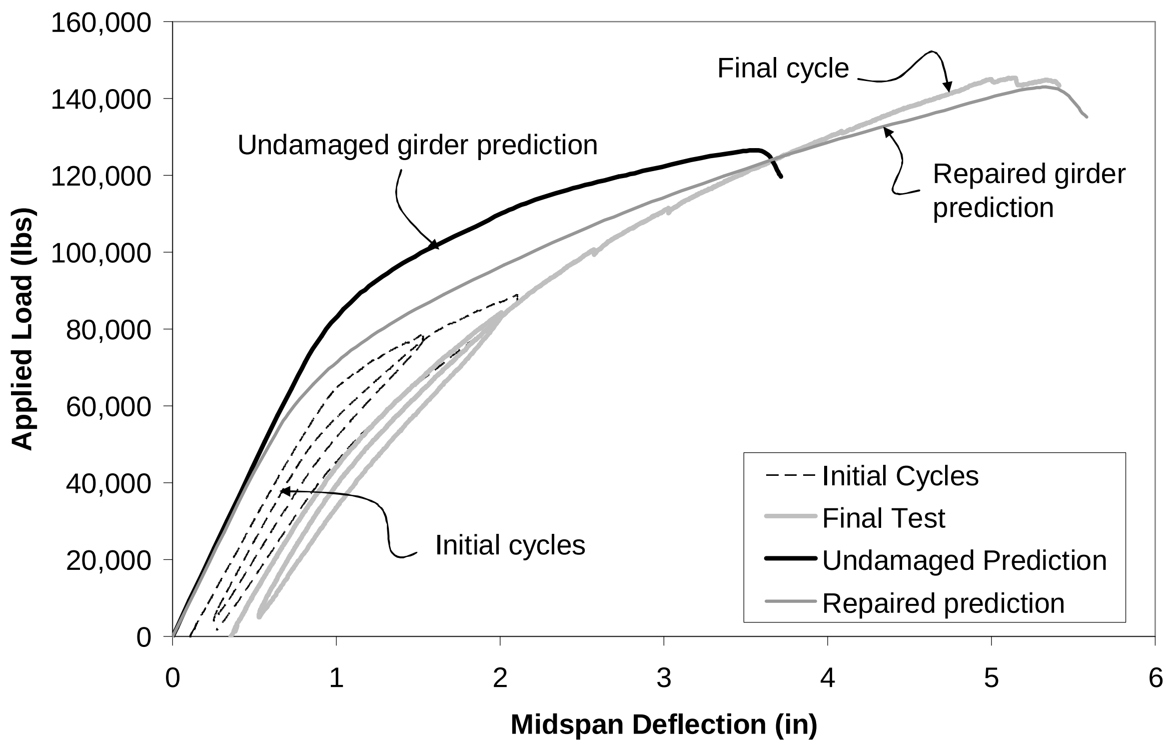

Figure 6.7 Load versus deflection of girder AASHTO3

The maximum measured tensile strain in the longitudinal CFRP at failure was 5760 με, significantly larger than the tensile strain measured in previous AASHTO flexural tests. The higher compressive strain capacity in the concrete led to a greater demand placed on the CFRP system which in turn led to a large increase in ultimate load compared to the undamaged girder. In this girder, tensile strain gauges were installed in the CFRP throughout the repaired area, and the measured tensile strain profile is shown in Figure 6.8. Also shown in the figure is the location of the 4.0 ft wide transverse U-wrap which encapsulated the area of simulated impact damage. At a distance of 216.5 in from the end of the CFRP the profile shows a strain peak, most likely the result of the strain gauge location near the toe of a flexural crack. The distance around midspan where the prestressing strands are yielding is also obvious in the figure, from approximately 98.4 to 236.2 in from end of the longitudinal CFRP.

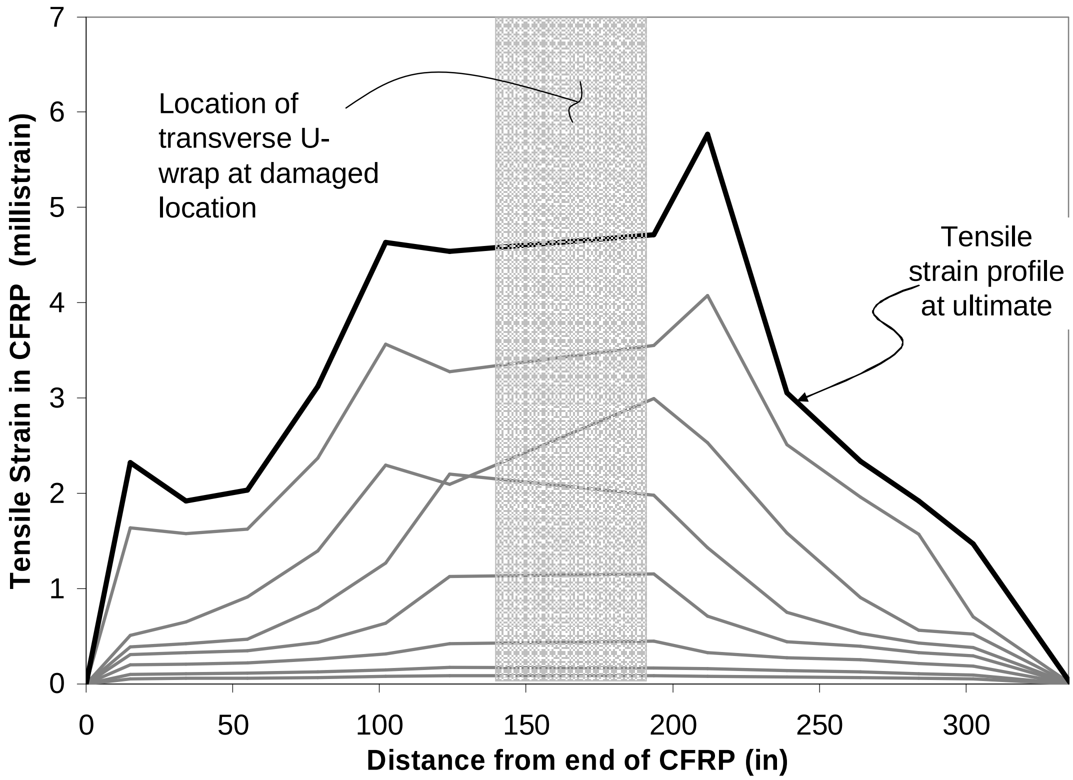

Figure 6.8 CFRP tensile strain profile during final static test of girder AASHTO3

Predicted versus Experimental

Similar to girder AASHTO2, in Figure 6.7 the load versus deflection predictions from cracked section analysis are shown for two scenarios: 1) the undamaged girder, and 2) the repaired girder with all CFRP. The undamaged girder prediction with the measured effective prestress force does not adequately reflect the measured load versus deflection behavior. This is likely the result of the poor condition of this girder upon delivery to the laboratory, with numerous impact events evident on one side. This internal damage and cracked nature of the beam could have resulted in the lower cracking load and stiffness compared to the prediction. The load versus deflection prediction for the repaired girder corresponds extremely well to the measured response of the girder. The predicted ultimate load of the repaired girder is 1.7 percent lower than the measured value. It should be noted that both the predicted scenarios show crushing of concrete as the failure mode, the same as the observed mode.

6.4 Shear Study

Two short span AASHTO Type II girders were tested under shear critical loading schemes. One girder was tested as a control specimen (AASHTO2C); the other girder was damaged and repaired using CFRP sheets and tested to failure (AASHTO2R). Summarized test results for the shear tests are provided in Table 6.3.

Table 6.3 Summarized test results for AASHTO girders tested in shear

Specimen Designation	AASHTO2C	AASHTO2R
Repair system	None	CFRP sheets
Cracking load (k)	226.4	256.3
Average crack width at failure (in)	0.148	0.019
Failure load (k)	413.7	446.3
Predicted failure load (k)	373	486
Failure mode	Web shear failure	Shear in right transfer zone followed by flexure-shear
Max tensile strain in longitudinal CFRP (με)	---	810
Max tensile strain in diagonal CFRP strut (με)	---	1920
Max compressive strain (με)	680	1400

AASHTO2C and AASHTO2R

The cracking behavior, tensile strain in the longitudinal and diagonal CFRP, ultimate behavior, and predicted versus experiment results and discussion will be presented for AASHTO2C and AASHTO2R in this section.

Cracking Behavior

Girder AASHTO2C and AASHTO2R were loaded in one cycle up to failure. During the loading process, several inclined cracks formed at 45 degrees from the support at various load levels. The number of cracks in the control specimen was visually obtained, however the cracks were not visible in the repaired girder as a result of the diagonal CFRP struts. In order to compare the average crack widths of the two specimens, it was assumed that the same number of cracks formed in the repair specimen that was visible in the control specimen. Figure 6.9 shows the average crack widths for both specimens at each of the three instrumented locations. It should be noted that the maximum crack widths formed closest to the loading point. The maximum crack width in AASHTO2C was 0.15 in and 0.02 in for AASHTO2R.

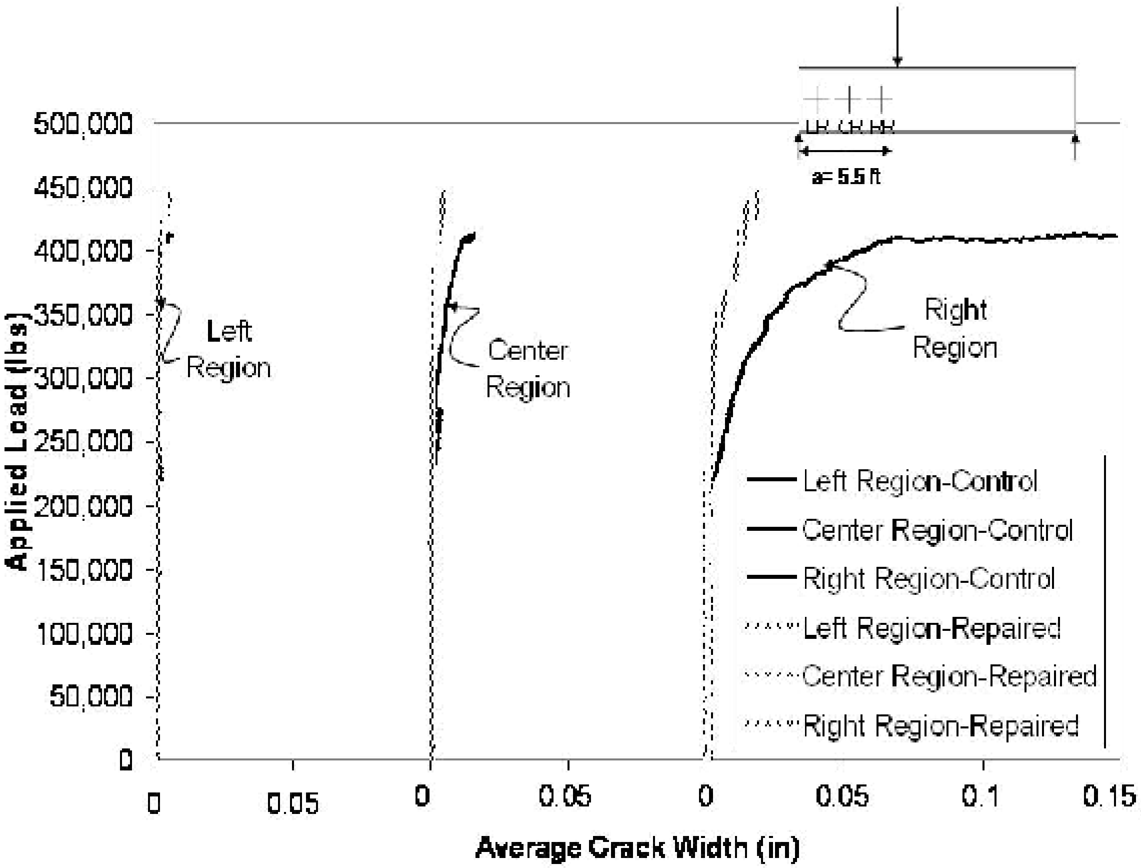

Figure 6.9 Average crack widths of AASHTO2C and AASHTO2R girders

Tensile Strain in CFRP

The tensile strain in the CFRP was measured at the right end of the longitudinal CFRP sheets. Figure 6.10 shows the load versus tensile strain plot for AASHTO2R. Several points that should be noticed were the presence of interfacial cracking, followed by plate-end debonding of the CFRP. The strain value near the termination point of the longitudinal CFRP was low (810 $\mu\varepsilon$) when plate-end debonding occurred. The presence of a U-wrap at this location would have minimized the plate-end debonding effects.

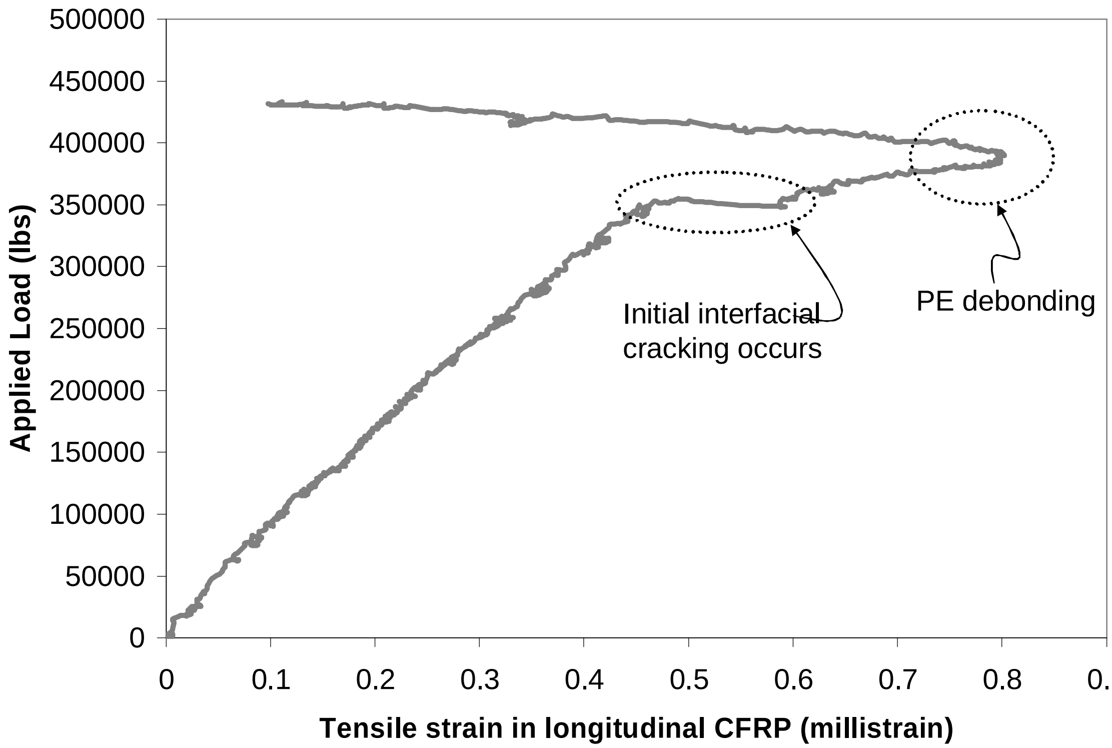

Figure 6.10 Tensile strain in longitudinal CFRP of girder AASHTO2R

The tensile strain at the center of each diagonal CFRP strut was also measured during the loading of AASHTO2C, as shown in Figure 6.11. This figure indicates that the largest inclined crack openings were located approximately half way between the left support and load plate, as expected. Also, the strain induced in the diagonal CFRP struts was much lower than the ACI Committee 440 (2002) rupture design value of 0.004 in/in, therefore not causing debonding or rupturing of the sheets.

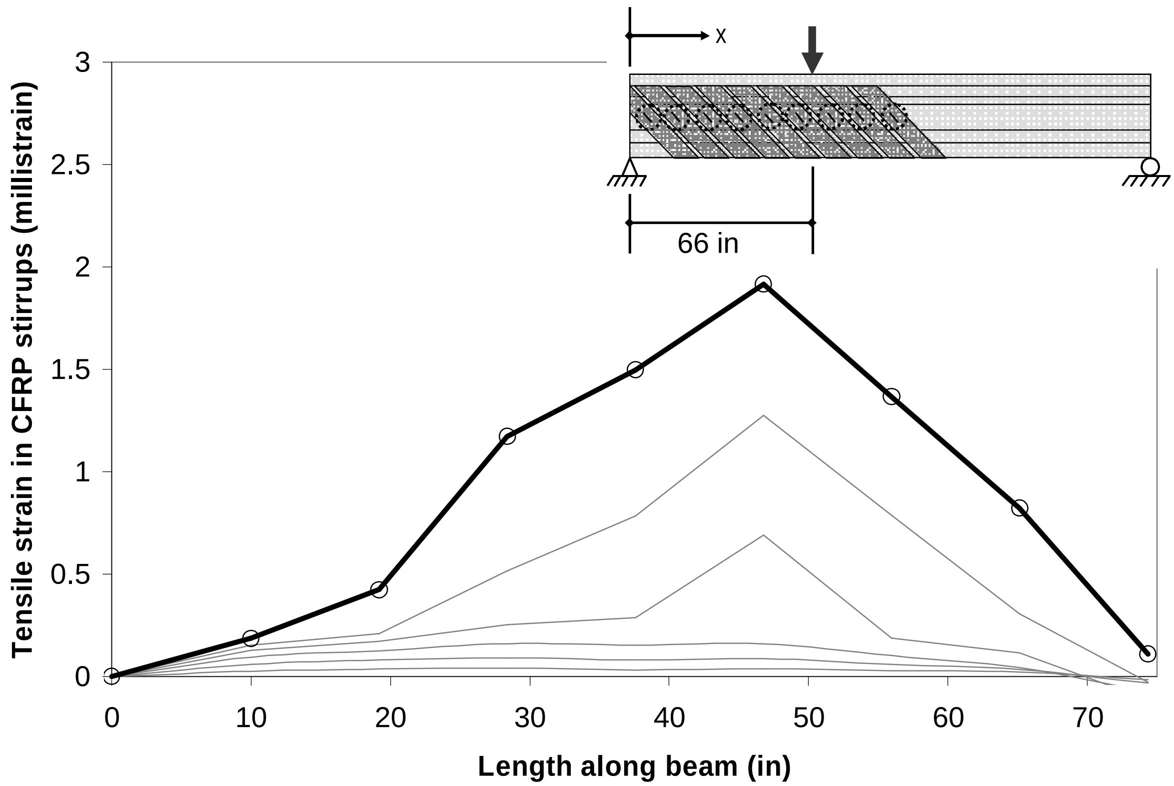

Figure 6.11 Distribution of tensile strain in diagonal CFRP struts

Behavior at Ultimate

The ultimate load versus deflection behavior of girders AASHTO2C and AASHTO2R are shown in Figure 6.12. Full descriptions of the static tests to failure are provided in Chapter 3. Failure of AASHTO2C initiated in the inclined cracks that formed on the shear-critical side of the test specimen. The failure of AASHTO2R initiated beyond the longitudinal CFRP sheets after shear failure in the right transfer region had occurred. As flexural shear cracks began propagating through the web, caused by the debonding of prestressing strands resulting from the failure in the transfer region, plate-end debonding occurred. The diagonal CFRP struts remained intact after the failure of AASHTO2R.

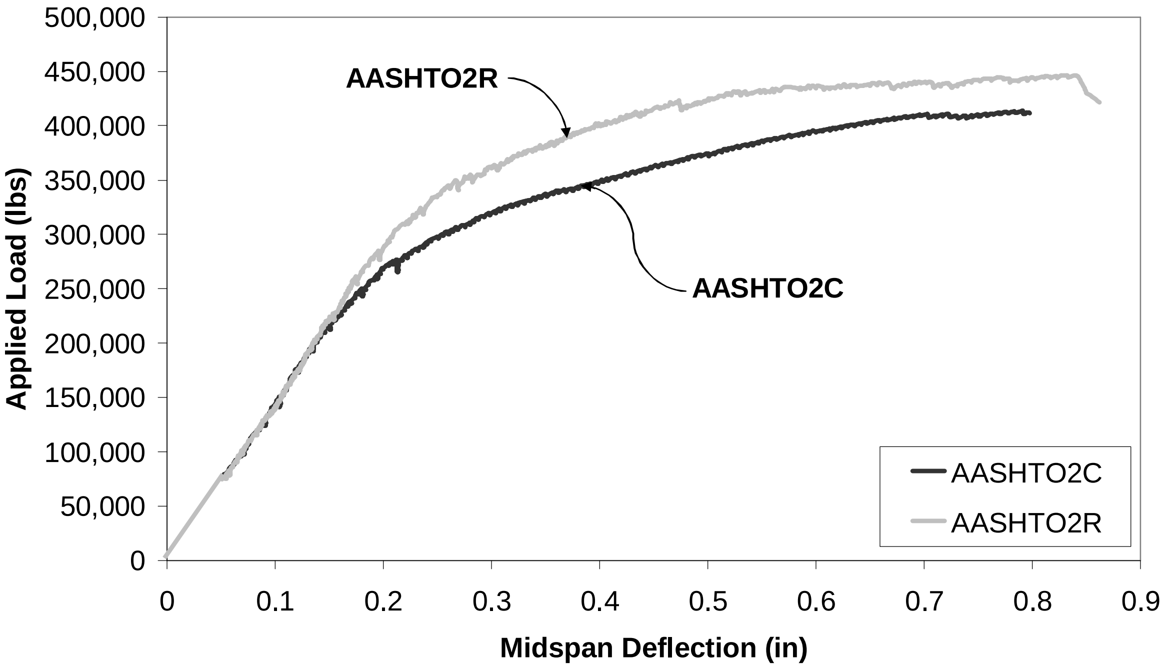

Figure 6.12 Load versus deflection of girders AASHTO2C and AASHTO2R

The initial stiffness of both AASHTO2C and AASHTO2R was roughly identical. The cracking load of the repaired specimen was greater than the control specimen and is shown in Figure 6.12. The ultimate load capacity of AASHTO2R was 7 percent higher than that of AASHTO2C, and the ultimate displacement was slightly enhanced. The maximum compressive strain reached in each of the tests was 680 $\mu\varepsilon$ and 1400 $\mu\varepsilon$ for girders AASHTO2C and AASHTO2R, respectively.

Predicted versus Experimental

The initial predicted shear capacity of AASHTO2R was 373 k, made using the PCI guidelines previously described in Section 6.2. The predicted shear capacity was less than the experimental ultimate load of 413.7 k . The test results clearly demonstrated that shear failure was the mode of failure in girder AASHTO2C, as previously shown in Figure 4.39. Therefore, an alternative method of examining the shear capacity of the girder was devised in hopes of more accurately predicting the shear failure load of girder AASHTO2C.3

After thoroughly examining the PCI (2006) equations for calculating shear capacity, and in comparison with AASHTO2C test results, it was discovered that replacing PCI's maximum effective depth of the prestressing strands (d) of 0.8 times the height (h) of the member with the true effective depth a far more accurate comparison to the test results could be obtained, as shown in Figure 6.13. It should be noted that the 0.8 times the height of the girder is intended for use as a conservative design value, however because this was an analysis of the girder and not the design, it was ignored. This method of examining the shear capacity will be referenced as the modified PCI method for here on out. The modified PCI method predicted an ultimate shear capacity of 414 k, similar to the experimental result of 413.7 k. It should be noted that the FRP U-wraps shown on the bottom of Figure 6.13were left over from the flexural repair of girder AASHTO2.

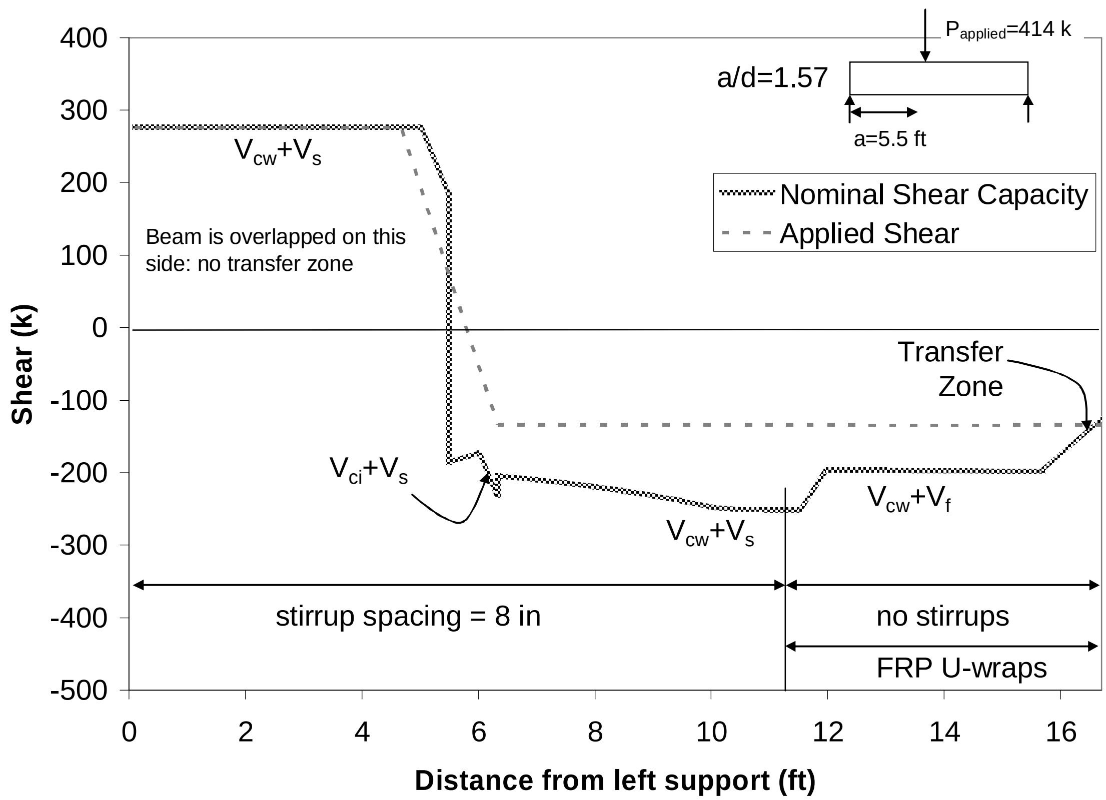

Figure 6.13 Modified AASHTO2C girder predicted and applied shear

The predicted shear capacity of the CFRP repaired AASHTO2R girder, shown in Figure 6.14, was determined using the modified PCI design guidelines previously presented in conjunction with ACI Committee 440 (2002) shear FRP design guidelines. The predicted shear failure load was 519 k, but the test specimen failed at 446 k, as shown in Figure 6.14. Shear failure to the left of the applied load, the shear-critical span, was not the failure mode of the test specimen, which led to further inspection of possible failure modes. In Figure 6.14, it is evident that the applied shear at the right end exceeded the allowable shear in the transfer region. Shear failure in the transfer region allowed the prestressing strands to debond, in turn lowering the moment capacity of the section on the right end. The moment capacity of the girder prior to debonding of the strands is shown in Figure 6.15, but became much less after the contribution of the prestressing strands is progressively lowered due to debonding.

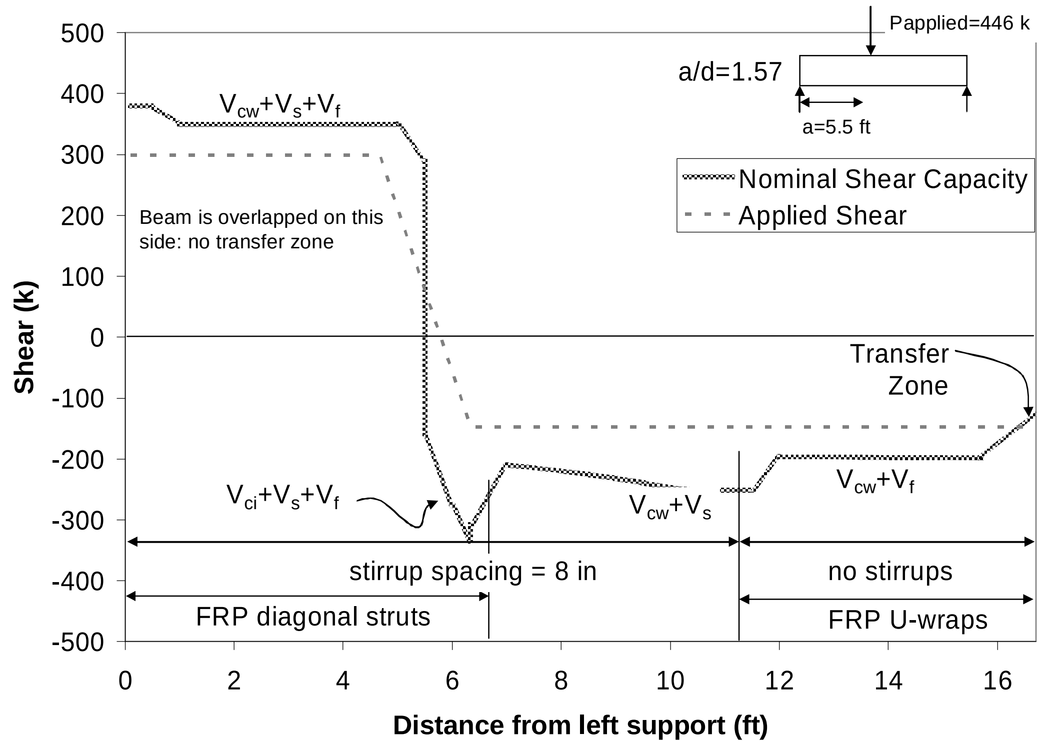

Figure 6.14 Predicted shear capacity versus the applied shear load of girder AASHTO2R

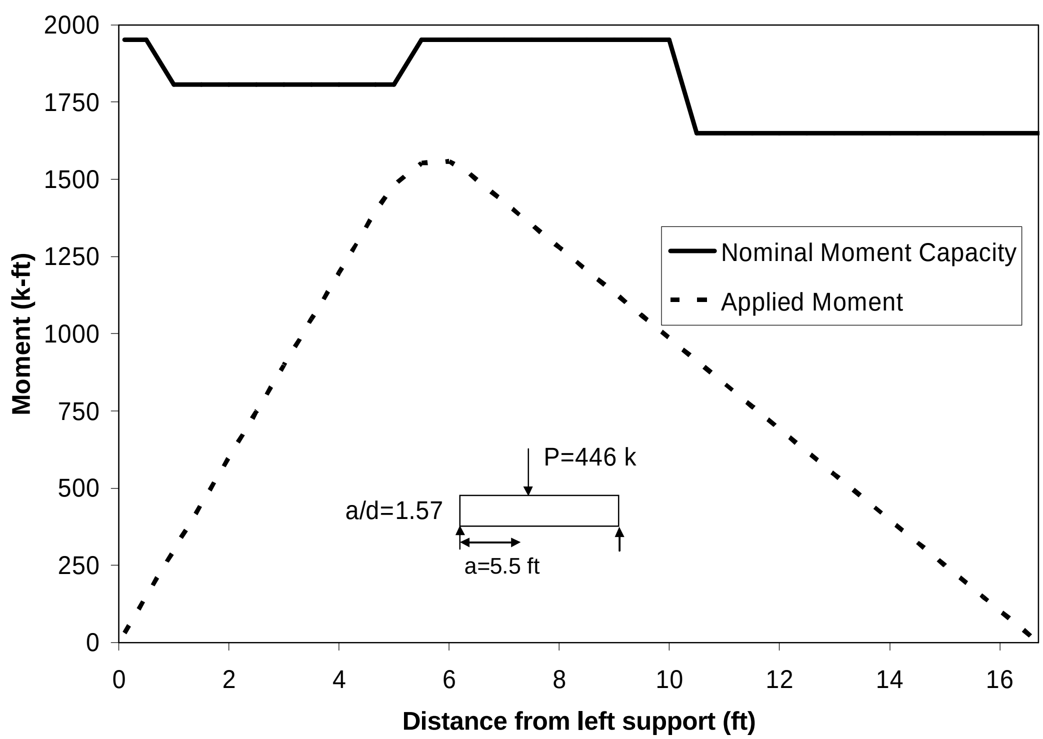

Figure 6.15 Repaired moment capacity of girder AASHTO2R

7 COST-EFFECTIVENESS AND VALUE ENGINEERING

7.1 Introduction

One of the goals of this research is to provide a complete evaluation including a cost-effectiveness and value engineering analysis of different FRP repair and strengthening techniques. Each FRP system was thoroughly analyzed to provide a comparison among the different techniques used in this study. In spite of the fact that the near surface mounted strengthening technique has proven to be the most structurally efficient (see Chapter 5), the preliminary findings show that the most cost-effective systems are the ones which use externally bonded CFRP sheets. Aspects considered in the value engineering analysis corroborate these findings. The results from the previous report, Final Report 2005, are included for comparison purposes.

7.2 C-Channel Strengthening

Cost Analysis

To closely resemble field conditions, the girders were placed side by side, as they would be on a bridge, on top of a steel substructure provided by the Department of Bridge Maintenance approximately 8.2 ft off the ground. The strengthening of the girders began in the winter of 2004 when temperatures at night dropped below recommended values for curing of the epoxy by the manufacturer. Therefore a plastic enclosure and a propane heater were provided to increase the surrounding temperature. This cost was assumed to be similar for all types of bridges repaired under these conditions and was not included as a parameter in the analysis.

To determine the cost-effectiveness of each strengthening technique, the following items were considered: 1) labor costs of the professional FRP applicators, 2) time taken to complete all tasks, 3) material costs, 4) equipment used for strengthening. The material costs include all primers, adhesives and CFRP required for field application for each technique. Equipment items include the rental of sandblasting pot, compressor, and sand. Also included in the equipment cost are items such as latex gloves, Tyvek© suits and plastic mixing buckets. For the externally bonded sheet systems, installation involved the use of paint rollers – so these are included. All other equipment (such as grinders, mixers, safety equipment, etc) is either assumed to be provided by the contractor or used equally in each of the strengthening systems. A summary of the labor tasks and time required for the installation of each of the strengthening systems is provided in Table 7.1. The results of the cost-effectiveness analysis are shown in Table 7.2. The labor costs were determined using a wage of $45 per hour. Consultation with several FRP installers produced this value which is commonly used for cost estimation in FRP strengthening work.

Table 7.1 Labor summary for C-Channel strengthening systems (in hours)

System Designation	NSM1	NSM2	EB1	EB2	EB4	EB5	EB6	EB7	SRP
Strengthening	NSM bars	NSM strips	EB strips	EB sheets	EB sheets	EB sheets	EB HM sheets	EB sheets	EB SRP
Gluing Strips	--	1	--	--	--	--	--	--	--
Concrete Repair	0.95	0.95	0.95	0.95	0.95	1.5	1.5	0.95	0.95
Groove cutting	5.5	5.5	--	--	--	--	--	--	--
Grinding / chipping	5.5	5.5	4	2	3.75	2	2	3	3
Sandblasting	0.3	0.3	0.93	0.93	0.75	0.5	0.5	1	1
Cutting of fiber	--	--	0.5	1	1.59	1.75	2.25	1.5	2
CFRP lay-up	5.63	5.63	10	8.75	11.59	9.95	14.3	11.2	17.4
Total hours / girder	17.88	18.38	13.88	13.63	18.63	15.7	20.55	17.65	24.35
Total hours / ft*	0.66	0.68	0.51	0.50	0.69	0.58	0.76	0.65	0.90

*length of strengthening equals 27 ft

Table 7.2 Cost effectiveness analysis for C-Channel CFRP strengthening systems

System Designation	NSM1	NSM2	EB1	EB2	EB4	EB5	EB6	EB7	SRP
Strengthening	NSM bars	NSM strips	EB strips	EB sheets	EB sheets	EB sheets	EB HM sheets	EB sheets	EB SRP
Main CFRP /ft	8.4	6.4	65.4	3.4	6.1	8.2	16.2	4.5	2.0
CFRP U-wraps /ft	-	-	3.4	3.4	3.7	3.4	3.2	2.2	1.6
Main adhesive /ft	7.4	7.4	4.2	1.5	-	3.6	7.5	3.6	2.5
U-wrap adhesive /ft	-	-	1.5	1.5	-	1.5	1.5	1.8	2.0
Equipment /ft	3.5	3.5	3.4	3.8	3.8	3.8	3.8	3.8	3.8
Labor /ft	30.4	31.3	23.7	23.3	31.7	26.8	35.1	29.4	40.5
Total cost /ft	49.8	48.6	98.8	36.9	45.4	47.2	67.2	44.1	52.5
% increase in strength*	8.4	6.4	65.4	3.4	6.1	8.2	16.2	4.5	2.0
Cost-Effectiveness**	0.140	0.142	0.060	0.087	0.402	0.470	0.024	0.209	0.269

* for girders tested under static loading conditions.
** based upon (percent increase in strength) / (total cost per foot)

The cost analysis indicates that the most cost-effective system, when comparing the variables described previously and combined with the percent increase in strength, was the normal modulus CFRP system used to strengthen girders EB4, EB5 and EB7. The NSM systems also performed well using these criteria. The only system with poor cost-effectiveness was the externally bonded CFRP strips (system EB1), due to the high costs of the CFRP material.

When CFRP was used to increase the ultimate flexural capacity by 20 percent (NSM1, NSM2 and EB1), the labor required for installation of a NSM system was substantially higher than for installation of an externally bonded system at the same strengthening level. If a NSM system was used to strengthen a girder by 60 percent, an appropriate increase in labor costs would be noted, most likely much higher than for the two systems strengthened to that level or higher with externally bonded CFRP sheets (EB4 and EB5). The difference in labor costs between EB5 (EB Sheets) and EB6 (EB HM Sheets) should be noted. Although the girders strengthened with system EB6 had more material, it wasn't only the amount of material that caused in increased labor costs. The contractors also said that the material itself was harder to work with and install than equivalent normal modulus CFRP sheets.

The steel reinforced polymer (SRP) strengthening system performed well in the cost effectiveness analysis, mainly as a result of the economical price of the SRP material which is roughly half the cost of similar CFRP systems. This reduction in cost was somewhat offset by the difficulty encountered in installation of the material, as the labor cost for installation of the system is the highest of all the girders strengthened. The labor estimate does not include the time spent in the repair to correct sagging SRP in one of the girders (SRPF), which is discussed in detail in the next section. If this repair is included in the analysis, the cost-effectiveness of the system is reduced by approximately 50 percent.

Value Engineering Analysis

Various items were considered in the strengthening of C-Channel girders from a value engineering perspective. The cost analysis cannot be used in a stand alone manner in deciding which CFRP strengthening system to apply. Many aspects particular to a certain project or design problem could lead to a decision making the use of certain systems unfeasible. The ability to provide guidance and forethought to the design problem from an engineering viewpoint is the goal of the value engineering analysis. One of the most important items that need to be considered prior to strengthening a C-Channel bridge is the condition of the bridge. The research team visited four C-Channel bridge sites in the course of the research. All bridges consisted of two simply supported spans with C-Channel girder superstructure systems.

Figure 7.1 Corrosion of bearing plate (left) and typical timber substructure (right)[1]

Figure 7.2 Concrete spalling repair (left) and corrosion of lower prestressing strand (right)[2]

From limited observations and from information given in the literature it can be concluded that some common problems encountered at C-Channel bridge sites are: 1) corrosion of lower prestressing strands near midspan resulting in longitudinal cracking and spalling (shown in Figure 7.1), 2) corrosion of the bearing plate at the support, resulting in spalling of concrete around bearing region (shown in Figure 7.1a), 3) shear cracks extending from area near support into the deck and 4) cracking of deck near midspan as a result of incorrect lifting maneuvers during original girder installation. In addition to these items observed with the superstructure elements, various other poor conditions can be found in the timber substructure (Figure 7.1b). Since strengthening may increase the posted capacity of the bridge, the timber substructure must be carefully evaluated to ensure that these increased loads do not lead to poor performance or deterioration. Therefore it is highly recommended to monitor the structural performance of any bridge strengthened using CFRP systems, especially the timber substructure. It is also essential to evaluate the efficiency of the timber substructure prior to installation of any strengthening technique.

The condition of the C-Channel girders may also lead to the use of particular systems which may be more effective. If the soffits, or webs, of a girder span have spalled concrete over a substantial length on either side of midspan, the use

---

[1] Corrosion of bearing plate is from Bridge 70 in Catawba County, NC. Timber substructure shown is from Bridge 43 in Carteret County, NC

of NSM systems could be problematic. If the concrete is damaged in the cover concrete below the lower prestressing strand, corrosion treatment of the strands and careful restoration of the concrete section should be performed prior to installation of the CFRP system. In the case of significant concrete damage, NSM systems may not be the best systems because of a danger of debonding failures despite their structural efficiency. An externally bonded system, with sufficient transverse CFRP U-wrap reinforcements would be the most effective choice.

It should be noted for C-Channel girders: even if the condition of the soffits is good, spalling of concrete may occur during the groove cutting process. If the two-bladed saw typically used for this purpose becomes slightly off-center, the groove could extend towards the edge of the soffit and spall off the concrete. This incident occurred numerous times during the installation process, since the width of the C-Channel soffit was only 2.5 in and the width of the groove is 0.75 in. One of the reasons the concrete saw bounced off the groove line was because of the presence of regular steel reinforcing stirrups which extended farther down than was specified on the plans. In some cases these stirrups were exposed at the bottom of the C-Channel girder, which had lead to corrosion in the stirrups and in the lower prestressing strand. Installation of a NSM system would be much more difficult if the bridge had many of these exposed stirrups which are in the region reserved for the NSM groove.

The width of the soffit may also control the configuration and level of strengthening since the geometry of the groove and width of the soffit often dictates the amount of NSM strengthening – whereas with externally bonded sheets an increase in ultimate load capacity of 73 percent was reached by increasing the number of sheet layers. The 20 percent increase in ultimate capacity was achieved using the NSM configurations; strengthening beyond this level was not feasible because of the width of the soffit. Strengthening using NSM systems could be extremely useful and effective for increasing the negative moment capacity for continuous span bridge decks located over the supports since many grooves can be cut efficiently in the concrete deck and the CFRP bars or strips inserted inside. For similar reasons, the strengthening of one-way slabs using NSM systems can be very effective (Hassan and Rizkalla 2002a).

Since all the strengthening work was performed under simulated field conditions, an evaluation of the difficulty of overhead installation can be made. Cutting of the NSM with the saw overhead can be a challenging task. If large numbers of girders are being strengthened using a NSM system, a guidance system should be constructed to locate the groove cutting in the correct position and to alleviate the weight burden on the installer. The easiest and simplest system to install overhead was the externally bonded strips. The installation of externally bonded sheets systems was slightly more challenging due to the need to apply pressure to the saturated sheets to ensure good adhesion.

---

[2]Concrete spalling repair is from Bridge 43 in Carteret County, NC. Corrosion of prestressing strand is from Bridge 14 in Pamlico County,

Installation of the systems using externally bonded strips were the most straightforward among the various systems considered in this investigation. In light of the possible debonding problems that could be encountered in this system, as well as the high cost of the material, it might not be the most effective solution to strengthening girders of this type. In addition, in order to control debonding of the CFRP plates, transverse CFRP U-wrap sheets are highly recommended.

The high modulus (HM) CFRP material, installed as either strips or sheets, are not the most effective material due to their limited ultimate strain capacity. Due to their brittle characteristics, handling and installation of the material requires careful attention to transportation and handling which increases the overall cost associated with this strengthening system.

Two C-Channels were strengthened with externally bonded steel reinforced polymer (SRP) material. During the strengthening operation several difficulties were encountered with SRP material with 0.03937 wires per in., mainly in SRP material that was bent, or meant to be rounded. For the longitudinal SRP, it was envisioned that the material would conform to the rounded soffit edge and bond to the concrete without leaving voids. For one of the soffits in girder SRPF, the SRP material was cut in the longitudinal direction in two places to relieve pressure that was present due to the wrapping. On the other soffit the SRP was left in one piece per layer, a configuration which resulting in sagging that was observed post-strengthening. To provide transverse strengthening to mitigate debonding SRP L-clips were provided, one on each side of the beam soffit at the required location. The L-clips were bent by the manufacturer to a specified angle of 90 degrees with a radius of 0.12 in. Due to the stiff nature of the SRP material with 0.03937 wires per in. in both the in-plane and out-of-plane directions, it was difficult to install the L-clips without using large amounts of epoxy material to fill voids. It is recommended that the SRP material not be used in situations where the material must be bent to conform to a particular surface.

Due to the fact that C-Channel type bridges typically span small streams and estuaries, the impact of a repair using CFRP must take into account its effect on the environment. It is recommended that the mixing of all the materials used in the repair be performed at a flat location away from streams and other environmentally sensitive areas due to the undesirable environmental problem which could occur due to a possible spill. Each of the strengthening systems in this investigation has their own set of drawbacks for the environment that may need to be considered in the selection process. The NSM systems use the least amount of adhesive during installation and therefore may be the safest option. However, it is recommended to isolate the superstructure of the bridge during cutting of the grooves required for the NSM system to prevent large quantities of concrete dust being released into the surrounding areas. Special precaution should be taken when mixing and applying the various primers, bonding agents and adhesives used in a wet lay-up type repair to prevent site contamination and health concerns. Safety precautions and environmental guidelines published in the recent NCHRP document (Mirmiran et al 2004) should be followed.

7.3 AASHTO Strengthening

The cost analysis of the CFRP repairs preformed on the AASHTO girders was similar to the C-Channel cost analysis since the installation of the CFRP repair system was carried out in a similar manner. All materials involved in the concrete repair and restoration were included: the concrete repair mortar, rust inhibitors, epoxy injection cost and the cost of the materials involved in the building of formwork.

At the site, a plastic enclosure was used and heated to provide comfort for the contractors and providing adequate curing temperatures for the adhesive. An equipment charge that was believed to be relevant for inclusion in the cost analysis was the rental of the sandblaster, sandblasting pot, compressor and sand. In addition, items such as Tyvek© suits, plastic gloves, mixing buckets and plastic rollers were also included. Items such as grinders, safety equipment and mixers were not included as it is assumed that their cost is covered by the contractors. Since the goal of the research in the repair scenario was to restore the original capacity of an undamaged girder, the cost-effectiveness cannot be evaluated as defined earlier. However, since all the CFRP repairs were successful in achieving their goals, the labor summary shown in Table 7.3 and the cost analysis shown in Table 7.4 could be of use and beneficial as an estimate of the expenses involved in a repair of this type. Since the only girder which was damaged by an overheight vehicle was AASHTO1 (Rizkalla et al. (2005)), several repair items such as epoxy injection have been included in the other girders even if the task was not performed. This was done in order to compare a baseline amount of damage. It should be noted that the labor cost per meter and total cost per meter should be used carefully because the actual length of repair depends on many different factors including the amount of concrete damage and number of ruptured prestressing strands. The length of the CFRP system for the girders repaired in flexure was taken as 28.9 ft, and for the girder repaired in shear the length was taken as 10 ft.

Table 7.3 Labor summary of CFRP repair of AASHTO girders

Task Description	AASHTO1	AASHTO2	AASHTO3	AASHTO2R
Chipping damaged concrete	4	4	4	4
Applying rust inhibitors	2.5	2.5	2.5	2.5
Constructing and installing formwork	3.2	3.2	3.2	3.2
Pouring concrete	19.83	8	8	8
Epoxy injection	5	5	5	5
Grinding	20	20	20	20
Sandblasting	9	8	8	6
Cutting fiber	3	5	5	8
Installing longitudinal CFRP reinforcement	15	15	15	10
Installing U-wrap CFRP reinforcement	12	13	13	22
Total hours / girder	93.53	83.7	83.7	88.7
Total hours / ft*	3.23*	2.89*	2.89*	8.87**

* length of repair = 28.9 ft.
** length of repair = 10 ft.

Table 7.4 Cost analysis of CFRP repair of AASHTO girders

System Designation	AASHTO1	AASHTO2	AASHTO3	AASHTO2R
Repair system	EB CFRP sheets	EB CFRP sheets	EB CFRP sheets	EB CFRP sheets
Repair Mortar	500	500	500	500
Rust Inhibitors	60	60	60	60
Epoxy Injection	100	100	100	100
Formwork Materials	700	700	700	700
Main Longitudinal CFRP	456	67.5	67.5	45
Tension strut CFRP	391.5	58.5	58.5	99
CFRP U-wraps	564	376.65	376.65	399.15
Equipment	265.5	265.5	265.5	265.5
Labor total ($45/hour)	4208.85	3762.2	3762.2	3987.0
Total cost	7245.85	5890.4	5890.4	6155.6
Total cost / ft*	249.91*	203.09*	203.09*	1373.19**

* length of repair = 28.9 ft.
** length of repair = 10 ft.

For the repair of the AASHTO girders in flexure (AASHTO1, AASHTO2, AASHTO3), the total cost per meter was similar for each. This is a result of the similar type of repair configuration, and the length of the CFRP repair, which was identical in each instance for structural comparison purposes. For each of these girders the time required to restore the concrete section was substantially less than the time required to install the CFRP repair system. In addition, the amount of longitudinal CFRP was only around 30 percent of the total cost of CFRP, the remaining material being used for transverse U-wraps and tension struts. This represents the importance of proper detailing in a flexural repair.

For the girder repaired in shear (AASHTO2R), the amount of time required to install the CFRP system was substantially longer than the flexurally repaired girders, mainly a result of the precision needed for installation of the transverse CFRP at an angle of 45 degrees.

Cost Analysis

Most of the findings presented in the value engineering analysis for the C-Channel girders strengthened with externally bonded CFRP wet lay-up systems are applicable for the repair of the AASHTO girder. Some other items specific to the AASHTO girder repair are discussed below.

In some cases, where the impact damage occurs near the supports, the desired length of development of CFRP sheets beyond the damaged region may not be possible. It would be recommended to provide for additional anchorage systems in this instance. Barnes and Mays (1999) have described a mechanical anchorage detail for CFRP plates which could be adapted for this purpose. The research team will study this problem as part of the project extension where one AASHTO Type II girder will be damaged near the supports and repaired using CFRP sheets.

In order to restore the original serviceability after an impact event resulting in a loss of prestress, the girder may have to have additional prestressing added – either in the form of external post-tensioning, splicing of the ruptured strands or application of prestressed CFRP sheets. The original ultimate capacity of the girder can be restored by repair using CFRP sheets.

Although the examination of different types of CFRP repair for impact damaged AASHTO girders is not being explored in the project extension, with a greater number of CFRP repair systems under field conditions, a better understanding of aspects related to value engineering can be obtained.

8 DESIGN GUIDELINES

8.1 Introduction

A previous chapter in an earlier report (Rizkalla et al. (2005)) suggests design guidelines for the installation of FRP systems. Similar information is in this chapter, including the design of SRP systems and so is up to date. Proper installation of the FRP system is essential in ensuring the performance desired by the designer. Correct techniques must be employed from the surface preparation to the application of the final protective coating, to ensure effective behavior of the FRP system. The recommendations provided in this chapter are based on the sizeable experience gained by conducting this research, as well as state-of-the-art installation procedures and guidelines found in the literature (Mirmiran et al. 2004, The Concrete Society 2003). Use of experienced contractors to perform the installation is essential and required for the proper installation of the system. Covered in the appendices are installation procedures for the strengthening systems examined in this research, including externally bonded CFRP precured strips and wet lay-up sheets, near surface mounted CFRP systems, and externally bonded steel reinforced polymer (SRP) systems.

Proper scheduling of any repair or strengthening operation using CFRP is essential. Typical repair projects require preparation of the surface, protection of the exposed steel reinforcement, and restoration of the concrete section which calls for a two-part mortar to be properly cured. The application of a CFRP system is also highly time dependent, including the use of a two-part structural epoxy with a specific pot-life. When using proper materials and techniques, a CFRP installation can take less time compared to a conventional repair or strengthening operation, and far less time than total bridge or girder replacement.

8.2 CFRP Repair and Strengthening Systems

Externally Bonded Pre-cured CFRP Laminate Installation

The installation of an externally bonded CFRP pre-cured laminate should begin by cutting the laminate to the specified dimensions and cleaning the CFRP surface. The adhesive should then be mixed in the appropriate ratio using a suitable electric mixer for the specified duration at ambient temperatures specified by the manufacturer. Using an adhesive bed, or guide is the best way to apply the adhesive to the CFRP laminate surface. The strip is placed longitudinally in the bed and the adhesive placed on one side of the metal plate. When the strip is pulled though the bed, a thin layer of adhesive is deposited on the CFRP strip in a triangular cross-section.

Figure 8.1 Adhesive bed for externally bonded CFRP laminate installation

The thickness of adhesive to be used should be specified by the laminate manufacturer. After adhesive application, the strip can be placed on the concrete substrate and pressed firmly to release entrapped air and change the dimension of the triangular adhesive cross section to a uniform thickness. Placement of clamping or shoring systems may be necessary in overhead applications for the duration of curing. After placement, the excess adhesive around the edges of the laminate should be wiped clean.

Externally Bonded Wet Lay-up CFRP Installation

All primers, putties and saturants should be mixed in the appropriate ratios with an electric mixer for the correct duration in ambient temperatures specified by the manufacturer. A primer coat is usually applied first to the concrete surface to penetrate open pores. Next, a bonding agent or putty is applied using a trowel to smooth the concrete surface and fill in small voids or gaps not adequately filled in during concrete repair and surface preparation. The putty is commonly made by mixing the primer/saturant with a thixotropic agent like untreated fumed silicon dioxide (Cabosil®). An approximate mixing ratio to the primer/saturant is 1:1 by volume.

Figure 8.2 Application of putty for wet lay-up

The saturation of the CFRP sheets is an integral part of the installation – impregnating the fibers of the sheet within an adhesive matrix. This is best performed with a resin-impregnating machine to ensure uniform saturation, but can be performed by hand using the following procedures: 1) impregnate one side of the sheet with saturant by using a paint roller, 2) flip the sheet over and saturated the other side similarly, 3) roll up the saturated sheet and let stand until the sheet becomes slightly hot to the touch.

Once the primer and putty applied to the concrete surface have become tack-free (depends on ambient temperatures) the saturated CFRP sheet may be installed as shown in Figure 8.3. The sheet is put in place by hand and rolled in the direction of the fibers using a plastic serrated roller.

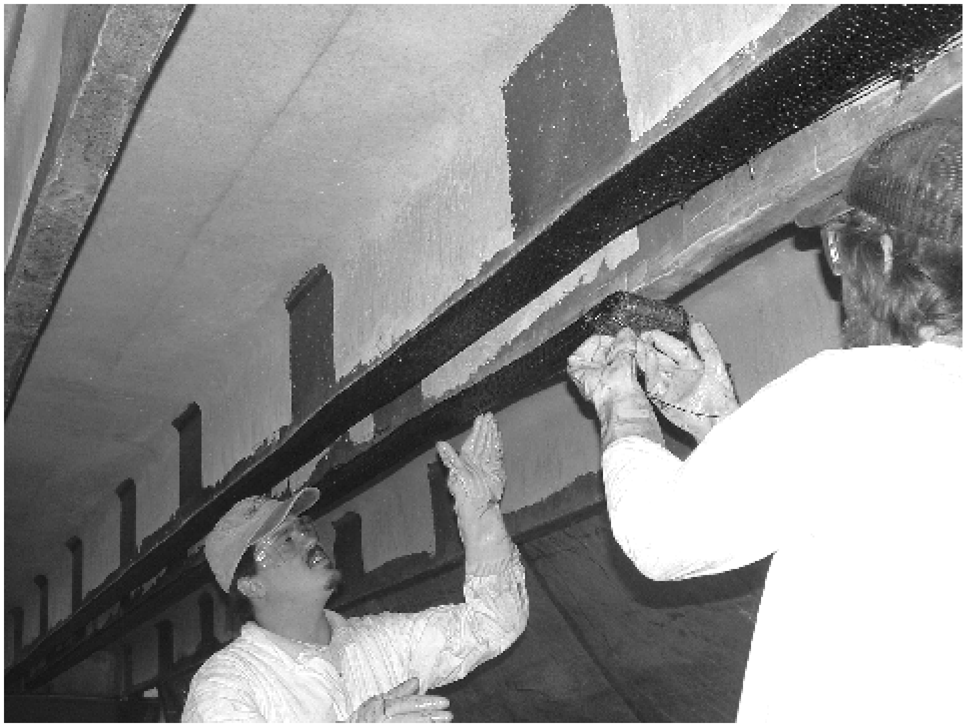

Figure 8.3 Installation of CFRP sheets

Rolling in a direction perpendicular to the fibers or with excessive force may fracture the fibers. Care must be taken to apply sufficient pressure to the sheets to release entrapped air and prevent sagging in overhead applications. Sufficient adhesive should be used around the edges of the CFRP sheets when wrapping around a soffit to prevent ponding effects.

Successive layers may be added by applying an additional layer of bonding agent or putty and installing another saturated sheet. Designs of more than five layers of CFRP wet lay-up sheets should be avoided. The manufacturer of each CFRP wet lay-up system may specify their own installation procedures that may differ slightly from the guidelines provided here.

8.3 Installation Recommendations

Shipping, Storage and Handling

FRP materials, in particular pre-cured laminates, should be shipped in impact resistant containers. All components of the FRP system must be stored properly in clearly marked containers in ambient temperatures 50-75.2° F. The shelf life of the FRP system components should be specified by the manufacturer and marked on containers. Correct handling of components of the FRP system is important to prevent damage or fiber misalignment. After cutting of

CFRP sheets, it is recommended that the sheets are rolled at a radius no tighter than 11.8 in (Mirmiran et al.2004). This is especially important for CFRP sheets made of a high modulus material. Rolling of high modulus CFRP pre-cured laminate strips is not recommended. While mixing the epoxy materials, it is important to scrape the buckets of each component to ensure that proper mixing ratios have been obtained. In addition, the epoxy materials should be kept out of direct sunlight during their working time.

Section Restoration

The restoration of a damaged prestressed concrete section can be a large task involving formwork and shoring or simply routine patching of lost cover concrete in the region below the lower prestressing strand. Before beginning restoration, all defective concrete should be removed in accordance with ACI Committee 546 (1996) using an appropriate jack-hammer or electric saw, to a depth of 0.5 in beyond the repair area in order to expose sound aggregates. Prior to application of the concrete repair material, the condition of the regular reinforcement and prestressing needs to be carefully evaluated. Discovery of corroded prestressing strands was found in some of the C-Channel bridges. In the flexural design of a CFRP strengthening system, it might be required to reduce the area of the prestressing strands in response to corrosion damage. To prevent further corrosion, application of a corrosion inhibitor is highly recommended. Cementitious, epoxy-modified products such as Sika Armatec© 110 EpoCem acts as an anti-corrosion coating in addition to a bonding agent for repairs to concrete and steel. An alternative, the two layer spray-on corrosion inhibitor Tyfo© CIS, can be used for restoration of the strands.

Figure 8.4 Application of corrosion inhibitor

Selection of the correct material to use in concrete repair is important. The repair material should have a compressive strength equal to or greater than the original concrete. Small areas of damage may be repaired with the same adhesive used in CFRP installation, and can be thickened by mixing with silica sand material. Any concrete voids larger than 0.5 in in diameter, should be repaired with an appropriate two-component polymer modified cementitious mortar. For overhead patching work, to be used in lifts of 1 to 2 in, the material Tyfo© P or SikaTop© 123 Plus is recommended. For large areas of concrete damage, where some amount of formwork is needed, the material Tyfo© PF or SikaRepair© 222 can be used in lifts up to 4 in.

One technique recommended by Shanafelt and Horn (1980) and Klaiber et al (1999) is to preload the bridge span with an appropriately sized truck during the concrete repair and curing. Once the truck is removed, this simple procedure can induce compressive stresses in the repaired concrete within the impacted region.

Surface Preparation

Once the engineer has approved the concrete repair and restoration, the surface preparation of the section may begin. The importance of a flat, smooth or convex surface is paramount in the performance of a FRP system to provide good bond characteristics and to prevent irregularities in the FRP from forming. Surface grinding should be performed on the concrete surfaces on which the FRP system will be applied, eliminating "all irregularities, unevenness and sharp protrusions" (Mirmiran et al. 2004). All surface paint, sealant or any other surface substance should be removed using a disk grinder. All sharp corners should be rounded to a minimum radius of 0.5 in (ACI 440R-02). All surface cracks in concrete larger than 0.01 in should be injected with epoxy.

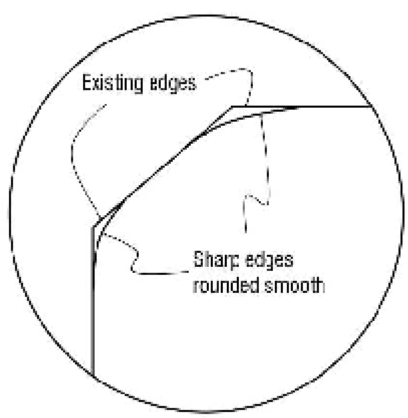

Figure 8.5 Chamfering Corners (from Mirmiran et al 2004)

The size of the groove used in NSM applications should be specified on the design specifications. For NSM bars, the width and depth of the groove should be twice the bar diameter (Hassan 2002). For NSM strips, the width of the groove should be approximately 3 times the width of the strip, and the height 1.5 times the width of the strip (Sena Cruz and Barros 2004).

Figure 8.6 Cutting of NSM groove

An electric saw with two diamond bit blades aligned to the correct width and depth should be used for cutting of NSM groove, as shown in Figure 8.6. After the two saw cuts are made, the concrete within the cuts can be removed using an electric chipper. Groove cutting for NSM systems should take care not to fracture any of the surrounding concrete. If concrete becomes damaged it may be repaired with structural two-part epoxy mixed with sand or an appropriate material.

For externally bonded CFRP system, surface cleaning of the concrete substrate after surface grinding is important in order to remove all dust and to open the pores of the concrete to guarantee good adhesion between the concrete and CFRP system. Sandblasting using Black Beauty© abrasive sand on all surfaces to be applied with CFRP is recommended. For NSM systems, sandblasting of the interior surfaces of the groove is recommended, although cleaning of the inside of the groove with compressed air or similar is sufficient.

8.4 Near Surface Mounted CFRP Installation

The installation of a NSM system is straightforward. The adhesive should first be mixed in the appropriate ratios using an electric mixer for the specified duration in ambient temperatures specified by the manufacturer. The CFRP bar or strip should be cut to the specified length, cleaned and placed at mid-depth of the NSM groove.

Figure 8.7 NSM bar in groove

The bar should then be lightly pressed to allow the adhesive to flow around the bar/strip cross section. The groove shall then be completely filled with additional adhesive and the surface leveled.

8.5 Use of Externally Bonded SRP

Although the installation of steel reinforced polymer (SRP) material is similar to the installation of wet lay-up CFRP systems, there are many differences that will be discussed in this section. The first item that needs to be mentioned is that the SRP material as currently manufactured is susceptible to rapid corrosion damage when exposed untreated to the elements. During the shipping of all spools of SRP material, it must be wrapped with plastic to keep out all moisture. Storage should also occur in a dry, cool place.

The cutting of SRP material is simple in the longitudinal direction (or direction of the wires). A razor blade knife can be used to cut the rubber-like grid that holds the wires together. Cutting in the transverse direction (across the fibers) requires careful selection of a specialized tool. For wires with diameter up to gauge 10, a pair of electric shears may be used. Bending of the SRP material should be done by the manufacturer or distributor prior to delivery to the site. A straight and bent piece of steel fiber sheet is shown in Figure 8.8. Careful consideration of the SRP design should aim to minimize the amount of bended SRP material that is used. For anchorage of an SRP longitudinal strengthening system, in lieu of U-wraps, two L-shaped clips should be used as shown in Figure 8.9.

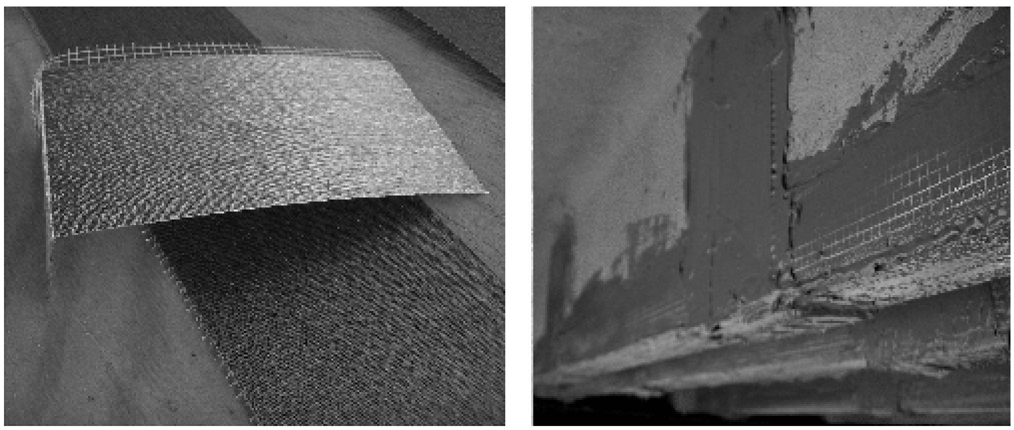

Figure 8.8 Steel reinforced polymer (SRP) system before (left) and after (right) installation

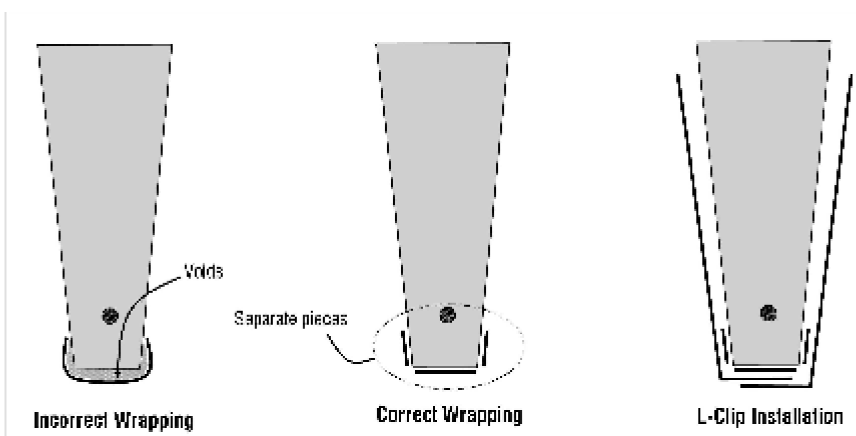

Figure 8.9 SRP installation recommendations

In the preparation for an SRP installation, the concrete surface should first be sandblasted or grinded to expose aggregates and open the pores of the concrete. If SRP L-clips or other wrapping is being installed, the corners should not be rounded, but prepared to the angle specified with no chamfer.

The SRP installation should be completed with epoxy systems specified by the manufacturer and appropriate for the purpose (overhead applications, etc.). Similar to a wet lay-up installation, a primer should be applied to the concrete surface and allowed to become tacky to the touch (approximately 30 minutes). A layer of the saturant is then placed on the surface where the SRP is to be applied. The SRP material is then put in place at the correct orientation and with the correct side up. The SRP should be pressed firmly and uniformly into the epoxy material. The white rubbery grid which holds the wires together also acts as an indicator of epoxy thickness: when the SRP has been pressed down sufficiently, the epoxy will be at the level of the grid material. An additional layer of the epoxy material should then be applied to completely cover the SRP surface. Comprehensive quality control processes should be implemented to ensure that all wire surfaces are completely covered with epoxy material, as the wires themselves are susceptible to corrosion. An installed SRP system is shown in Figure 8.8.

Due to problems encountered in wrapping the SRP material with 25.9 wires per in. around the soffit of the concrete C-Channels strengthened in this research, it is recommended that the SRP be cut into multiple pieces as shown in Figure 8.9. This relieves outward pressure caused by the transverse stiffness of the material and prevents voids from forming between the concrete and SRP.

9 INSPECTION GUIDELINES

9.1 Introduction

Effectiveness of repair and strengthening systems, with fiber reinforced polymer (FRP) material, is highly dependent on the bond of the FRP material to the concrete surface. To ensure successful and proper installation of the FRP system requires practical and effective inspection procedures to ensure the effectiveness of the strengthening and repair systems. This chapter discusses the various inspection methods commonly used to ensure proper installation of FRP strengthening/repair systems including the current design guidelines provided by the national and international codes. This chapter presents the experimental program undertaken in this study to demonstrate the most promising technique for inspection using the pull-off test and its effectiveness in identifying any improper installation of the system. Recommendations for inspection procedures for FRP repaired systems are discussed.

The following sections review the current available inspection methods and their use to examine proper installation of FRP repair and strengthening systems for concrete bridges and structures.

9.2 Visual Inspection

The visual inspection of FRP should be done thoroughly and routinely. Several codes and design guidelines recommend continuous detailed records of the inspection, as the most important part of visual inspection is noticing the changes of the repaired area over time. The inspector should check the FRP surfaces for crazing, cracking and delamination as well as locations of possible changes in adhesive thickness. Crazing is the appearance of fine, random surface cracks due to moisture and temperature. The FRP system should be checked for dampness due to long term exposure to water as moisture can lead to major FRP deterioration. The concrete surface surrounding the repair should also be checked for any additional cracking and/or corrosion. As visual inspection relies solely on the inspectors' abilities to observe, it is also recommended the inspector use auxiliary visual aids to improve the view of the surface.

9.3 Various Inspection Tests

There are several types of inspection tests that have been carried out by researchers, both in the field and laboratory, which have been successful in identifying problem areas in repaired concrete structure with FRP. Generally these tests fall under two categories: nondestructive (NDT) and partially non-destructive (PDT) methods. Various NDT and PDT methods are discussed in the following section. The most effective PDT method, typically used by the industry, is known as the pull-off test.

Partially Destructive Testing (PDT)

This section provides the various PDT methods available in the literature and that are used by the industry to inspect the appropriate installation of the FRP repaired and strengthening system for concrete bridges and structures. PDT methods usually provide a better assessment of the strengthening/repair system but as they damage part of the structure, therefore, it may be more costly to the owner due to the cost of repair the damaged parts.

Pull-off test

The pull-off test is one of the most effective and commonly used PDT methods for the inspection of FRP systems. The pull-off test can be used to determine the tensile strength of the concrete substrate before installation of the FRP system as shown in Figure 9.1. It can be also used to determine the bond strength between the concrete surface and the FRP system and to provide the adequacy of passing or failing of the installed FRP material. The three modes of failure typically expected when using the pull-off tests are: failure in the concrete substrate, failure at the laminate-concrete interface or failure in the epoxy adhesive layer.

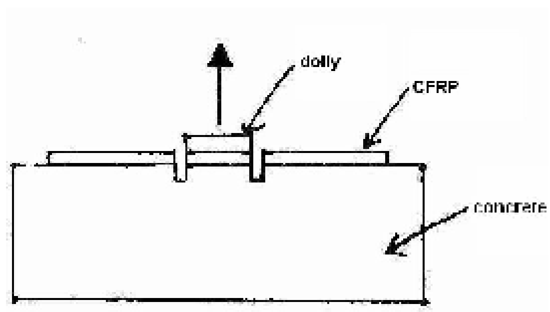

Figure 9.1 Pull off Test

Shear test

Many organizations recommend the use of the shear test, as show in Figure 9.2, to determine the bond quality of the adhesive. In this test a FRP strip is adhered to the concrete surface and extended partially beyond the end of the structure. The strip is then gripped at the free end and pulled in direct tension (pure shear) until failure. Fracture by rupture of the FRP material occurs when the FRP material tears as it is being pulled. Failure of the bond at the FRP-concrete interface occurs when the FRP material is pulled off of the concrete surface. Failure of the concrete beneath the FRP strip occurs when chunks of concrete rip away with the pulled FRP strip but the strip stays in one piece.

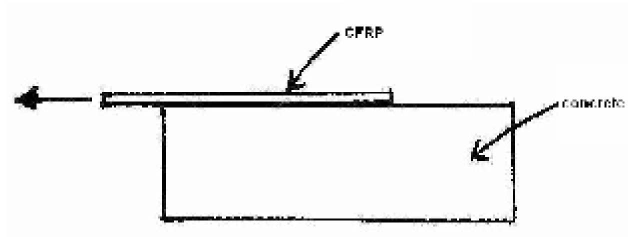

Figure 9.2 Shear Test

Torque test

The torque test is similar to the adhesion pull-off test in terms of set up and preparation, as shown in Figure 9.3. The only difference is the nature of the applied forces. With the surface adherence torque test, a circular dolly is subjected to a pure twisting motion, instead of being pulled in direct tension, through the use of a calibrated torque wrench. This method can be used to evaluate the bond of the FRP strengthening/repair system to the concrete specimen.

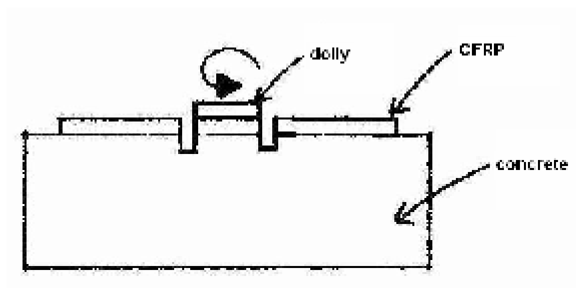

Figure 9.3 Torque Test

Coring

Coring through the FRP repair, as shown in Figure 9.4, can used to determine the laminate thickness and number of plies. The small cores taken from the structure can be visually inspected. As with all PDT methods, the cores need to be located at relatively low stressed zones within the structure.

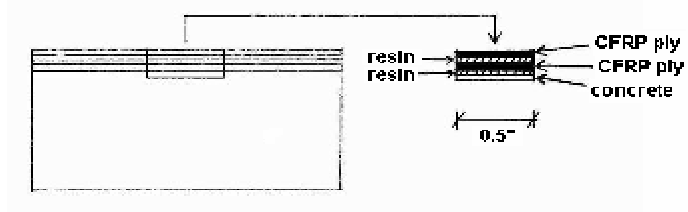

Figure 9.4 Cured Thickness Test

Laboratory tests

It is recommended to test witness panels and resin cups made from the materials used in the field at the time of application of the system. These tests provide data related to the curing status, hardness and tackiness of the adhesive. It is further recommended that the inspector typically compare these test results to the material properties of the adhesive and FRP provided by the manufacturers for comparison.

Nondestructive Testing

This section discusses the various NDT methods available in the literature and used by the industry to inspect the appropriate installation of the FRP repaired and strengthening system for concrete bridges and structures. A nondestructive test is a method in which the testing does not disable or destroy the structure nor impair its future usefulness.

Tapping test (Acoustic Sounding)

When two materials are bonded together, the sound of tapping on the surface, as shown in Figure 9.5, is different from the sound of each material individually. A “full” or low-frequency sound could be heard when the FRP materials are fully bonded in comparison to “hollow” or high-frequency sounds which reflect delamination of the FRP from the concrete surface. The main advantage of the tap test is its relative ease to perform. Tapping on FRP strips can give valuable information as to where potential voids are present between the laminate and concrete. Inspectors must first be trained to recognize the difference between bonded and unbonded laminates.

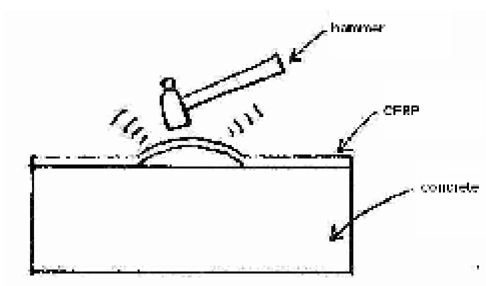

Figure 9.5 Acoustic Hammering

Ultrasonic technology

Ultrasonic pulsed echo technology uses high frequency ultrasonic signals can be used to scan the FRP-concrete interface. Ultrasonic transparency techniques use low frequency ultrasonic signals to scan paths orthogonal to the strengthened surface. A pulse is sent between two different points and the transmission time of the pulse is recorded. Voids or defects in the laminate will increase the transmission time as the pulse will be redirected onto another path in the concrete to avoid the defects as illustrated in Figure 9.6. For the inspector to analyze the results he/she must first find an area with no voids and record the specimen's "normal" or control transmission time. The effectiveness of these techniques is limited to "gaseous" defects such as air bubbles or gas film detachments and requires smooth FRP surfaces. FRP areas next to edges or with small bending radius cannot be tested with this method. Only those with proper training can effectively use this technology, it is very time consuming and should only be used on critical bond areas.

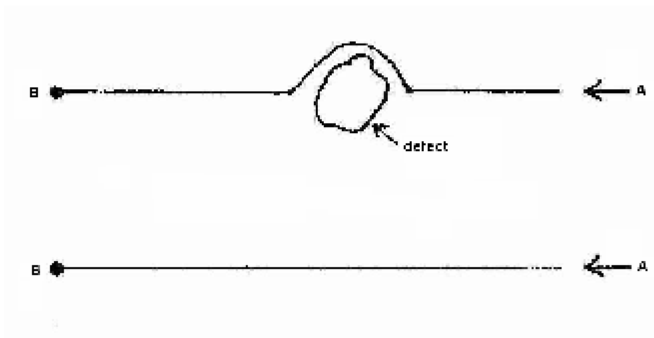

Figure 9.6 Ultrasonic detection of defects

Thermography

Thermography technology is based upon the transfer and/ or loss of heat in a structure. The specimen can be externally heated by many different mediums. If the FRP surface is heated in strengthened structure, the cooler concrete substrate below will draw heat away from the FRP. Heat transfer occurs at different rates between well bonded and debonded areas; the larger the delamination the slower the transfer rate and the hotter the area, as illustrated in Figure 9.7. Infrared thermometers and cameras can be used to detect the different areas of heat. Images, taken at various stages of cool down, show the "hot pocket" or delamination locations between the specimen and FRP sheets.

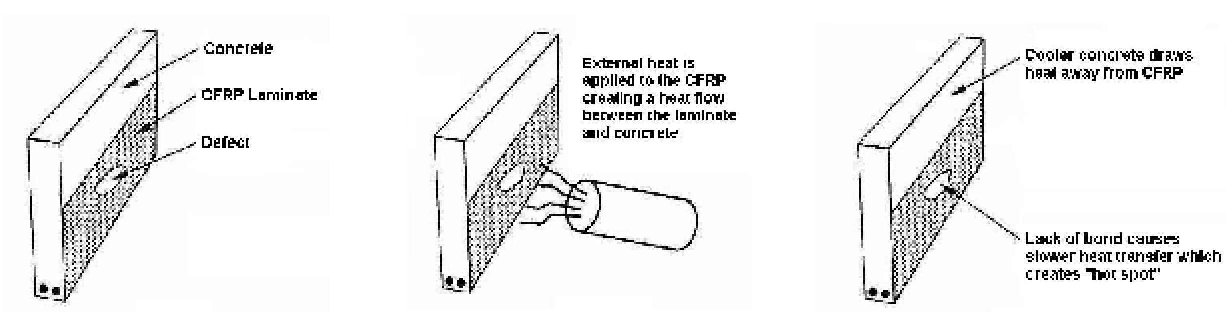

a) CFRP system with defect b) external heat applied c) "hot spot" forms

Figure 9.7 Infrared Thermography

Impulse radar

Impulse radar can be used to detect reinforcement, voids, pipes, etc as well as local humidity within a specimen. This technology allows the thickness of layered structures and rebar or tendon duct positions to be relatively easy to estimate. Very short impulse waves (<1 ns) are sent across the concrete specimen by a tie bow or horn antenna at frequencies typically between 500 MHz and 2.5 GHz. The impulses are then reflected back at different rates due to the dielectric properties of the different materials within the specimen. The reflected impulses are recorded by a second antenna.

Acoustic Methods

Acoustic methods are slower than radar but could be more reliable. This method can be used as a back up when engineers become unsure about measurements taken by radar. A pulse is sent between two sensors with a glycerin gel acting as a coupling agent. The pulse is either detected by the receiving sensor or by other sensors on the FRP plate. Depth of range for this method depends on material properties: porosity, aggregate size and moisture content. Typical depth ranges into the structure are 11.8 in to 19.7 in.

Laser Shearography

Laser speckle shearing interferometry, also known as laser shearography, is a large-area nondestructive method based on laser interferometry. The concrete structure is covered with a relatively low intensity laser light and the image recorded with a digital shearography camera for a reference. After heating of the structure another image is recorded. These two images are superimposed on top of each other to determine the defects. A major advantage of this method is that the pictures are permanent records easily used for comparisons to determine any delamination growth over time.

9.4 National and International Codes and Installation Guidelines

The following provides review of the current national and international codes, guidelines and literature that discuss the inspection of various FRP systems both in the field and laboratory.

American Concrete Institute

ACI 440 Committee 440 (2002) regulates the use of witness panels and pull-off tests to evaluate difference aspects of an installed FRP system. It recommends that in-place load tests confirm the installed behavior of the member strengthened with FRP. Witness panels should be used to evaluate tensile strength and modulus, hardness, lap splice length and gel time of the FRP materials. ACI recommends that standards set forth by ASTM D 3039 and ISIS Canada

(1998) be followed when testing witness panels. ASTM D 3418 should be followed for the mixing and subsequent testing of sample cups of resin for level of cure. When appropriate, simple visual inspections can also be made on site to determine resin tackiness and hardness. Visual inspection should also look for fiber orientation and kinks or waves in the wet lay-up sheets system. ACI Committee 440 recommends that any fibers misaligned by more than 5% should be evaluated by an engineer. The FRP should also be checked for changes in color, debonding, peeling, blistering, cracking, crazing and deflections.

ACI recommended inspection tests include acoustic sounding (hammer sounding or tapping), ultrasonics and thermography. These tests should be able to detect delaminations or air voids, of 2.0 in^2 or greater, between FRP layers as well as between the FRP and concrete. For wet lay-up systems delaminations smaller than 2 in^2 can be ignored. For precured systems, all delaminations must be looked at. Pull-off tests, governed by ACI 503R-93 or ASTM D 4541 or by the methods set forth by ISIS Canada (1998), are also recommended. ACI 503R-93 is a guide of the quality control for the selection and application of adhesives and also suggests the use of a pull-off tester for field tests of the adhesion. ASTM D 4541 gives more specific steps to follow when conducting the actual pull off test. Tension adhesion strengths should exceed 200 psi and failure of the sample should occur at the concrete substrate. Cores may also be taken, typically with 0.5 inch diameters, for further visual inspection of the cured laminate thickness.

Canadian Standards Association

The Canadian Standards Association (2002) (CSA) states that all areas repaired with FRP should be inspected according to the manufacturer's specifications. The installed FRP system should be checked for voids and delaminations. Direct pull-off tests should be conducted to verify the bond between the FRP system and concrete substrate. The CSA recommends that a pull-off test of the concrete substrate be done alone before the FRP is installed to give a baseline failure stress level. The pull-off test is considered successful when the tensile stress reaches the design stress or the baseline failure stress level. The frequency and number of pull-off tests shall be determined by the contractor and owner.

The Concrete Society

The Concrete Society has published several guidelines that cover the installation and subsequent inspection of FRP, in particular Technical Report 55 (2000) and Technical Report 57 (2003). TR55, the first document to address the inspection of FRP with regard to British code, lists several long-term items inspectors should take note of when maintaining a structure repaired with FRP. All building/bridge owners are prompted to design a regular visual inspection regime for strengthened elements. All materials used during strengthening should be included in a Health and Safety File, including all initial faults in the FRP such as minor areas of delamination as well as regions where the strengthening is the most critical. TR57 puts great importance on the first inspection after installation, as this will be used as a reference point for future inspections. Visual inspections should occur annually with more detailed inspections every few years, depending on the structure. FRP should be inspected for debonding or other imperfections through the tap test. While thermal and acoustic methods are currently available they may be more applicable in a lab than in the field. In TR57, the Concrete Society recommends the use of a light hammer or coin for as instrumentation for the tap test. They also recommend that the entire repaired area should be tested by this method. In general the Concrete Society follows standards set forth by the British Standards Institution.

Upon immediate installation, particularly with the wet lay-up system, the orientation of the FRP sheets must be checked. TR57 states that the inspector should record where there are any fibers misaligned by more than 0.4 in as well as where there are any noticeable folds or kinks in the FRP wet lay-up system. The visual inspection should check for signs of crazing, cracking or delamination. The concrete structure surrounding the repair should also be checked for cracking, corrosion or other signs of deterioration. Any damage to the protective layer suggests the possibility of damage to the composite underneath. Additional samples of the FRP should be bonded to the structure away from the strengthened region. These samples are to be inspected and tested as part of the inspection regime and should not be covered with any protective layers. Installing instrumentation, i.e. strain gauges, to monitor the structure during and after strengthening could be good indicators of a problem with the installation. It is recommended to keep the FRP as safe from moisture as possible, i.e. blocked up sewers and gutters, as well as safe from any cleaning solvents, future grit-blasting of the concrete structure, etc.

The Concrete Society believes that pull-off tests on a control specimen, at regular intervals, are the best way to test the condition of the adhesive. They recommend that there be five pull-off tests for each “representative” area. There are many organizations that address the use of a pull-off tester including ACI, which suggest the use of ASTM standards, the International Concrete Research Institute (ICRI) and the Concrete Society suggest the British Standards Institute (BS) methods. The British standard, BS EN 1542 is very similar to ASTM D 4541. The only major differences are that BS EN 1542 stipulates that there be a minimum of five bond tests carried out for each test specimen (ASTM requires three for statistical analysis), that the concrete surface be grit-blasted and that coring of the test area be done before the dolly is adhered onto the surface, instead of after.

It is advised that the adhesive debonding of FRP plates and shells be tested using visual and sonic methods (which may also be used on FRP fabric) while thermography is an option for all three FRP systems. Adhesive voids in FRP plates, shells and fabrics may also be detected using ultrasonic methods and in-situ pull-off tests. There are however no current standards governing these methods. The Concrete Society states that acoustic methods are only successful in a laboratory setting as they have had no success in detecting debonding along FRP plates on an actual structure. They have had only some success with thermograhic technologies on actual structures by heating the FRP surface with a high-powered flashgun, scanning the structure at intervals of hot and cold. This method could pick up voids and laminate debonding but gave no idea to the quality of adhesion. It is recommended that the bonding of FRP plates to concrete and the wet lay-up system be inspected using the tap test for the entire repaired area. It is recommended that extra FRP samples be placed away from the strengthened region in a non critical zone for field testing. The Barnes Bridge in Manchester had samples of FRP, one with a "perfect" bond and one with complete debonding, so on site inspectors could have a handy demonstration of what they were to be listening for when completing the tap test on the actual repair. Extra FRP samples can also be bonded to smaller, individual concrete samples and left alongside the structure. They recommend that testing samples not be covered with protective layering.

fib (The International Federation for Structural Concrete)

The International Federation for Structural Concrete (*fib*) recommends several tests for the inspection of FRP after installation. They believe quality control can be achieved through the combination of NDT and PDT methods. They caution that only NDT should occur at critical areas on the specimen; critical areas include areas of high-stress levels and anchorage zones. While separate test areas may be necessary for quality control, all tests should be performed under the same conditions.

Visual inspection should be done at the critical bond zones to look for the presence of voids immediately after installation. Recommended PDT methods include the pull-off test, surface adherence shear test and the surface adherence torque test. Non-destructive tests include the tap test, ultrasonic pulsed echo techniques, ultrasonic transparency techniques, thermography, impact spectrum analysis and surface acoustic wave propagation. *fib* recommends steps and guidelines to follow for each of these tests including the specific use of a steel stick with rounded 0.2 diameter tip for the tap test. It is recommended that at least three bond tests be performed at 3 and/or 7 days after initial installation of the system. *fib* states that thermography has been successful in direct dynamic conditions. Their specimen was at thermal equilibrium, placed under homogeneous heat and then recorded as it cooled down. Defects were located as hot (or cool) spots. Several limitations arose when dealing with thick overlays and with materials that had high thermal conductivity (i.e. CFRP).

Highways Agency

The Highways Agency report BD 84/02 (2002) states that contractors must inspect FRP properties as well as the FRP bond to concrete. The number of tests, type of tests and properties measured shall be predetermined by both the manufacturer and client. FRP properties shall be determined by the tensile and/or compressive testing of coupons made from sample laminates during installation. Testing the FRP's bond to concrete shall be done by installing sample laminates to separately made concrete test pieces, which should be left at the repair site, and then tested for bond strength. Visual inspections shall be done to ensure that the fibers are aligned, straight and uniform, fully covered by resin and that there is no trapped air.

Technical report BA 30/94 (1994) states that inspections should occur every six months for the first two years after completion. It recommends that an inspection procedure manual be prepared and include all technical literature relating to products and equipments used as well as procedures to be followed. It recommends the visual examination and tapping of FRP sheets with a hammer to make sure there is no audible evidence of debonding.

ISIS Canada

The Intelligent Sensing for Innovative Structures Canada Research Network (2004) design guide lists several steps to follow when inspecting FRP. ISIS states that it is the duty of the FRP material manufacturers to train the installation crew and verify their ability to follow and complete the steps required for installation; this includes training those responsible for inspecting the FRP after installation.

ISIS recommends the inspection of FRP before, during and after installation. The inspection report should record the size and number of delaminations, level of cure, adhesion strength, laminate thickness, fiber alignment and FRP and adhesive material properties. Sample resin cups and FRP plate specimens should be made onsite for laboratory testing. A visual inspection should be made to ensure the fibers, specifically for the wet lay-up system, are orientated in the right direction. Any fiber misalignment of more than 5 degrees from the intended alignment should be immediately reported to the Engineer.

After the completion of the installation on-site bond tests should be done to verify the bond strength of the FRP system. The presence of delaminations needs to be detected and analyzed for their size, number and location relative to the overall repair area. ISIS recommends hammer sounding, ultrasonic and thermography technologies as inspection methods capable of detecting such delaminations.

They recommend that the cure of the FRP adhesive should be evaluated through the testing of sample plate specimens or resin cup samples. These tests should be run following the guidelines set down by ASTM Standard D3418 in the laboratory. In-situ, a physical observation of resin tackiness and hardness may be sufficient. ACI 503R-93 or ASTM D4541 should be followed when completing tensile tests of the adhesion strength using a pull-off tester. The frequency of the tests will depend on the size and difficulty of the project. Small core samples, 0.6 inches in diameter, should be taken to determine laminate thickness. These tests should be done away from high stress areas or splice areas on the structure.

Japan Society of Civil Engineers

The Japan Society of Civil Engineers (JSCE) makes several recommendations for the inspection of FRP as part of their Concrete Engineering Series. Continuous fiber sheets should be checked during and immediately after installation for installed position, wrinkles, lifting or peeling and the thickness of the impregnation resin. They state that the performance of the adhesive can be determined by a "bond strength test." The tensile strength performance of continuous fiber sheets during construction is generally checked by means of existing test data obtained at similar environments and conditions but can be checked using test specimens fabricated on site when considered necessary. The JSCE gives some guidelines about bond strength tests and the inspection of the FRP sheets. The code mentions that the repair system must be inspected on site to make sure that the resin has impregnated the fibers thoroughly but does not specify how this should be done.

National Cooperative Highway Research Program

National Cooperative Highway Research Program's (NCHRP) Report 514 gives comprehensive but still general guidelines as to what the inspector should look for after installation of the FRP system in the field. NCHRP recommends many applicable methods for the inspection of various FRP systems after installation. They include visual inspection, acoustic tap testing, pull-off tests, laboratory testing of witness panels and resin-cup samples, and taking core samples. Report 514 also gives specifications as to what to look for when inspecting FRP as well as how often it should be checked. After the initial inspection for waves or kinks in the sheets, NCHRP suggests a cure time of 24 hours before the tap test can reasonably be preformed. According to NCHRP any instrument will do for the tap test as long as it can detect any voids larger than 2 in^2. They also recommend that an area suspect of delamination should be struck at least every 1 ft^2. NCHRP suggests that the inspectors consult ACI and ASTM standards for guidelines on when and how to judge the repaired system. They do require a minimum of three pull-off tests with at least one test per span or 1000 ft^2. NCHRP recommends that a pull-off test occur on a FRP sample on the concrete substrate before the final installation begins. NCHRP gives guidelines as to who can be responsible for the QA/QC of the repair. They also developed a system of checklists for contractors to follow, including one specifically for the inspection of the system post application. The checklist, FORM NO. QAP 15, addresses the tap test as well as the pull-off test.

9.5 Other Literature and Future Techniques

The American Society for Nondestructive Testing (2006) offers many publications for further information on various NDT methods and their uses. Publications include handbooks detailing infrared and thermal testing (volume 3), acoustic emission testing (volume 6) and ultrasonic testing (volume upcoming). The handbooks discuss the applications of NDT for various industries including certain uses of FRP within infrastructure. The organization also provides standards for the qualification and certification of nondestructive testing personnel.

Clarke (2002) recommends the inspection of the FRP repaired system at all stages, especially right after the installation for a preliminary 'as installed' assessment. The author stresses that visual and routine inspections are a vital part of any FRP repair system with attention being paid to the concrete just as much as the FRP. The author recommends the use of the tap test as well as the pull off test.

The Florida Department of Transportation (FDOT) conducted a study to determine the accuracy of infrared thermography (IRT) to inspect FRP composites before, during and after load tests. The IRT research included both laboratory and field tests. The FDOT determined that, in the laboratory, thermography has great potential to identify unbonded areas in FRP systems near the surface but that as the thickness of the laminate increased identifying defects became unrealistic. In the field, IRT identified defects caused during installation as well as damage caused by an accident, though this damage was only identified within the area of the impact. The FDOT concluded that IRT works well only for detecting near surface defects or in single-layer systems.

The need for better understanding of NDT methods was discussed in Helmerich et al. (2006). Several NDT technologies that could be used in the inspection of a FRP system, such as pulse-phase thermography, impulse-radar and acoustic methods, were investigated. The need for additional software development for data analysis regarding these methods, as well as a standard system for assessment of a FRP system, was also explored. The paper suggests that NDT will be more effective once a combination of the different methods is standardized. Currently the authors are focusing part of their research on the mixing of acoustic methods and impulse radar and researching the applications of thermography. Specifically they are determining how pulse-phase thermography is being used for the quality assurance of repair and strengthening using a CFRP system. The two main things being checked are the quality of strengthening after the application of the repair system and the effect of heavy static, impact and cyclic loading on the debonding of the system. To evaluate the application, as well as the accuracy of the thermographic procedure, tests were conducted using two types of specimens. FRP strengthened surfaces were heated with different heating units, such as radiators or a flash light installation, for one minute, then cooled and recorded with the thermographic camera for five minutes. The analysis of the thermographic data received gave good contrast of the debonded areas.

The paper concludes that the main problems with NDT methods are integration issues between NDT data and damage models.

The use of microwave NDT techniques, particularly an open-ended rectangular waveguide, to locate delaminations between FRP layers and a concrete specimen were discussed in Hughes et al. (2002). The paper concluded that microwave technology could be used to successfully locate real delaminations as well as distinguish the difference between real delaminations and false ones.

Kaiser et al. (2004) makes distinctions between NDT, non destructive evaluation (NDE) and non destructive inspection (NDI). While NDT and NDI both refer to the inspection process, NDE is the assessment of the effect the found damage may have on the repaired system. The paper also goes into detail about the use of a calibrated torque wrench to perform inspection tests on FRP samples along with the standard pull-off test. As visual inspection relies solely on the inspectors' abilities to observe, the authors also recommend the use of magnifying lenses and auxiliary light sources to improve the view of the specimen and repair.

Two types of NDI methods, thermography and laser shearography, are discussed in Newman and Zweben (2002). Both tests were declared successful when used to located voids in a FRP repair but the publication states that the laser shearography had several advantages over thermography. While thermography showed the cross sectional size and placement of defects, the shearography method also showed whether the defect was an intrusion or extrusion. Shearography technology can also be used with different types of structural excitation besides heating including mechanical loading.

Mosallam et al. (2006) found that an assessment of the bondline condition of FRP-jacketed RC columns using infrared thermography was not reliable. The resulting images were determined untrustworthy based upon the uncontrollable variability in the amount of heat and the timing of taking the photo during cool down. Also the researchers found it difficult to heat the specimens on-site and found that heating the FRP before it was fully cured lessened the integrity of the repair. The current technology also only produces a 2-D image so there is no way to determine the depths of the voids and the heat could not adequately penetrate thick composite layers.

The long term durability of FRP strengthening systems was studied by Schiebel et al. (2001). The initial tests were successful in that they showed good cohesion between the laminate and concrete structure. The researchers adhered five strips of CFRP at the end of the bridge, away from traffic lanes and the reinforced area, to perform a series of tests on these strips once every five years. The researchers will use the values determined by the pull-off and torsion tests to evaluate the performance of the bond behavior over time.

Taljsten (2002) recommended several tests to determine the presence of voids in a FRP system. The report suggested that the Engineer check the bond joint and composite for possible voids, blisters or discoloration and, in particular, examine critical zones, such as anchorage zones. After the initial application, it is suggested that the final surface be covered with a finishing layer and / or fire protection. The report states that normally voids should be detected by means of "tapping" the bonded surface with a hammer or even a coin. Other methods to be used include ultrasonic pulsed echo techniques, ultrasonic transparency techniques and thermography in direct dynamic conditions.

Tumialan et al. (2001) suggests that a complete visual and acoustic tap test inspection should be performed after at least 24 hours for initial resin cure, and that any delaminations less than 2 in^2 can be ignored. It is also stated that direct pull-off tests can effectively verify tensile bond between FRP sheets and concrete substrate.

9.6 Inspection Demonstration at North Carolina State University

The following section covers the application of one of the most recognized FRP inspection procedures known as the pull-off test. Several organizations and publications recommend the use of a portable adhesive tester to check the bond strength in a FRP repair as well as the tap test to determine areas of delamination in the repaired area. It demonstrates the effectiveness and ease of using a pull-off test to determine the presence of delaminations between the repair system and concrete specimen based on the maximum tensile strength.

The concrete specimen used to evaluate the effectiveness of this inspection method consisted of a 15 foot long surface of a prestressed precast C-Channel type bridge girder provided by the North Carolina Department of Transportation (NCDOT) for project 2004-15. The concrete surface was divided into three distinct zones, each approximately 60 in by 20 in, and tested for various FRP strengthening systems for a total of 153 pull off tests. Precured and different number of layers for the wet lay-up system were evaluated with built in known defects and different surface preparation as given in Table 9.1.

Table 9.1 Test Matrix

	Unprepared Surface			Sandblasted Surface			Grinded Surface		
Defects	None	Level 1	Level 2	None	Level 1	Level 2	None	Level 1	Level 2
Precured	5	5	5	4	5	5	4	5	5
1 Layer Wet Lay-up	5	5	5	5	5	5	5	5	5

2 Layer Wet Lay-up	5	5	5	5	5	5	5	5	5
Baseline	5			5			10		

The concrete surface was prepared by a grinder to remove any dirt and loose material as recommended for the installation of FRP. The first section was lightly grinded to remove any left over asphalt and dirt, and therefore considered as almost unprepared surface. The second section, grinded surface, was ground with a diamond tooth blade until the top cement layer was totally removed and the aggregate was exposed. The third section was sandblasted to open the pores of the concrete until the surface was a relatively uniform height and roughness. As the concrete specimen was an old NCDOT C-Channel bridge girder there were several surface areas where the concrete had been worn down too far into the aggregate. Therefore the installation of the FRP system was not uniform across the surface of the C-Channel, particularly on the unprepared and sandblasted surfaces.

The demonstration consisted of three FRP systems: two inch wide precured FRP system, five inch wide 1-layer and five inch wide 2-layer wet lay-up systems. ASTM D 4541 was followed to evaluate the pull-off strength of the adhesion on the concrete specimen. ASTM required several steps for the preparation of the test site. The selected surface area was flat, rigid and large enough to accommodate the replicate tests; statistically only three replications are required to adequately characterize the test area but at least four were adhered for each test case. Each test site was surrounded by only enough extra surface area to accommodate the testing apparatus. The pull-off tester was a Hilti Test Meter 4 is shown in Figure 9.8.

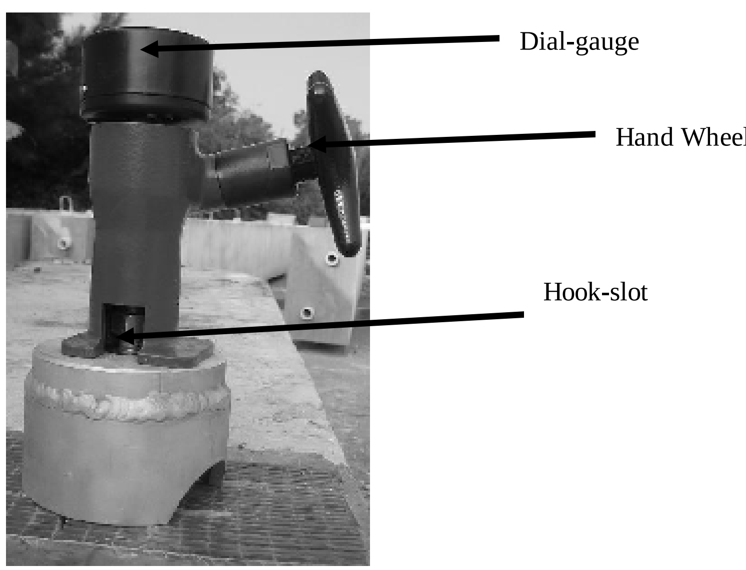

Figure 9.8 Testing Apparatus

Rectangular steel plates (testing dollies) were fabricated at 2.25 in^2 x 3/8 in, with centered 0.5 in diameter threaded holes. A four inch diameter aluminum stand was fabricated to stand over the dollies and allow for direct tensile testing of the specimens by the pull-off tester. Figure 9.9 shows a circular plate, with a 1.0 in diameter hole in the center that was welded to the top of the stand in order to provide a stable support for the pull-off tester to stand on.

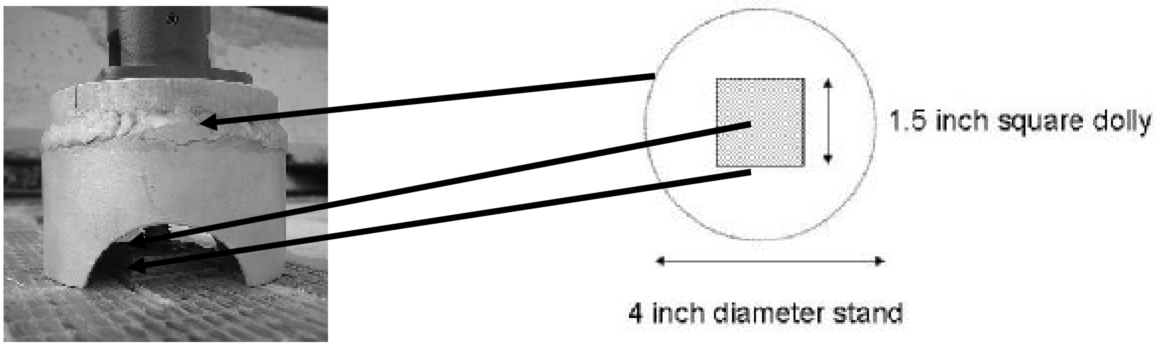

Figure 9.9 Stand and Dolly

Each surface area had three distinct sections of dollies; those with no defects, Level 1 defects and Level 2 defects. Dollies with "no defects" were adhered directly to the FRP. To achieve Level 1 and Level 2 defects masking tape, made specifically to adhere to concrete, was placed directly on the concrete surface. The dollies were then adhered to the specimen, horizontally centered on the masking tape strip.

The induced Level 1 defect consisted of a 0.5 in strip of masking tape which was centered to induce a defect equivalent to 0.75 in^2 or 33.33% of the total repaired area.

The induced Level 2 defect consisted of a 1.0 in strip which resulted in a defect of 1.5 in^2 or 66.67% of the total repaired area. The masking tape was placed directly on the concrete specimen before the application of the FRP strips/sheets. The FRP systems were adhered to the concrete specimen per manufacturer's instructions. The two levels of defected areas along with the no defect surface is schematically shown in Figure 9.10 and Figure 9.11, for the precured strips and wet-lay up system, respectively.

The system was allowed to cure for 7 days after which a cutting wheel was used to cut through the FRP, along the four sides of the dollies, and into approximately 0.6 in +/- 0.2 in of the concrete. A threaded rod was screwed into the dolly and the stand was placed perpendicular to the FRP strips over the dolly. The rod was then inserted into the pull-off tester as it attached flush with the stand. A tensile force was applied using the pull-off tester, following the fabricators instructions, until the block of material was detached. The force was applied with approximate rate of 150 psi/s up to failure.

The nature of failure was recorded, whether it occurred in the concrete substrate or at the concrete/adhesive interface or at the adhesive/FRP interface or within the FRP itself. This failure was qualified by noting the percent of adhesive failure, looking specifically at the interfaces and layers involved. For specimens with an induced partial debonded surface, the amount of exposed debonded surface to specimen cross sectional area ratio was determined. The pull-off strength was determined based on the measured maximum load divided by the total surface area of the dolly. The measured strength of the concrete tensile strength using the same procedure was used as a baseline for comparison reasons. For all cases the strength was determined based on averaging the values for pull-off tests on each of the surface preparations.

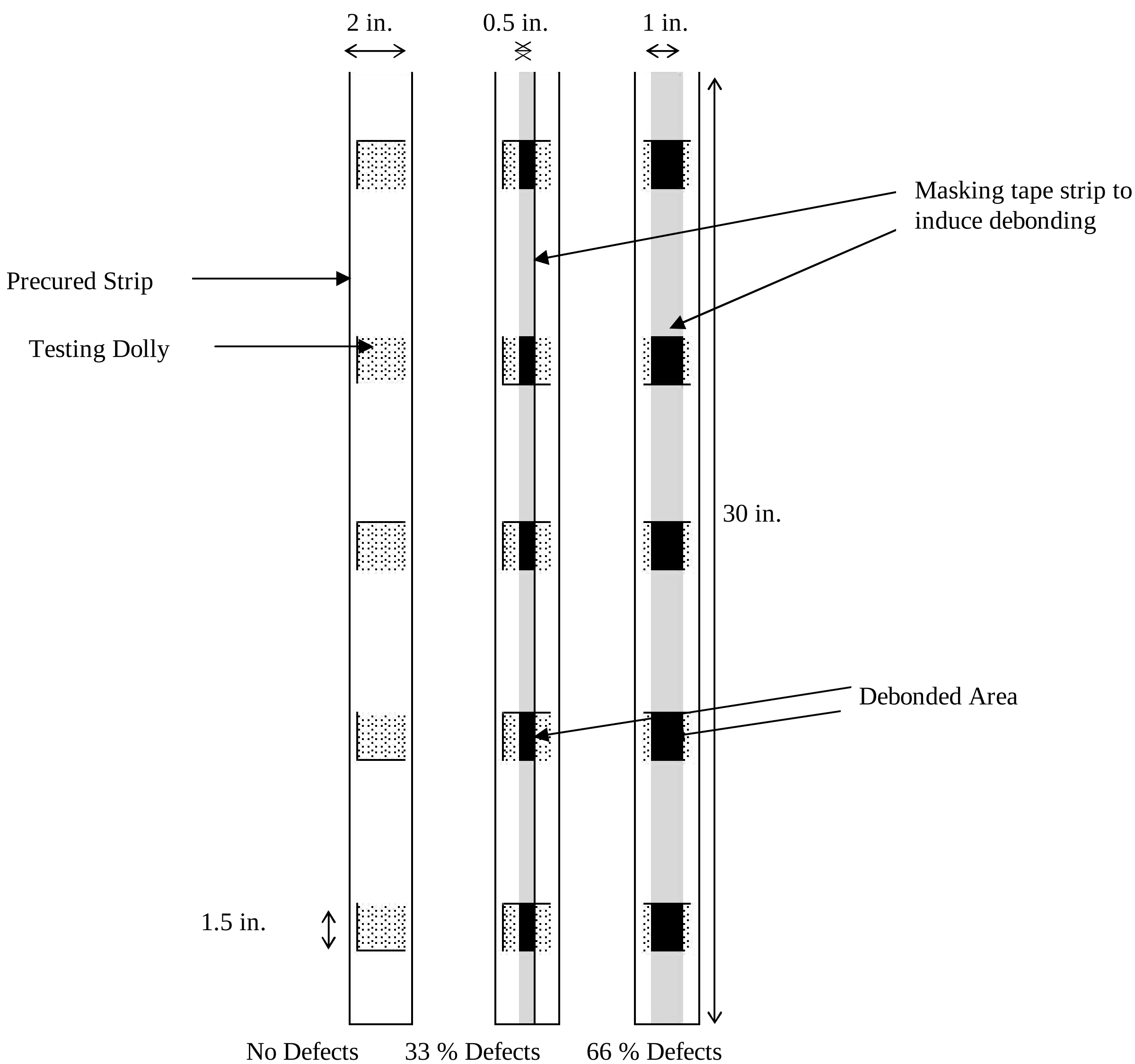

Figure 9.10 Precured Strips

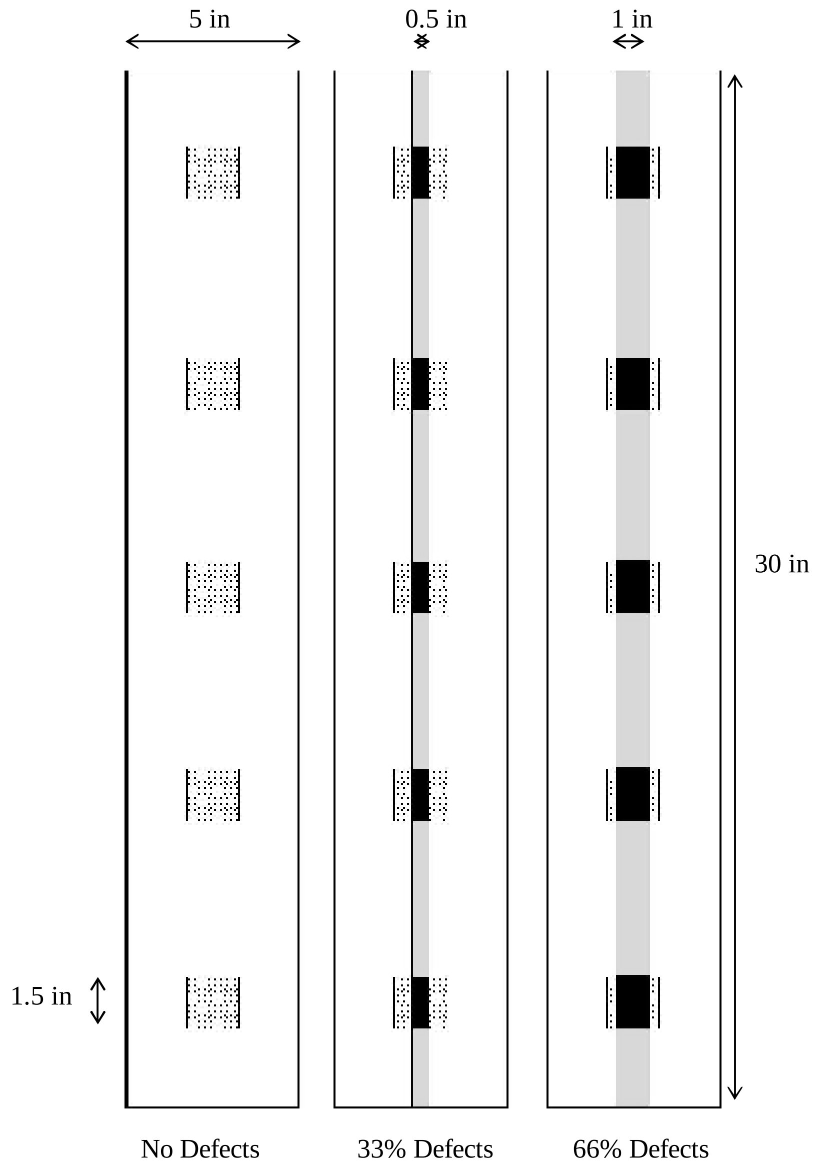

Figure 9.11 Wet Lay-up Systems

Test Results

Test results did not suggest a clear relationship linking the three surface preparations used for the three different FRP systems used in this study; however, it provided clear evidence of their capability of the inspection procedure to identify the defects. The average of the measured strength for the three surface preparations showed that they are all reduced proportional to the area of defect for each of the FRP systems considered in this study.

Failure at the adhesive interface, instead of the concrete layer, occurred for only 10 out of the 133 specimens tested. All of the 10 failures occurred for the wet lay-up FRP systems. The grinded surface accounted for six of that failure type. Six of the adhesive interface layer failures occurred for Level 1 defects, three occurred for Level 2 and one occurred for the specimen without defects. Failures of all the specimens without defect occurred within the concrete.

The loss of the measured tensile force from the testing device for the specimens with different levels of defects was compared to results of specimens without defects in Table 9.2.

Table 9.2 Measured tensile force of specimens without defects and with Level 1 and 2 defects

Strengthening System	% Defects	Type of Surface Preparation		
		Unprepared	Grinded	Sandblasted
Precured	Level 1 (33% defects)	13.30	20.27	28.87
	Level 2 (66% defects)	25.80	51.94	57.80
1 Layer Wet Lay-up	Level 1 (33% defects)	21.31	41.87	12.24
	Level 2 (66% defects)	40.46	59.32	61.20
2 Layer Wet Lay-up	Level 1 (33% defects)	31.06	26.97	3.54
	Level 2 (66% defects)	40.55	49.43	32.15

Test Results of Precured System

For the Precured System the unprepared surface was less sensitive to the level of induced defects in comparison to the other three surface preparations. The measured tensile forces for the sandblasted surface were proportional to the area of defect consequently provided more accurately prediction of the effect of the defect induced into the repair system.

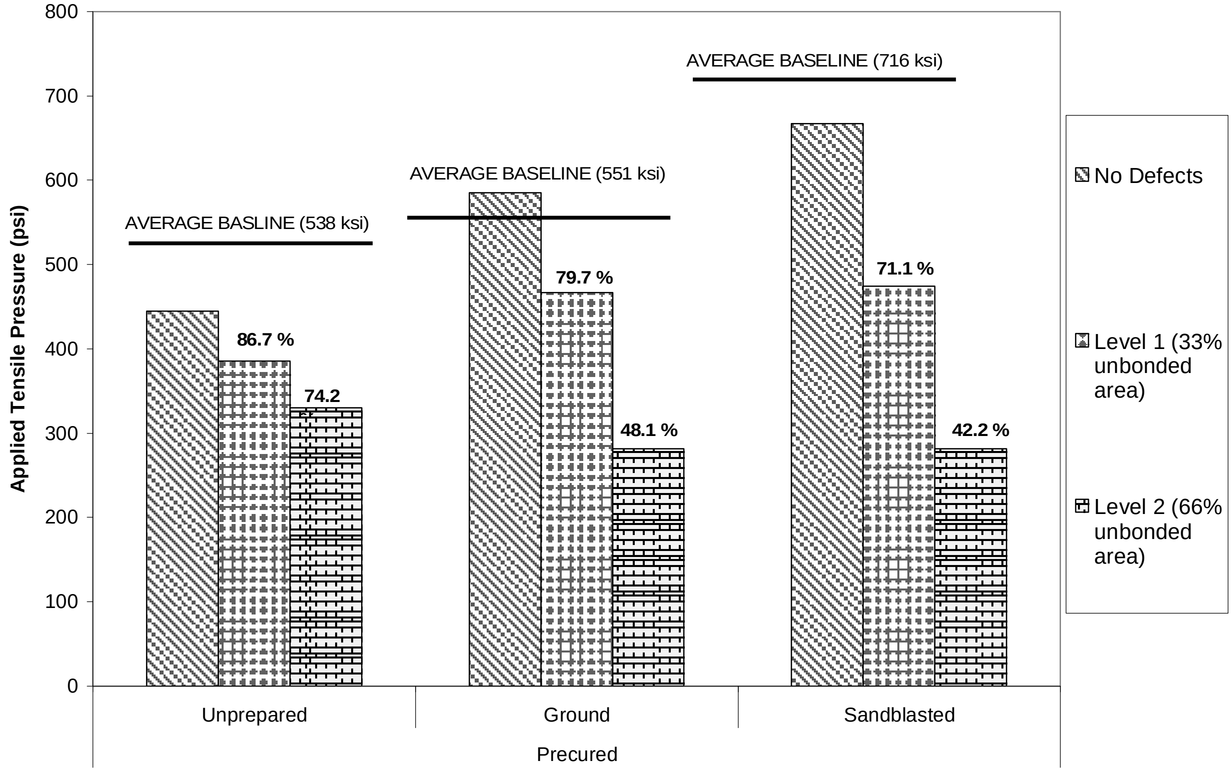

Figure 9.12 Precured System Test Results

Test Results of the Wet Lay-up System

The wet lay-up systems with both unprepared and grinded surfaces provided good prediction of the level of the induced defect in the bonded surface area, as shown in Figure 9.13. Test results reflected lower bond strength of the one and two layer wet lay-up system with sandblasted preparation as shown in Figure 9.13 and Figure 9.14, respectively.

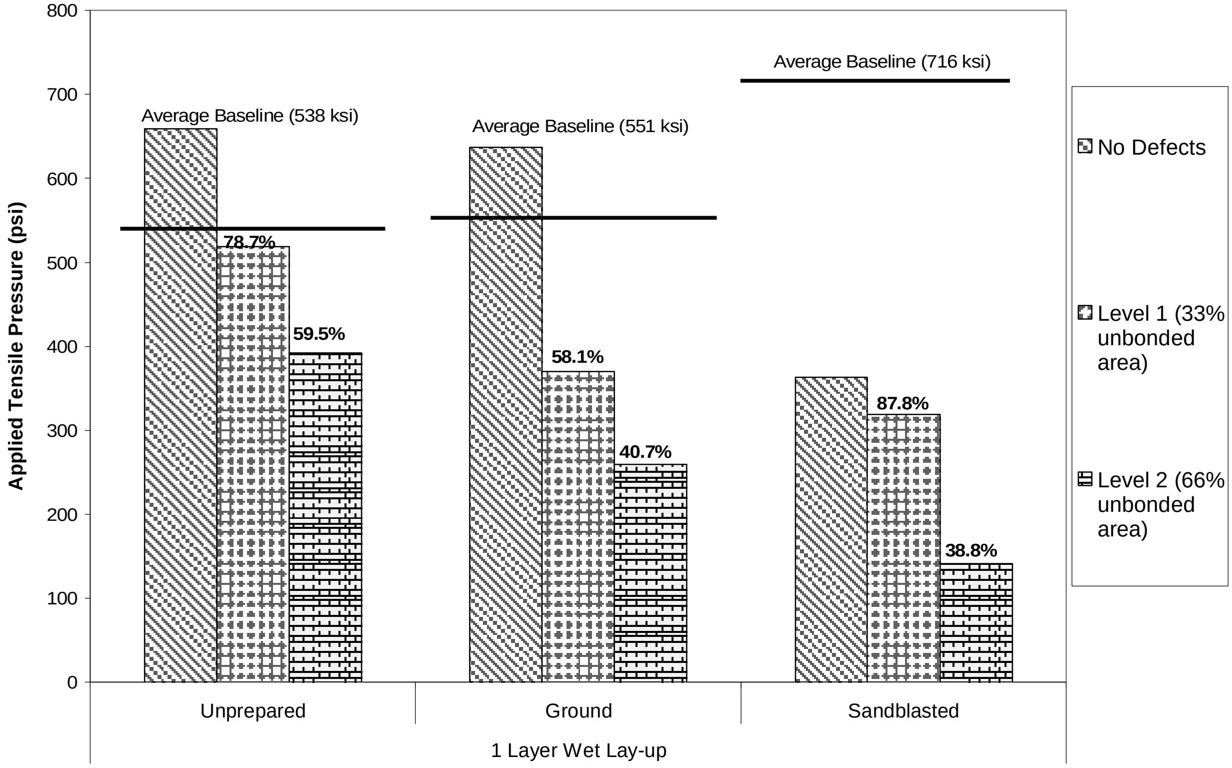

Figure 9.13 1 Layer Wet Lay-up System Results

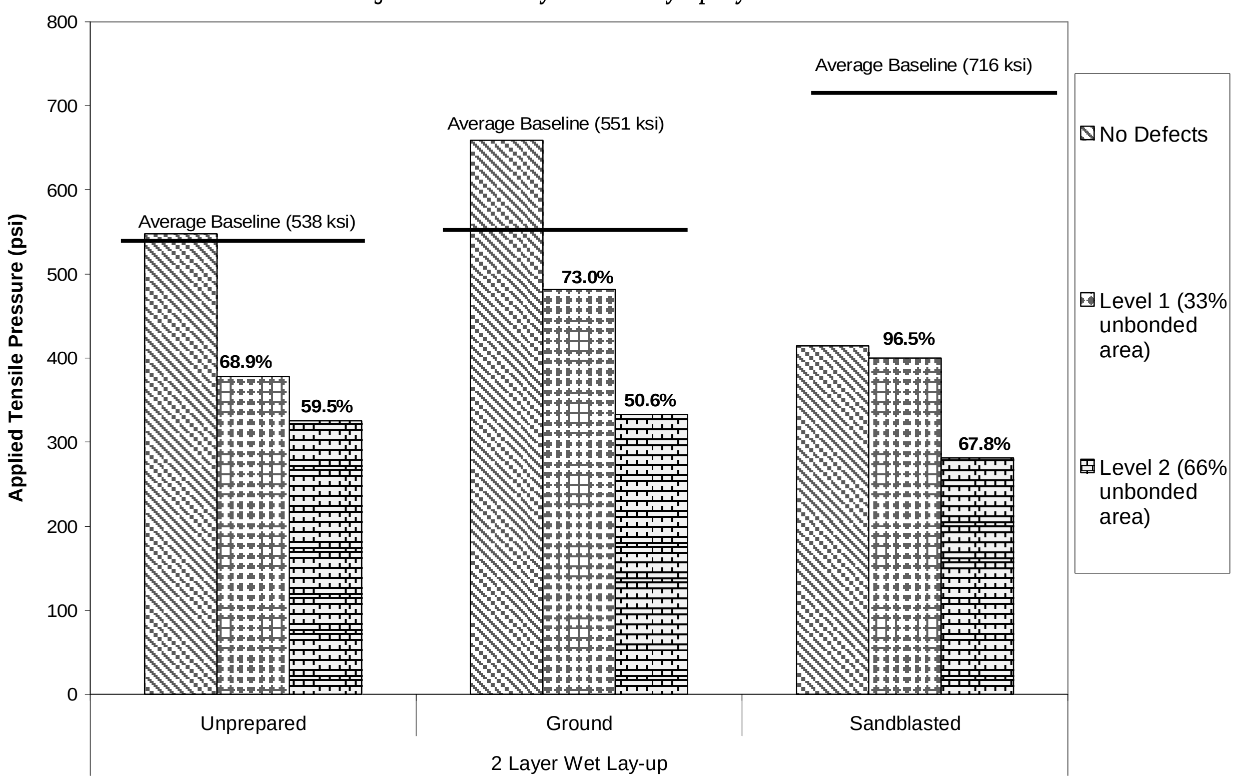

Figure 9.14 2 Layer Wet Lay-up System Results

Summary of the research findings

Based on analysis of the tests results, it became evident that the pull-off test is an excellent tool to determine the presence of areas of delamination between FRP sheets and a concrete surface. The tensile strength values even show that the pull-off test was able to "determine" the area of defects in the system. The pull-off tester requires very little training and is easy to manipulate for either field or laboratory use with minimum effort and time.

Test results indicted also that the ACI 440 criterion of bond failure at 200 psi is not conservative enough; however, due to the importance of bond for the entire repair system, it is highly recommended for practical application.

9.7 Recommended Inspection Procedure

Based upon the literature review of the different inspection methods and the recommendations of the various published codes and technical reports, as well as the experience of the research team and inspection demonstration, several recommendations are made for the inspection of concrete bridges repaired or strengthened with FRP System.

Inspection Checklist:

1. Record all materials used to strengthen or repair the specimen in an organized file.
2. After application of FRP system, immediately perform preliminary inspection and record the "as installed" condition. Note location of any visual flaws in the FRP material. The initial visual inspection is crucial, since it will form a baseline for subsequent inspections. It is also important to assess the effectiveness of the FRP system, in particular the presence of fiber misalignment, folds or kinks.
3. The owner, contractor, engineer must come to an agreement about what tests are necessary for the inspection of the repair system used in the field. It is recommended that the pull off test and tap testing should be carried out by a qualified inspector. It is also recommended that witness panels and resin cups be tested in order to determine the strength and material behavior of the material used.
4. The "inspector" should have specific training in the use of the pull off tester as well as the sound of the fully bonded, partially bonded and unbonded areas.
5. As the pull-off test should cause localized discontinuity of the repaired area it is recommended that the pull off should be conducted on extra FRP samples placed away from the repaired area. Five pull-off tests should be preformed for each representative area. The pull off tests should be carried out no earlier than 7 days after completion of the FRP system. The owner may elect to have the pull off test carried out on the actual structure but in an area away from the high stressed zones.
6. Tap tests should be preformed on the actual repaired area after careful visual inspection of the repair. A practice tap test box should be constructed to educate inspectors on the difference in sounds between bonded

and unbonded laminate and left on-site for in-situ inspection comparison. The tap test should be carried out with a steel rod and preformed no earlier than 24 hours after the application of the system to allow enough cure time.

7. Detailed records must be kept of the FRP repair system in order to keep track of the deterioration of the system over time. This report should include delamination size, location, and quantity as well as any physical changes in the FRP and surrounding concrete structure over time

10 CONCLUSIONS

10.1 Summary

The overall structural behavior and cost effectiveness of FRP strengthening or repair systems for concrete highway bridges was studied. The behavior was examined under the effect of two loading conditions: extreme loading simulated by a monotonic load to failure, and service loading using fatigue loading. The structural behaviors of the strengthening and repair systems were evaluated under these conditions. The behavior was simulated using an analytical model which predicts the flexural behavior of the strengthened and repaired girders including failure mode. The entire experimental program in this research consisted of testing 26 full-scale prestressed concrete bridge girders. Twenty-one girders were tested after strengthening with various FRP systems, and five impact damaged girders were tested after repair to examine their behavior. The research indicates that FRP systems are effective for strengthening/repair of concrete highway bridges. This report also includes a review of the various inspection methods and the recommended practical and effective inspection procedures to ensure effectiveness of the strengthening and repair systems. The following section briefly describes specific findings related to the strengthening/repair of prestressed concrete highway bridge girders.

10.2 Conclusions

Strengthening of C-Channel Girders

A series of twenty-one prestressed concrete C-Channels were tested under static and fatigue loading conditions to assess the performance of various FRP strengthening systems. Based on the experimental and analytical analysis the following conclusions can be drawn:

1. Proper design and installation of a CFRP strengthening system can maintain the same failure mode of crushing of concrete in the compression zone, therefore preserving the ductile structural response of the unstrengthened girders.
2. Externally bonded CFRP sheets are the most cost-effective strengthening technique and are the most suitable technique for the C-Channel type of girder.
3. The most structurally efficient strengthening technique used is the near surface mounted (NSM) CFRP bars or strips system (Rizkalla *et al*. (2005)).
4. The ultimate flexural capacity of prestressed concrete bridge girders can be increased substantially using CFRP materials. The flexural capacity of the C-Channel girders tested in this research program could be increased by as much as 73 percent with the use of externally bonded CFRP sheets.

5. The use of steel reinforced polymer (SRP) materials to strengthen prestressed concrete bridge girders is a structurally viable and cost effective alternative to CFRP systems.
6. The use of transverse CFRP U-wraps for externally bonded CFRP systems is required to ensure proper bonding.
7. For externally bonded CFRP wet lay-up systems, the measured tensile strain in the CFRP outperformed the values provided by the manufacturer.
8. The crack spacing and crack widths at service and at ultimate can be substantially reduced using CFRP strengthening. Crack widths observed during the testing of the C-Channels were reduced by as much as 400 percent using CFRP materials in comparison to the unstrengthened girder.
9. Stiffness of C-Channel girders can be increased by using high modulus CFRP materials. Based on strictly a serviceability criterion, the high modulus CFRP materials outperformed the normal modulus CFRP materials.
10. Strengthening using CFRP materials can reduce the stress ratio in the prestressing strands due to their effectiveness in controlling crack widths and increasing the overall stiffness.
11. The most fatigue critical component in a CFRP strengthened prestressed concrete bridge girder are the prestressing strands. The level of the induced stress ratio in the prestressing strands under the effect of the increased live load, including impact factor, should be kept below limits specified in AASHTO Section 5.5.3.3 (2004), which for the C-Channel girders is 18.1 ksi for straight and 10.1 ksi for harped prestressing strands.

Repair of AASHTO Girders

Due to the increasing frequency of overheight vehicular impact and rising costs of complete replacement of the damaged girder, the structural behavior of CFRP repaired prestressed concrete beams were studied to determine the effectiveness of the repair system. Damage in flexure and shear critical zones, including loss of concrete and rupturing of prestressing strands was examined. Every specimen's original undamaged flexure/shear capacity was successfully restored using externally bonded CFRP sheets. An analytical model for restoring the ultimate load capacity of all four repaired girders was performed using existing design guidelines.

CFRP Repair to Restore Flexural Strength

Two AASHTO Type II girders were damaged at or near midspan, repaired with longitudinal and transverse CFRP sheets. The girders were tested under flexurally critical loading up to failure. The specific research findings can be summarized as follows:

1. Based on the testing regime, it was possible to repair an impact-damaged girder with up to an 18 percent loss of prestressing force using CFRP sheets.

2. Test results showed that the deflection at ultimate stage of repaired girders is the same magnitude as the undamaged girder.
3. Test results indicate that a 20 loss of the stiffness of the damaged girder compared to the undamaged girder occurred due to the loss prestressing strands. Following the restoration of the concrete section and application of the CFRP, the girder gained 50 percent of the lost stiffness
4. Results from the fatigue test of AASHTO1(Rizkalla et al. (2005)) demonstrated that a CFRP repaired AASHTO Type II prestressed girder can withstand 2 million cycles of cyclic loading with very little loss of stiffness or residual deflection.

CFRP Repair to Restore Shear Strength

Two AASHTO Type II girders were tested using small shear span-to-depth ratio to simulate critical shear conditions. One girder was tested as a control specimen and the second girder was damaged near the support and repaired using longitudinal and diagonal U-wraps of CFRP sheets. The following conclusions can be drawn:

1. Shear failure occurred for the undamaged prestressed concrete girder when loaded at shear span-to-depth ratio of 1.57.
2. Test results showed that a damaged AASHTO Type II girder with 14 percent loss of prestressing force and loss of one inch of the thickness of the concrete in the web can be repaired using CFRP sheets to restore its original capacity.
3. The use of CFRP sheets reduced the shear crack widths of the repaired girder in comparison to the control specimen.

Flexure and Shear Modeling Using CFRP

Several analytical models were examined and used to predict both the flexural response and shear response of a repaired prestressed concrete girder. The following conclusions can be drawn from these two models:

1. Assuming a perfect bond, test results showed that the flexural behavior of an undamaged as well as CFRP strengthened or repaired prestressed member can be predicted using cracked section analysis.
2. Comparison of test results and predicted values showed that PCI and ACI Committee 440 guidelines accurately predict the shear both with and without the presence of CFRP strengthening/repair systems.

Inspection Guidelines

1. Record all materials used to strengthen or repair the specimen in an organized file.
2. After application of FRP system, immediately perform preliminary inspection and record the “as installed” condition. Note location of any visual flaws in the FRP material. The initial visual inspection is crucial, since it

will form a baseline for subsequent inspections. It is also important to assess the effectiveness of the FRP system, in particular the presence of fiber misalignment, folds or kinks.

3. The owner, contractor, engineer must come to an agreement about what tests are necessary for the inspection of the repair system used in the field. It is recommended that the pull off test and tap testing should be carried out by a qualified inspector. It is also recommended that witness panels and resin cups be tested in order to determine the strength and material behavior of the material used.
4. The "inspector" should have specific training in the use of the pull off tester as well as the sound of the fully bonded, partially bonded and unbonded areas.
5. As the pull-off test should cause localized discontinuity of the repaired area it is recommended that the pull off should be conducted on extra FRP samples placed away from the repaired area. Five pull-off tests should be preformed for each representative area. The pull off tests should be carried out no earlier than 7 days after completion of the FRP system. The owner may elect to have the pull off test carried out on the actual structure but in an area away from the high stressed zones.
6. Tap tests should be preformed on the actual repaired area after careful visual inspection of the repair. A practice tap test box should be constructed to educate inspectors on the difference in sounds between bonded and unbonded laminate and left on-site for in-situ inspection comparison. The tap test should be carried out with a steel rod and preformed no earlier than 24 hours after the application of the system to allow enough cure time.
7. Detailed records must be kept of the FRP repair system in order to keep track of the deterioration of the system over time. This report should include delamination size, location, and quantity as well as any physical changes in the FRP and surrounding concrete structure over time

10.3 Future Work

Although a great deal has been investigated as part of this research program, there is a need for additional work to optimize the design cover additional important details. This section itemizes the direction that major research should be headed, and is broken down into two sections: FRP strengthening and FRP repair.

FRP Strengthening Systems

The effect of U-wrap debonding mitigation was examined only briefly in this research. Future work should aim to characterize the effect of U-wraps at the support to mitigate plate-end (PE) debonding, and throughout the beam to reduce the propensity for intermediate crack (IC) debonding. Two types of analysis could be used in the future to predict the effect of U-wraps: 1) a shear friction approach similar to the simple model proposed by Larson et al. (2004) and Reed and Peterman (2004), or 2) strut and tie modeling.

In the C-Channel strengthening program, the CFRP was wrapped around the soffit of the girder, which changed the location of interface cracking from the extreme tensile side of the beam in the concrete paste layer to the level of the wrapping. Similar to the work of Seracino et al. (2005) for near surface mounted CFRP systems, the effect of wrapping should be further examined and analytical techniques identified to predict its failure.

Considerable research into the durability of FRP materials has been conducted. A recent report has been drafted on the durability of CFRP materials used with concrete by ACI Committee 440 (2006). The durability of steel reinforced polymer (SRP) materials with concrete needs to be explored before implementing long-term strengthening solutions.

The analytical model described here was calibrated against a database of strengthened reinforced concrete beams loaded under three and four point bending. Future research needs to confirm the postulated effect of other loading conditions on the interface shear stress, including distributed loads and continuous beams and strengthening in negative moment regions. The effect of side plating on IC debonding strains in unclear from research by Breña et al. (2005). Since this type of plating could be useful in strengthening building structures where obstructions block access to the tensile side of the member, more experimental and analytical work should be performed in this area. In addition, the debonding mechanisms in partially prestressed members should be further examined, including the magnitude of interface shear stress.

In several of the beams tested as part of this research, an innovative fiber optic sensor interferometer was installed within the adhesive layer of the CFRP strengthening system to measure tensile strains (Jiang et al. 2006). Although only able to measure global strains over the length of the member, next generation fiber optic ribbons with Bragg gratings are under development which has the potential to give the complete envelope of tensile strains.

A research project is currently underway at North Carolina State University on FRP inspection techniques. The ability of owners to determine the effectiveness of their FRP strengthening and repair system is important for full implementation. Various inspection techniques will be reviewed and evaluated in the future report including the “tap test”, pull-off testers, and infrared thermography.

The most important future research step is implementation of the strengthening and repair systems described in this report. Load testing and field measurement of displacements and strains under real loading conditions is important for widespread use.

FRP Repair Systems

The AASHTO girders tested as part of this research had a composite deck only the width of the top flange of the prestressed girder as a result of the extraction of the girders from the superstructure for transport. The large effective width of many composite bridge girders could change the failure modes described in this research from concrete crushing to failure of FRP system. More research on composite bridge girders with a large tributary width is needed.

Due to the effectiveness of the CFRP repair system, none of the AASHTO girders examined in this research failed due to rupture or debonding of the FRP system. Higher levels of prestressing loss should be examined (greater than the 18 percent loss in the current research) and FRP repair systems should be examined without the presence of debonding mitigation to understand more fully the fundamental behavior.

Experimental and analytical investigations should be performed in future research on the full response of the system after an impact event. Field monitoring of a bridge before and after an impact event and following CFRP repair would be useful. In addition, long term monitoring should be applied to a CFRP repair system to determine the demand placed on the system over time and system degradation. The effectiveness of pre-loading an impact-damaged bridge prior to concrete repair in order to induce compressive strains in the concrete also needs to be examined, including field validation.

RECOMMENDATIONS

The main objective of this research was to evaluate the cost-effectiveness and value engineering of various CFRP repair and strengthening systems for prestressed concrete bridge girders. As a result of the study, the following recommendations can be made:

1. When properly designed, CFRP systems are a viable, practical, and cost-effective strengthening technique that can be used to increase the live load of prestressed concrete bridge girders up to 40 percent.
2. When properly designed, CFRP systems can be used effectively as a repair technique to regain the original capacity of impact damaged AASHTO Type II bridge girders with one ruptured prestressing strand and significant loss of concrete section.
3. Inspection of all strengthening and repair systems is easy to perform and practical to examine the effectiveness of the installed system.

IMPLEMENTATION

This research has shown that the Response 2000© program is an accurate analysis tool adequate to design any CFRP repair and strengthening system for prestressed concrete bridge girders. Using the design recommendations presented in Chapter 8, CFRP systems are a practical and cost-effective strengthening technique. Field application of the systems using existing bridges is highly recommended. The bridge should be instrumented and structurally monitored to observe behavior under real field conditions, including environmental effects.

REFERENCES

Aas-Jakobsen, K., (1970) "Fatigue of Concrete Beams and Columns", Trondheim NTH Institutt for Betonkonstruksjoner, Bulletion No. 70-1, pp. 148.

Aboutaha, Riyad S. "Rehabilitation of Reinforced Concrete Beams by the Use of Bonded Steel Plates." ACI Special Publication SP-174 p.225-244, April 1, 1998.

ACI 440.2R-02 "Guide for the Design and Construction of Externally Bonded FRP Systems for Strengthening Concrete Structures." Published by the American Concrete Institute, Farmington Hills, MI, pp 13, 2002.

ACI Committee 215, (1997) "Considerations for Design of Concrete Structures Subjected to Fatigue Loading (ACI 215R-74 revised 1997)", ACI Manual of Concrete Practice, American Concrete Institute.

ACI Committee 318, (2005) "Building Code Requirements for Structural Concrete and Commentary," ACI Manual of Concrete Practice, American Concrete Institute.

ACI Committee 440, (1996) "State-of-the-Art Report on FRP for Concrete Structures (ACI 440R-96)", ACI Manual of Concrete Practice, American Concrete Institute.

ACI Committee 440, (2002) "Design and Construction of Externally Bonded FRP Systems for Strengthening Concrete Structures (ACI 440.2R-02)", ACI Manual of Concrete Practice, American Concrete Institute.

ACI Committee 440, (2006) "Guide to the durability of Fiber Reinforced Polymers (FRP) composites used with concrete," Draft document 440.1R, American Concrete Institute.

ACI Committee 503, (1996),"Use of Epoxy with Concrete", ACI 503R-93, American Concrete Institute.

ACI Committee 546, (1996) "Concrete Repair Guide", (ACI 546R-96), ACI Manual of Concrete Practice, American Concrete Institute.

Adams, R.D. (2004) *Adhesive Bonding*, Woodhead Publishing Ltd, Cambridge, England, 543 p.

Adhikary, B.B. and Mutsuyoshi, H. "Behavior of Concrete Beams Strengthened in Shear with Carbon-Fiber Sheets." Journal of Composites for Construction. 8.3 (2004): 258-264.

Adimi, R.M., Rahman, A.H., Benmokrane, B., (2000) "New Method for Testing Fiber-Reinforced Polymer Rods under Fatigue", Journal of Composites for Construction, Vol. 4, No. 4.

Aidoo, J., Harries, K.A. and Petrou, M.F. (2006) "Full-scale Experimental Investigation of Repair of Reinforced Concrete Interstate Bridge using CFRP Materials," accepted to ASCE Journal of Bridge Engineering.

Aidoo, J., Harries, K.A., and Petrou, M.F. (200X) "Fatigue behavior of CFRP strengthened reinforced concrete bridge girders," *submitted to ACI Structural Journal*.

Alkhrdaji, T., Barker, M., Chen, G., Mu, H., Nanni, A., Yang, X. (2001) "Destructive and Non-Destructive Testing of Bridge J857, Phelps County, Missouri", MoDOT Report RDT01-002A.

Ahmed, O., and Van Gemert, D., (1999) "Effect of longitudinal carbon fiber reinforced plastic laminates on shear capacity of reinforced concrete beams," *Proceedings of the Fourth International Symposium on Fiber Reinforced Polymer Reinforcement for Reinforced Concrete Structures*, Baltimore, MD, pp. 933-943.

Ahmad, I. (2004) "Shear Response and Bending Fatigue Behavior of Concrete-Filled Fiber Reinforced Polymer

American Association of State Highway and Transportation Officials, (2004) "AASHTO LRFD Bridge Design Specifications", AASHTO.

American Society for Nondestructive Testing. July 2006. Web site: http://www.asnt.org/

ASTM. 4541, *Standard test method for pull-off strength of coatings using portable adhesion testers*. American Society for Testing and Materials, West Conshohocken, Pennsylvania.

Arduini, M., Di Tommaso, A., Nanni, A., (1997) "Brittle failure in FRP plate and sheet bonded beams," *ACI Structural Journal*, V. 94, No. 4, pp. 363-370.

Arduini, M., Nanni, A., and Romagnolo, M., (2002) "Performance of Decommissioned RC Girders Strengthened with FRP Laminates," *ACI Structures Journal*, Vol. 99, No. 5, Sept.-Oct., pp. 652-659.

Asplund, S. O., (1949) "Strengthening Bridge Slabs with Grouted Reinforcement", ACI Structural Journal V.20, No. 4, pp.397-406.

Barnes, R.A., Mays, G.C., (1999) "Fatigue Performance of Concrete Beams Strengthened with CFRP plates", Journal of Composites for Construction, Vol. 3, No. 2.

Bažant, Z., Planas, J. (1998) *Fracture and Size Effect in Concrete and other Quasibrittle Materials*, CRC Press, New York.

Bentz, E.C. (2000) "Section Analysis of Reinforced Concrete Members", Ph.D. Thesis, University of Toronto, 2000.

Bizindavyi, L., Neale, K.W. (1999) "Transfer lengths and bond strengths for composites bonded to concrete," *Journal of Composites for Construction*, Vol. 3, No. 4, pp. 153-160.

Bonacci, J.F. and Maalej, M. (2000) "Externally bonded fiber-reinforced polymer for rehabilition of corrosion damaged concrete beams," *ACI Structural Journal*, 97(5), pp. 703-711.

Breña, S.F., Kreger, M.E., Wood, S.L., (2005) "Fatigue Tests of Reinforced Concrete Beams Strengthened using Carbon Fiber Reinforced Polymer Composites", ACI Structural Journal, Vol. 102, No. 2.

Bresler, B., and Pister, K.S. (1958) "Strength of concrete under combined stresses," *Journal of the American Concrete Institute*, Vol. 30, No. 3, pp. 321-345.

British Standards Institution. BS EN 1542. ***Products and systems for the protection and repair of concrete structures-Test methods-Measurement of bond strength by pull-off.*** 1999.

Brosens, K. (2001) "Anchorage of externally bonded steel plates and CFRP laminates for the strengthening of concrete elements," Dissertation, Catholic University of Lueven, Belgium.

Budelman, H., and Husemann, U. (2005) "Effect of repeated live loads on bond capacity of externally bonded CFRP plates," *Proceedings of the Third International Conference on Composites in Construction*, Lyon, France.

Buyukozturk, O., Gunes, O., and Karaca, E. (2004) "Progress on understanding debonding problems in reinforced concrete and steel members strengthened using FRP composites," *Construction and Building Materials*, Vol. 18, No. 1, pp. 9-19.

Canadian Standards Association, (2000) "Design and Construction of Building Components with FRP", Canadian Standards Association Report S806-00.

Carolin, A. Nordin, M. and Taljsten, B. (2001) "Concrete Beams Strengthened with Near Surface Mounted Reinforcement of CFRP." Proceedings of the International Conference on FRP Composites in Civil Engineering, Hong Kong, China, pp. 1059-1066.

Carolin, A. (2003) "Carbon Fiber Reinforced Polymers for Strengthening of Structural Elements", Doctoral Thesis, Luleå University of Technology.

Ceroni, F., Pecce, M., Prota, A., and Manfredi, G. "Flexural Strengthening of RC Beams using Emerging Materials: Cracking Behavior." Proceedings of the International Conference FRP Composites in Civil Engineering – CICE 2004 – Seracino (2004): 171-178.

Chahrour, A., and Soudki, K., (2005) "Flexural Reponse of Reinforced Concrete Beams Strengthened with End-Anchored Partially Bonded Carbon Fiber Reinforced Polymer Strips." *Journal of Composites in Construction*; Vol. 9, No. 2, pp. 170-177.

ChemRex. EMACO® T430 2002. 9 August 2006 <http://www.cadeco.com/productfiles/MasterBuilders-EmacoT430.pdf>.

Chen, W.F. (1988) *Plasticity for Structural Engineers*, Springer-Verlag, New York, 606 p.

Chen, J.F., and Teng, J.G., (2001) "Anchorage strength models for FRP and steel plates bonded to concrete," *Journal of Structural Engineering*, Vol. 127, No. 7, pp. 784-791.

Chen, J.F., Yang, Z.J., and Holt, G.D. (2001) "FRP or steel plate-to-concrete bonded joints: effect of test methods on experimental bond strength," *Steel and Composite Stuctures*, Vol. 1, No. 2, pp. 231-244.

Chen, J.F., Yuan, H., and Teng, J.G., (2005) "Analysis of debonding failure along a softening FRP-to-concrete interface between two adjacent cracks," *Proceedings of the International Symposium on Bond Behavior of FRP in Structures (BBFS 2005)*, pp. 103-111.

Clarke, John. ***Installing, inspecting and monitoring FRP-strengthened concrete structures.*** Concrete. Vol. 36, No. 2, February 2002, 34-36 pp.

Collins, M.P., and Mitchell, D., (1997) *Prestressed Concrete Structures*, Response Publications, Canada.

Concrete Society, The, (2004) "Design Guidance for Strengthening Concrete Structures using Fibre Composite Materials", Technical Report 55, The Concrete Society, United Kingdom.

Concrete Society, The, (2003) "Strengthening Concrete Structures Using Fibre Composite Materials: Acceptance, Inspection and Monitoring", Technical Report 57, The Concrete Society, United Kingdom.

Coronado, C.A., and Lopez, M.M. (2005) "Modeling of FRP-concrete bond using nonlinear damage mechanics," *Proceedings of the 7th International Symposium on Fiber Reinforced Polymer Reinforcement for Concrete Structures*, Kansas City, Mo, pp. 373-390.

Coronado, C.A, and Lopez, M.M. (2006) "Sensitivity analysis of reinforced concrete beams strengthened with FRP laminates," *Cement and Concrete Composites*, Vol. 28, No. 1, pp. 102-114.

De Lorenzis L. and Nanni, A., (2001a) "Shear Strengthening of Reinforced Concrete Beams with Near-surface Mounted Fiber Reinforced Polymer Rods", ACI Structural Journal, Vol. 98, No. 1, pp.60-68.

De Lorenzis L. and Nanni, A. (2001b) "Characterization of NSM FRP Rods as Near-Surface Mounted Reinforcement," Journal of Composites for Construction, May 2001, pp. 114-121.

De Lorenzis, L., Miller, B., and Nanni, A. (2001) "Bond of FRP laminates to concrete," *ACI Materials Journal*, Vol. 98, No. 3, pp. 256-264.

De Lorenzis L. and Nanni, A., (2002) "A Bond Between Near-surface Mounted FRP Rods and Concrete in Structural Strengthening", ACI Structural Journal, Vol. 99, No. 2, pp. 123-132.

Dias, S., Juvandes, L., Figueiras, J. (2004) "Strengthening of reinforced concrete structures in bending with CFRP," *Revista IBRACON de Estructuras (Instituto Brasileiro de Concreto),* Vol. 1., No. 1., pp. 1-19.

Di Ludovico, M., (2003). "Experimental Behavior of Prestressed Concrete Beams Strengthened with FRP." Report CIES 03-42, University of Missouri-Rolla, MO.

Di Ludovico, M., Nanni, A., Prota, A., & Cosenza, E. (2005). Repair of Bridge Girders with Composites: Experimental and Analytical Validation. ACI Structural Journal, 102(5), 639-648.

El-Hacha, R., Filho, J., Rizkalla, S., and Melo, G., (2004) "Static and Fatigue behavior of Reinforced Concrete beams strengthened with different FRP Strengthening techniques", Proceedings of the 2nd International Conference on FRP Composites in Civil Engineering (CICE 2004), Adelaide, Australia.

El-Hacha, R., Rizkalla, S. (2004) "Near-Surface-Mounted Fiber-Reinforced-Polymer Reinforcements for Flexural Strengthening of Concrete Structures," ACI Structural Journal, Vol. 101, No. 5, September-October 2004.

El-Mihilmy, M.T., and Tedesco, J.W. (2001) "Prediction of anchorage failure for reinforced concrete beams strengthened with fiber-reinforced polymer plates," ACI Structural Journal, V. 98, No. 3, pp. 301-314.

El-Tawil, S., Ogunc, C., Okeil, A., Shahawy, M. (2001) "Static and fatigue analysis of RC strengthened with CFRP laminates, " *ASCE Journal of Composites for Construction,* Vol. 5, No. 4, pp. 258-267.

El-Tawil, S. and Okeil, A. M. (2002) "LRFD Flexural Provisions For PSC Bridge Girders Strengthened with CFRP Laminates," ACI Structural Journal, Vol. 99, No. 2, pp. 300-310.

Fang, T.Q. (2002) "Study on U-shaped sheet behavior of anti-debonding in the concrete beam reinforced flexurally with FRP," Master's thesis, Tsingua University, China.

Fanning, P.J., and Kelly, O., (2001) "Ultimate response of RC beams strengthened with CFRP plates," *Journal of Composites for Construction*, V. 5, No. 2, pp. 122-127.

Fédération Internationale du Béton (2001) "Externally bonded FRP reinforcement for RC structures," *fib Bulletin 14*, Task Group 9.3 FRP Reinforcement for concrete structures.

Feldman, Lisa R., Jirsa, James O., and Kowal, Edward S.. "Repair of Bridge Impact Damage." Concrete International. 20.2 (1998): 61-66.

fib (The International Federation For Structural Concrete) Externally *bonded FRP reinforcement for RC Structures*, The Federation, Lausanne, Switzerland, 2001, 130pp.

Florida Department of Transportation. Summary of Final Report, BC354-55, CFRP Repair of Impact-Damaged Bridge Girders, Volume II-Inspection of FRP Composite Repairs Using Infrared Thermography. January 2005

Fyfe Co. LLC. Tyfo SCH-41 Composite Using Tyfo S Epoxy. 2006. 7 July 2006 <http://www.fyfeco.com/products/compositesystems/sch-41.html>.

Fyfe Co. LLC. Tyfo P® Polymer Cement Modified Mortar. 2002. 9 August 2006 <http://www.fyfeco.com/products/concreterepair/pdf/p.pdf l>.

Gao, B., Leung, W.H., Cheung, C.M., Kim, J.K., Leung, C.K.Y., (2001) "Effects of adhesive properties on strengthening of concrete beams with composite strips," *Proceedings of the International Conference on FRP Composites in Civil Engineering*, Hong Kong, pp. 423-432.

Garden, H.N., Quantrilll, L.C., Hollaway, L.C., Thorne, A.M., and Parke, G.A.R. (1998) "An experimental study of the anchorage length of carbon fibre composite plates used to strengthen reinforced concrete beams," *Construction and Building Materials*, Vol 12, pp. 203-219.

Garden, H.N. and Hollaway, L.C. (1998) “An experimental study of the influence of plate-end anchorage of carbon fibre composite plates used to strengthen reinforced concrete beams,” *Composite Structures*, Vol. 42, pp. 175-188.

Grace, N.F, and Singh, S.B. (2005) “Durability Evaluation of Carbon Fiber-Reinforced Polymer Strengthened Concrete Beams: Experimental Study and Design,” *ACI Structural Journal*, Vol. 102, No. 1, pp. 40-53.

Grace, N.F., Abdel-Sayed, G. and Ragheb, W.F. (2002) “Strengthening of concrete beams using innovative ductile fiber-reinforced polymer fabric,” *ACI Structural Journal*, Vol. 99, No. 5, pp. 692-700.

Green, P.S., Boyd, A.J., Lammert, K., and Ansley, M. (2004) “CFRP repair of impact-damaged bridge girder Volume 1: Structural evaluation of impact-damaged prestressed concrete I girders repaired with FRP materials,” Florida Department of Transportation Structures Research Report 922, 194 p.

Hag-Elsafi, O., Kunin, J., Alampalli, S., Conway, T. (2001) “Strengthening of Route 378 Bridge over Wyantskill Creek in New York using FRP laminates,” *Special Report 135*, New York State Department of Transportation, 58 p.

Harmon, T.G., Kim, Y.J., Kardos, J., Johnson, T., Stark, A. (2003) “Bond of surface mounted fiber-reinforced polymer reinforcement for concrete structures,” ACI Structural Journal, 100(5), pp. 557-564.

Hassan, T., and Rizkalla, S., (2002) “Flexural Strengthening of Prestressed Bridge Slabs with FRP Systems”, PCI Journal, V. 47, No. 1, pp. 76-93.

Hassan, T., (2002) “Flexural Performance and Bond Characteristics of FRP Strengthening Techniques for Concrete Structures”, PhD. Thesis, University of Manitoba, Winnipeg, Canada.

Hassan T. and Rizkalla, S. (2003) “Investigation of Bond in Concrete Structures Strengthened with Near Surface Mounted CFRP Strips”, ASCE, Journal of Composites for Construction, Vol. 7, No.3, pp.248-257.

Hassan, T., Rizkalla, S., (2004) “Bond Mechanism of NSM FRP Bars for Flexural Strengthening of Concrete Structures”, ACI Structural Journal, Vol. 101, No. 6, November-December 2004.

Hearing, B. (2000) “Delamination in reinforced concrete retrofitted with fiber reinforced plastics,” PhD Thesis, Massachusetts Institute of Technology, Cambridge, MA.

Heffernan, P.J., Erki, M.A., (2004) “Fatigue Behavior of Reinforced Concrete Beams Strengthened with Carbon Fiber Reinforced Plastic Laminates”, Journal of Composites for Construction, V. 8, No. 2.

Helmerich, Rosemarie, Ernst Niederleithinger and Herbert Wiggenhauser. *A toolbox with Non-Destructive Testing Methods for the Condition Assessment of Railway Bridges*. TRB 2006 Annual Meeting

Highways Agency. BD 84/02, *Strengthening concrete bridge supports using fibre-reinforced polymers*, The Agency, London 202.

Highways Agency. BA 30/94, *Strengthening of concrete highway bridges using externally bonded plates*, Design manual for roads and bridges.

Hines, W.W., and Montgomery, D.C. (1990) Probability and statistics in engineering and management science, John Wiley and Sons, New York.

Hognestad, E. (1951) “A study of combined bending and axial load in reinforced concrete members,” Bulletin Series No. 399, University of Illinois Engineering Experiment Station.

Hughes, D., M. Kazemi, K. Marler, R. Zoughi, J. Myers and A. Nanni. *Microwave Detection of Delaminations Between Fiber Reinforced Polymer (FRP) Composite and Hardened Cement Paste.* CP615, Review of Quantitative Nondestructive Evaluation Vol. 21, ed. by D.O. Thompson and D.E. Chimenti, 2002

Hutchinson, R. and Rizkalla, S. “Shear Strengthening of AASHTO Bridge Girders Using CFRP Sheets.” ACI Special Publication SP-188, November 1999, pp 945-958.

Hutchinson, R., Tadros, G., Kroman, J., and Rizkalla, S., "Use of Externally Bonded FRP Systems for Rehabilitation of Bridges in Western Canada", ACI Special Publications, SP-215, November 2003, pp. 239-248.

ISIS Canada. Strengthening reinforced concrete structures with externally-bonded fibre-reinforced polymers. Manual No.4, Report ISIS-MO5-00, ISIS Canada, University of Manitoba, Winnipeg, Canada, 2001.

Japan Society of Civil Engineers, (2001) “Recommendations for Upgrading of Concrete Structures with use of Continuous Fiber Sheets”, Concrete Engineering Series 41, Japan.

Jiang, G., Van Vickle, P. and Peters, K. (2006) "Monitoring of FRP strengthened structures using a modified time of flight interferometer," Proceedings of the 2006 International Mechanical Engineering Conference and Exposition, Chicago, IL.

Jones, R., Swamy, R.N., and Charif, A. (1988) "Plate separation and anchorage of reinforced concrete beams strengthened by epoxy-bonded steel plates," *The Structural Engineer,* Vol. 66, No. 5, pp. 85-94.

Joyner, Jonathon "Inspection and Maintenance Procedures for CFRP Rehabilitated Reinforced Concrete Bridge Girders", 2005.

Juvandes, L., Figueiras, J.A., and Marques, A.T. (1998) "Strengthening of concrete beams with CFRP laminates," Proceedings of the Second International Conference on Composites in Infrastructure (ICCI 1998) Tucson, Arizona, pp. 83-90.

Kaiser, H. & Karbhari, V.M. (2004). Non-destructive testing techniques for FRP rehabilitated concrete –1: a critical review. *International Journal of Materials & Product Technology*, *21*(5), 349-384.

Kaminska, M.E. and Kotynia, R. (2000) Experimental Research on RC beams strengthened with CFRP strips, Report No. 9, Department of Concrete Structures, Technical University of Lodz, Poland.

Khaloo, A.R. "Shear Repair of Reinforced Concrete Beams Using Post-Tensioning." ACI Special Publication SP-193 p. 519-550, 1 August 2000.

Khoman, N., Foster, S.J., and Smith, S.T., (2004) "Debonding failure in CFRP strengthened concrete beams," Proceedings of the the Second International Conference on FRP Composites in Civil Engineering (CICE 2004), Adelaide, Australia, pp. 505-512.

Kishi, N., Mikami, H., Matsuoka, K.G., Kurihasi, Y. (2001) "Failure behavior of flexural strengthened RC beams with AFRP sheet," Proceedings of the Fifth International Conference on Fiber-Reinforced Plastics for Reinforced Concrete Structures, Cambridge, UK, pp. 87-95.

Klaiber, F. W., Wipf, T.J., Kempers, B.J., (1999) "Field Laboratory Testing of Damaged Prestressed Concrete (P/C) Girder Bridges", Iowa Department of Transportation Report HR-397.

Kotynia, R. and Kaminska, M.E. (2003) Ductility and failure mode of RC beams strengthened for flexure with CFRP, Report No. 13, Department of Concrete Structures, Technical University of Lodz, Poland.

Larson, K.H., Peterman, R.J., Rasheed, H.A. (2005) "Strength-Fatigue Behavior of Fiber Reinforced Polymer Strengthened Prestressed Concrete T-Beams." Journal of Composites for Construction, 9(4), 313-326.

Larson, K.H., Rasheed, H.A., and Peterman, R.J. (2004) "Developing a Non-linear Strength-Fatigue Design Procedure for FRP Strengthening of Prestressed Concrete Girders." Proceedings of 17th ASCE Engineering Mechanics Conference, Newark, DE, June 13-16 2004.

Leung, C.K.Y., and Tung, W.K., (2001) "A Three parameter model for debonding of FRP from concrete substrate," *Proceedings of the International Conference on FRP Composites in Civil Engineering*, Hong Kong, China, pp. 373-379.

Li, A., Assih, J, and Delmas, Y. "Shear Strengthening of RC Beams with Externally Bonded CFRP Sheets." <u>Journal of Structural Engineering.</u> 127.4 (2001): 374-380.

Ludovico, Marco Di. "Experimental Behavior of Prestressed Concrete Beams Strengthened with FRP." Report CIES 03-42, University of Missouri-Rolla, Rolla, MO, 2003.

Ludovico, Marco Di, Nanni, A., Prota, A., and Cosenza, E. "Repair of Bridge Girders with Composites: Experimental and Analytical Validation." <u>ACI Structural Journal.</u> 102.5 (2005): 639-648

MacGregor, James G. and Wight, James K. <u>Reinforced Concrete: Mechanics and Design.</u> Upper Saddle River, New Jersey: Pearson Education, Inc., 2005.

Maeda, T., Asano, Y., Sato, Y, Ueda, T, and Kakuta, Y. (1997) "A study on bond mechanism of carbon fiber sheet," *Proceedings of Third International Symposium on Non-Metallic (FRP) Reinforcement for Concrete Structures (FRPRCS3)*, Sapporo, Japan, pp. 279-286.

Maeda, T., Komaki, H., Tsubouchi, K., Murakami, K. (2002) "Strengthening Effect of Carbon Fiber Sheet Adhesion Method using flexible layer," *Transactions of the Japan Concrete Institute*, Vol 23, pp. 185-192.

Malek, A. M., Saadatmanesh, H., and Ehsani, M. R., "Prediction of Failure Load of RC Beams Strengthened with FRP Plate Due to Stress Concentration a the Plate End," *ACI Structural Journal*, V. 95, No. 1, 1998, pp. 142-152.

Matthys, S. (2000) “Structural behavior and design of concrete members strengthened with externally bonded FRP reinforcement,” Dissertation, University of Ghent, Belgium.

Meier, U. (1986) “Future use of advanced composites in bridge construction engineering,” *I Mech E Conference Publications (Institution of Mechanical Engineers),* p 217-233.

Meier, U. (1987) “Proposal for a carbon fibre reinforced composite bridge across the Straight of Gibraltar at its narrowest point,” Proceedings of the Institution of Mechanical Engineers, Part B: Management and Engineering Manufacturing, V 201, B2, 1987.

Micelli, F., Annaiah, R., and Nanni, A. “Strengthening of Short Span RC-T Joists With FRP Composites.” ASCE Journal for Composites in Construction. 6.4 (2002): 264-271.

Miller, A.D. (2006) “Repair of Impact-Damaged Prestressed Concrete Bridge Girders Using Carbon Fiber Reinforced Polymer (CFRP) Materials,” Master’s Thesis, North Carolina State University.

Mirmiran, A, Shahawy, M., Nanni, A., Karbhari, V., (2004) “Bonded Repair and Retrofit of Concrete Structures using FRP Composites”, National Cooperative Highway Research Program (NCHRP) Report 514, Transportation Research Board.

Mosallam, Ayman, Maria Feng, Medhat Haroun. Advances in Remote Sensing and Nondestructive Evaluation of Bridges and Structures. International Conference on Bridge Management Systems Monitoring, Assessment and Rehabilitation, March 21-23, 2006, Cairo, Egypt

Mukhopadhyaya, P., Swamy, N. (2001) “Interface shear stress: a new design criterion for plate debonding,” Journal of Composites for Construction, Vol. 5, No. 1, pp. 35-43.

Muller, J.F. and Dux, P.F., (1994) “Fatigue of prestressed concrete beams with inclined strands”, ASCE Journal of Structural Engineering, Vol. 120, No. 4.

Naaman, A.E. “Fatigue in Partially Prestressed Concrete Beams: Summary of Ten Years of Research”, International Symposium on Fatigue and Fracture in Steel and Concrete Structures, 1991.

Nanni, A, (1999) "Composites: Coming on Strong", Concrete Construction, vol. 44, p. 120.

Nanni, A., Di Ludovico, M., Parretti, R., (2004) “Shear Strengthening of a PC bridge girder with NSM CFRP rectangular bars”, Advances in Structural Engineering, Vol. 7, No. 4.

National Research Council of Italy (2004) “Guidelines for the design, execution and control of strengthening interventions by means of fibre-reinforced composite,” CNR-DT 200.

Neubauer, U., and Rostásy, F.S., (1999) “Bond failure of concrete fiber reinforced polymer plates at inclined cracks – experiments and fracture mechanics model,” Proceedings of Fourth International Symposium on Non-Metallic Reinforcement for Cocnrete Structures (FRPRCS4), pp. 369- 392.

Newman, John and Carl Zweben. *Nondestructive inspection of composite-strengthened concrete structures*. 47th International SAMPE Symposium, May 12-16, 2002, Page 691-702

Nguyen, D.M., Chan, T.K., Cheong, H.K., (2001) “Brittle failure and bond development length of CFRP-concrete beams,” *Journal of Composites for Construction*, V. 5, No. 1, pp. 12-17.

Niedermeier, R.P., (2001) *Zugkraftdeckung bei klebearmierten Bauteilen,* Doctoral Thesis (in German), Technischen Universität München.

Nilson, A.H. (1991) *Design of Concrete Structures*, McGraw Hill, New York, 904 p.

Oehlers, D.J., (1990) “Reinforced Concrete Beams with Plates Glued to their Soffits”, Journal of Structural Engineering, V.118, No. 1.

Oehlers, D. J., and Moran, J. P. (1990) ‘‘Premature failure of externally plated reinforced concrete beams.’’ *Journal of Structural Engineering*. Vol. 116 No. 4, 978–995.

Oehlers, D.J., Seracino, R., (2004) “Design of FRP and Steel Plated RC Structures”, Elsevier Press, London.

Oehlers, D.J, Seracino, R., and Smith, S.T. (2006) “Design guideline for RC structures retrofitted with FRP and metal plates: beams and slabs,” Draft 3 submitted to Standards Australia, January 2006.

Olson, S.A., French, C.W., and Leon, R.T. (1992) “Reusability and Impact Damage Repair of Twenty-Year-Old AASHTO Type III Girders”, Research Report No. 93-04, University of Minnesota, Minneapolis, Minn.

Overman, T.R., Breen, J.E., and Frank, K.H., (1984) “Fatigue Behavior of pretensioned concrete girders”, Research Report 300-2F, Center for Transportation Research, Austin, TX.

Quattlebaum, J., Harries, K. A., and Petrou, M. F. (2004) “Comparison of three CFRP flexural retrofit systems under monotonic and fatigue loads.” *Journal of Bridge Engineering*, 10(6), 731–740.

Pan, J.L., and Leung, C.K.Y, (2005) “FRP debonding under the presence of multiple cracks along a concrete beam,” *Proceedings of the International Symposium on Bond Behavior of FRP in Structures (BBFS 2005), Hong Kong, China*, pp. 283-290.

PCI Design Handbook. 6th ed. Chicago, IL: Precast/Prestressed Concrete Institute, 2006.

Pham, H., and Al-Mahaidi, R. (2004) “Bond characteristics of CFRP fabrics bonded to concrete members using wet lay-up method,” *Proceedings of the Second International Conference on FRP Composites in Civil Engineering*, Adelaide, Australia, pp. 407-412.

Popovics, S. (1973) “A numerical approach to the complete stress-strain curve of concrete,” *Cement and Concrete Research*, Vol. 3, pp. 583-599.

Pornpongsaroj, P., and Pimanmas, A. (2003) “Effect of end wrapping on peeling behavior of FRP-strengthened beams,” *Proceedings of the Sixth International Conference on Fiber-Reinforced Polymers for Reinforced Concrete Structures (FRPRCS6)*, pp. 277-286.

Precast and Prestressed Concrete Institute (2006) *PCI Design Handbook*, Sixth edition, Chicago, IL.

Prota, A., Manfredi, G., Nanni, A., Cosenza, E., and Pecce, M. “Flexural Strengthening of RC Beams using Emerging Materials: Ultimate Behavior.” Proceedings of the International Conference FRP Composites in Civil Engineering – CICE 2004 – Seracino (2004).

Prota, A., Tan, K.Y., Nanni, A., Pecce, M., and Manfredi, G. (2006) “Performance of shallow reinforced concrete beams with externally bonded steel-reinforced polymer,” *ACI Structural Journal*, Vol. 103, No. 2, pp. 163-170.

Rabbat, B.G., Kaar, P.H., Russell, H.G., Bruce, R.N., (1985) “Fatigue tests of pretensioned girders with blanketed and draped strands”, PCI Journal, Vol. 105, No. 4.

Rabinovich, O., and Frostig, Y. (2000) “Closed-form high-order analysis of RC beams strengthened with FRP strips,” *ASCE Journal of Composites for Construction, Vol. 4, No. 2., pp. 65-74.*

Rahimi, H., and Hutchinson, A., (2001) ”Concrete beams strengthened with externally bonded FRP plates,” *ASCE Journal of Composites for Construction*, 5(1), pp. 44-56.

Rao, C. and Frantz, G.C., (1996) “Fatigue tests of 27-year old prestressed concrete bridge box beams”, PCI Journal, Vol. 41, No. 5.

Raoof, M., Zhang, S. (1997) “Insight into the structural behaviour of reinforced concrete beams with externally bonded plates,” *Proceedings of the Institution of Civil Engineers, Structures and Buildings*, v 122, n 4, Nov, 1997, p 477-492.

Reed, C.E., Peterman, R.J. (2004) “Evaluation of Prestressed Concrete Girders Strengthened with Carbon Fiber Reinforced Polymer Sheets”, *ASCE Journal of Bridge Engineering*, Vol. 9, No. 2.

Reeve, B.Z. (2005) “Effect of adhesive stiffness and CFRP geometry on the behavior of externally bonded CFRP retrofit measures subject to monotonic loads,” Thesis, University of Pittsburgh.

Ritchie, P.A., Thomas, D.A., Lu, L.W.,a nd Connelly, G.M. (1991) “External reinforcement of concrete beams using fiber reinforced plastics,” *ACI Structural Journal*, Vol. 88, No. 4, pp. 490-500.

Rizkalla, S. and Hwang, L., "Crack Prediction for Members in Uniaxial Tension at Any Given Loading Stage", Journal of the American Concrete Institute, Vol. 81, No. 6, November 1984, pp. 572-579.

Rizkalla, S., Rosenboom, O.A., and Miller, A.D. “Value Engineering and Cost Effectiveness of Various Fiber Reinforced Polymer (FRP) Repair Systems.” Final Report Research Project 2005-10, July 2005, North Carolina DOT, Raleigh, NC.

Roberts, T.M., and Haji-Kazemi, H. “Approximate analysis of shear and normal stress concentrations in the adhesive layer of plated RC beams”, Structural Engineer, Vol 67, No. 17 Mar 1989

Rosenboom, O.A. “Behavior of FRP Repair/Strengthening Systems for Prestressed Concrete.” Ph.D Dissertation, North Carolina State University, Raleigh, NC, 2006.

Rosenboom, O.A. and Rizkalla, S. “Flexural Behavior of Aged Prestressed Concrete Girders Strengthened with Various FRP Systems.” Accepted for publication in Construction and Building Materials, 2006.

Saadatmanesh, H., Ehsani, M.R., (1991) "RC beams strengthened with GFRP plates, I: Experimental study," *ASCE Journal of Structural Engineering*, 117(11), pp. 3417-3433.

Saito, M., and Imai, S., (1983) "Direct Tensile Fatigue of Concrete by the Use of Friction Grips", ACI Journal, V. 80, No. 5, pp. 431-438.

Sallam, H.M., Saba, A.M., Shahin, H.H., Abdel-Raouf, H. (2004) "Prevention of peeling failure in plated beams," *Journal of Advance Concrete Technology*, Vol 2, No. 3, pp. 419-429.

Schiebel, S., Parretti, R., Nanni, A., (2001) "Repair and Strengthening of Impacted PC Girders on Bridge A4845", Missouri Department of Transportation Report RDT01-017/RI01-016.

Schilde, K., and Seim, W., (2004) "Experimental and numerical investigations of bond between CFRP and concrete." Proceedings of FRP Composites in Civil Engineering (CICE 2004), Adelaide, Australia.

Sebastian, W.M. (2001) "Significance of midspan debonding failure in FRP-plated concrete beams," *Journal of Structural Engineering*, V. 127, No. 7, pp. 792-798.

Sebastian, W.M. (2002a) "Sensitivities of strength and ductility of plated reinforced concrete sections to preexisting strains," *Journal of Structural Engineering*, V. 128, No. 5, pp. 624-636.

Sebastian, W.M. (2002b) "Prediction of interface shear stresses in elastoplastic moment-varying zones of advanced composite material-strengthened concrete members," *Journal of Structural Engineering*, V. 128, No. 9, pp. 1212-1221.

Sena Cruz, J.M. and Barros, J.A.O. (2004) "Bond Between Near-Surface Mounted Carbon-Fiber-Reinforced Polymer Laminate Strips and Concrete", *Journal of Composites for Construction*, Vol 8, No. 6. pp. 519-527.

Seracino, R., Oehlers, D.J., and Saifulnaz, M.R.R., (2005) "Towards a generic model of the intermediate crack debonding resistance of plates adhesively bonded to concrete," *Proceedings of the International Symposium on Bond Behavior of FRP in Structures (BBFS 2005)*, pp. 271-276.

Shahawy, M., Beitelman, T.E. (1999) "Static and fatigue performance of RC beams strengthened with CFRP laminates," *ASCE Journal of Structural Engineering*, Vol. 125, No. 6, pp. 613-621.

Shanafelt, G.O. and Horn, W.B. "Damage Evaluation and Repair Methods for Prestressed Concrete Bridge Members." National Cooperative Highway Research Program Report 226, Transportation Research Board, 1980.

Sharif, A., Al-Sulaimani, G.J., Basunbul, I.A., Baluch, M.H., and Ghaleb, b.N. (1994) "Strengthening of initially loaded reinforced concrete beams using FRP plates," *ACI Structural Journal*, Vol. 91, No. 2, pp. 160-168.

Shen, H.S., Teng, J.G., and Yang, J., (2001) "Interfacial stresses in beams and slabs bonded with thin plate," *Journal of Engineering Mechanics*, V. 127, N. 4, pp. 399-406.

Shin, Y.S., and Lee, C., (2003) "Flexural behavior of reinforced concrete beams strengthened with carbon fiber-reinforced polymer laminates at different levels of sustaining load," *ACI Structural Journal*, V. 100, No.2, pp. 231-239.

Sika Corporation. SikaTop®123 PLUS 2003. 9 August 2006 <http://www.sikaconstruction.com/tds-cpd-SikaTop123PLUS-us.pdfl>.

Smith, S.T., and Teng, J.G., (2001) "Interfacial stresses in plated beams," *Engineering Structures*, V. 23, pp. 857-871.

Smith, S.T., and Teng, J.G., (2002a) "FRP strengthened RC beams. I: review of debonding strength models," *Engineering Structures*, Vol. 24, pp. 385-395.

Smith, S.T., and Teng, J.G., (2002b) "FRP strengthened RC beams. II: assessment of debonding strength models," *Engineering Structures*, Vol. 24, pp. 397-417.

So, M, and Harmon, T.G. (200X) "Cover delamination of R/C members with surface mounted FRP reinforcement." ACI Structural Journal, in review.

Spadea, G., Bencardino, F., and Swamy, R.N. (1998) "Structural Behavior of composite RC beams with externally bonded CFRP," *Journal of Composites for Construction*, Vol. 2, No.3, pp. 132-137.

Stallings, J.M., Tedesco, J.W., El-Mihilmy, M., McCauley, M. (2000) "Field Performance of FRP Bridge Repairs." *Journal of Bridge Engineering*, Vol 5, No. .5, pp. 107-113.

Standards Australia, (200X) "Draft design guideline for RC structures retrofitted with FRP and metal plates: beams and slabs," a draft submitted to Standards Australia Feb. 2006.

Swamy, R.N., Hobbs, B., and Roberts, M. (1995) "Structural Behaviour of Externally Bonded, Steel Plated RC Beams after Long-Term Exposure," *The Structural Engineer*, Vol. 73, No. 16.

Takács, P. F., and Kanstad T., (2002) "Strengthening Prestressed Concrete Beams with Carbon Fiber Reinforced Polymer Plates", NTNU Report R-9-00, Trondheim, Norway.

Takahashi, Y., and Sato, Y. (2003) "Flexural behavior of RC beams externally reinforced with carbon fiber sheets," *Proceedings of the Sixth International Symposium on Fiber Reinforced Polymer Reinforcement for Reinforced Concrete Structures (FRPRCS6)*, Singapore, pp. 237-246.

Takeda, K., Mitsui, Y., Murakami, K, Sakai, H., Nakamura, M. (1996) "Flexural behavior of reinforced conrete beams strengthened with carbon fibre sheets," *Composites Part A*, 27A, pp. 981-987.

Täljsten, B. (1994) *Strengthening of existing concrete structures with epoxy bonded plates of steel or fibre reinforced plastics*, Doctoral thesis, Luleå University of Technology.

Täljsten, B. (1997) "Strengthening of beams by plate bonding," *Journal of Materials in Civil Engineering*, Vol. 9, No. 4, pp. 206-212.

Täljsten, B. (2002) *FRP Strengthening of Existing Concrete Structures: Design Guidelines*, Luleå University of Technology, Sweden.

Tan, K.H., and Mathivoli, M., (1999) "Behavior of preloaded reinforced concrete beams strengthened with carbon fiber sheets," *Proceedings of the 4th International Symposium on Fiber Reinforced Polymer Reinforcement for Concrete Structures (FRPRCS4), Baltimore, MD, pp. 159-170.*

Teng, J.G., Chen, J.F., Smith, S.T., Lam, L. (2002) *FRP Strengthened RC Structures*, John Wiley and Sons, Ltd, England.

Teng, J.G., Smith, S.T., Yao, J., Chen, J.F. (2003) "Intermediate crack-induced debonding in RC beams and slabs," *Construction and Building Materials*, Vol. 17, pp. 447-462.

Teng, J.G., Lu, X.Z., Ye, L.P., and Jiang, J.J., (2004) "Recent research on intermediate crack-induced debonding in FRP strengthened RC beams," *Proceedings of Advanced Composite Materials in Bridges and Structures (ACMBS)*, Calgary, Alberta, Canada, July, pp. 1-12.

Teng, J.G., and Yao, J., (2005) "Plate-end debonding failures of FRP or steel-plated RC beams: a new strength model," *Proceedings of the International Symposium on Bond Behavior of FRP in Structures (BBFS)*, pp. 291-298.

Teng, J.G., Yuan, H., and Chen, J.F., (200X) "FRP-to-concrete interfaces between two adjacent cracks: theoretical model for debonding failure," *International Journal of Solids and Structures*, in press.

Tumialan, G., Serra, P., Nanni, A. and Belarbi, A. (1999). "Concrete cover delamination in reinforced concrete beams strengthened with carbon fiber reinforced polymer sheets," *Proceedings of the Fourth International Symposium on Fiber Reinforced Polymer Reinforcement for Reinforced Concrete Structures*, Maryland, USA, 725-735.

Tumialan, J.G., Huang, P.C, Nanni, A. (2001) "Strengthening of an Impacted PC Girder on Bridge A10062." Final Report RDT01-013/RI99-041, Missouri DOT, St. Louis County, MO, 41 pp.

Triantafillou, T.C., Plevris, N. (1992), "Strengthening of RC beams with epoxy-bonded fibre-composite materials," *Materials and Structures*, Vol. 25, pp. 201-211.

Ulaga, T., Vogel, T., and Meier, U. (2003) "Bilinear stress-slip model: theoretical background and significance," *Proceedings of Sixth International Symposium on Fiber Reinforced Polymer Reinforcement for Reinforced Concrete Structures*, Singapore, pp. 153-162.

Valcuende, M., Benlloch, J., and Parra, C.J. (2003) "Ductility of reinforced concrete beams strengthened with CFRP strips and fabric," *Proceedings of the Sixth International Conference on Fiber Reinforced Polymers for Reinforced Concrete Structures*, Singapore, pp. 338-346.

Walton, J.M., Yeung, Y.C.T., (1986) "The Fatigue Performance of Structural Strands of Pultruded Composite Rods", Mechanical Engineering Publications Ltd.

Watson Bowman Acme Corporation. Wabo®MBrace Saturant, 2002. 9 August 2006. <http://www. degussa-cc-la.com/paises/caribbean/productos/mbracesaturant-eng.pdf>.

Wang, C.Y., and Ling, F.S., (1998) "Prediction for the debonding failure of cracked RC beams with externally bonded FRP sheets," Proceedings of the Second International Conference on Composites in Infrastructure (ICCI 98), Tuscon, AZ, pp. 549-563.

Eric W. Weisstein. (2006) "Kolmogorov-Smirnov Test." From MathWorld--A Wolfram Web Resource. http://mathworld.wolfram.com/Kolmogorov-SmirnovTest.html

Yao, J., Teng, J.G., and Lam, L. (2005) "Experimental study on intermediate crack debonding in FRP-strengthened RC flexural members," *Advances in Structural Engineering*, 8(4), pp. 365-395.

Ye, L.P., Lu, X.Z., and Chen, J.F. (2005) "Design proposals for the debonding strength of FRP strengthened RC beams in the Chinese design code," *Proceedings of the International Symposium on Bond Behavior of FRP in Structures (BBFS 2005), Hong Kong, China, December.*

Yoshizawa, H., and Wu, Z. (1997) "Analysis of debonding fracture properties of CFS strengthened RC member subject to tension," *Proceedings of Third International Symposium on Non-Metallic (FRP) Reinforcement for Concrete Structures (FRPRCS3)*, Sapporo, Japan, pp. 287-294.

Yuan, H., Wu, Z., and Yoshizawa, H., (2001) "Theoretical solutions on interfacial stress transfer of externally bonded steel/composite laminates," *Journal of Structural Mechanics and Earthquake Engineering*, No. 675, pp. 27-39.

Yuan, H. and Wu, Z., (1999) "Interfacial fracture theory in structures strengthened with composite of continuous fiber," *Proceedings of Symposium of China and Japan: Science and Technology of 21st Century*, Tokyo, Sept., pp. 142-155.

Zhang, G.F., Kishi, N., and Mikami, H., (2003) "Influence of material properties of FRPs on strength of flexural strengthened RC beams," Proceedings of the Sixth International Symposium on FRP Reinforcement for Concrete Structures (FRPRCS6), Singapore, pp. 327-336.

Zhao, L., and Toutanji, H. (2004) "Verifications of some design equations of beams externally strengthened with FRP composites," Proceedings of the the Second International Conference on FRP Composites in Civil Engineering, Adelaide, Australia, pp. 499-503.

Ziraba, Y.N., Baluch, M.H., Basunbul, I.A., Sharif, A.M., Azad, A.K., and Al-Sulaimani, G.J., (1994) "Guidelines toward the design of reinforced concrete beams with external plates," ACI Structural Journal, V. 91, No. 6, pp. 639-646.

Zobel, R.S. and Jirsa, J.O. (1998) "Performance of Strand Splice Repair in Prestressed Concrete Bridges", PCI Journal v.43 (6) (1998) (72-84).

Zobel, R.S., Jirsa, J.O., Fowler, D.W., and Carrasuqillo, R.L. "Evaluation and Repair of Impact-Damaged Prestressed Concrete Bridge Girders." Report CTR 1370-3F, University of Texas, Austin, TX.

APPENDIX A – DESIGN EXAMPLE WITH RESPONSE 2000

A.1 Introduction

This appendix provides a design example to illustrate the various steps involved in the design of a CFRP flexural repair system for a prestressed concrete bridge girder. The analysis is based on a cracked section analysis, which is performed using the RESPONSE 2000© analysis program. The program is available to download free of cost, along with the instruction manual, at http://www.ecf.utoronto.ca/~bentz/home.shtml.

A.2 Problem Statement

A simply supported 50 ft AASHTO Type II concrete bridge girder prestressed with sixteen 0.5 in diameter 270 ksi straight strands, as shown in Figure A.1, was impacted by an overheight vehicle 3 ft from midspan. The impact caused significant loss of the concrete section as well as the rupture of three prestressing strands, or 18.8 percent loss of prestressing force. The objective is to restore the original flexural capacity of the member.

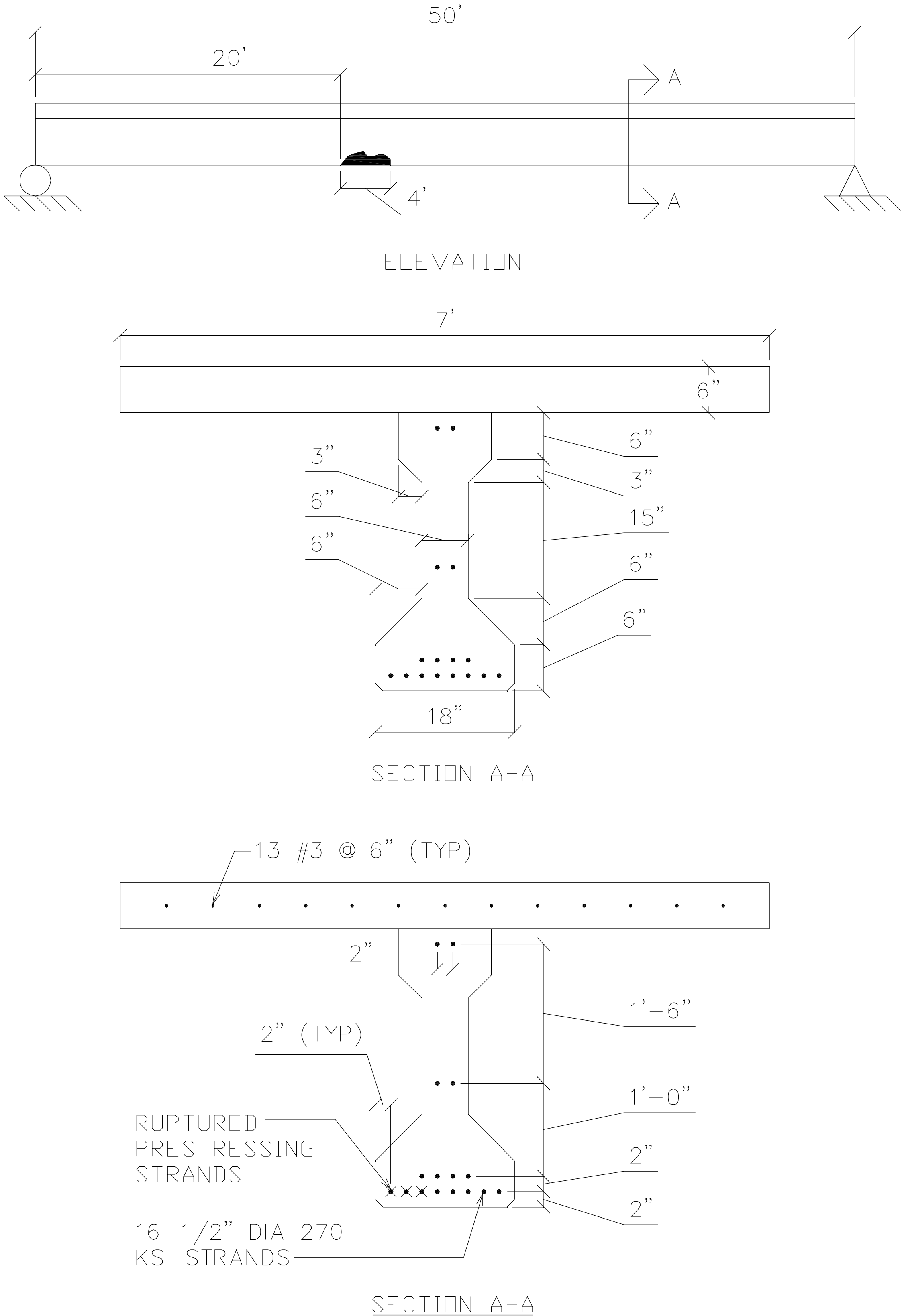

Figure A.1 Elevation and cross section of AASHTO Type II girder to repaired with CFRP

Testing of core samples taken from the girder indicates a concrete compressive strength in the girder of 6000 psi and A 3000 psi deck strength. The composite deck is 7 ft wide by 6 in thick. The cross sectional area of each strand is A_{ps} = 0.167 in^2. Assume an initial prestress level of 0.7 f_{pu} and a total prestress loss of 20 percent. Use the Ramberg-Osgood equation for the stress-strain relationship of the strand:

$$f_p = E_p e_{ps}\left[A + \frac{1-A}{\left[1+\left(Be_{ps}\right)^C\right]^{1/C}}\right] \tag{A-1}$$

where A = 0.015, B = 108, and C = 10, and E_p = 29000 ksi. Assume a rupture strain of 0.06 in/in. Non-prestressed reinforcement in the composite deck consists of thirteen #3 longitudinal bars spaced at 6 in and #4 closed-loops stirrups spaced at 9 in throughout the length of the girder.

It is proposed to use externally bonded CFRP wet lay-up sheets as the repair system. The material properties provided by the manufacturer are:

Ultimate tensile strength for design laminate:	143,000 psi
Laminate thickness:	0.04 in
Tensile Modulus:	13.9 x 10^6 psi
Ultimate elongation:	1.0%

A.3 Analysis of the Undamaged Section

The first step in the design is to conduct a flexural analysis of the undamaged section in order to predict the ultimate flexural strength of the girder.

Input of the Material and Geometric Properties

It is assumed that the reader is familiar with the RESPONSE 2000© Instruction Manual. Additional recommendations for input are described below:

1. The cross section of the AASHTO Type II girder can be chosen from the set of predefined shapes.
2. The material properties of the concrete can be automatically calculated by RESPONSE 2000© for the given value of f_c'.
3. The effective width of the composite deck, 59.4 in for this example, should be used to account for the difference in concrete strengths.
4. The material constants of the Ramberg-Osgood equation are required to define the characteristics of the type of prestressing steel used.

5. The prestrain in the prestressing strands can be calculated using the Ramberg-Osgood equation by first calculating the stress in one of the prestressing strands after losses, then dividing the effective prestressing force by the modulus of elasticity and multiplying by 100 to determine the prestrain value in units of millistrain:

$$\text{prestrain} = \frac{f_{pe}}{E_{ps}} * 100 \tag{A-2}$$

where $$f_{pe} = 0.7 f_{pu} \left(1 - 0.2\right) \tag{A-3}$$

Moment-Curvature Response of the Section

Using RESPONSE 2000©, the moment versus curvature behavior of the prestressed section is easily obtained by clicking SOLVE >> SECTIONAL RESPONSE. The section response is shown in Figure A.2. Note that the mode of failure indicated is crushing of the concrete in the compression region of the girder. The undamaged section capacity was found to be 1960.9 k-ft.

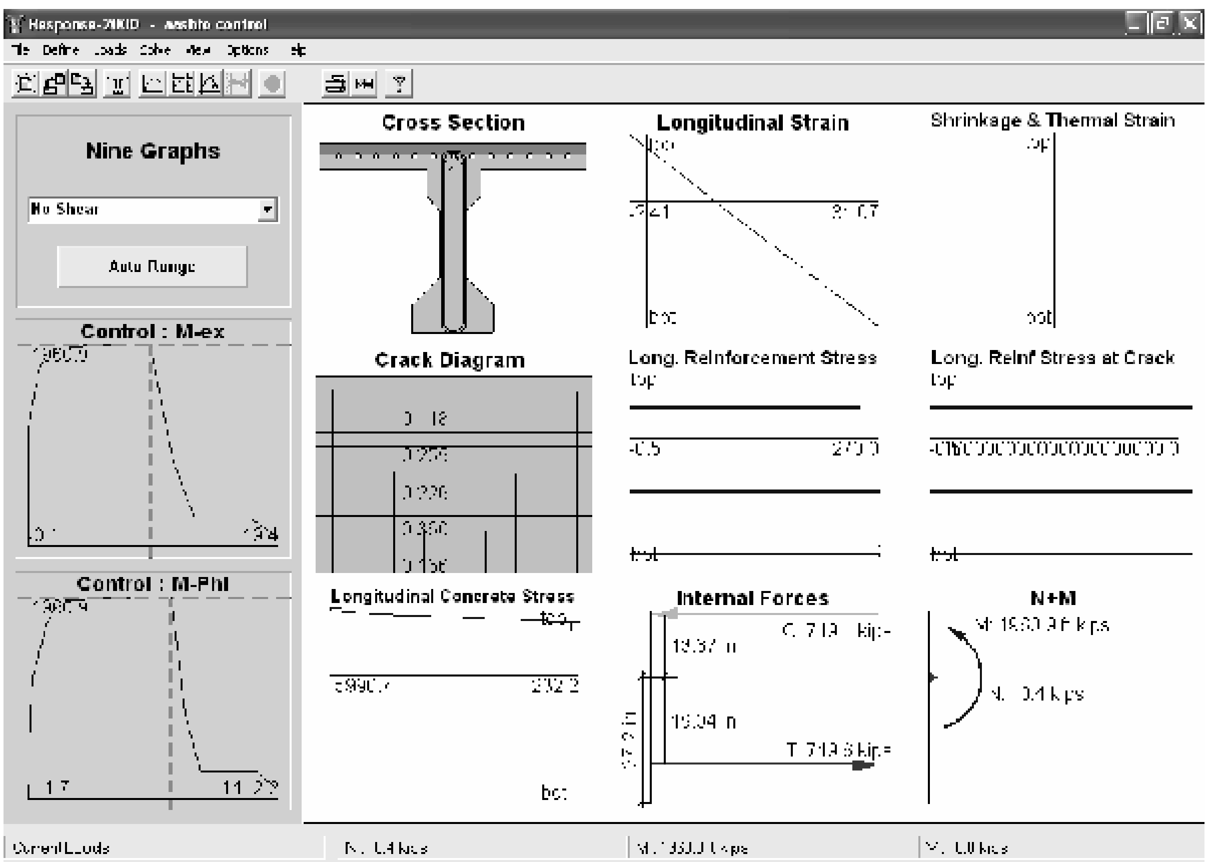

Figure A.2 Section analysis from RESPONSE 2000© of undamaged section

A.4 Analysis of the Damaged Section

After determining the undamaged flexural capacity of the section, the next step is to determine the damaged flexural capacity of the section. This is done by removing the proper number of prestressing strands from the cross section. It is important to not change the cross section to account for removal of damaged concrete, in that this will incorrectly redistribute the initial prestressing forces. The damaged section capacity was found to be 1535.8 k-ft.

A.5 Design of the Longitudinal CFRP

After analyzing the undamaged and damaged sections, the next step is to choose the required amount of longitudinal CFRP to restore the original flexural capacity of the section.

Design Material Properties

The material properties provided by the manufacturer should be considered initial properties and should be appropriately reduced to account for environmental degradation. ACI Committee 440 (2002) recommends an environmental reduction factor (C_E) of 0.85 to be applied to the ultimate tensile strength (f^*_{fu}) and rupture strain (e^*_{fu}) provided by the manufacturer for Carbon Fiber Reinforced Polymer materials subjected to exterior exposure. Therefore, the design ultimate strength (f_{fu}) and rupture strain (e_{fu}) can be calculated as:

$$f_{fu} = C_E f^*_{fu} \qquad \text{(A-4)}$$

$$= 0.85 \cdot (143)$$

$$= 121.5 \text{ ksi}$$

$$e_{fu} = C_E e^*_{fu} \qquad \text{(A-5)}$$

$$= 0.85 \cdot (0.01)$$

$$= 0.0085 \text{ in/in}$$

using the reduced properties, the elastic modulus of the CFRP (E_f) can be calculated:

$$E_f = \frac{f_{fu}}{e_{fu}} \qquad \text{(A-6)}$$

$$= \frac{121.5}{0.0085}$$

$$= 14{,}300 \text{ ksi}$$

Input Material and Geometric Properties of CFRP

In consultation with the developer of the RESPONSE 2000© program, the procedure below should be followed for input of the material characteristics of CFRP:

1. The CFRP material properties should be input as "Longitudinal Reinforcement".
2. The "Elastic Modulus" should be input as E_{frp}. The "e-Strain Hardening" can be entered as $1000 \times e_{fu}$. The "Rupture Strain" should be entered as $2 \times 1000 \times e_{fu}$, a value recommended by the developer of the program.
3. When defining the FRP as "Longitudinal Reinforcement", the appropriate area and location of the FRP should be specified, even if it is located outside the concrete cross-section.
4. RESPONSE 2000© will unrealistically predict a large horizontal shear in the cover concrete below the lower prestressing strand if the transverse non-prestressed reinforcement is terminated at the bottom of the web. The transverse steel should extend to the centroid of the FRP to eliminate this problem; even though it will be located outside of the concrete cross-section.

Design of the Longitudinal CFRP

The task of this step is to determine the amount of CFRP required to restore the ultimate flexural capacity of the damaged section. Based on section analysis of the unstrengthened section, the ultimate flexural capacity was found to be 1960.9 k-ft. Similarly, the ultimate flexural capacity of the damaged section was found to be 1535.8 k-ft. We need to add sufficient CFRP to gain an internal moment capacity of 425.1 k-ft. After several trials, it was found that two layers of CFRP 16 in wide gives an area of CFRP, $A_{FRP} = (2)(0.04)(16) = 1.28$ in^2, which exceeds our required moment capacity with a value of 1979.1 k-ft, as shown in Figure A.3. It should be noted that the mode of failure predicted by RESPONSE 2000[2] for the repaired section was rupturing of the longitudinal CFRP.

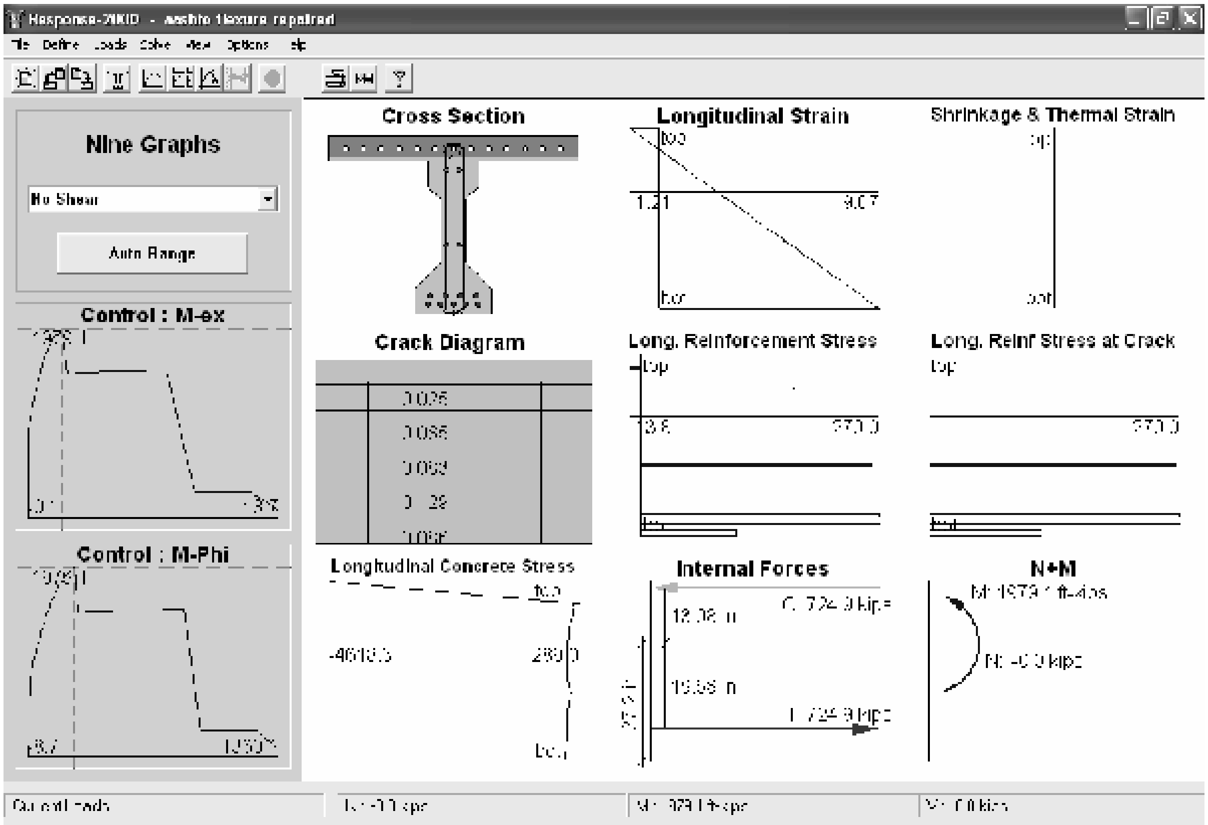

Figure A.3 Section analysis from RESPONSE 2000© of CFRP repaired section

Stress Ratio in Prestressing Strands

According to design guidelines presented in Rizkalla et al.2005, the stress ratio in straight prestressing strands should not exceed 5 percent under service loading. This must be confirmed in order to prevent the rupture of prestressing strands under cyclic service loading. The dead load moment due to the self weight of the girder and the composite deck can be determined assuming that the unit weight of concrete is 150 lbs/ft^3 as follows:

$$w_{DLg} = 0.384 \ \text{k/ft}$$

$$w_{DLd} = 0.525 \ \text{k/ft}$$

$$M_{DL} = \frac{(0.384 + .525)\cdot(50)^2}{8}$$

$$= 284.1 \ \text{k-ft}$$

The maximum allowable live load was determined as the load that induced a maximum tensile stress in the extreme bottom of the concrete flange equal to $3\sqrt{f'_c}$ psi, which is specified by the AASHTO (2004) code for service loading in corrosive environments. The corresponding allowable live load moment is equal to 556.1 k-ft, therefore the service loading conditions will vary between a minimum value of:

$$M_{DL} = 284.1 \text{ k-ft}$$

and a maximum value of:

$$M_{DL+LL} = 840.2 \text{ k-ft}$$

From the "Section Response" screen in the lower left corner is the "Control: M-Phi" plot. The cursor on this plot can be moved to show the corresponding strains, stresses and forces acting on the section at any given value of moment. At values of moments equal to the DL and the DL+LL shown above, the stress in the reinforcing can be determined using Response 2000© and is given in Table A.1. Using the following equation, the stress ratio can be calculated for the 270 ksi prestressing strands:

$$SR_{ps} = \frac{f_{ps2} - f_{ps1}}{f_{pu}} \times 100 \qquad \text{(A-7)}$$

Table A.1 Stress ratios in the prestressing strands of repaired AASHTO girder

Prestressing strand location	Bottom
Type of strand	Straight
Stress at DL, ksi	145.5
Stress at DL+LL, ksi	153.3
SRps, %	2.89
SRps limit from guidelines, %	5

The analysis indicated that the stress ratios in prestressing strands of the repaired girder at the service loading levels are below the specified values recommended in the design guidelines.

Check Deflections

AASHTO (2004) specifies in Article 2.5.2.6.2 a maximum deflection (Δ_{max}) due to dead load and vehicular live load of:

$$\Delta_{\max} = \frac{l_g}{800} \tag{A-8}$$

where l_g is the girder span length (in inches). For our girder span, this limit corresponds to 0.75 in. The dead and live load moments previously found can be resulted into concentrated loads at midspan from:

$$P_{DL} = \frac{(284.1)\cdot(4)}{50}$$

$$= 22.7 \text{ k}$$

$$P_{LL} = \frac{(556.1)\cdot(4)}{50}$$

$$= 44.5 \text{ k}$$

The service load level, P_s, at which the deflection should be calculated should include the dead load, P_{DL}, and the live load, P_{LL}, multiplied by the impact factor, IM, as follows:

$$P_s = 22.7 + 44.5$$

$$= 67.2 \text{ k}$$

In RESPONSE 2000©, the full member response can be calculated by entering various properties under LOAD >> FULL MEMBER PROPERTIES. The values given below correspond to a simply supported girder, 50 ft clear span, loaded with a concentrated load at midspan.

1. "Length subjected to shear" equal to half of the girder span, 300 in.
2. "Constant Moment zone on right" equal to zero.
3. Use "Constant shear analysis", "support on bottom", and "Load on continuous beam, load on top", to create a simply supported girder.

The full member response of the girder can be calculated by clicking on SOLVE >> MEMBER RESPONSE. Due to symmetry, RESPONSE 2000© only calculates the response of half of the member, so the load versus deflection plot shown in the lower left hand corner is half of the actual member response. The deflection at half the service load, $P_s/2$, is 0.20 in, therefore the AASHTO deflection criteria is satisfied. The member response is shown in Figure A.4.

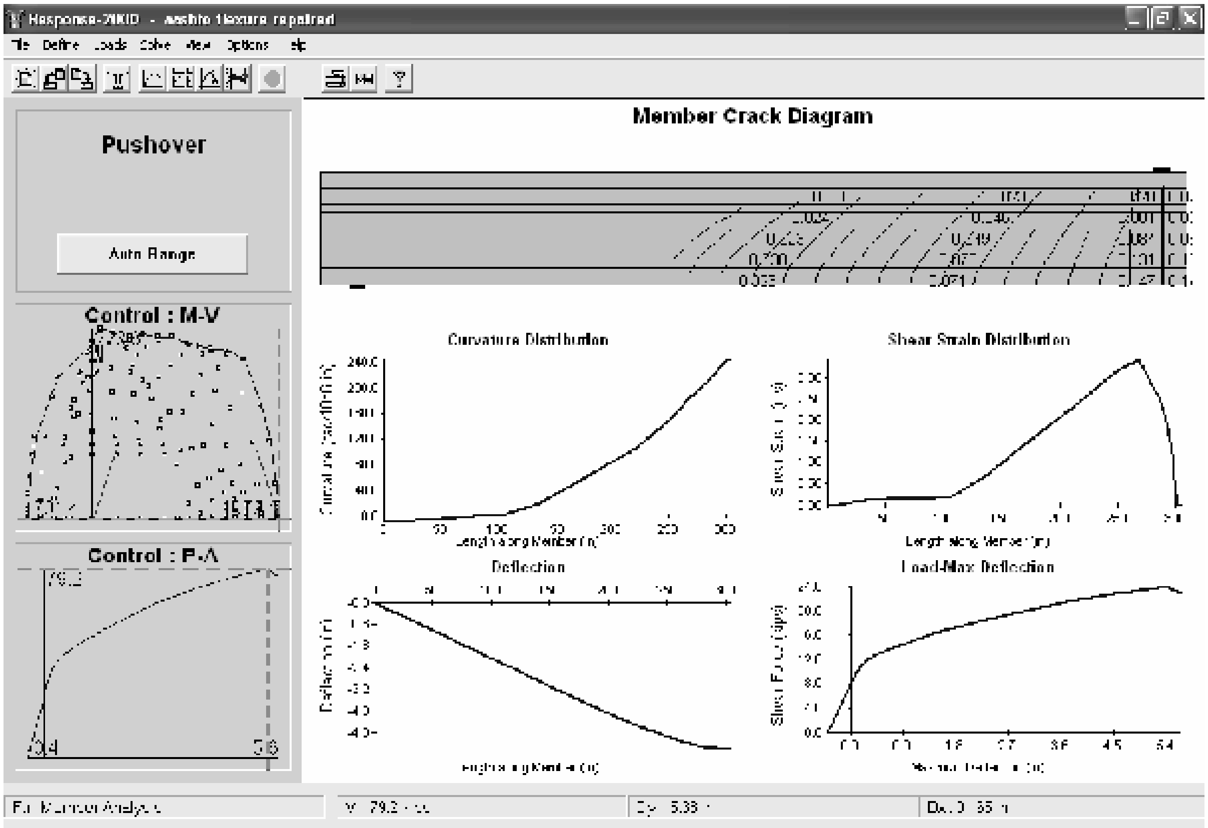

Figure A.4 Member response of CFRP repaired girder

A.6 CFRP Detailing

To ensure full usage of material capacities and to control premature failures due to debonding, the following detailing should be included in the design:

1. Each layer of longitudinal CFRP must extend past the damage a length equal to or greater than the development length of the prestressing strands.
2. The termination of the longitudinal CFRP sheets should be staggered to minimize plate-end debonding effects.
3. To further control plate-end type debonding, 12 in wide transverse CFRP U-wraps should be provided at the termination point of each layer of the longitudinal CFRP. The U-shape should extend to the top flange on both sides of the girder.
4. Additional transverse U-wraps, identical to the ones described above, should be provided at intervals of 3 ft or less along the length of the longitudinal CFRP to control possible intermediate crack debonding.
5. Continuous 2 ft wide transverse U-wraps should be provided, with minimum spacing in between, at the location of the repair mortar to minimize cracking in the non-prestressed region.

APPENDIX B – PARAMETRIC STUDY

B.1 Introduction

This appendix provides a design example to illustrate the various steps involved in the design of a CFRP system to repair lateral impact damage of a prestressed concrete bridge girder near a support. The analysis is based on guidelines proposed by the Precast/Prestressed Concrete Institute (PCI) Design Handbook (2006) for the shear strength of prestressed concrete members and ACI Committee 440 (2002) proposed guidelines for the contribution of CFRP used in shear applications.

B.2 Problem Statement

A simply supported 50.0 ft AASHTO Type II concrete bridge girder prestressed with sixteen 0.5 in diameter 270 ksi straight strands, as shown in Figure B.1, was impacted by an overheight vehicle 3 ft from the face of the left support. The impact caused a loss of the concrete section along a 4 ft length of the girder, including the loss of 3 in of the web cross section, as well as rupturing three prestressing strands. The primary objective is to restore the original shear capacity of the member.

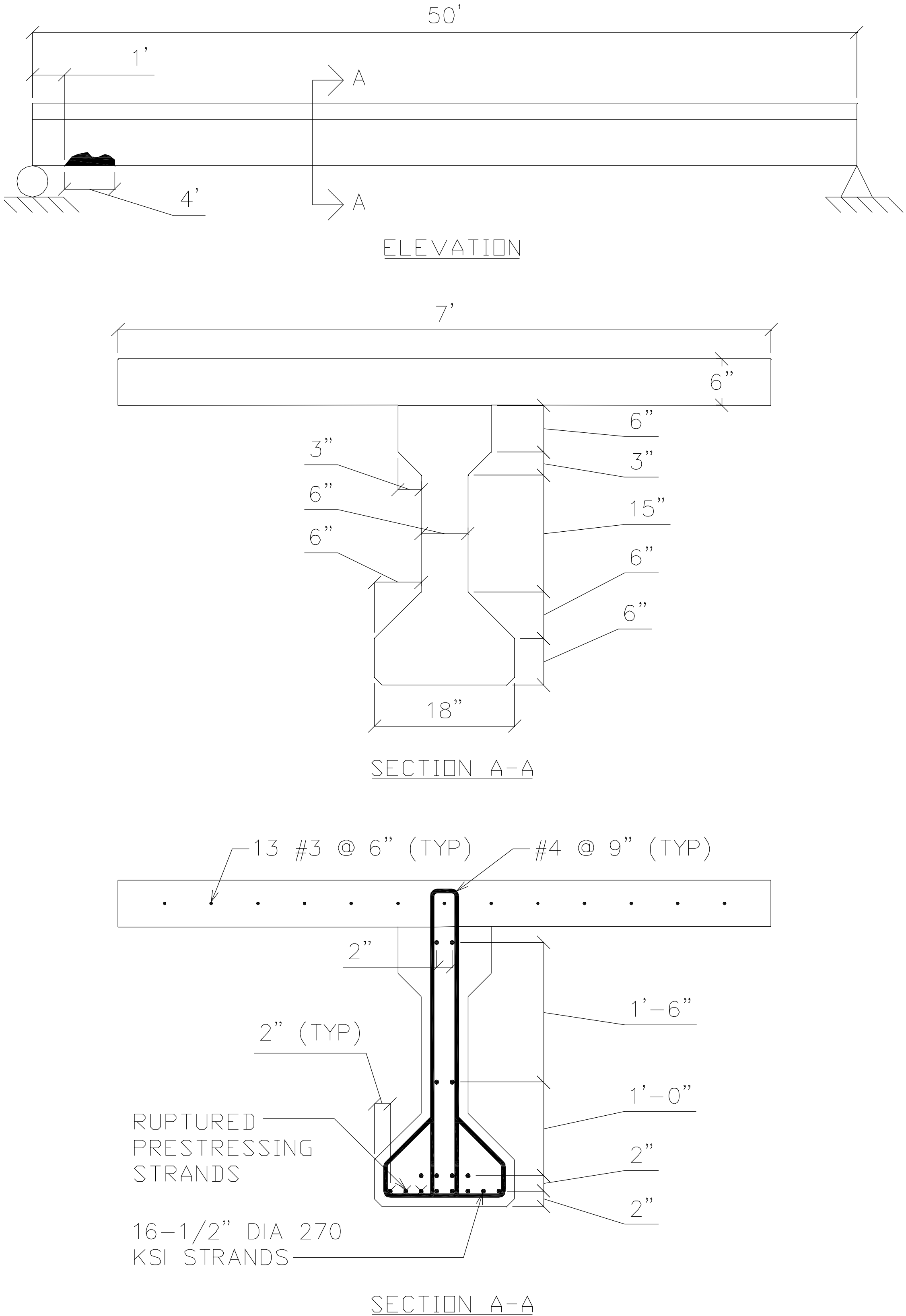

Figure B.1 Elevation and cross section of AASHTO Type II girder repaired with CFRP

The composite deck is 7 ft wide by 6 in thick. Testing of core samples taken from the girder indicates a concrete compressive strength in the girder of 6000 psi and 3000 psi in the deck. The cross sectional area of each strand is A_{ps} = 0.167 in^2 Assume an initial prestress level of 0.7 f_{pu} and a total prestress loss of 20 percent. Use the Ramberg-Osgood equation for the stress-strain relationship of the strand:

$$f_p = E_p e_{ps} \left[A + \frac{1-A}{\left[1+\left(Be_{ps}\right)^C\right]^{1/C}} \right] \tag{B-1}$$

with A = 0.015, B = 108, and C = 10, and E_p = 29000 ksi. Assume a rupture strain of 0.06 in/in. Non-prestressed reinforcement in the composite deck consists of thirteen #3 longitudinal bars spaced at 6 in and #4 closed-loops stirrups spaced at 9 in throughout the length of the girder. It is proposed to use externally bonded CFRP wet lay-up sheets as the repair system. The material properties provided by the manufacturer are:

Ultimate tensile strength for design laminate:	143,000 psi
Laminate thickness:	0.04 in
Tensile Modulus:	13.9 x 10^6 psi
Ultimate elongation:	1.0%

B.3 Analysis of the Undamaged Section

The first step in the design is to conduct a shear analysis of the undamaged girder at various intervals to predict the nominal shear strength at each section. The nominal shear strength, $V_n = V_c + V_s$ is found by adding up the contribution of the concrete and the steel stirrups at each section. Since the nominal shear capacity changes at each section, this example shows a sample calculation of the shear capacity of the section at the centerline of the damage, or 3 ft from the left support.

In order to calculate the shear capacity of a prestressed member, the applied loads first need to be determined. Finding the critical shear loading scheme for the girder was performed using AASHTO (2004) moving truck load design guidelines. After several iterations, the critical loading scheme was determined and is shown in Figure B.2. Due to the location of the damage, it was decided that the critical loading scheme would induce the largest constant shear force throughout the damaged region.

From the PCI Design Handbook (2006), the contribution of the concrete (V_c) to the shear capacity of the section is the lesser value of V_{cw} and V_{ci}, calculated as follows:

$$V_{ci} = 0.6\sqrt{f_c^{'}}b_w d + V_d + \frac{V_i M_{cr}}{M_{\max}} \tag{B-2}$$

$$= 0.6\sqrt{6000}(6)(33.75)/1000 + 20.01 + \frac{(51.36)(23,467)}{1,849}$$

= 681 k

and

$$V_{cw} = \left(3.5\sqrt{f_c^{'}} + 0.3 f_{pc}\right)b_w d + V_p \tag{B-3}$$

$$= \left(\left(\frac{3.5\sqrt{6000}}{1000}\right) + 0.3(404/369)\right)(6)(33.75) + 7.4$$

= 128 k

where V_d is the shear force caused by the unfactored dead load, V_i is the factored shear force at a section due to externally applied loads, M_{cr} is the cracking moment of the section, $M_{\max}$ is the maximum factored moment at a section due to externally applied loads, f_{pc} is the compressive stress in concrete at the centroid due to effective prestressing forces, and V_p is the vertical component of the effective prestress force at the section centroid. M_{cr} is the cracking moment and can be calculated as:

$$M_{cr} = \left(\frac{I}{y_t}\right)\left(6\sqrt{f_c^{'} + f_{pe} - f_d}\right) \tag{B-4}$$

where I is the moment of inertia, y_t is the distance from the top of the girder to the center of gravity, f_{pe} is the compressive stress in the concrete at the extreme tension fiber due to the effective prestressing force, and f_d is the stress due to service dead load. Since $V_{cw} < V_{ci}$, then the contribution of concrete to the nominal shear strength of the girder is 128 k .

The contribution of the steel stirrups (V_s) to the shear capacity of the section is primarily dependent on the size of the reinforcing bar used and the spacing between bars. The stirrup contribution is calculated as follows:

$$V_s = \frac{A_v f_y d}{s} \tag{B-5}$$

$$= \frac{(0.44)(60)(33.75)}{9}$$

$$= 99 \text{ k}$$

where A_v is the area of the shear reinforcement, f_y is the yield stress of the shear reinforcement, and s is the spacing between stirrups. The shear contribution of the stirrups is 99 k.

The total nominal shear strength (V_n) is 128 + 99 = 227 k. The nominal shear capacity of the entire girder was calculated at different sections in the same manner as above, except in the transfer region of the prestressing strands. The transfer region is defined as $50d_b = 50*0.5$ = 25 in, where d_b is the diameter of the prestressing strand. In order to account for this lesser bond strength in the transfer region, PCI (2006) guidelines specify that the shear capacity at the end of the girder be governed by $3.5\sqrt{f_c'}\,(b_w)(d)$ = $3.5\sqrt{6000}\,(6)(33.75)$ = 54.9 k. A linear interpolation is then performed between this value and the shear capacity 25 in from the end of the girder. The nominal shear capacity and the factored applied shear load along the entire length of the girder are shown in Figure B.2. The factored applied loading diagram shown in Figure B.2 was calculated using a dead load factor of 1.2, a live load factor of 1.7, and an impact factor of 1.33, all per AASHTO (2004).

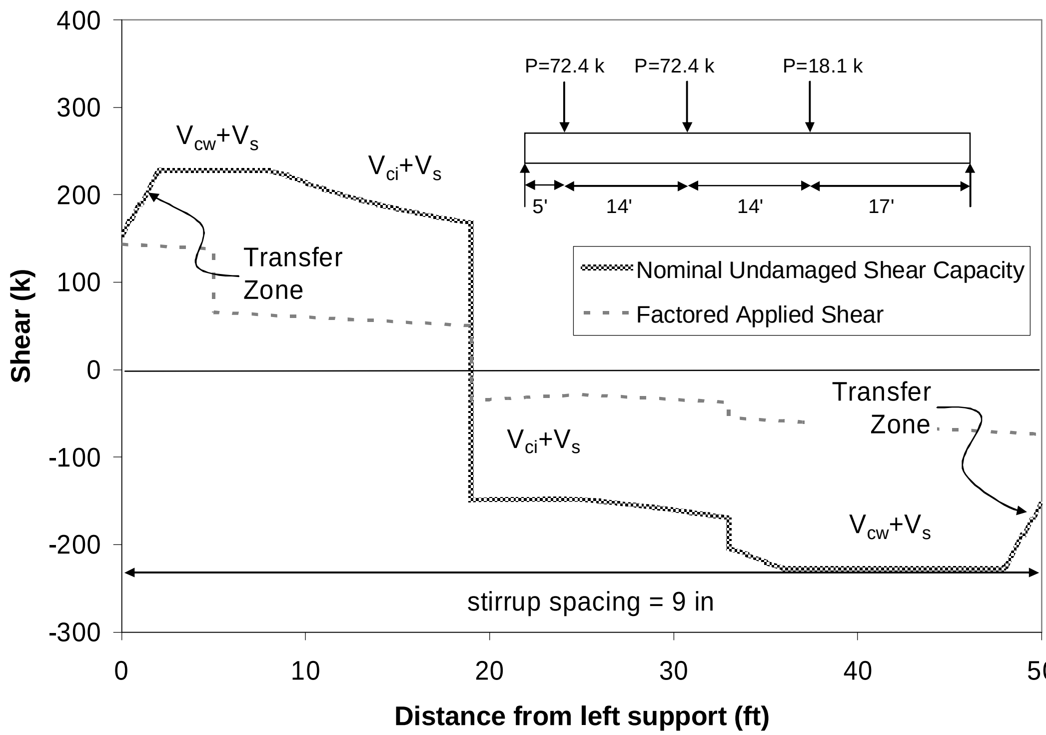

Figure B.2 Nominal undamaged shear capacity of AASHTO Type II girder

B.4 Analysis of the Damaged Section

The next step in the design of a CFRP shear repair system is to analyze the nominal shear strength of the damaged girder. This is performed in the same manner as previously described for the undamaged section, except several changes are made to correspond with the lateral impact damage. Unlike the flexural design example shown in Appendix A, the shear design model requires that the loss of concrete section be included as well as the loss of prestressing strands. The most critical variable in a shear-critical specimen is the width of the web (b_w). The girder is evaluated at various sections along the entire length to determine the nominal shear capacity envelope. A sample calculation of the damaged section 3 ft from the left support, the same location examined in detail above, is presented below. V_c is calculated in the same manner as before using equation B.2 and B.3, as shown:

$$V_{ci} = 0.6\sqrt{6000}(3)(33.75)/1000 + 20.01 + \frac{(51.36)(25,605)}{1,849} \qquad \text{(B-2)}$$

$$= 736 \text{ k}$$

and $$V_{cw} = \left(\left(\frac{3.5\sqrt{6000}}{1000}\right) + 0.3(328/291)\right)(3)(33.75) + 7.4 \qquad \text{(B-3)}$$

$$= 69.1 \text{ k}$$

Since $V_{cw} < V_{ci}$, then the contribution of concrete to the nominal shear strength of the girder is 69.1 k, which is 58.9 k less than the undamaged concrete section shear capacity contribution.

The contribution of the steel stirrups changes throughout the length as a result of the width of the web changing through the damaged section. Per PCI (2006), the maximum allowed contribution of the steel stirrups, $V_s = 8\sqrt{f_c^{'}}b_w d$, exceeds the direct calculation of the stirrups contribution.

$$V_s = 8\sqrt{f_c^{'}}b_w d \qquad \text{(B-6)}$$

$$= 8\sqrt{6000}(3)(33.75)$$

$$= 62.7 \text{ k}$$

Therefore, the contribution of the steel stirrups at this location is 62.7 k which is 36.3 k less than the undamaged section stirrup shear capacity contribution. As previously described, the transfer zone at each end of the girder was taken into account, but in addition to the transfer zones at the ends of the girder, a third transfer zone is created beyond the ruptured prestressing strands that must be taken into account. To be conservative, it is assumed that all prestressing strands are affected in this other transfer zone, not just the ruptured ones. The nominal shear capacity of the entire girder was calculated at different sections in the same manner as above and plotted with factored applied loads in Figure B.3.

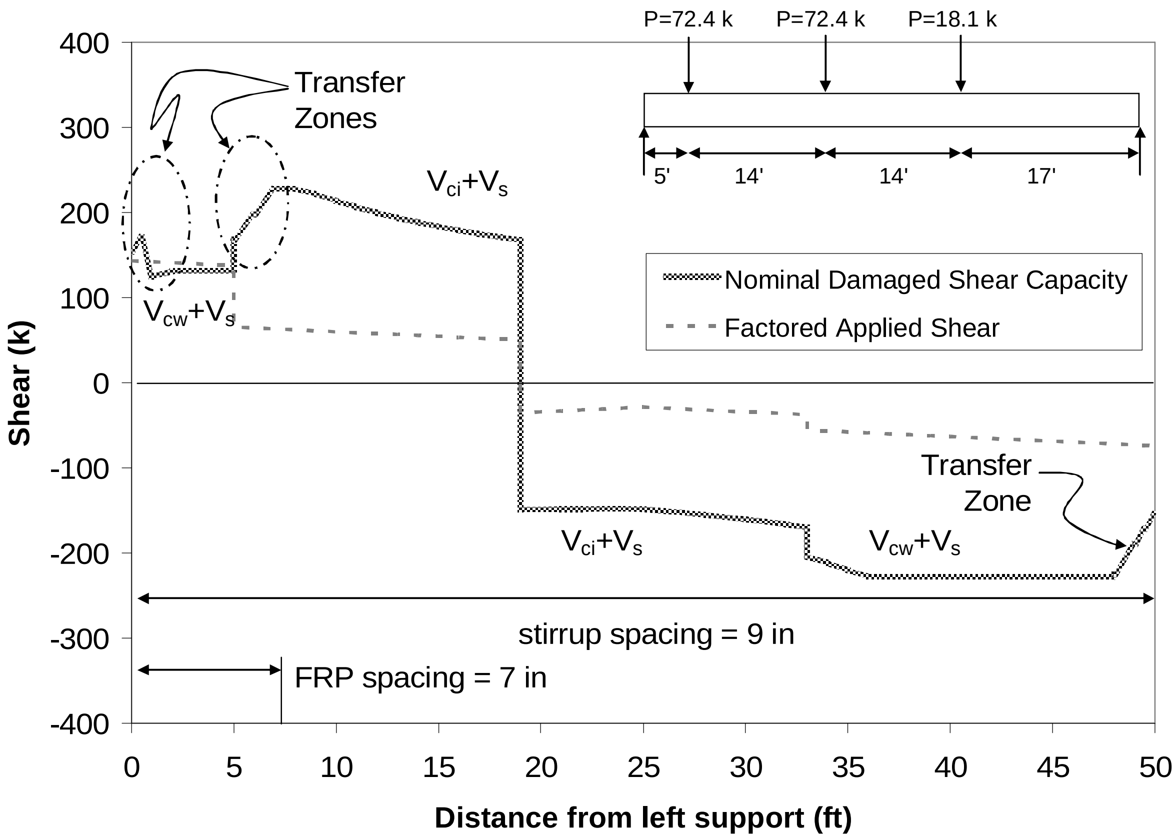

Figure B.3 Nominal damaged shear capacity of AASHTO Type II girder

B.5 Design of the Transverse CFRP

After the analysis of the undamaged and damaged sections, the next step is to choose the required amount of transverse CFRP to restore the original shear capacity at each section along the length of the girder.

Design Material Properties

The material properties provided by the manufacturer should be considered initial properties and should be appropriately reduced to account for environmental degradation. ACI Committee 440 (2002) recommends an environmental reduction factor (C_E) of 0.85 to be applied to the ultimate tensile strength (f^*_{fu}) and rupture strain (e^*_{fu}) provided by the manufacturer for CFRP materials subjected to exterior exposure. Therefore, the design ultimate strength (f_{fu}) and rupture strain (e_{fu}) can be calculated as:

$$f_{fu} = C_E f^*_{fu} \tag{B-7}$$

$$= 0.85 \cdot (143)$$

$$= 121.5 \text{ ksi}$$

$$e_{fu} = C_E e^*_{fu} \tag{B-8}$$

$$= 0.85 \cdot (0.01)$$

$$= 0.0085 \text{ in/in}$$

using the reduced properties, the elastic modulus of the CFRP (E_f) can be calculated:

$$E_f = \frac{f_{fu}}{e_{fu}} \tag{B-9}$$

$$= \frac{121.5}{0.0085}$$

$$= 14{,}300 \text{ ksi}$$

Design of the Transverse CFRP

The task of this step is to determine the amount of CFRP required to restore the nominal shear capacity at each section along the girder. Again for this example, we will analyze the same section, 3 ft from the left support, which was previously analyzed in the undamaged and damaged example. From these previous examples, analysis of the undamaged and damaged sections yielded nominal shear capacities of 227 k and 132 k respectively. For this particular section, we need to add sufficient CFRP to increase the shear capacity by $227 - 132 = 95$ k . At this point, the ACI Committee 440 (2002) recommendations for shear contribution of CFRP are used. After several trials, it was found that 1 layer of 6 in wide CFRP sheets, with a 1.0 in space between sheets, oriented at 45 degrees to the left of horizontal would provided a shear contribution of 101.4 k, which exceeds our deficit of 95 k. The steps involved using the ACI Committee 440 (2002) guidelines are as follows. First, an area (A_{fv}) of transverse CFRP is chosen, which is calculated as follows:

$$A_{fv} = 2nt_f w_f \tag{B-10}$$

$$= 2(1)(.04)(6)$$

$$= 0.48 \text{ in}^2$$

where n is the number of layers, t_f is the thickness of each layer, and w_f is the width of each layer of CFRP. The next step is to find the active bond length of the FRP (L_e), which is the length over which the majority of the bond stress is maintained. The active bond length is calculated as shown:

$$L_e = \frac{2500}{\left(nt_f E_f\right)^{0.58}} \tag{B-11}$$

$$= \frac{2500}{\left((1)(.04)(14,300)(1000)\right)^{0.58}}$$

$$= 1.14 \text{ in}$$

where E_f is the modulus of elasticity calculated using Equation B.9. The next step is to calculate the bond reduction modification factors k_1 and k_2. k_1 accounts for the concrete strength while k_2 accounts for the wrapping scheme used, which in our case is U-wraps. These factors are calculated as shown:

$$k_1 = \left(\frac{f_c'}{4000}\right)^{2/3} \tag{B-12}$$

$$= \left(\frac{6000}{4000}\right)^{2/3}$$

$$= 1.31$$

$$k_2 = \frac{d_f - L_e}{d_f} \text{ for U-wraps} \tag{B-13}$$

$$= \frac{28 - 1.14}{28}$$

$$= 0.96$$

where $f_c^{'}$ is the compressive strength of the concrete and d_f is the depth of the FRP shear reinforcement taken from the centroid of the tension steel to the top of the transverse sheet. After determining the modification factors, the next step is to determine the bond reduction factor (k_v) as shown:

$$k_v = \frac{k_1 k_2 L_e}{468 e_{fu}} \leq 0.75 \tag{B-14}$$

$$= \frac{(1.31)(0.96)(1.14)}{(468)(0.0085)}$$

$$= 0.36$$

where e_{fu} is found using Equation B.8. The next step is to determine the effective strain in the FRP at failure (e_{fe}), as follows:

$$e_{fe} = k_v e_{fu} \leq 0.004 \tag{B-15}$$

$$= (0.36)(0.0085)$$

$$= 0.00306 \text{ in/in}$$

After finding the effective strain, the next step is to find the effective stress at failure (f_{fe}) as shown below:

$$f_{fe} = e_{fe} E_f \tag{B-16}$$

$$= (0.00306)(14,300)$$

$$= 44.0 \text{ ksi}$$

The final step is to determine the unreduced nominal shear strength (V_f) provided by the transverse FRP, as shown:

$$V_f = \frac{A_{vf} f_{fe} (\sin a + \cos a) d_f}{s_f} \tag{B-17}$$

$$= \frac{(0.48)(44.0)(\cos(45) + \sin(45))28}{7}$$

$$= 119.4 \text{ k}$$

where α is the angle of inclination of the FRP (in degrees), and s_f is the spacing of the transverse FRP reinforcement.

Lastly, V_f must be reduced by $\psi = 0.85$ to account for any uncertainties in the material properties, therefore $\psi V_f = 101.4\text{ k}$. Figure B.4 shows the repaired shear capacity along with the undamaged shear capacity at each section of the girder; for comparative purposes. The factored applied load is also shown in Figure B.4 It is evident that the repaired capacity is higher than the original capacity throughout the entire member length.

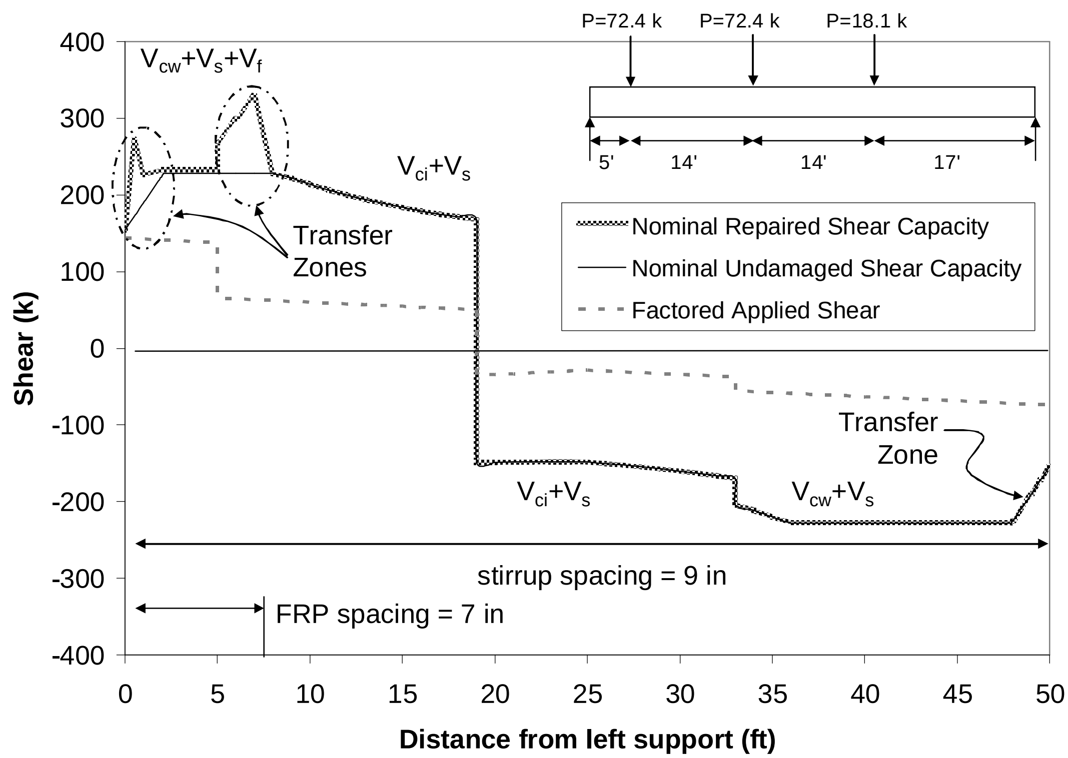

Figure B.4 Nominal shear capacity of undamaged and repaired girder

B.6 Design of the Longitudinal CFRP

The design of the longitudinal CFRP to restore the flexural capacity of the section should be performed in the same manner as previously described in Appendix A. The design calls for two layers of 16 in wide sheets to restore the flexural capacity. These longitudinal sheets should begin at the left support and extend for a minimum of 8 ft according to the CFRP detail recommendations provided.

B.7 CFRP Detailing

The following details, in conjunction with the details laid out in Appendix A for flexural repairs using CFRP materials, should be included to ensure full effectiveness of the individual CFRP sheets and CFRP repair system as a whole:

1. The diagonal CFRP struts should be continuous from the top flange on one face to the opposite side of the bottom flange, forming a crossing pattern on the bottom with the strut on the opposite face.
2. To further control plate-end type debonding, one 12 in wide transverse CFRP U-wrap should be provided at the centermost termination point of the bottom layer of the longitudinal CFRP. The U-wrap should extend to the top flange on both sides of the girder.
3. To account for the outward forces created, one longitudinal layer of CFRP should be provided on each side of the girder at the intersection of the bottom flange and bottom of the web.